

Estudio de las propiedades en columna y
superficie del aerosol atmosférico en la zona
centro-norte de la Península Ibérica:
énfasis en aerosol desértico

María Ángeles Burgos Simón



Universidad de Valladolid

FACULTAD DE CIENCIAS

DEPARTAMENTO DE FÍSICA TEÓRICA, ATÓMICA Y ÓPTICA

TESIS DOCTORAL:

**Estudio de las propiedades en columna y
superficie del aerosol atmosférico en la zona
centro-norte de la Península Ibérica: énfasis
en aerosol desértico**

Presentada por María Ángeles Burgos Simón
para optar al grado de doctora por la
Universidad de Valladolid

Dirigida por:

Dra. Victoria E. Cachorro Revilla

Dr. David Mateos Villán

Este trabajo ha sido realizado en el
Grupo de Óptica Atmosférica de la Universidad de Valladolid



Certificado

Dra. Victoria E. Cachorro Revilla, Catedrática de Universidad en Física Aplicada, como Tutora y Directora del presente trabajo y Dr. David Mateos Villán, Investigador Post-doctoral Juan de la Cierva-Incorporación, como Director del presente trabajo

CERTIFICAN:

Que la memoria titulada: “Estudio de las propiedades en columna y superficie del aerosol atmosférico en la zona centro-norte de la Península Ibérica: énfasis en aerosol desértico”, presentada por Dña. María Ángeles Burgos Simón para optar al grado de Doctora en Física por la Universidad de Valladolid, ha sido realizada bajo nuestra dirección en el Departamento de Física Teórica, Atómica y Óptica de la Universidad de Valladolid.

Y para que conste, y en cumplimiento de la legislación vigente, firmamos el presente certificado en Valladolid, a 22 de Noviembre de 2016.

Fdo.: Dra. Victoria E. Cachorro Revilla

Fdo.: Dr. David Mateos Villán

Agradecimientos

Un sueño sólo puede triunfar sobre la realidad si se le da la oportunidad - Stanislaw Lem

Es la guinda del pastel, el momento en que echas la vista atrás y tienes la oportunidad de agradecer a todos los que te han acompañado en uno de los caminos más importantes de tu vida.

Y así, quisiera empezar por el principio, agradeciendo a mis abuelos y abuelas, porque ni las desgracias ni los cerros de esparto fueron capaces de detenerlos. A mi tío Antonio, porque nos regalaste tu infancia y muchos años después, este es un logro que he podido cosechar gracias a tu esfuerzo. A mis padres, porque no habría podido escribir esta tesis si vosotros no me hubieseis enseñado cómo utilizar una cuchara, y porque éste es el resultado de esa frase que dice que todo largo camino comienza por un paso, vosotros habéis estado desde el primero al último, en los que tropezaba, en los caía, en los que saltaba, en los que bailaba... Por ser un constante ejemplo de superación, lucha, valores, dedicación, amor y apoyo. Dicen que el verdadero arte aparece cuando haces algo muy difícil haciendo creer al que te está viendo que no te cuesta nada, vosotros habéis tirado siempre del carro sin que nosotras nos diéramos cuenta de lo que costaba, de las dificultades, del esfuerzo, de los quebraderos de cabeza mes a mes, de los viajes que empiezan a las 5 de la mañana y terminan a las 5 de la mañana del día siguiente o las lavadoras que terminan después de la media noche... en definitiva habéis hecho arte con nuestra familia en el día a día y ese es el mejor aprendizaje que nos podemos llevar de vosotros. Gracias por los regalos y también por la exigencia, por los consejos pero sobre todo por los regaños. A mi hermana, porque aunque tengas la tremenda suerte de tenerme como hermana, puede que sea recíproco. No hay que ser la mayor para ser un ejemplo a seguir.

De vital importancia es toda la gente que ha trabajado conmigo codo a codo durante estos años. Quiero agradecer a mis dos tutores, Victoria y David, por su constante esfuerzo y paciencia. Por la constancia y empeño en el trabajo que se incluye en esta memoria así como por hacer de mí una mejor científica e investigadora. Victoria, creo que siempre me asombraré al recordar como en tu cabeza puede caber tanta información y conocimiento y mi objetivo es que en la mía alguna vez todas las estanterías estén ordenadas y llenas como las tuyas. Gracias por tu esfuerzo porque sin personas como tú sería imposible hacer todo esto realidad. David, puedes que no sea capaz de devolverte todo lo que me llevo de ti: las gráficas, la redacción, el saber estar, la ilusión en cada cosa que haces, el trabajo duro... sabes que has sido mucho más que un tutor durante estos años, un compañero, un amigo y un ejemplo a seguir. Gracias a los dos, no podría haber dado con dos tutores mejores y eso es algo que no tiene precio. Si la vida es una cadena de favores, espero que me llegue la hora de transmitir todo lo que he aprendido de vosotros y ser capaz de hacerlo con todo el esmero y la excelencia con la que vosotros lo habéis hecho.

Pero mi carrera profesional no empezó aquí, sino en Valencia, y quiero agradecer a Vicente Caselles por ser el primero que creyó en mí y me dio la oportunidad para recorrer este camino. A Enric Valor, Vicent García, César Coll i els companys i companyes de la Universitat de València, gràcies per la saviesa i moments compartits. El començament d'un camí sempre marca el recorregut i tothom desitjaria poder fer-ho com jo ho vaig fer al costat de personnes com vosaltres.

A Ángel de Frutos, por complementar mi formación con temas tan diversos como la música, las películas, la política, la historia... ¡Es tan enriquecedor rodearse de gente con tanto conocimiento que no se puede imaginar un puesto de trabajo más interesante hasta en la hora del café! A Yasmine, porque sin aprender de ti hubiera sido un camino tortuoso, tus lecciones y consejos tanto profesionales como personales han sido de gran influencia para mí. A Carlos, por estar siempre al pie del cañón y saber sacar tiempo de donde no hay para leer los amenos artículos que le encargábamos. A Ramiro, por ser un apoyo desde el primer día que llegué a la

ciudad y porque aunque te metas conmigo y te hagas el duro sé que en el fondo has acabado cogiéndome cariño. A Cristian, porque de “lunes a jueves” nos llenas el despacho de alegría. A Rober, porque el escritorio de al lado es algo que une mucho. A Carlos Baladrón, ¡qué suerte haber sido tu compañera de docencia! Gracias por tu amabilidad y disponibilidad para resolver mis dudas y por las charlas y cafés llenos de anécdotas de las que aprender. Y a todos los demás compañeros del departamento que día tras día hacen de este trabajo, un camino apasionante y divertido.

Y por suerte mi experiencia no se queda dentro de las fronteras, Guten Tag Herr Christopher Ritter, für die große professionelle Entwicklungschance gestatteteb sie mir die Untersuchung in Potsdam. Vielen Dank für die wissenschaftlichen Erklärungen und der Aufmerksamkeit mir gegenüber, vom Tag der Tag der Ankunft bis zu meiner Abreise und dass ich mich wie zu Hause fühlen konnte. Das war eines der schönsten und profitabelsten Erfahrungen in meinem Leben. Vielen Dank dass sie mir das ermöglicht haben.

Ale, Vero, Bea, Teru, Diego, Rodrigo, Edu, Alejandra, Alberto Marcos, por los cafés, comidas y ratos que hemos compartido, con gente como vosotros el trabajo es un poco menos trabajo. A los del pasillo amarillo, Marina, Bea, Javichuelo, Miguelón, Sandra, Sergio, Mariana...porque aunque aún no haya terminado de sumar todos los enteros positivos sé que entre todos lo conseguiremos. Marina, ahora será difícil compartir piso con alguien más porque vaya si has puesto el listón alto, gracias por todo porque aunque no te lo dijera...sí que te echaba de menos (un poquito, eh!) cuando te ibas aunque fuera un día o dos. Y muy especialmente a ti, Hernán, por ser mi constante apoyo e ilusión durante este tiempo.

También me gustaría agradecer a mis tíos y tías, por el granito o granote de arena que cada uno aporta en mi vida. A mis primos y primas (*Blondi*, tú también), por compartir conmigo el valor de la familia. Alba, mi prima pequeña y tan grande a la vez. Sara, porque ya que soy tu prima preferida tendré que dedicarte alguna línea ¿no? La verdad es que es difícil escribirle algo a la escritora de la familia, así que lo resumiré en que los abrazos de garrapata (o Koala, que es más mono) nunca desaparezcan aunque nos hagamos mayores.

A mis amigas de Castalla, porque a pesar de lo rancia y ermitaña aún no me han echado del grupo (aunque Palazón se esfuerce). A Carme, Inés y Bea, ¡diez años ya! Por ser de esas a las que hablas poco y ves menos y sin embargo un minuto sobra para que sea como si aún estuviésemos de reuniones en las habitaciones. ¡Sois los mejores regalos personales que la vida universitaria me ha dado! A Noe (Juanjo y Aitana) y Jose, sin vosotros puede que esta tesis se hubiera realizado pero seguro que le hubiesen faltado las risas, disparates y cartas que sólo puedes compartir con los que están igual de locos que tú. Sin duda, ¡Física valió la pena por ese cuarto de carrera! (y mientras escribo esto pienso en nuestro viaje fin de carrera seis años después y con la familia ampliada a Berlín). Gracias Jose por tu hospitalidad en tierras germanas, por no enseñarme la ciudad y ser sin embargo el mejor guía que he podido tener. Gracias Noe por estar siempre dispuesta a escucharme y a hacer un hueco por mí, volver a casa siempre es gratificante si te espera gente como tú. Yuri, Dani... os he dejado preparados unos tupperts de cocido para cuando me vaya, para que no paséis hambre.

A Ana Sanz, por ser un referente de mujer en mi vida y por darle a estos cuatro años las agujetas necesarias para que el camino fuera más agradable. A Sara, porque estos años han sido sobre todo buenos, pero estoy segura que en Berlín y Canarias nos lo pasaremos también muy bien ;). A María Mozo, Ana Zamorano, Silvia, Elena, Cleofé... ¡Por todos los chasés que nos quedan por bailar! Y como no, Patri, porque aunque hayas decidido estudiar química sabes que siempre contarás con mi apoyo (!!!por las turboletas!!!).

Y a todos los que en mayor o menor medida me han acompañado durante estos años y de los que sin duda han dejado algo bueno en mi vida. Y a ti, lector, por tu interés y paciencia en las líneas que siguen...

A mis padres, Juan Pedro y MªÁngeles,
y a mi hermana, Clara

ÍNDICE

| | |
|--------------------------------------------------------------------------------------------------------------------------------|----|
| ÍNDICE..... | 11 |
| PUBLICACIONES..... | 13 |
| Compendio de artículos de la tesis doctoral..... | 13 |
| Trabajos presentados en congresos nacionales e internacionales..... | 13 |
| Otras publicaciones desarrolladas durante el periodo doctoral..... | 16 |
| RESUMEN | 17 |
| ABSTRACT | 19 |
| 1. Introducción, objetivos y estructura de la tesis | 21 |
| 1.1. Introducción | 21 |
| 1.1.1. Estado del arte | 21 |
| 1.1.2. Redes de monitorización de aerosoles y estudios previos | 23 |
| 1.1.3. Zona de estudio: Península Ibérica y comunidad de Castilla y León..... | 26 |
| 1.2. Objetivos | 28 |
| 1.3. Estructura de la tesis | 29 |
| 2. Medidas y metodología..... | 31 |
| 2.1. Estaciones de medida, bases de datos y otras informaciones..... | 31 |
| 2.2. Metodología | 35 |
| 2.3. Metodología de “Detección de episodios desérticos” | 37 |
| 2.3.1. Metodología de detección de episodios desérticos..... | 37 |
| 2.3.2. Caso estudio: Octubre, 2014 | 40 |
| 3. Resultados | 45 |
| 3.1. Estudio comparativo de las propiedades en superficie y columna de los aerosoles en dos estaciones de fondo regional | 45 |
| 3.1.1. Resumen gráfico..... | 45 |
| 3.1.2. Resumen..... | 45 |
| 3.1.3. Artículo 1 | 48 |
| 3.2. Inventario de intrusiones desérticas en el centro-norte de la Península Ibérica durante el periodo 2003-2014..... | 61 |
| 3.2.1. Resumen gráfico..... | 61 |
| 3.2.2. Resumen..... | 61 |
| 3.2.3. Artículo 2 | 63 |

| | |
|------------------------------------------------------------------------------------------------------------------------------------------------------------|-----|
| 3.3. Propiedades microfísicas y ópticas del aerosol desértico y sus mezclas en estaciones de fondo regional del centro-norte de la Península Ibérica | 87 |
| 3.3.1. Resumen gráfico | 87 |
| 3.3.2. Resumen | 87 |
| 3.3.3. Artículo 3 | 90 |
| CONCLUSIONES | 107 |
| REFERENCIAS | 111 |

PUBLICACIONES

Compendio de artículos de la tesis doctoral

- Bennouna, Y., Cachorro, V.E., Mateos, D., Burgos, M.A., Toledano, C., Torres, B., de Frutos, A.M., 2016. Long-term comparative study of columnar and surface mass concentration aerosol properties in a background environment. *Atmos. Environ.*, 140, 261-272, <http://dx.doi.org/10.1016/j.atmosenv.2016.05.061>.
- Cachorro, V.E., Burgos, M.A., Mateos, D., Toledano, C., Bennouna, Y., Torres, B., de Frutos, A.M., Herguedas, A., 2016. Inventory of African desert dust events in the North-central Iberian Peninsula in 2003-2014 based on Sun photometer and PM_x data. *Atmos. Chem. Phys.*, 16, 8227-8248, doi: 10.5194/acp-16-8227-2016.
- Burgos, M.A., Mateos, D., Cachorro, V.E., Toledano, C., de Frutos, A.M., 2016. Aerosol properties of mineral dust and its mixtures in a regional background of north-central Iberian Peninsula. *Sci. Total. Environ.*, 572, 1005-1019, <http://dx.doi.org/10.1016/j.scitotenv.2016.08.001>.

Trabajos presentados en congresos nacionales e internacionales

- Burgos, M.A., Mateos, D., Cachorro, V.E., Toledano, C., Velasco-Merino, C., González, R., Calle, A., de Frutos, A.M., 2016. Fingerprints of Aerosol Mineral Dust and its Mixtures on Optical and Microphysical Properties. IV Iberian Meeting on Aerosol Science and Technology. Aveiro, Portugal. Awarded with the Best Student Poster Prize.
- Mateos, D., Burgos, M.A., Cachorro, V.E., Toledano, C., Velasco-Merino, C., González, R., Guirado, C., Calle, A., de Frutos, A.M., 2016. Identification of atmospheric high turbidity episodes using different aerosol measurement techniques. IV Iberian Meeting on Aerosol Science and Technology. Aveiro, Portugal.

- Velasco-Merino, C., Toledano. C., Cachorro, V.E., Mateos, D., González, R., Burgos, M.A., Guirado, C., Calle, A., de Frutos, A.M., 2016. Impact of long-range transport on Saharan dust aerosol optical and microphysical properties. IV Iberian Meeting on Aerosol Science and Technology. Aveiro, Portugal.
- Mateos, D., Burgos, M.A., Cachorro, V.E., Toledano, C., Velasco-Merino, C., González, R., Calle, A., de Frutos, A.M., 2016. Impact of desert dust outbreaks in the aerosol load levels of a rural background environment between 2003 and 2014. 8th International Workshop on sand/Duststorms and Associated Dustfall. Lisbon, Portugal.
- Burgos, M.A., Cachorro, V.E., Mateos, D., Toledano, C., de Frutos, A.M., 2016. Oral Presentation: Aerosol characterization at columnar and Surface levels based on a long-term desert dust inventory in North-central Iberian Peninsula. 8th International Workshop on sand/Duststorms and Associated Dustfall. Lisbon, Portugal.
- Cachorro, V.E., Mateos, D., Toledano, C., Burgos, M.A., Bennouna, Y., Torres, B., Fuertes, D., González, R., Guirado. C., Román, R., Velasco-Merino, C., Marcos, A., Calle, A., de Frutos, A.M., 2015. Climatological classification of five sectors in the Iberian Peninsula using columnar (AOD, alpha) and surface (PM₁₀, PM_{2.5}) aerosol data supported by air mass apportioning. European Geosciences Union General Assembly 2015. Vienna, Austria.
- Burgos, M.A., Cachorro, V.E., Mateos, D., Toledano, C., Román, R., Velasco-Merino, C., González, R., Calle, A., de Frutos, A.M., 2015. Characterization of desert dust aerosol properties over Castilla y León in 2003-2013. III Iberian Meeting on Aerosol Science and Technology. Elche, Spain.
- Mateos, D., Cachorro, V.E., Toledano, C., Burgos, M.A., Bennouna, Y., Torres, B., Fuertes, D., González, R., Guirado, C., Román, R., Velasco-Merino, C., Calle, A., de Frutos, A.M., 2015. Climatological study about columnar and surface aerosol load in the Iberian Peninsula. III Iberian Meeting on Aerosol Science and Technology. Elche, Spain.

- Mateos, D., Cachorro, V.E., Toledano, C., Burgos, M.A., Bennouna, Y., Torres, B., Fuertes, D., González, R., Velasco-Merino, C., Román, R., Calle, A., de Frutos, A.M., 2015. Differences and similarities between surface and columnar aerosol climatology in the Iberian Peninsula. VIII Workshop Lidar Measurements in Latin America (WLMLA). Cayo-Coco, Cuba.
- Cachorro, V.E., Burgos, M.A., Toledano, C., Mateos, D., Bennouna, Y., Fuertes, D., González, R., Román, R., Velasco-Merino, C., Calle, A., de Frutos, A.M., 2015. Long-term Inventory of Desert Dust Outbreaks in Palencia Site (North-central Spain). VIII Workshop on Lidar Measurement in Latin America. Cayo-Coco, Cuba.
- Mateos, D., Cachorro, V., Marcos, A., Bennouna, Y., Toledano, C., Burgos, M. A., de Frutos, A.M., 2014. Aerosol load at the surface in the Iberian Peninsula during the last 25 years. 41st Annual European Meeting on Atmospheric Studies by Optical Methods. Stockholm, Sweden.
- Cachorro, V.E., Burgos, M.A., Bennouna, Y., Toledano, C., Torres, B., Mateos, D., Marcos, A., de Frutos, A.M., 2014. Climatology and interannual variability of desert dust outbreaks over north-central Spain in the 2000s. 41st Annual European Meeting on Atmospheric Studies by Optical Methods. Stockholm, Sweden.
- Cachorro V.E., Burgos, M.A., Bennouna, Y., Toledano, C., Torres, B., Mateos, D., Marcos, A. de Frutos, A.M., 2014. Characterization of PM_x Data Belonging to the Desert-Dust-Inventory Based on AOD-Alpha RIMA-AERONET Data at Palencia-Autilla Stations. II Iberian Meeting on Aerosol Science and Technology. Tarragona, Spain.
- Mateos, D., Cachorro, V.E., Marcos, A., Bennouna, Y., Toledano, C., Burgos, M.A., de Frutos, A.M., 2014. Temporal Characterization of Particulate Matter over the Iberian Peninsula to Support the Brightening Phenomena in the Last Decades. II Iberian Meeting on Aerosol Science and Technology. Tarragona, Spain.
- Cachorro, V.E., Burgos, M.A., Bennouna, Y., Toledano, C., Torres, B., Herguedas, A., González-Orcajo, J., de Frutos, A.M., 2013. Inventory of desert dust aerosols over the North-center region of Spain (2003-2012). VII Workshop on Lidar Measurements in Latin America. Pucón, Chile.

- Bennouna, Y., Cachorro, V.E., Burgos, M.A., Toledano, C., Herguedas, A., González-Orcajo, J., de Frutos, A.M., 2013. Relationships between AOD-Alpha and PM_x in the North-central area of Spain from long term records of AERONET and EMEP. VII Workshop on Lidar Measurements in Latin America (VII WLMLA). Pucón, Chile.
- Bennouna, Y., Cachorro, V.E., Toledano, C., Torres, B., Burgos, M.A., González, R., Fuertes, D., de Frutos, A.M., 2013. A climatological study of the relations between AOD-a and PM_x for north-central Spain. Davos Atmosphere and Cryosphere Assembly (DACA). Davos, Switzerland.
- Cachorro, V.E., Burgos, M.A., Bennouna, Y., Toledano, C., Torres, B., Herguedas, A., González, J., de Frutos, A.M., 2013. Inventory of desert dust aerosols in the region of Castilla y León (2003-2012). I Iberian Meeting on Aerosol Science and Technology. Évora, Portugal.
- Bennouna, Y., Cachorro, V.E., Burgos, M.A., Toledano, C., Herguedas, A., González, J., de Frutos, A.M., 2013. The Relations between AOD and PM_x from long-term data for North-central Spain. I Iberian Meeting on Aerosol Science and Technology. Évora, Portugal.

Otras publicaciones desarrolladas durante el periodo doctoral

- Mateos, D., Cachorro, V.E., Toledano, C., Burgos, M.A., Bennouna, Y., Torres, B., Fuertes, D., González, R., Guirado, C., Calle, A., de Frutos, A.M., 2015. Columnar and Surface aerosol load over the Iberian Peninsula establishing annual cycles, trends, and relationships in five geographical sectors. Sci. Total. Environ., 518–519, 378–392, doi: 10.1016/j.scitotenv.2015.03.002.
- Bennouna, Y.S., Cachorro, V.E., Burgos, M.A., Toledano, C., Torres, B., de Frutos, A.M., 2014. Relationships between columnar aerosol optical properties and surface particulate matter observations in north-central Spain from long-term records (2003–2011). Atmos. Meas. Tech. Discuss., 7, 5829–5882, doi: 10.5194/amtd-7-5829-2014.

RESUMEN

El impacto de los efectos directos e indirectos de los aerosoles atmosféricos en el balance radiativo del sistema Tierra-Atmósfera genera una enorme problemática de aspectos climáticos con consecuencias tanto en el campo científico como social que hace necesaria su monitorización y análisis global a largo plazo. Los diferentes trabajos que componen esta tesis doctoral se basan, fundamentalmente, en las siguientes magnitudes: Espesor Óptico de Aerosoles (AOD) y Exponente de Ångström (AE) proporcionadas por la red AERONET (AErosol RObotic NETwork) que ofrecen información sobre toda la columna atmosférica, y las diversas fracciones de Materia Particulada (PM_x , $x=10$ o $2.5\text{ }\mu\text{m}$) obtenidas de la red EMEP (European Monitoring and Evaluation Programme) que dan información de lo que ocurre a nivel de superficie. Las magnitudes AOD y PM_{10} dan cuenta de la carga de aerosol mientras que AE y la fracción $PM_{2.5}/PM_{10}$ (PM ratio) indican el tamaño de las partículas. Además, aplicando un algoritmo de inversión a los datos de radiancia de cielo y AOD de la red AERONET se genera una serie de parámetros como la distribución de tamaños, el radio efectivo, el volumen de concentración, la esfericidad, el albedo de dispersión simple o el factor de asimetría, que representan las propiedades microfísicas y ópticas de los aerosoles. Todas estas magnitudes han sido analizadas en este trabajo de tesis doctoral a fin de obtener su completa caracterización en la zona de estudio.

Con objeto de ampliar el conocimiento sobre los aerosoles atmosféricos en la zona centro norte de la Península Ibérica (PI), se analizan, bajo un enfoque climatológico que abarca 12 años de medidas (2003-2014), las dos bases de datos mencionadas que nos ofrecen información complementaria en columna y superficie. Una de las principales características del área en la que se centra esta tesis doctoral es que presenta una estación de AERONET (Palencia, de la cual es responsable el Grupo de Óptica Atmosférica de la Universidad de Valladolid desde el año 2003) y otra de EMEP (Peñausende, Zamora) muy cercanas y que permiten la realización de un estudio de este tipo. Cabe destacar que pocas regiones en la península e incluso en Europa poseen series de datos simultáneas de estas características y duración. Ambas estaciones han sido caracterizadas como estaciones de fondo regional limpio alejadas de grandes núcleos urbanos o industriales por lo que además de ser representativas del área, permiten la detección de eventos de alta turbiedad atmosférica. Debido a la localización geográfica de la zona de estudio y a su cercanía con la mayor fuente de aerosol

de origen natural desértico del hemisferio Norte, el desierto del Sahara, el trabajo aquí presentado se ha centrado en la detección, estudio y caracterización de este tipo de aerosol.

La relación entre las concentraciones a nivel de superficie y los datos en columna ha mostrado ser de especial interés a la hora de realizar estudios de caracterización de aerosoles desde un punto de vista climatológico. Por tanto, en este trabajo hemos caracterizado en primer lugar la zona de estudio obteniendo sus principales características: ciclo anual de intensidad y parámetro de tamaño de las partículas, estadísticas básicas, promedios anuales y tendencias.

Una vez caracterizadas las principales magnitudes de aerosoles en el área de estudio, se ha desarrollado y aplicado una metodología para la detección de intrusiones de aerosol desértico a partir de una inspección visual de la información principal AOD-AE-PM₁₀ y el análisis de cierta información complementaria. La metodología cuenta con la ventaja de que permite la clasificación de los días con intrusión de aerosol desértico en dos grupos, el “D” (Desert) que corresponde a aquellos con un fuerte carácter desértico, y el “MD” (Mixed Desert), en los que el aerosol desértico presenta mezcla, en mayor o menor medida, con otros tipos de aerosoles. Gracias a la evaluación de este inventario, se han podido establecer los ciclos anuales y la evolución temporal de la ocurrencia de días y episodios de intrusión desértica así como la contribución de éstos a los valores totales de la carga de aerosol en columna (AOD) y superficie (PM₁₀). Los escenarios sinópticos que propician la llegada de dichas intrusiones también han sido analizados.

En último lugar, y para caracterizar completamente las intrusiones desérticas en el área de estudio, se han analizado en detalle sus propiedades microfísicas y ópticas así como las relaciones entre ellas, mostrando que establecer distintos tipos de intervalos en función del peso de la fracción fina mejora la interpretación de las relaciones entre todas estas propiedades.

ABSTRACT

Atmospheric aerosols cause direct and indirect effects in the earth-atmosphere radiative budget generating climatic problems with consequences in scientific and social fields that make necessary to monitor and analyze them in a long-term basis. The different studies that compose this doctoral thesis are based, mainly, on the following quantities: Aerosol Optical Depth (AOD) and Ångström Exponent (AE) provided by the AERONET network (AErosol RObotic NETwork) which give information on the aerosol content of the entire atmospheric column, and the different fractions of the Particulate Matter (PM_x , $x=10$ or $2.5\text{ }\mu\text{m}$) obtained from EMEP (European Monitoring and Evaluation Programme) network, which give information on the aerosol concentration at surface level. The AOD and PM_{10} quantities are related to the aerosol load meanwhile AE and $PM_{2.5}/PM_{10}$ (PM ratio) indicate the size predominance of the aerosol particles. Moreover, an inversion algorithm can be applied to the AOD and sky radiance measurements obtained from AERONET in order to generate parameters that give information about aerosol microphysical and optical properties, such as size distribution, effective radius, volume concentration, fraction of spherical particles, single scattering albedo or asymmetry factor. All these quantities have been analyzed in this research to obtain their complete characterization in the study area.

With the aim to broadening the knowledge about atmospheric aerosols in the north-central Iberian Peninsula (IP), the above mentioned datasets, which provide complementary information at surface and columnar level, have been analyzed under a climatological approach, covering 12 years of measurements (2003-2014). One of the main characteristics of the area under study in this research is that it counts with an AERONET site (Palencia, run by the Atmospheric Optics Group of the Universidad de Valladolid since year 2003) and an EMEP site (Peñausende, Zamora), that are close together and allow a long-term study of these properties. It also should be mentioned that few Spanish or European regions own simultaneous long-term databases of these characteristics. Both sites have been defined as clean continental background sites, far away from industrial or urban nuclei, so they are representative of the study area as well as they allow the detection of atmospheric turbidity episodes. Due to the geographical location of the area and its closeness to the larger desert dust source of the northern hemisphere, the Sahara desert, this work has been focused on the detection, study and characterization of Saharan dust aerosol.

The relationship between surface level concentration and columnar quantities under a climatological perspective is of major interest for atmospheric studies. In this work we have characterized the study area obtaining the main features: annual cycle for intensity and particle size predominance, basic statistics, annual means and trends.

Once the main aerosol quantities were established for the area, a methodology for the detection of desert dust intrusions has been developed and applied. This methodology is based on a visual inspection of the core information AOD-AE-PM₁₀ and the analysis of certain ancillary information. An advantage of this methodology is that it classifies those days with desert dust intrusion in two groups: “D” (Desert) type which is composed of those days with a strong desert dust character and “MD” (Mixed Desert) type containing those days presenting dust, that is mixed, in a greater or lesser extent, with other aerosol types. After the evaluation of this desert dust inventory, the annual cycle and temporal evolution of the number of desert dust event days and episodes have been established, as well as their contribution to the total aerosol load both in the entire column (AOD) and at surface level (PM₁₀). The synoptic scenarios that favor these intrusions have also been analyzed.

Finally, and with the aim to deeply characterizing desert dust intrusions, microphysical and optical properties have been analyzed as well as the relationships among them. The investigation shows that when different intervals are established as a function of the fine mode fraction of the size distribution, these surface-column relationships show higher correlation.

1. Introducción, objetivos y estructura de la tesis

1.1. Introducción

1.1.1. Estado del arte

Los aerosoles atmosféricos, definidos como el conjunto de partículas sólidas o líquidas en suspensión en un medio gaseoso el tiempo suficiente como para ser medidas (Willeke and Baron, 1993), son objeto de estudio en las ciencias atmosféricas desde hace varias décadas (Boucher et al., 2013). Pueden ser emitidos directamente a la atmósfera (mecanismo de formación primaria) o surgir a partir de reacciones químicas (mecanismo de formación secundaria) que involucran tanto a los aerosoles como a los gases precursores de éstos como el H_2SO_4 , NH_3 , compuestos orgánicos, etc. Para determinar sus efectos, se estudian varias características como su forma, tamaño, composición química, etc.

Según su origen, diferenciaremos entre aerosoles naturales o antropogénicos. Algunos ejemplos de aerosoles naturales son el polvo mineral del desierto, las cenizas volcánicas, el polen, etc., y entre los de origen antropogénico nos encontramos con el aerosol urbano o el continental contaminado, etc. Independientemente de su origen, los aerosoles producen efectos radiativos directos e indirectos en el balance del sistema Tierra-atmósfera. Los efectos directos se deben principalmente a la interacción con la radiación solar y terrestre a través de procesos de absorción y dispersión, y los efectos indirectos a que actúan como núcleos de condensación en el proceso de formación de nubes e influyen en sus propiedades microfísicas y ópticas (como el albedo) y por tanto en la precipitación (Haywood and Boucher, 2000; Lohmann et al., 2010; Boucher et al., 2013). El efecto final producido podrá ser de calentamiento o enfriamiento y dependerá simultáneamente de varios factores como la proporción entre el número y tamaño de las partículas y la altura a la que se encuentren en la atmósfera, entre otros. Por tanto, para comprender el cambio climático, es necesario conocer y comprender las características de los aerosoles, su distribución a escala global y regional y las interacciones que tienen lugar ya sea con otros aerosoles, nubes y/o radiación. Además, son un punto de especial relevancia en diversas áreas del conocimiento (Schwartz et al., 1996; Künzli et al., 2000; Dockery, 2001) debido a su composición química, a su influencia en ciclos naturales: biogeoquímicos, del carbono o ciclos de energía (Martínez-García et al., 2011; Knippertz and Stuut, 2014), a los efectos que producen en la salud y en la visibilidad

atmosférica dificultando por ejemplo el transporte aéreo, las operaciones militares (De Deckker et al., 2008) o a los problemas que causan en la agricultura (McTainsh et al., 1990).

Entre los aerosoles de origen natural, el aerosol desértico juega un papel importante por su fuerte impacto en el sistema terrestre debido a su distribución global y temporal. Estas características presentan una gran variabilidad y son por tanto uno de los principales problemas a la hora de estudiarlos en detalle. Las partículas crustales de polvo que se originan en las zonas áridas y semi-áridas del planeta, son inyectadas a la atmósfera gracias a la acción de los vientos originados a nivel de superficie y son responsables del 13% de las emisiones de aerosol natural a escala global, aportando megatoneladas de materia particulada a la atmósfera (Goudie and Middleton, 2006; Knippertz and Stuut, 2014; Viana et al., 2014). En el hemisferio norte, los desiertos de Sahara y Sahel son las principales fuentes de polvo desértico, emitiendo más de 200 Tg por año a través de diferentes procesos de resuspensión que dan como resultado capas de aerosol a grandes altitudes que pueden ser transportadas largas distancias a través del Océano Atlántico, llegando tanto a Europa como al continente Americano. A través de procesos como sedimentación gravitacional, turbulencias o precipitación, los aerosoles desérticos son eliminados de la atmósfera y el fenómeno de deposición en plantas, nieve o hielo, glaciares, suelo u océanos produce cambios en la radiación solar reflejada, así como el transporte de nutrientes a ecosistemas lejanos (Prospero, 1999; Prospero et al., 2002, Kaufman et al., 2005; Guirado et al., 2014).

El transporte de aerosoles en general y de aerosol desértico en particular a otras zonas del planeta puede provocar consecuencias de diversa índole, cuyo impacto puede ser evaluado correctamente si se conocen las propiedades físicas y químicas del aerosol en cuestión. Se podrá distinguir entre impactos causados en las zonas fuente, en la atmósfera y en las zonas de deposición del aerosol. En general, el impacto dependerá de la composición química y mineralógica, de la fracción de mezcla, de la concentración mísica, de la distribución de tamaño, de la morfología y forma de las partículas... (Formenti et al., 2011). Por ejemplo, para evaluar el efecto radiativo de los aerosoles desérticos mediante modelos, el desconocimiento de determinados parámetros físicos o químicos puede conllevar la obtención de resultados poco precisos e incluso erróneos, lo que pone de manifiesto la importancia de conocer en detalle las propiedades de dichos aerosoles (Knippertz and Stuut, 2014).

1.1.2. Redes de monitorización de aerosoles y estudios previos

Varias metodologías y diversos instrumentos han sido desarrollados en los últimos años con objeto de obtener información a escala tanto global como regional de las partículas atmosféricas, evaluar su variabilidad temporal o informar sobre las posibles fuentes de aerosol e identificar los procesos de transporte que los escenarios meteorológicos sinópticos propician. La teledetección activa o pasiva, con sensores a bordo de satélites o medidas de diferentes instrumentos en la superficie (como radiómetros, LIDAR, etc...), se utiliza junto con la ayuda de modelos para extraer la máxima información posible. A su vez, las llamadas mediciones “in-situ” de material particulado (bien a nivel de superficie o en plataformas aéreas), parte de las cuales se basan en extraer muestras que serán analizadas en el laboratorio, sirven para obtener, generalmente, su composición química. Las técnicas de teledetección estudian la extinción (a través de los procesos de absorción y dispersión) que provoca la interacción de los aerosoles con la radiación solar-terrestre y por tanto será función de la longitud de onda de ésta y de las características o propiedades del aerosol presente en la atmósfera.

En este contexto, las redes de monitorización de aerosoles a nivel de superficie cobran especial relevancia: EMEP (European Monitoring and Evaluation Programme) es una red mundial compuesta actualmente por 852 estaciones de medida (<http://ebas.nilu.no/default.aspx>) que fue creada tras la firma en 1979 de la convención de contaminación atmosférica transfronteriza, como medida central para la protección del medio ambiente. Esta red proporciona a la comunidad científica datos de calidad contrastada (EMEP, 2014) sobre contaminantes atmosféricos, deposición y niveles de concentración másica de materia particulada (PM_x , en μgm^{-3} , con el subíndice “x” se indica que las mediciones tendrán en cuenta partículas con un diámetro aerodinámico menor al indicado) con los que es posible analizar y asesorar sobre el transporte transfronterizo de los contaminantes y establecer un marco para desarrollar acciones coordinadas entre diversos países para reducir la contaminación atmosférica.

La concentración másica de la materia particulada es una magnitud física que da cuenta de la carga de aerosol a nivel de superficie, siendo por tanto un parámetro de referencia a la hora de evaluar la calidad del aire. El PM_{10} hará referencia a las partículas inhalables y es una magnitud que generalmente se utiliza para medir la carga de aerosol presente en la atmósfera (medida de la inmisión), mientras que $PM_{2.5}$ hará referencia a las conocidas como partículas

finas que están asociadas con efectos peligrosos para la salud humana ya que su eficiencia para penetrar en el sistema respiratorio es mayor que la de las partículas gruesas (EMEP, 1996; Pope, 2000). El cociente entre estas dos magnitudes, $PM_{2.5}/PM_{10}$ o PM ratio, será por tanto un indicador del tamaño predominante de las partículas y la diferencia entre $PM_{10}-PM_{2.5}$ es una magnitud que puede asociarse a la fracción de partículas gruesas (diámetros entre 2.5 y 10 μm). Tanto instituciones nacionales como internacionales han establecido valores umbrales máximos para las diferentes fracciones de PM con vistas a proteger la salud humana y reducir el número de días que presentan contaminación antropogénica (WHO, 2006; EC, 2008). Para el PM_{10} , el valor a partir del cual se considerará que existe una excedencia en los niveles de contaminación se ha fijado en $50 \mu g m^{-3}$, el cual no deberá ser sobrepasado 35 veces al año.

Utilizando fotómetros solares de teledetección pasiva como principal instrumento, AERONET (AErosol RObotic NETwork) nace en la década de 1990, establecida por NASA (National Aeronautics and Space Administration) y la Universidad de Lille, como una red mundial de medida de aerosoles a nivel de superficie que ha ido extendiéndose y cuenta actualmente con más de 400 estaciones (Holben et al., 1998) desde las que se mide la irradiancia solar directa y la radiación difusa del cielo. El objetivo principal es monitorizar las propiedades de los aerosoles para un periodo largo de tiempo así como proveer de una base de datos global y estandarizada que permita establecer y comparar climatologías, validar datos de satélites o modelos de aerosoles, entre otros. Las principales ventajas que ofrece AERONET son: la estandarización de los instrumentos de medida, de sus calibraciones, de las secuencias de medidas realizadas de forma rutinaria y automática, el tratamiento de datos y el libre acceso a las bases de datos resultante de calidad asegurada. Actualmente, los únicos laboratorios de calibración de los fotómetros que componen la red se encuentran en Goddard (EEUU), la Universidad de Lille (Francia), y la Universidad de Valladolid (España), siendo el Observatorio de Izaña (CIAI-AEMET) el lugar de calibración de los Másteres de los que hacen uso Valladolid y Lille.

El parámetro principal que proporciona AERONET, utilizado para medir la carga en columna del aerosol, es el AOD (Aerosol Optical Depth, en inglés) o espesor óptico de los aerosoles. El AOD se determina a partir de la ley de Beer-Bouguer-Lambert:

$$I(\lambda) = I_0(\lambda) \cdot e^{-AOD(\lambda) \cdot m} \quad (1)$$

con las medidas de irradiancia a nivel del suelo (I) e irradiancia extraterrestre (I_o), y siendo m la llamada masa óptica. El AOD se obtiene a diferentes longitudes de onda y describe la extinción que sufre la radiación solar al atravesar la columna atmosférica debido a la presencia de aerosoles. Esta metodología se basa en la interacción radiación-partícula. De la dependencia espectral del AOD se puede derivar información sobre el tamaño de las partículas presentes en la atmósfera. Así, el exponente de Ångström (AE) puede ser utilizado para la distinción de partículas según su tamaño. Su rango varía entre 0 (partículas más gruesas) y 4 (partículas más finas). Una herramienta para clasificar y diferenciar los diferentes tipos de aerosoles es el diagrama de dispersión entre la cantidad de aerosoles presentes en la atmósfera (AOD) y el tamaño de éstos (AE). Según la región del diagrama en la que se sitúen los valores de AOD-AE será posible discriminar entre aerosoles continentales, (limpio, promedio, contaminado), marítimo (limpio, contaminado, tropical), desértico, ártico, antártico urbano... (D'Almeida et al., 1991; Hess et al., 1998; Eck et al., 1999; Vergaz et al., 2005; Toledano et al., 2007a). El modelo OPAC (Optical Properties of Aerosols and Clouds) presentado por Hess et al. (1998) proporciona valores característicos de parámetros radiativos de diferentes tipos de aerosoles genéricos. En la Figura 1 se muestran algunos ejemplos de la posición sobre el diagrama AE-AOD que ocupan diferentes tipos de aerosoles obtenidos a partir de los valores proporcionados por el modelo OPAC.

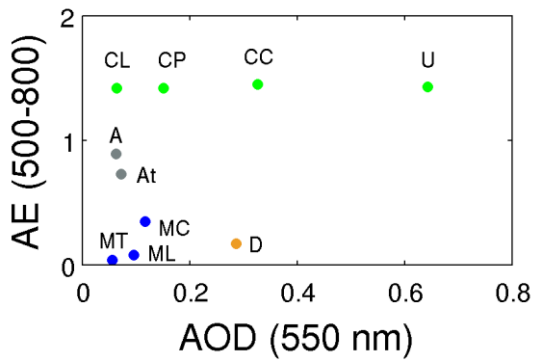


Figura 1: Diagrama AE (500-800 nm) – AOD (550 nm) con los tipos de aerosoles dados por el modelo OPAC: continental limpio (CL), continental promedio (CP), continental contaminado (CC), urbano (U), ártico (A), antártico (At), marítimo tropical (MT), marítimo continental (MC), marítimo limpio (ML) y desértico (D).

Los datos que proporcionan estas redes globales de monitorización no solo se han utilizado para la clasificación de las propiedades según el tipo de aerosol, sino que también se han obtenido resultados en relación a las climatologías, comportamientos estacionales o tendencias sobre los últimos 20-30 años. Una de las particularidades del estudio de los aerosoles es que no se dispone de series de datos o registros más antiguos. De hecho, estudios

recientes intentan estimar valores de AOD a partir de parámetros históricos como las horas de sol (por ejemplo, Sanchez-Romero et al., 2016). Los datos de PM_x proporcionados por EMEP han servido como base para estudiar la tendencia decreciente de los promedios anuales en diversos países Europeos en los últimos 40 años (EMEP, 2011,2014; Barmpadimos et al., 2012; Cusack et al., 2012; Tørseth et al., 2012; Boucher et al., 2013; Querol et al., 2014). A su vez, Mateos et al., (2014b, 2015) obtienen resultados similares estudiando los datos de AOD proporcionados por AERONET sobre diversas áreas de la Península Ibérica entre 2000 y 2013.

Debido a que el AOD es función de la concentración másica de los aerosoles, diversos estudios investigan las relaciones entre el AOD y el PM_x, la deposición másica, la concentración másica/volúmica de aerosoles en columna (Cachorro and Tanré, 1997; Pelletier et al., 2007; Kokhanovsky et al., 2009; Toledano et al., 2012; entre otros). En concreto, se puede estudiar la relación teórica entre el AOD (magnitud representativa de la extinción en toda la columna atmosférica) y la concentración volúmica en columna a través de la definición del factor de eficiencia másico/volúmico (Fraser et al., 1984; Kokhanovsky, et al., 2009), sin embargo, éste no es un problema sencillo de abordar por lo que algunos autores han optado por establecer relaciones empíricas (Prats et al., 2011; Toledano et al., 2012).

1.1.3. Zona de estudio: Península Ibérica y comunidad de Castilla y León

La Península Ibérica (PI) constituye un área de especial interés debido a que registra una amplia variabilidad de eventos de alta turbiedad atmosférica. Como resultado de la influencia del Océano Atlántico, el Mar Mediterráneo, el continente Europeo y el desierto del Sahara, en la PI se produce una importante variabilidad espacio-temporal de aerosoles y de mezclas de éstos. Diversos estudios ya han establecido el ciclo anual que siguen los aerosoles en diferentes áreas o sectores de la PI diferenciados según su topografía y orografía (Cachorro et al., 2000a, b; Alados-Arboledas et al., 2003; Vergaz et al., 2005; Toledano et al., 2007a; Estellés et al., 2007; Bennouna et al., 2013; Mateos et al., 2014b). Sin embargo, el todavía corto periodo disponible (muchas estaciones de la península por debajo de 10 años de datos) puede dar lugar a que el ciclo anual sufra determinados cambios a medida que se incorporen nuevos años. Debido a la cercanía de la PI al continente africano, los episodios de intrusión de material crustal son frecuentes, intensificando los valores de la carga de aerosol medido en toda la columna atmosférica (AOD) o a nivel de superficie (PM_x). Además, los diferentes escenarios sinópticos que propician la llegada de dichas intrusiones, dan como resultado

diferencias en el comportamiento estacional del aerosol desértico (Escudero et al., 2005; Toledano et al., 2007b; Basart et al., 2009; Valenzuela et al., 2012; Cachorro et al., 2016). Las intrusiones de origen desértico que llegan a la PI se suelen caracterizar por su corta duración, entre 2 y 3 días, siendo durante los meses de verano cuando se registran los episodios más largos y una mayor frecuencia de ocurrencia respecto a los otros meses. Durante los meses de verano, las recirculaciones de masas de aire y la escasa precipitación pueden aumentar el tiempo en el que una intrusión ocurre sobre la PI y dificultar la separación entre eventos sucesivos (Rodríguez et al., 2002; Escudero et al., 2005). También se detecta otro pico de frecuencia de intrusiones al final de invierno comienzo de primavera en los meses de febrero y marzo. En relación al balance radiativo, el aerosol desértico presenta una eficiencia de forzamiento radiativo de -70 Wm^{-2} en el sur-este de la PI (Valenzuela et al., 2014). Otros estudios dan cuenta de los efectos en la salud humana, mostrando que aumenta la tasa mortalidad debida a problemas cardiovasculares y respiratorios durante episodios desérticos en España (Pérez et al., 2012; Reyes et al., 2014).

En el presente trabajo, centraremos nuestro interés en los aerosoles atmosféricos medidos en la Península Ibérica y, en concreto, en su región centro-norte en gran parte ocupada por la Comunidad Autónoma de Castilla y León (CyL). Dicha comunidad forma parte de la Meseta Norte a una altitud aproximada de 800 m s.n.m. Varios sistemas montañosos de altitudes en torno a los 2000-2500 m rodean dicha meseta reduciendo la influencia tanto del Océano Atlántico como del Mar Mediterráneo y quedando la zona caracterizada por un clima continental. La comunidad de Castilla y León es una de las comunidades con menos densidad de población de España, contando con una extensión de 94193 km^2 y una población de alrededor de 2.5 millones de personas censadas en 2012. Las condiciones de baja turbiedad, siendo una de las regiones menos contaminadas de Europa, y las bases de datos existentes en la región posibilitan un estudio desde el punto de vista climatológico (ver Sección 2.1. Estaciones de medida, bases de datos y otras informaciones). Además, el impacto de las intrusiones de alta turbiedad atmosférica debida a polvo desértico es relevante en toda la base Mediterránea y en concreto en la zona de estudio. Durante las intrusiones de masas de aire africanas se alcanzan los valores más altos registrados en PM_{10} y de parte de los valores más altos registrados en AOD. Estudios anteriores realizados en Castilla y León (Rodrigo et al., 2012) muestran la necesidad de ampliar la detección de intrusiones desérticas sobre esta región.

1.2. Objetivos

El objetivo principal de esta tesis doctoral es el estudio y caracterización de las propiedades de los aerosoles durante intrusiones desérticas que ocurren en la región de Castilla y León mediante el análisis conjunto de medidas en superficie y en columna.

Este objetivo general da lugar a los siguientes objetivos específicos que se van a desarrollar en los tres artículos de los que consta la tesis:

1. Estudio de las relaciones de las medidas de aerosol en superficie (PM_{10} y PM ratio) y columna (AOD y AE), enfatizando su evolución en las intrusiones desérticas.
2. Creación de un inventario de intrusiones desérticas sobre la zona de estudio basado en el desarrollo y aplicación de una metodología de detección de dichos eventos.
3. Evaluación de la contribución del aerosol desértico a la carga total de aerosol, tanto para los valores de AOD como de PM_x .
4. Análisis de los parámetros microfísicos y radiativos de los aerosoles en los días que conforman el inventario de intrusiones desérticas, estableciendo sus relaciones.

La Tabla 1 recoge las principales tareas desarrolladas en la tesis doctoral indicando el artículo en el que han sido desarrolladas.

Tabla 1: Tareas desarrolladas y artículo correspondiente:

| TAREAS | ARTÍCULO |
|-------------------------------------------------------------------------------------------------------------------------------------------------------------------------------------------------------------------------------------------|----------|
| Caracterizar las propiedades de los aerosoles a través de sus ciclos anuales, variabilidad interanual y tendencias | 1 |
| Estudiar el comportamiento de cada par de magnitudes: AOD-AE, PM ₁₀ -PM ratio | 1 |
| Interpretar las relaciones entre la carga del aerosol y el tamaño de las partículas en superficie y columna (AOD-PM ₁₀ y AE-PM ratio) | 1 |
| Detectar e identificar los eventos de alta polución atmosférica causados por aerosol de origen desértico | 2 |
| Establecer un inventario detallado y fiable de intrusiones desérticas, basado, principalmente, en el análisis simultáneo de datos de superficie (PM ₁₀) y columna (AOD-AE) | 2 |
| Estudiar las principales características de las intrusiones desérticas: ciclo anual, variabilidad interanual y tendencias | 2 |
| Calcular la contribución del aerosol desértico a la carga total de aerosol en superficie y columna | 2 |
| Estudiar en detalle las propiedades en columna cuando tenemos asegurada la presencia de aerosoles desérticos: AOD, AE, distribución de tamaños, concentración en volumen, esfericidad, albedo de dispersión simple y factor de asimetría. | 3 |
| Comparar algunas de las propiedades en columna con datos de concentración mísica en superficie | 3 |
| Definir varios intervalos de interés en función de la fracción fina del aerosol presente distinguiendo entre intrusiones más puras y condiciones de mezcla con predominancia o no de material crustal. | 3 |
| Realizar un estudio detallado de las principales propiedades teniendo en cuenta los intervalos establecidos | 3 |
| Obtener factores como la eficiencia de extinción o el factor de escala en función de los intervalos establecidos | 3 |

1.3. Estructura de la tesis

El trabajo de investigación que se presenta en esta memoria para optar al grado de Doctora en Física por la Universidad de Valladolid se ha realizado siguiendo la modalidad de compendio de publicaciones. Los tres artículos que componen la tesis doctoral han sido aceptados y publicados en revistas científicas pertenecientes al primer cuartil dentro de su categoría. Así, los objetivos mencionados en la sección anterior se distribuyen en la tesis en tres capítulos, cada uno de los cuales se corresponde con uno de los artículos. Comenzaremos citando las referencias bibliográficas correspondientes a los artículos que componen la tesis doctoral:

- Artículo 1 (A1): Bennouna, Y., Cachorro, V.E., Mateos, D., Burgos, M.A., Toledano, C., Torres, B., de Frutos, A.M., 2016. Long-term comparative study of columnar and surface mass concentration aerosol properties in a background environment. *Atmos. Environ.*, 140, 261-272, <http://dx.doi.org/10.1016/j.atmosenv.2016.05.061>. Factor de Impacto: 3.459. Categoría: Environmental sciences; Meteorology & atmospheric sciences (Journal Citation Report, JCR, 2015). Posición: 42/225, primer cuartil.

- Artículo 2 (A2): Cachorro, V.E., Burgos, M.A., Mateos, D., Toledano, C., Bennouna, Y., Torres, B., de Frutos, A.M., Herguedas, A., 2016. Inventory of African desert dust events in the North-central Iberian Peninsula in 2003-2014 based on Sun photometer and PM_x data. *Atmos. Chem. Phys.*, 16, 8227-8248. doi: 10.5194/acp-16-8227-2016. Factor de impacto: 5.114. Categoría: Meteorology & atmospheric sciences (JCR, 2015). Posición: 6/84, primer cuartil.
- Artículo 3 (A3): Burgos, M.A., Mateos, D., Cachorro, V.E., Toledano, C., de Frutos, A.M., 2016. Aerosol properties of mineral dust and its mixtures in a regional background of north-central Iberian Peninsula. *Sci. Total. Environ.*, 572, 1005-1019, <http://dx.doi.org/10.1016/j.scitotenv.2016.08.001>. Factor de impacto: 3.976. Categoría: Environmental Sciences (JCR, 2015). Posición: 32/225, primer cuartil.

La memoria pretende exponer de forma clara y precisa la coherencia y conexión temática de la investigación subyacente a las publicaciones. Así, se ha considerado que la estructura que permite exponer de la mejor manera posible la relación temática de las publicaciones y la relevancia de su aportación conjunta es la que se explica a continuación.

Esta Sección 1 sirve de marco que contextualiza el tema de estudio así como el estado del arte en la región analizada y presenta los objetivos perseguidos durante la realización de la tesis doctoral. La Sección 2 se divide en tres subsecciones en las que se introduce, en primer lugar, las estaciones de medida y las bases de datos utilizadas, que es parte común en los tres artículos. A continuación, la Sección 2.2 da cuenta de la metodología e idea general subyacente en el grueso del trabajo de tesis doctoral, mientras que la Sección 2.3 refleja en detalle la metodología explicada y utilizada en el Artículo 2 para la detección de episodios de alta turbiedad atmosférica de origen desértico. Dicha metodología merece especial mención en esta memoria debido a su relevancia dentro del trabajo, sirviendo de base para la realización de los Artículos 2 y 3.

En la Sección 3 se presentan los resultados correspondientes a cada uno de los artículos. Dicha sección se divide en tres subsecciones para facilitar su lectura. Se hará en primer lugar un breve resumen gráfico del artículo correspondiente así como un resumen escrito en el que se detallan los principales resultados obtenidos y a continuación se facilitará el artículo completo en su versión publicada en inglés. La Sección 3.1 que corresponde al artículo 1,

presenta la valoración inicial de la comparación entre las magnitudes básicas en superficie y columna en la zona de estudio, caracterizándolas y estudiando las relaciones entre ellas. La Sección 3.2 que recoge el artículo 2, presenta el inventario de intrusiones desérticas de 12 años en la región de Castilla y León y evalúa el impacto que tienen los episodios desérticos sobre los valores totales de carga de aerosol. En último lugar, la Sección 3.3 muestra los resultados obtenidos en el artículo 3, en el que se han caracterizado las intrusiones desérticas y en el que se estudiarán las principales propiedades microfísicas y ópticas de dicho tipo de aerosol y sus mezclas.

2. Medidas y metodología

2.1. *Estaciones de medida, bases de datos y otras informaciones*

Las dos estaciones principales de medida utilizadas en este estudio, pertenecientes a la Comunidad Autónoma de Castilla y León, se sitúan en Peñausende (41.24 N, 5.910 O, 750m s.n.m.) y Palencia (41.99 N, 4.52 O, 750m s.n.m., ver Figura 2). Palencia es una pequeña ciudad (alrededor de 100.000 habitantes) situada a unos 50 km al norte de la ciudad más grande de CyL, Valladolid, y Peñausende es un pequeño pueblo perteneciente a la provincia de Zamora, situado a unos 100 km al este Valladolid. Ambas estaciones están por tanto aisladas de grandes núcleos urbanos e industriales, presentando condiciones atmosféricas excepcionalmente limpias y pueden ser consideradas como estaciones de fondo regional para el estudio que aquí se presenta. Este punto será especialmente relevante a la hora de detectar, clasificar y estudiar episodios de origen desértico ya que podrán ser observados con claridad al influir de manera significativa sobre las condiciones de fondo regional características de dichas estaciones.

En la estación de Peñausende se llevan a cabo medidas de PM_x de forma rutinaria desde el año 2001. Los datos aquí recogidos son los oficiales con los que trabaja la comisión Europea y su calidad está garantizada (Pey et al., 2013). Para este estudio, se han utilizado los datos comprendidos entre el periodo 2003-2014, debido a que durante los dos primeros años no existen medidas simultáneas de la base de datos de AERONET. Las medidas tanto de PM_{10} como de $PM_{2.5}$ se llevan a cabo en base diaria y en promedio, un 90% de los días de cada año

presentarán medidas útiles para nuestro estudio. Además, para obtener los valores del ratio PM_{2.5}/PM₁₀ es necesario que haya medida simultánea de ambas variables. La base de datos de PM_x de Peñausende será esencial para el estudio tanto de las relaciones superficie-columna así como para la detección y caracterización de las intrusiones desérticas. Cabe mencionar, que en la detección de episodios desérticos se usarán como apoyo los datos de dos estaciones cercanas, Campisábalos (41.28° N, 33.14° W, 1360m s.n.m) y Barcarrota (38.48° N, 6.92° W, 492m s.n.m.) con la finalidad de conocer por dónde han penetrado tales intrusiones sobre la IP procedentes del continente africano. La Figura 2 muestra la localización geográfica de las dos estaciones de medida de la red AERONET y las tres de la red EMEP que se han utilizado para el estudio.

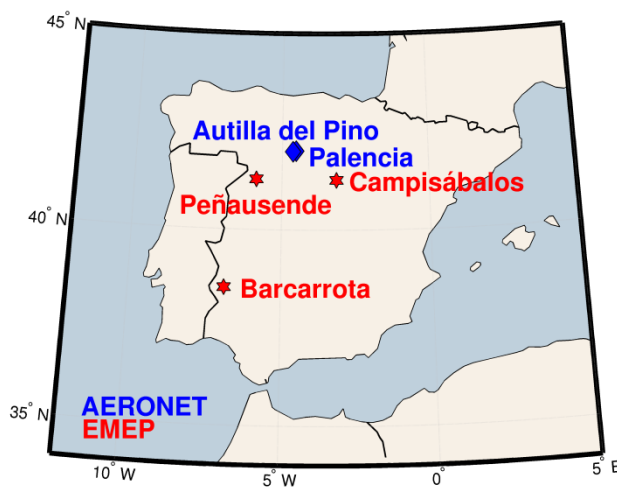


Figura 2: Localización geográfica de las estaciones de medida utilizadas pertenecientes a las redes AERONET y EMEP.

Con respecto a las medidas de aerosol en columna, el Grupo de Óptica Atmosférica de la Universidad de Valladolid posee un fotómetro solar multibanda CE-318 de CIMEL Electronique, que está situado a las afueras de Palencia, en la Escuela Técnica Superior de Ingenierías Agrarias de la Universidad de Valladolid. La base de datos de radiación con la que se obtendrán las variables AOD y AE comprende desde 2003 a 2014, con un hueco en los años 2009 y 2010 que será completado con los datos de la estación de Autilla del Pino, situada a tan sólo 7 km de Palencia y con las mismas características que ésta (Bennouna et al., 2013). En este caso, en torno al 67% de las medidas diarias son válidas cada año para el estudio. Esta base de datos así constituida es una de las más largas medidas en la Península

Ibérica (Mateos et al., 2014a). Según los protocolos seguidos por AERONET, los valores brutos de AOD que se obtienen a través de la radiación solar directa son los que conforman el nivel 1.0 y entre éstos, algunos pueden estar contaminados por la presencia de nubes. Tras la utilización de un algoritmo (“cloud screening”) para filtrar los datos contaminados obtendremos el nivel 1.5 y finalmente, se obtendrá el nivel 2.0 tras aplicar los valores de la pre- y post- calibración del instrumento y una inspección manual a la base de datos (Smirnov et al., 2000). Los datos de nivel 2.0 son de calidad asegurada y serán los utilizados para el análisis, caracterización y todos los resultados obtenidos en este estudio. Únicamente, para la detección de eventos desérticos puede ser de ayuda analizar y ver la evolución de los datos de niveles inferiores (nivel 1.5 e incluso nivel 1.0). La base de datos que utilizaremos se compone de datos de AOD medidos a una longitud de onda de 440nm y de datos de AE obtenidos a partir de las medidas realizadas entre 440-870nm.

Se expone a continuación una diferencia importante en relación al procedimiento de medida de AOD y PM_x que es necesario tener en cuenta al leer este trabajo. Las medidas de fotómetro son instantáneas, cada 15 minutos y en condiciones de cielo despejado a diferencia de las de PM_x , que proporcionan información integrada sobre 24 horas y sin restricción de cielo despejado. Además, una aclaración pertinente tras introducir la localización de las estaciones de medida es que la distancia entre Palencia y Peñausende (~ 100 km) no es un obstáculo a la hora de comparar la información recabada en superficie y columna puesto que entre ellas no hay ninguna fuente relevante de aerosoles ni accidentes geográficos a tener en cuenta. De este modo, y puesto que ambas estaciones son representativas de las condiciones de fondo de la zona centro-norte de la Península Ibérica, cuando se da un evento de alta turbiedad atmosférica es simultáneamente registrado en ambas bases de datos. Sin embargo, otros aspectos como la diferencia entre los procedimientos de medida de AOD y PM_x parece tener un papel más importante a la hora de justificar las diferencias entre ambas.

En la Tabla 2 se muestra una descripción detallada del número de días con medida disponible de AOD y de PM_{10} para cada una de las bases de datos utilizadas y para el periodo 2003-2014. En términos generales, la base de datos de PM_{10} presenta una cobertura mayor (90.1%) que la de AOD (67.2%), obteniendo un 63.2% de días datos simultáneos en ambas bases de datos. El muestreo anual de AOD más bajo es el del año 2003 con un 42.8% de datos, debido a que no hubo medidas los tres primeros meses de ese año, seguido del año 2006 con 190 días de medidas disponibles (52.1%), mientras que es el año 2012 presenta un menor muestreo para el PM_{10} con 315 datos (86.1%). Los años con mayor muestreo en ambas

bases de datos son 2005 (80.8%) y 2011 (93.2%) para AOD y PM₁₀ respectivamente. El número de días con medidas disponibles por mes alcanza su valor máximo para ambas bases de datos en julio con un 89.5% y 95.7% para AOD y PM₁₀ respectivamente y su mínimo en enero con un 36.0% y un 75.5%.

Tabla 2: Número de días (y porcentaje entre paréntesis) anual y mensual (periodo 2003-2014) de las dos bases de datos, PM_x (EMEP) y AOD (AERONET), utilizadas en este estudio.

| | 2003 | 2004 | 2005 | 2006 | 2007 | 2008 | 2009 | 2010 | 2011 | 2012 | 2013 | 2014 | total |
|------------------|--------|--------|--------|--------|--------|--------|--------|--------|--------|--------|--------|--------|--------|
| AOD | 156 | 265 | 295 | 190 | 271 | 280 | 256 | 244 | 269 | 252 | 220 | 249 | 2947 |
| (%) | (42.8) | (72.4) | (80.8) | (52.1) | (74.2) | (76.5) | (70.1) | (66.8) | (73.7) | (68.9) | (63.3) | (68.2) | (67.2) |
| PM ₁₀ | 330 | 338 | 330 | 339 | 336 | 317 | 329 | 331 | 340 | 315 | 328 | 316 | 3949 |
| (%) | (90.4) | (92.4) | (90.4) | (92.9) | (92.1) | (86.6) | (90.1) | (90.7) | (93.2) | (86.1) | (89.9) | (86.6) | (90.1) |
| | Ene | Feb | Mar | Abr | May | Jun | Jul | Ago | Sep | Oct | Nov | Dic | total |
| AOD | 134 | 215 | 230 | 223 | 296 | 258 | 333 | 320 | 312 | 255 | 199 | 172 | 2947 |
| (%) | (36.0) | (63.4) | (61.8) | (61.9) | (79.6) | (71.7) | (89.5) | (86.0) | (86.7) | (68.6) | (55.3) | (46.2) | (67.2) |
| PM ₁₀ | 281 | 297 | 344 | 332 | 352 | 336 | 356 | 354 | 331 | 342 | 321 | 303 | 3949 |
| (%) | (75.5) | (87.6) | (92.5) | (92.2) | (94.6) | (93.3) | (95.7) | (95.2) | (91.9) | (91.9) | (89.2) | (81.5) | (90.1) |

Cabe mencionar que a la hora de llevar a cabo la detección de los episodios desérticos, será de relevancia la consideración de otra información auxiliar que citamos a continuación y explicaremos con más detalle en la Sección 2.3, dedicada a explicar la metodología seguida para detectar las intrusiones desérticas. Esta información auxiliar será: a) información de nubosidad obtenida a partir de los productos del sensor satelital MODIS (Moderate Resolution Imaging Radiometer); b) mapas de AOD proporcionados por GIOVANNI (Geospatial Interactive Online Visualization ANd aNalysis Infrastructure) y MODIS; c) predicciones obtenidas a partir de modelos como NAAPS (Navy Aerosol Analysis and Prediction System); d) mapas meteorológicos de presión a nivel de superficie; e) mapas meteorológicos de altura geopotencial a 700hPa proporcionados por NOAA (National Oceanic and Atmospheric Administration) con los que se han establecido los escenarios sinópticos que propician la llegada de las intrusiones desérticas a la IP y f) masas de aire que llegan a Palencia a las 12:00 UTC calculadas con ayuda del modelo HYSPLIT (Hybrid Single-Particle Lagrangian Integrated Trajectory, Stein et al., 2015) a tres alturas distintas (500, 1500 y 3000m s.n.m) y 120 horas atrás en el tiempo, siendo los datos de entrada al modelo los proporcionados por la base de datos GDAS1 (Global Data Assimilation System) (Draxler et al., 2014). La Sección 2.3 muestra un caso estudio donde se ve directamente la

aplicación y uso de toda esta información complementaria a la hora de detectar eventos desérticos de alta turbiedad.

2.2. Metodología

La metodología que se ha seguido en el trabajo de tesis doctoral comienza analizando las magnitudes representativas de carga y tamaño de aerosol en superficie (PM_{10} y PM ratio) y columna (AOD y AE) para todos los días del periodo 2003-2014. Estudiar todos los días que componen el período es la base para conocer las estadísticas básicas de estas magnitudes principales como los valores medios, medianas, variabilidad... A su vez, el enfoque climatológico subyacente al estudio ha permitido establecer los ciclos anuales y las tendencias de dichas variables. A continuación, se han estudiado las relaciones entre estas magnitudes con la ayuda de diagramas de dispersión: a) AE-AOD para diferentes intervalos de PM_{10} y PM ratio, b) PM ratio- PM_{10} para diferentes intervalos de AOD, c) PM_{10} -AOD para diferentes intervalos tanto de AE como de PM ratio y d) PM ratio-AE para diferentes intervalos de AOD y PM_{10} . Además, debido a la diferente resolución temporal con la que se obtienen los valores en superficie o columna, se ha asignado a cada valor instantáneo de AOD-AE el valor diario de PM_{10} -PM ratio correspondiente. Se ha concluido esta parte del trabajo estudiando la correlación entre las variables PM_{10} y AOD a través de diferentes procedimientos: con valores instantáneos, medias diarias, mensuales y mediante un estudio por intervalos. En la Sección 3.1 se presentan los resultados correspondientes a este apartado y el Artículo 1 en el que se han publicado.

Debido a la importancia que juegan las intrusiones de origen desértico en la Península Ibérica (ver Sección 1.1.3) se ha decidido crear un inventario de dichos episodios utilizando como base la metodología propuesta en Toledano et al. (2007b) y Rodrigo (2012). La Sección 2.3 explica en detalle esta metodología de detección de episodios desérticos: los umbrales necesarios que se han personalizado para nuestro estudio y el uso de información complementaria que se ha consultado. También se da un ejemplo de un caso estudio para una mejor compresión. Se ha considerado relevante incluir esta información como una sección en esta memoria debido a la importancia que tiene en el conjunto del trabajo.

Una vez creado el inventario de intrusiones desérticas se ha procedido a caracterizar el ciclo anual, la variabilidad interanual y las tendencias así como a calcular la contribución del aerosol desértico a la carga total tanto en superficie como en columna. Para cuantificar las

tendencias se ha utilizado el estimador Theil-Sen y el test Mann-Kendall. Las contribuciones de aerosol desértico a la carga total de aerosol en columna (AOD) y superficie (PM_{10}) se calcularán de la siguiente manera: al valor medio (mensual o anual) de la variable en cuestión considerando todos los días (AOD_T) se le restará el valor medio considerando todos los días excepto aquellos que han sido clasificados como desérticos ($AOD_{NoDesértico}$):

$$Contribución = AOD_T - AOD_{NoDesértico} \quad (2)$$

Y análogamente se ha procedido para calcular la contribución desértica a los niveles totales de PM_{10} . Esta metodología asume que toda la carga de aerosol del día considerado es debida al aerosol desértico y se puede considerar como una hipótesis válida visto los bajos niveles de fondo que presenta la zona de estudio. La información relativa al inventario y a éstos primeros resultados en relación a los días desérticos se recoge en la Sección 3.2 y en el Artículo 2.

Para ampliar el conocimiento de los aerosoles desérticos se ha procedido a realizar una caracterización completa de éstos, estudiando sus propiedades microfísicas y radiativas. Los resultados correspondientes así como el artículo que los recoge (A3) se presentan en la Sección 3.3. Se han calculado las estadísticas básicas, las relaciones AE-AOD con la ayuda de diagramas de dispersión para diferentes intervalos de PM_{10} y PM ratio y los ciclos anuales de las magnitudes principales. A continuación se han estudiado las propiedades microfísicas a partir de la distribución de tamaños y las relaciones entre la concentración volúmica de partículas, la esfericidad y el AE o PM ratio. Se han establecido tres zonas o intervalos para diferenciar las intrusiones desérticas en función de la predominancia de las partículas finas en la mezcla con el aerosol desértico lo que ha permitido estudiar la correlación entre magnitudes en función del intervalo al que pertenecen. En último lugar, se ha estudiado la dependencia espectral de algunas propiedades radiativas como el albedo de dispersión simple o el factor de asimetría.

Consideramos muy relevante la realización del inventario de aerosoles desérticos en nuestra zona de estudio y fundamentalmente la evaluación de la contribución de los aerosoles desérticos al valor total del AOD, por ser la primera vez que se realiza en la Península Ibérica y a nivel europeo. También es importante el cálculo de ésta contribución sobre los valores totales del PM_x ya que es la primera vez que se ha evaluado sobre las fracciones de $PM_{2.5}$ y $PM_{10-2.5}$.

2.3. Metodología de “Detección de episodios desérticos”

2.3.1. Metodología de detección de episodios desérticos

La metodología seguida para la detección de intrusiones desérticas comienza con una inspección visual de los valores instantáneos de AOD y AE y de los valores diarios de PM₁₀, PM_{2.5} y su ratio, siendo ambas bases de datos la información principal considerada. Hemos de resaltar que el inventario lo que contabiliza son días, es decir, días completos donde se considera que los niveles que se alcanza de los parámetros estudiados son característicos de un evento de aerosol desértico.

Aunque la detección de eventos de aerosoles de origen desértico se ha basado fundamentalmente en la inspección visual mencionada, debe basarse en unos criterios más objetivos, y por eso se precisa establecer los valores umbrales que definen un evento de alta turbiedad. Como es obvio, para establecer esos valores umbrales debería conocerse la climatología o bien los valores estadísticos de una zona o área de estudio. Sin embargo, esos datos sólo se conocían parcialmente puesto que este estudio comenzó en el año 2006 y las bases de datos disponibles, como ya se ha mencionado, comenzaron en 2001 y 2003, respectivamente. Así pues, basándonos en el análisis de los datos disponibles, así como en resultados obtenidos por nuestro grupo en trabajos anteriores (Cachorro, et al., 2000a, b; Toledano, et al., 2007a, b; Bennouna et al., 2013; 2014), se establecieron valores umbrales de AOD y PM₁₀ para indicar los valores a partir de los cuales se podía considerar que hay una intrusión de alta turbiedad en la zona de estudio. Estos valores fueron: AOD>0.18 y PM₁₀>13 μgm^{-3} (Rodrigo, 2012; Bennouna et al., 2013; 2014) y eran susceptibles de modificarse a lo largo del tiempo a medida que se iban analizando nuevos años debido a la variabilidad que en sí presentan los valores anuales y estacionales de los aerosoles. Sin embargo, en la re-evaluación final realizada en 2014 no consideramos necesaria esta modificación ya que la versatilidad que nos da el análisis visual ha demostrado que no se precisaba. Debemos enfatizar que la observación de los valores instantáneos del AOD a lo largo del día nos hará clasificar si ese día se incluye o no dentro del inventario (los datos de PM_x son valores diarios) de episodios de aerosoles desérticos y en algunas ocasiones ese día puede presentar solo unas horas de evento desértico. El inventario no se basa en considerar valores medios diarios del AOD, y en ello radica la dificultad de realizar este inventario “manual” pero a su vez nos garantiza una muy alta fiabilidad incluso en la identificación de eventos débiles.

Además de estos valores umbrales de AOD y PM_x se deben establecer también valores umbrales para AE y el PM ratio, indicativos del tamaño de las partículas presentes en la atmósfera y que nos ayudarán a discernir el tipo de aerosol registrado. Para nuestro estudio, la magnitud principal será el AE, permitiéndonos discernir aquellas intrusiones de aerosol desértico puro ($AE < 1.0$), las que presentan un cierto grado de mezcla con aerosol desértico ($1.0 < AE < 1.5$), y las intrusiones con predominancia de partículas finas ($AE > 1.5$), o no desérticas. En estos tres rangos de AE, tenemos pues, aerosol desértico puro y mezclas con distinta influencia de otros tipos de aerosol. El PM ratio tomará valores próximos a cero para los casos de aerosol desértico puro y aumentará hasta llegar a la unidad en las mezclas conforme se incremente el peso o predominancia de partículas finas. En este caso establecer tres rangos como en el caso del parámetro AE no es tan evidente. Ello nos llevó a estudiar las relaciones entre estos 4 parámetros mencionados (Artículo A1).

Analizaremos las tres estaciones de EMEP mencionadas anteriormente: Peñausende como estación principal y Campisábalos y Barcarrota como estaciones de apoyo. Se escogen estas tres estaciones en concreto por dos motivos fundamentales. En primer lugar, por estar situadas en áreas rurales de fondo regional donde la detección de intrusiones Saharianas es posible y en segundo lugar, debido a que la distinta localización geográfica de las estaciones será una ayuda a la hora de determinar el camino que ha seguido la intrusión. La dirección por la que ha llegado la intrusión podrá ser establecida con las medidas de Peñausende si entra por el oeste, Barcarrota si entra por el sur-oeste, o Campisábalos si entra por el sureste hasta llegar a nuestra estación.

Una vez establecido un episodio basado en los datos dados por el fotómetro y los datos de PM_x , nos ayudaremos de información auxiliar para corroborar si ciertamente estamos ante un evento desértico, y analizar más en detalle los días que componen dicho evento. Así, las masas de aire a tres alturas distintas (500, 1500 y 3000m s.n.m) serán útiles para determinar tanto el origen del aerosol medido como el camino recorrido hasta llegar a la Península. Debido a que las intrusiones desérticas pueden ser transportadas largas distancias a altitudes superiores a la capa límite de la atmósfera se escoge la altura de 3000m s.n.m., y los otros dos niveles nos darán información sobre lo que ocurre cerca de la superficie y alrededor de la capa límite obteniendo así información del transporte vertical de los aerosoles. La información de la nubosidad presente durante los días estudiados obtenida a partir de los productos MODIS será de utilidad al contrastarla con la que se observa en la evolución temporal de los datos AOD-AE de los niveles 1.0 y 1.5. Además, la información obtenida por los mapas de AOD

proporcionados por MODIS nos ayudará a determinar el camino y longitud de las plumas desérticas de los eventos estudiados. La información obtenida del modelo NAAPS será también contrastada a su vez para comprobar si está de acuerdo con las otras informaciones de las que se dispone. Se analizarán también los mapas meteorológicos de presión a nivel de superficie y de altura geopotencial a 700 mb proporcionados por NOAA con ánimo de clasificar los distintos escenarios sinópticos que propician las intrusiones desérticas.

La identificación de eventos llevada a cabo a través del estudio detallado de cada día por un observador humano permitirá diferenciar las intrusiones fuertes, moderadas y débiles así como las mezclas de polvo desértico con otro tipo de aerosol. Por tanto, se clasificarán los días incluidos en el inventario en dos subgrupos, desérticos puros (D) y desérticos mezcla (MD). Ambas categorías presentarán gran parte de la evolución de los valores instantáneos de AOD por encima del valor umbral establecido de 0.18 y el valor diario de PM₁₀ será superior a 13 μgm^{-3} . Parte de los valores instantáneos del AE, indicativos del tamaño predominante de las partículas presentes en la atmósfera, estarán por debajo de 1.0 para los días clasificados como D y entre 1.0 y 1.5 para aquellos días MD. Esta clasificación será de especial relevancia más adelante a la hora de obtener resultados y establecer conclusiones.

La dificultad de la diferenciación entre varios tipos de intrusiones reside en que no siempre todas las informaciones son completamente concordantes entre sí, como se demuestra al comparar las masas de aire con los valores de AOD y éstos con los valores de PM_x. A su vez, los altos valores del AOD y la alta variabilidad que caracterizan a los eventos desérticos hacen que se confundan con la nubosidad, como hemos comprobado en cantidad de casos, ya que el algoritmo de AERONET de filtrado de nubes (cloud screening) no es perfecto. Otro efecto muy importante es el desfase o retardo temporal entre los valores del AOD y PM_x debido al fenómeno de la deposición de las partículas que se precisa para medir los valores de PM_x. El observador humano tendrá que tener en cuenta las consecuencias del fenómeno de deposición. Si una intrusión es detectada en columna por los valores de AOD y sabemos por las retro-trayectorias que ha entrado a una determinada altura, es posible que los niveles de PM₁₀ tarden en ser superiores al valor umbral y reflejar la intrusión. Esto es así ya que puede ocurrir que la intrusión tenga lugar únicamente en las capas atmosféricas más altas (las capas atmosféricas más bajas no presentan aerosol) y son por tanto los aerosoles que viajan en altura los que tienen que ser depositados en la superficie para poder ser medidos, pudiendo tardar en producirse esta deposición de uno a tres días.

2.3.2. Caso de estudio: Octubre, 2014

En el ejemplo que mostramos a continuación analizaremos el episodio desértico que tuvo lugar durante los días comprendidos entre el 19 y el 31 de octubre de 2014. Este episodio se caracteriza por su complejidad y larga duración, resultando así octubre de 2014 como el mes de octubre con más días de intrusión desértica de los doce años considerados. Las Figuras 3 y 4 muestran la evolución temporal de los valores instantáneos de AOD-AE y diarios de PM₁₀-PM ratio, respectivamente. Una de las características que podemos ver es cómo mientras que la evolución temporal de AOD no siempre supera su valor umbral establecido, los valores de PM₁₀ sí que superan su correspondiente umbral de 13 μgm^{-3} (excepto para el día 22). Por su parte, el valor de AE nos indica clara predominancia en todos los días de partículas gruesas, lo que puede corroborarse al analizar los bajos valores del PM ratio en la Figura 4. La peculiaridad de este episodio es que no es habitual ver esos valores tan bajos de AE junto a valores tan bajos de AOD, sobre todo los días 25, 26 y 27. El seguimiento simultáneo de la evolución en los valores de PM₁₀ de nuestras tres estaciones de interés (Peñausende, Barcarrota y Campisábalos) indica una amplia pluma de intrusión que evoluciona de manera similar en dichas estaciones. Esta intrusión también vino caracterizada por una alta nubosidad como ponen de manifiesto las imágenes RGB de MODIS así como los valores en el nivel 1 de AOD de AERONET, filtrados en el nivel 1.5.

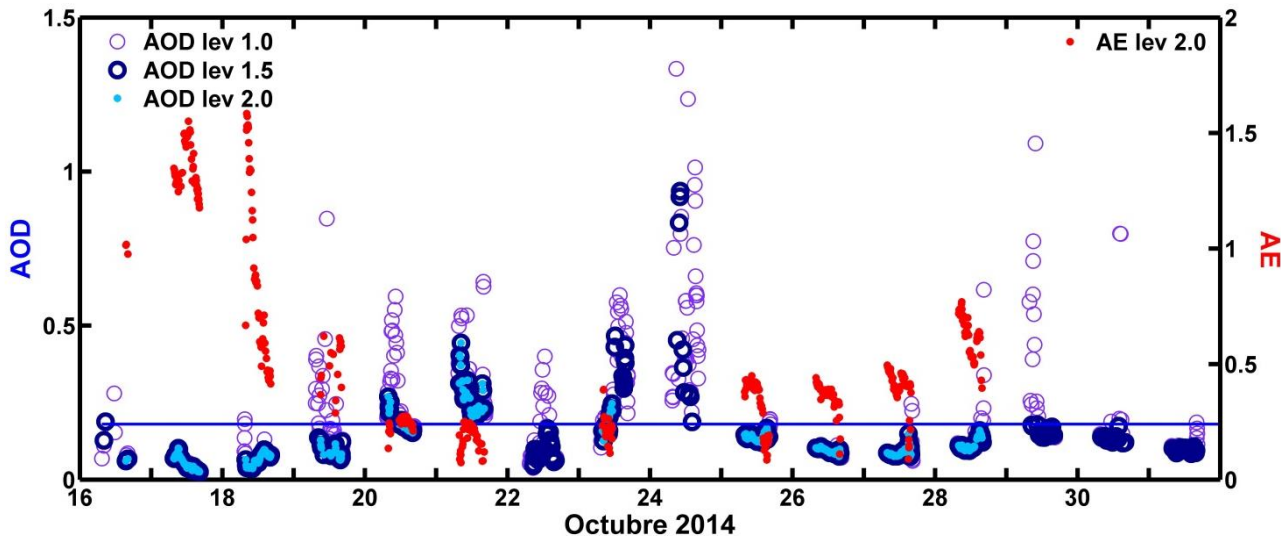


Figura 3: Evolución temporal de los valores instantáneos de AOD y AE para la estación de Palencia.

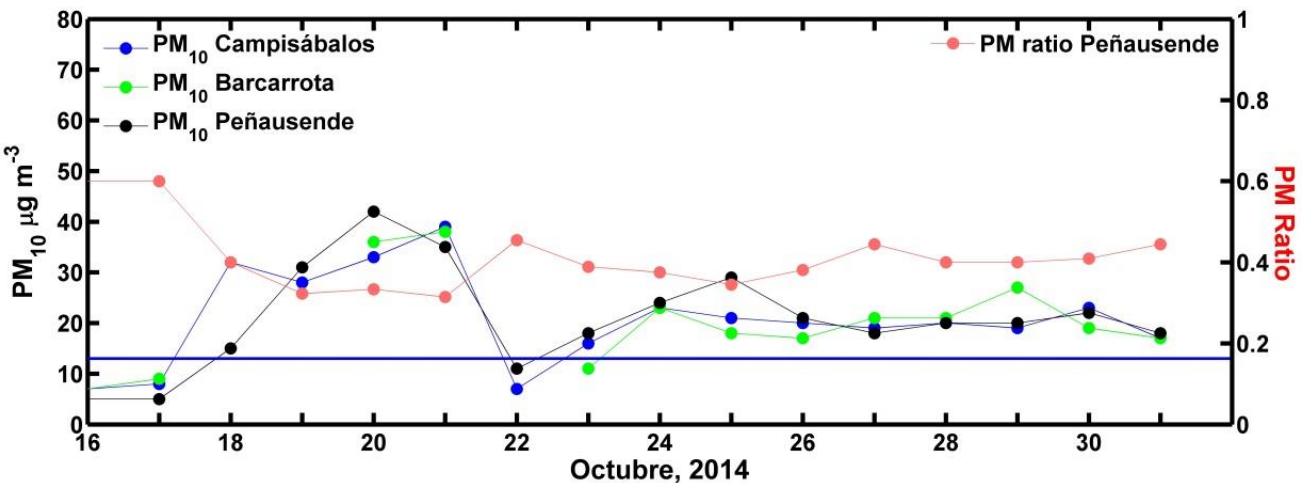


Figura 4: Evolución temporal de los valores diarios de PM₁₀ para las estaciones de Peñausende, Barcarrota y Campisábalos, y el valor diario del PM ratio para Peñausende.

Cuando se analizan los posibles días que componen o no un episodio se revisa la información complementaria para cada uno de los días en cuestión. En concreto, las Figuras 5, 6 y 7 muestran dicha información como ejemplo para el día 20 de Octubre (la Figura 6 añade también información sobre el día 26).

En el panel izquierdo de la Figura 5 se puede observar el origen y camino seguido por las retro-trayectorias de las masas de aire, lo que pone de manifiesto la influencia desértica durante este día para las tres alturas analizadas. En el panel derecho de dicha figura, podemos observar que la imagen RGB-MODIS presenta zonas de cierta cobertura nubosa por lo que cabe esperar que haya algunos huecos durante el día en los valores instantáneos de nivel 1.5 y 2 de AOD-AE debido a dicha nubosidad. Las zonas de esta imagen que presentan claros indican que es posible que haya medidas correctas durante este día que sirvan para apreciar la evolución de las variables y poder detectar así si hubo o no presencia de aerosol desértico.

La predicción del modelo NAAPS muestra cuatro mapas por día para los siguientes elementos de interés: polvo desértico, sulfatos, concentración de polvo desértico a nivel de superficie y humo. Como se puede observar en la Figura 6, el día 20 (4 mapas de la izquierda) presenta predicción de polvo desértico en columna y en superficie mientras que para el día 26 el modelo muestra que no habrá impacto desértico, lo que conlleva una cierta incongruencia al analizar lo que ocurre a nivel de superficie puesto que el valor de PM₁₀ para este día es superior a su valor umbral. Sin embargo, tampoco es de esperar una predicción muy precisa

antes unos valores tan bajos del AOD, dado que para este día, solo se detecta la intrusión en los valores de PM₁₀.

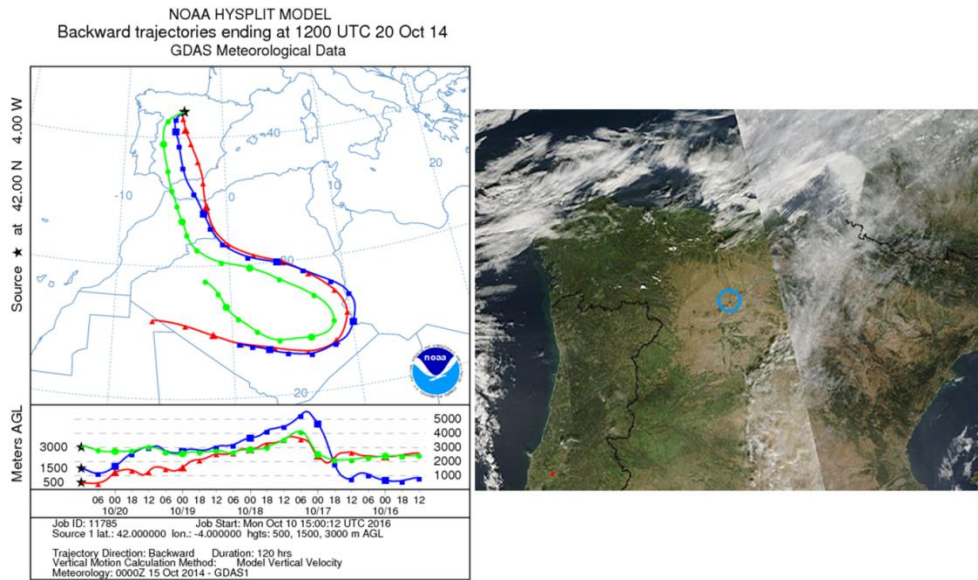


Figura 5: Información complementaria utilizada para la clasificación de episodios desérticos. Día 20 de Octubre de 2014. Izquierda: retro-trayectorias de las masas de aire (HYSPLIT). Derecha: imagen RGB (MODIS).

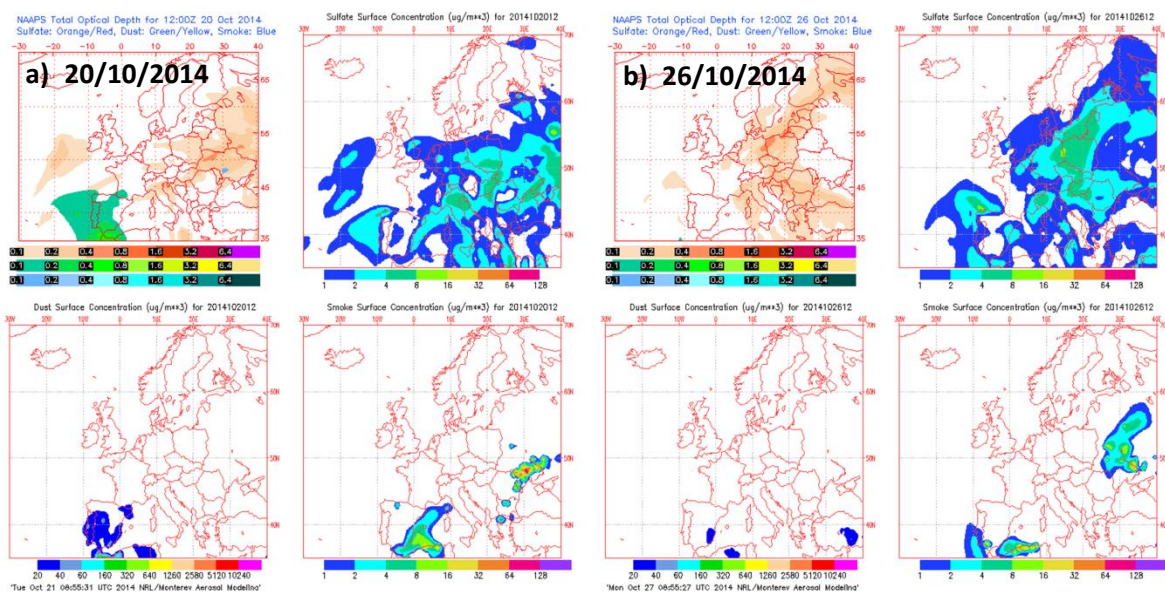


Figura 6: Información complementaria utilizada para la clasificación de episodios desérticos. Predicción alta turbiedad (NAAPS). Los cuatro mapas de la izquierda pertenecen al día 20 de Octubre, los 4 de la derecha, al día 26 de Octubre.

La Figura 7 está compuesta por el mapa de AOD proporcionado por MODIS (izquierda) y los mapas meteorológicos tanto de presión a nivel de superficie (derecha arriba) como de altura geopotencial calculada a 700mb (derecha abajo) proporcionados por NOAA a través de la página web <http://www.esrl.noaa.gov/psd/data/histdata/>. En primer lugar, la imagen de AOD muestra como el día 20 presenta una clara pluma desértica que llega a la PI por la zona de Gibraltar (lo que concuerda con la información obtenida por las retro-trayectorias). Además, los mapas meteorológicos nos permiten clasificar el escenario sinóptico que propicia la intrusión estudiada. En este caso, el escenario sinóptico es el denominado depresión Atlántica (“AD”, Atlantic Depression en inglés, Escudero et al., 2005), caracterizado por un sistema de bajas presiones tanto a nivel de superficie como en altura en la zona de las Azores que puede ser el causante de intrusiones de polvo sahariano por el sur de la PI en todas las alturas atmosféricas (de nuevo información que concuerda con la obtenida a través de las retro-trayectorias de las masas de aire).

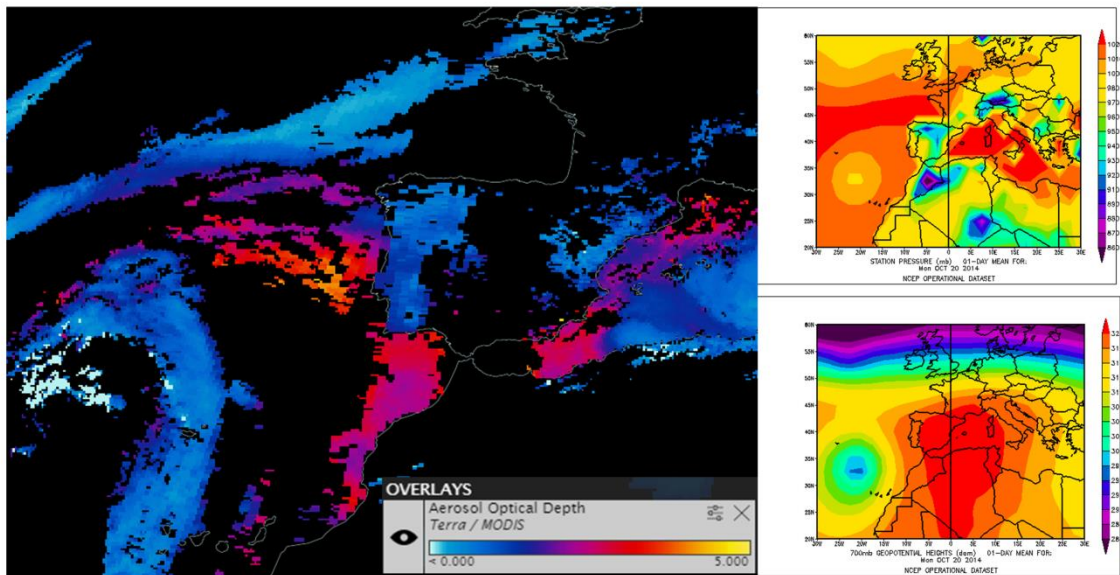


Figura 7: Información complementaria utilizada para la clasificación de episodios desérticos. Día 20 de Octubre de 2014. Izquierdo: mapa de AOD proporcionado por MODIS con una escala de AOD de 0 a 5. Derecha: mapa de la Presión a nivel de superficie (arriba) y de la altura geopotencial a 700mb (abajo).

Una vez analizadas todas las fuentes de información y concretados los días que formarán parte del episodio, se realiza una tabla resumen con la información más importante a tener en cuenta. La Tabla 3 presenta para este caso estudio los datos más relevantes contenidos en el inventario. Cada día es clasificado como D o MD de acuerdo a los criterios previamente establecidos para los valores de AE. En este caso, puesto que los valores del AE están por

debajo de 1.0, todos los días han sido clasificados como tipo D excepto el día 31, que debido al descenso tanto en AOD (nivel 1.5) como en PM₁₀ y al ligero aumento de PM ratio y AE (nivel 1.5, no mostrado aquí) ha sido clasificado como MD. Las retro-trayectorias observadas durante los días que componen este episodio han pasado por las zonas Desértica (D) y Atlántica (A), que son dos de las zonas con fuerte influencia de aerosol desértico. También se indica la presencia o no de nubosidad. Se añaden los valores medios diarios de PM₁₀, PM_{2.5}, PM_{10-2.5}, PM ratio, AOD y AE (nivel 2.0) y el número que define el escenario sinóptico que propicia la intrusión. Indicaremos el número de datos instantáneos de nivel 2.0 de la red AERONET para asegurar la validez de la media diaria. En general, si un día cuenta con menos de 3 datos instantáneos, los valores de AERONET no son considerados puesto que pueden no ser significativos del día en cuestión, sin embargo esta regla tiene excepciones, si manualmente se comprueba en eventos fuertes la veracidad de los datos. Finalmente, se hace notar la no coincidencia en la huella que ciertos casos de días de naturaleza desértica dejan en las base de datos de AOD-AE y de PMx. Esto conlleva a que se generarían inventarios diferentes si se analizara únicamente una de estas dos bases de datos por separado, y a su vez estos inventarios serían diferentes al que hemos obtenido al tomar ambas conjuntamente.

Tabla 3: Información contenida en el inventario relativa a los casos de estudio. D: Desértica, MP: Marítimo-Polar, L: Local, A: Atlántica. El valor de AOD y AE corresponde a la media diaria.

| Fecha | Tipo Evento | Retro-trayectoria (500/1500/3000) | PM ₁₀ | PM _{2.5} | PM ₁₀ -PM _{2.5} | PM ratio | AOD | AE | Escenario Sinóptico | Num. Datos Instantaneos AERONET |
|------------|-------------|-----------------------------------|------------------|-------------------|-------------------------------------|----------|------|------|---------------------|---------------------------------|
| 19/10/2014 | D | D/D/D Poca Nubosidad | 31 | 10 | 21 | 0.32 | 0.09 | 0.50 | 2 | 17 |
| 20/10/2014 | D | D/D/D Sin Nubosidad | 42 | 14 | 28 | 0.33 | 0.18 | 0.24 | 2 | 33 |
| 21/10/2014 | D | D/D/D Poca Nubosidad | 35 | 11 | 24 | 0.31 | 0.27 | 0.18 | 2 | 36 |
| 22/10/2014 | D | MP/MP/MP Sin Nubosidad | 11 | 5 | 6 | 0.45 | N/A | N/A | 2 | N/A |
| 23/10/2014 | D | MP/MP/D Nubosidad Media | 18 | 7 | 11 | 0.39 | 0.18 | 0.23 | 2 | 18 |
| 24/10/2014 | D | MP/MP/D Nubosidad Media | 24 | 9 | 15 | 0.38 | N/A | N/A | 2 | N/A |
| 25/10/2014 | D | L/A/L Sin Nubosidad | 29 | 10 | 19 | 0.34 | 0.14 | 0.33 | 2 | 49 |
| 26/10/2014 | D | L/L-C/L-A Sin Nubosidad | 21 | 8 | 8 | 0.38 | 0.09 | 0.36 | 2 | 49 |
| 27/10/2014 | D | L/L/L Sin Nubosidad | 18 | 8 | 10 | 0.44 | 0.09 | 0.40 | 2 | 49 |
| 28/10/2014 | D | D/D/D Nubosidad Media | 20 | 8 | 12 | 0.40 | 0.11 | 0.63 | 2 | 43 |
| 29/10/2014 | D | D/D/D Nubosidad Media | 20 | 8 | 12 | 0.40 | N/A | N/A | 2 | N/A |
| 30/10/2014 | D | D/D/D Sin Nubosidad | 22 | 9 | 13 | 0.41 | N/A | N/A | 2 | N/A |
| 31/10/2014 | MD | L/L/D Nubosidad Media | 18 | 8 | 10 | 0.44 | N/A | N/A | 2 | N/A |

2. Resultados

3.1. Estudio comparativo de las propiedades en superficie y columna de los aerosoles en dos estaciones de fondo regional

3.1.1. Resumen gráfico

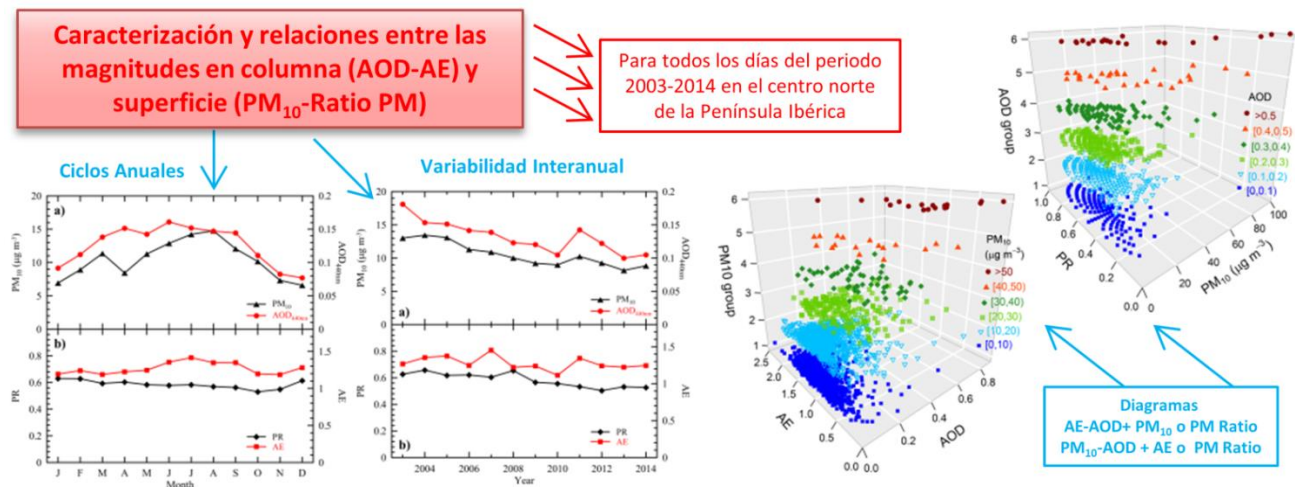


Figura 8: Resumen gráfico del A1.

3.1.2. Resumen

El primer estudio realizado, que sirve de base para los posteriores, se ha centrado en el análisis comparativo de las propiedades de los aerosoles en columna y superficie en el área centro-norte de la Península Ibérica a partir de los datos medidos entre enero de 2003 y diciembre de 2014. En cuanto a las magnitudes que nos darán cuenta de la carga de aerosol, utilizaremos PM_x (concentración másica a nivel de superficie) y AOD (índice que nos da la cantidad o carga de aerosol considerando toda la columna atmosférica), ya que a pesar de su diferente significado son magnitudes complementarias. Para estudiar el tamaño de las partículas utilizaremos el PM ratio (superficie) y el AE (columna).

Se realizó inicialmente un estudio global de caracterización de la evolución temporal y de los parámetros estadísticos correspondientes que se refleja en la obtención del comportamiento de los ciclos anuales. Así, el ciclo anual de PM₁₀ muestra dos máximos a lo largo del año (uno a final de invierno – principio de primavera y otro en verano) y el ciclo de AOD (cuya forma es cercana a la de una campana) muestra sólo un máximo en verano. Es por

tanto, la presencia de éstos dos máximos en el ciclo anual del PM₁₀, el hecho diferencial entre los ciclos anuales estudiados. Para explicar parcialmente estas diferencias, hay que subrayar el hecho de que en el área estudiada, son las intrusiones de aerosol desértico las que mayormente influirán en los valores de PM₁₀, en contraposición al AOD, cuyos valores se verán influidos tanto por intrusiones desérticas como por aerosoles de pequeño tamaño, las denominadas partículas finas provenientes de la quema de biomasa de los incendios forestales, o bien episodios de contaminación antropogénica. En cuanto a las magnitudes referentes al tamaño de las partículas, el ciclo anual del PM ratio muestra pequeñas variaciones a lo largo del año, con valores ligeramente superiores en invierno. A su vez, el ciclo anual del AE también muestra valores casi constantes con medias ligeramente menores en invierno-primavera en comparación con las de verano-principio de otoño.

Las diferentes relaciones que existen entre AOD, AE, PM₁₀ y PM ratio se han estudiado desde una perspectiva climatológica, obteniendo una caracterización general de esa zona de estudio correspondiente a un ambiente de fondo regional. Las relaciones entre estas cuatro magnitudes se han analizado a través de diagramas de dispersión, los cuales son de utilidad a la hora de visualizar relaciones no lineales entre los diferentes parámetros y dan una idea muy global de la posibilidad de establecer grupos o clasificaciones entre los diferentes tipos de aerosoles (aunque con fronteras muy difusas). A pesar de la base teórica que explica la relación entre las magnitudes consideradas, la variedad de tipos de aerosoles implicados así como los complejos procesos físico-químicos y atmosféricos que tienen lugar, y la dependencia de otros factores implicados en ellos, da lugar a que se hayan considerado y establecido relaciones de tipo empírico.

En un primer paso, se han estudiado las relaciones AE-AOD y PM ratio- PM₁₀ en función de las correspondientes magnitudes de superficie y columna, respectivamente. La mayoría de los promedios diarios de los valores AE-AOD son los esperados para un área clasificada como continental limpia. Trabajando a partir del valor promedio diario de AOD para todos los días del periodo se puede establecer un umbral de AOD~0.2 para considerar eventos de alta polución. Así, los casos de alta turbiedad representan el 18% del total de la base de datos de AOD. Si se estudian estos mismos diagramas utilizando los valores instantáneos podemos obtener más detalle en cuanto a eventos que presentan valores extremos así como aquellos casos con mezcla de varios tipos de aerosoles. En cuanto al análisis de PM₁₀-PM ratio, los casos de alta turbiedad caracterizados por valores de PM₁₀ superiores a 20 µg m⁻³ representan el 12% de los datos de PM₁₀. El análisis de los datos muestra la limitación de los mismos,

pues al ser valores diarios de PM_x muy bajos y valores enteros, representativos de zonas limpias de fondo rural, da lugar a una discretización de los valores del PM ratio, que tiene como consecuencia que no se vea tan claramente información importante al analizar los diagramas de estos parámetros.

Al estudiar las dos variables que tienen en cuenta el tamaño de los aerosoles, se obtiene una baja correlación en los diagramas AE-PM ratio. Ciertamente las variaciones de los valores diarios son importantes pero no así en las medias mensuales o anuales como ya se ha mencionado. La baja correlación observada de estas dos variables es una característica de la zona de estudio, y parece ser una tónica general en la relación entre ellas. Los resultados también muestran que el AE representa el tamaño de las partículas mejor que el PM ratio ya que éste es un ratio entre concentraciones (y con un rango de variación menor, de 0 a 1 frente a 0-4 del AE) mientras que el AE contiene la dependencia espectral del AOD. De acuerdo a la teoría de Mie la variación espectral del AOD contiene más información útil en relación al tamaño de las partículas, sin embargo debido a la compleja interacción entre éstas y la radiación, este parámetro tampoco es extremadamente sensible al tamaño de las partículas.

Debido a que magnitudes como el AOD están siendo proporcionadas por sensores a bordo de satélites, lo que ofrece la ventaja de una gran cobertura espacial, estudios anteriores han intentado determinar o estimar la concentración de PM_{10} o $PM_{2.5}$ a partir de estos valores del espesor óptico de aerosoles de la columna (Pelletier et al., 2007; Schaap et al., 2009; Kokhanovsky et al., 2009). Visto el interés de este tipo de estudios centrados en establecer relaciones empíricas entre la carga del aerosol en superficie y columna, hemos estudiado en detalle la correlación entre las bases de datos de AOD y PM_{10} en nuestra área de estudio y durante el periodo seleccionado. Las correlaciones son pobres para los valores diarios ($R=0.58$), mejorando al considerar promedios mensuales ($R=0.74$) y anuales ($R=0.89$). El análisis global de estas 4 magnitudes sobre una determinada zona de estudio demuestra que lo correcto es establecer relaciones o correlaciones tomando los datos base sobre intervalos o rangos de valores (“bines”) de estas variables y no sobre valores puntuales, diarios. Las relaciones o correlaciones entre ellas presentan más un carácter climatológico que puntual, a no ser que estos sean de carácter bastante intenso.

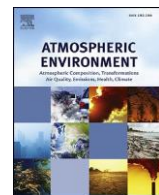
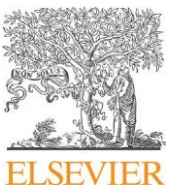
Al depender éstas correlaciones de la estación de medida, el rango de valores de AOD y PM_{10} de nuestro estudio será menor comparado con áreas de mayor contaminación. Una de las razones por las que la correlación entre éstas variables es moderada es la gran variabilidad

de aerosoles en un corto rango de valores de AOD y PM₁₀ debido a las condiciones limpias de fondo del área de estudio, donde las partículas que prevalecen son de tamaño medio o fino y tienen una influencia mayor en el AOD que en el PM₁₀.

El análisis de la evolución temporal de la carga de aerosol durante las últimas décadas resulta vital para poder comprender fenómenos como el dimming (decrecimiento) o el brightening (aumento) en los niveles de radiación solar registrados en superficie. Además, en las últimas décadas instituciones tanto nacionales como internacionales han establecido límites a los valores de PM_x con el objetivo de disminuir la contaminación y proteger la salud pública y el medio ambiente (EC, 2008). De este modo, ya se han encontrado tendencias anuales decrecientes en varios países europeos (Cusack et al., 2012; Querol et al., 2014). Teniendo esto en cuenta, hemos estudiado la evolución temporal de las dos bases de datos principales, obteniendo que los promedios anuales de AOD y PM₁₀ muestran tendencias decrecientes similares, situándose en torno al 40% y 38% (PM₁₀ y AOD, respectivamente) en los 12 años estudiados. Estos resultados se han corroborado en otro estudio en el que ha participado la doctoranda (Mateos et al., 2015), en el que se ha encontrado una evolución en torno al -30% por década en la cantidad de material particulado en la PI desde la década de los 80. Las tendencias decrecientes encontradas en nuestro estudio, relativas tanto a la carga de aerosol en superficie como en columna incluyen las posibles variaciones en las tendencias de los aerosoles de origen antropogénico y natural. La tendencia del aerosol natural de origen desértico será estudiada más adelante (Sección 3.2). Además, nuestro trabajo muestra que el PM ratio presenta una reducción en los promedios anuales del 22% (debido al hecho que el PM_{2.5} presenta una reducción del 60%) y apenas una reducción del 8% para el AE.

A pesar de las limitaciones encontradas en este estudio, se puede concluir que la sinergia superficie-columna en las bases de datos de larga duración estudiadas puede ser explorada de forma cuantitativa y obtener información de utilidad en la caracterización de aerosoles y tendencias desde una perspectiva climatológica. La originalidad del trabajo se basa en el hecho de que no se encuentran trabajos publicados donde se analicen las relaciones de los parámetros o variables de aerosoles en superficie y columna con tanto detalle y sobre una base de datos tan larga que permite un análisis con una perspectiva climatológica del área de estudio.

3.1.3. Artículo 1



Long-term comparative study of columnar and surface mass concentration aerosol properties in a background environment

Y.S. Bennouna, V.E. Cachorro*, D. Mateos, M.A. Burgos, C. Toledano, B. Torres,
A.M. de Frutos

Atmospheric Optics Group (GOA), University of Valladolid (UVA), Valladolid, Spain



h i g h l i g h t s

- Long-term surface and columnar aerosol data in a background environment are analysed.
- The best correlation between AOD and PM₁₀ is obtained using yearly means.
- High turbidity events show weak correlation of surface and aerosol properties.

article info

Article history:

Received 14 December 2015

Received in revised form

27 May 2016

Accepted 30 May 2016

Available online 2 June 2016

Keywords:

Aerosol optical depth

Particulate matter

High turbidity events

Columnar and surface relationships

Aerosol climatology

abstract

The relationship between columnar and surface aerosol properties is not a straightforward problem. The Aerosol Optical Depth (AOD), Ångström exponent (AE), and ground-level Particulate Matter (PM_x, $x \leq 10$ or 2.5 μm) data have been studied from a climatological point of view. Despite the different meanings of AOD and PM_x both are key and complementary quantities that quantify aerosol load in the atmosphere and many studies intend to find specific relationships between them. Related parameters such as AE and PM ratio (PR = PM_{2.5}/PM₁₀), giving information about the predominant particle size, are included in this study on the relationships between columnar and surface aerosol parameters. This study is based on long measurement records (2003–2014) obtained at two nearby background sites from the AERONET and EMEP networks in the north-central area of Spain. The climatological annual cycle of PM_x shows two maxima along the year (one in late-winter/early-spring and another in summer), but this cycle is not followed by the AOD which shows only a summer maximum and a nearly bell shape. However, the annual means of both data sets show strong correlation ($R \approx 0.89$) and similar decreasing trends of 40% (PM₁₀) and 38% (AOD) for the 12-year record. PM₁₀ and AOD daily data are moderately correlated ($R \approx 0.58$), whereas correlation increases for monthly ($R \approx 0.74$) and yearly ($R \approx 0.89$) means. Scatter plots of AE vs. AOD and PR vs. PM₁₀ have been used to characterize aerosols over the region. The PR vs. AE scatterplot of daily data shows no correlation due to the prevalence of intermediate-sized particles. As day-to-day correlation is low (especially for high turbidity events), a binned analysis was also carried out to establish consistent relationships between columnar and surface quantities, which is considered to be an appropriate approach for environmental and climate studies. In this way the link between surface concentrations and columnar remote sensing data is shown to provide useful information for aerosol characterization from a climatological context, despite some limitations.

© 2016 Elsevier Ltd. All rights reserved.

1. Introduction

A common reference indicator for particulate air quality is the concentration of particulate matter (PM) at ground level, which is

given in units of mass per unit volume of air (mg m⁻³). The PM size fraction represented by PM₁₀ and PM_{2.5} are the most available and commonly used metrics. The PM₁₀, often called "inhalable particles" (EMEP, 1996; Brown et al., 2013), refers to particle fraction with aerodynamic diameters less than 10 μm. In the same way, PM_{2.5} or "fine particles" (diameters below 2.5 μm) is another measure of particulate matter. The latter is associated to hazardous effects, having far greater efficiency than "coarse particles"

* Corresponding author.

E-mail address: chiqui@goa.uva.es (V.E. Cachorro).

(2.5×10^{-10} Mm) to penetrate the respiratory system and reach the alveolar regions. Consequently, PM₁₀ is usually used as a standard for measuring aerosol loading, while PM_{2.5} is linked to health and visibility impacts (Pope III, 2000; Pope III and Dockeri, 2006).

In the last decades national and international institutions have set limits and guide values for the concentration of various PM size fractions with the aim to protect public health and environment (Delucchi et al., 2002; WHO, 2006; EC, 1999, 2008). Although so far this objective has not been universally achieved (Füssel and Jol, 2012), decreasing trends in yearly average have been observed in many European countries (EMEP, 2011, 2014; Tørseth et al., 2012; Cusack et al., 2012; Boucher et al., 2013; Querol et al., 2014). These reductions are certainly attributed in a great part to the application of these abatement strategies of air pollution (EMEP, 2014). A significant effort has been dedicated to the implementation of continuous ground-based "in-situ" monitoring networks. The European Monitoring and Evaluation Programme (EMEP) established these networks with the goal of studying Long-Distance Atmospheric Pollution. This network provides to scientific community and governments quantitative information on the transport of air pollutants across national boundaries, associated deposition and concentration levels (Tørseth et al., 2012; EMEP, 2011, 2014). However the EMEP PMx observations are too sparse to resolve the large spatial and temporal aerosol variability and thus other measurement techniques, such as remote sensing at ground-based or satellite platform, may also be used.

Other networks for aerosol studies are based on powerful remote sensing techniques, like AERONET (Aerosol Robotic Network), which was created in the 1990's as a federation of national and regional networks managed by NASA. It is a dense network of ground-based sun photometers providing a continuous database of remotely sensed aerosol measurements at more than 400 sites around the globe (Holben et al., 1998). Such networks constitute a valuable source of information for the establishment of local and regional aerosol characterization and climatology (Holben et al., 2001; Dubovik et al., 2002; Toledano et al., 2007a; Bennouna et al., 2011, 2013; Mateos et al., 2015).

The primary aerosol parameter provided by remote sensing is the Aerosol Optical Depth (AOD), describing the extinction of the electromagnetic radiation in a given atmospheric column attributed to aerosols at a given wavelength. This is the key parameter for measuring the columnar aerosol load. The advantage of this methodology using radiation-particle interaction is the complementary information provided by AOD wavelength dependence, related to the size of particles. The Ångström exponent (AE) derived from AOD wavelength dependence is the parameter supporting this kind of information being the smallest this parameter the largest the particles. However, the AOD is a complex function of the aerosol mass concentration, mass extinction efficiency, relative humidity, and vertical distribution of aerosols, and hence several authors have investigated the relationships between AOD and columnar aerosol volume/mass concentration, surface PMx, mass deposition, or other quantities (Cachorro and Tanré, 1997; Kacenelenbogen et al., 2006; Pelletier et al., 2007; Kokhanovsky et al., 2009; Rohen et al., 2011; Toledano et al., 2012; among others).

The AOD, as a parameter representing the extinction over the whole atmospheric column, has a theoretical link with columnar particle volume concentration or columnar mass concentration through the definition of volume/mass efficiency factor (Cachorro and Tanré, 1997; Kokhanovsky et al., 2009; Toledano et al., 2012), but the link of these columnar properties with surface concentration given by PM₁₀ (or PM_{2.5}) measurements is not a straightforward problem and hence empirical relationships are usually established (e.g., Estellés et al., 2012; references herein; Rohen et al., 2011).

In this context and restricting the study to AOD data given by ground-based observations we are interested in the relationships AOD-PM₁₀ including derived quantities such as Ångström exponent (AE) and ratio of PMx fractions (PM_{2.5}/PM₁₀), related with particle size, which also need to be involved in the study of these relations. Thus, the objective of this work is to investigate in detail the relations between these four complementary parameters from a climatological point of view relying on 12 years of overlapping AOD and PMx data (2003e2014) over two background stations of the large region of "Castilla y Leon" in the North-central Iberian Peninsula. This plateau presents a clean continental background aerosol without local pollution and it is adequate for this kind of study. The sites belong to EMEP and AERONET-Europe networks respectively, which certify the quality of the used data. To our knowledge this is the first time that this kind of study is carried out taking an area with these characteristics and lengthy records, emphasizing the climatological aspect.

It is relevant to note here that in the study area the highest levels of PMx are attributed to desert dust intrusions (Rodríguez et al., 2001; Escudero et al., 2005, 2007; Toledano et al., 2007a; Cachorro et al., 2008), because events of high AOD can also be due to external anthropogenic pollution (showing less influence on PMx values). Impact of desert dust aerosols on AOD (Toledano et al., 2007b; Cachorro et al., 2013) and PMx (Querol et al., 2009; Cachorro et al., 2014; Pey et al., 2013) are of particular interest for the Mediterranean Basin because they have a strong influence on the relationships established hereafter which opens new perspective on their potential use in aerosols studies.

The paper begins by introducing the region of study (section 1) and the description of the datasets (section 2). The results are presented in several sections. Section 3.1 gives a brief analysis of the annual cycle, interannual variability and temporal trends. In section 3.2, columnar scatter plots of AOD-AE and surface scatter plots PM₁₀-PR are examined in order to address general findings in terms of general aerosol characterization. Section 3.3 establishes and analyses the relationship PM₁₀-AOD and section 3.4 the PR-AE one. Section 3.5 gives the latter relationships under the analysis of binned data.

2. Measurement sites and data

The locations of the two sites used in this study are presented in

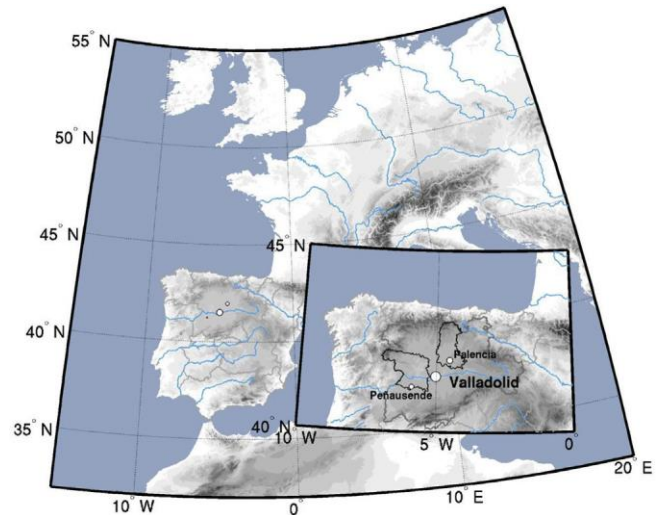


Fig. 1. Map of the area of study showing the location of the EMEP site of Peñausende and the AERONET site of Palencia within the region of "Castilla y Leon" in Spain.

Fig. 1: the rural village of Peñausende (41.24 N, 5.90 W, 985 m. a.s.l.) and Palencia City (41.99 N, 4.52 W, 750 m a.s.l.), both belonging to the autonomous community of “Castilla y León” (CyL). This region located in the North Central part of the Iberian Peninsula lies on the northern plateau of Spain (Castilian Plateau), which has an average altitude of ~800 m, and is crossed by the Duero River, forming a narrow valley. The Castilian Plateau is surrounded by mountains (about 2000e2500 m) that reduce Atlantic and Mediterranean influences, thus leading to the continental climate characterizing this region. The CyL region spans a territory of 94,193 km² with 27 inhabitants per km², making it the most sparsely populated region of Spain. The biggest metropolitan center of the region is Valladolid City (~400,000 habitants). The small city of Palencia (~100,000 inhabitants) is located about 50 km to the northeast of Valladolid. The little village of Peñausende (~500 habitants) is located in the province of Zamora, about 100 km to the east of Valladolid. Both Palencia and Peñausende sites, are relatively well isolated from big urban and industrial centers, and can therefore be classified as regional background sites.

At Peñausende, PMx measurements have been carried out continuously since 2001 by means of gravimetric methods, however we only used data from 2003 onward for the overlapping period with AOD data. The samples are collected on quartz fiber filters using MCV-PM1025 high-volume samplers operating at an average flow rate of 30 m³ h⁻¹ with 10 mm/2.5 mm cut-off inlets. Sample treatment, analytical procedures and quality assurance were performed according to the details described in the EMEP Manual for Sampling and Chemical Analysis (EMEP, 1996). The PM₁₀ and PM_{2.5} samplings were carried out on a daily basis. **Table 1** sums up the number of EMEP PMx measurements available by year. On average, 90% of yearly data are usable. The PR values are derived from the two independent PMx measurements when both are available.

Columnar aerosol properties, here aerosol optical depth and Ångström exponent, are derived by direct sun and sky radiation sunphotometer measurements. The AOD gives the total load of aerosol over the vertical column and it is generally measured at various wavelengths. This spectral wavelength dependence defines the AE parameter related to particle size (Cachorro et al., 2000; Vergaz et al., 2005; Toledano et al., 2007a), and thus gives information about the prevalence of fine or coarse fractions. The AERONET AOD at 440 nm and the AERONET derived value for AE, using wavelengths in the range 440e870 nm, are used in this study.

A Cimel sunphotometer belonging to RIMA (Iberian Network for Aerosol Measurements) located at the outskirts of Palencia (University Campus, Superior Technical School of Forestry and

Table 1
Yearly statistics of EMEP PM₁₀, PM_{2.5}, and AERONET AOD data counts in the region of study for the period 2003e2014.

| Year | N. days and (%) PM ₁₀ | N. days and (%) PM _{2.5} | N. days and (%) AOD-AE |
|-------|----------------------------------|-----------------------------------|------------------------|
| 2003 | 330 (90.41%) | 317 (86.85%) | 156 (42.74%) |
| 2004 | 338 (92.35%) | 329 (89.89%) | 265 (72.40%) |
| 2005 | 330 (90.41%) | 340 (93.15%) | 295 (80.82%) |
| 2006 | 339 (92.88%) | 324 (88.77%) | 190 (52.05%) |
| 2007 | 336 (92.05%) | 327 (89.59%) | 271 (74.25%) |
| 2008 | 317 (86.61%) | 320 (87.43%) | 280 (76.50%) |
| 2009 | 329 (90.14%) | 321 (87.95%) | 256 (70.14%) |
| 2010 | 331 (90.68%) | 326 (89.32%) | 244 (66.85%) |
| 2011 | 340 (93.15%) | 339 (92.88%) | 269 (73.70%) |
| 2012 | 315 (86.07%) | 334 (91.26%) | 252 (68.85%) |
| 2013 | 328 (89.86%) | 336 (92.05%) | 220 (60.27%) |
| 2014 | 316 (86.58%) | 310 (84.93%) | 249 (68.22%) |
| Mean | 329 (90.12%) | 326 (89.53%) | 245 (67.25%) |
| Total | 3949 | 3923 | 2947 |

Agricultural Engineering) and operating in the frame of AERONET-EUROPE (Holben et al., 1998; Goloub et al., 2012), provided continuous aerosol measurements from 2003 to 2014 with the exception of a long period between 2009 and 2010. This gap in Palencia data was completed by values from Autilla station, another nearby RIMA-AERONET site (3 km apart from Palencia city; Bennouna et al., 2013). Raw AOD data provided every 15 min by direct sun radiation measurements are cloud-contaminated (level 1.0), thus an automatic cloud screening algorithm (Smirnov et al., 2000) is applied to obtain level 1.5. The final data level named “quality assured” level 2 is the one used in this study, where pre- and post-calibration are accounted for with a final manual inspection according to AERONET protocols. The AOD accuracy for level 2 AERONET is about 0.01 in the visible and near infrared spectral regions (Eck et al., 1999).

We must emphasize that the distance between both monitoring sites (~100 km) is not an obstacle to link the aerosol properties in this representative area of the North-central Spain, because the plateau between them with no relevant local aerosol sources and where external events of high turbidity are clearly identified at both sites at the same time. Otherwise, the different intrinsic measurement techniques (one based on 24 h filters for PMx values which represent an accumulative measure while daily sunphotometer data are based on nearly instantaneous, every 15-min, values) seem to play a major role on the AOD-PMx differences.

3. Results

3.1. Climatological annual cycle, variability and trends of AOD, PMx, AE and PR

A quick description of the annual cycle from 2003 to 2014 is shown for AOD, AE, PM₁₀ and PR quantities in Fig. 2, and Fig. 3 presents their respective interannual variability; associated statistical values are reported in Tables 2e5. At Peñausende the mean value and standard deviation of PM₁₀ is $10.6 \pm 9.0 \text{ mg m}^{-3}$ and the AOD at Palencia is 0.13 ± 0.09 , given a ratio of 81.5 mg m^{-3} per unit of AOD (near 100). What stands out is the high standard deviations of 85% and 69% respectively, indicating high variability (also shown by Tables 2 and 3). The most important feature is the low level of

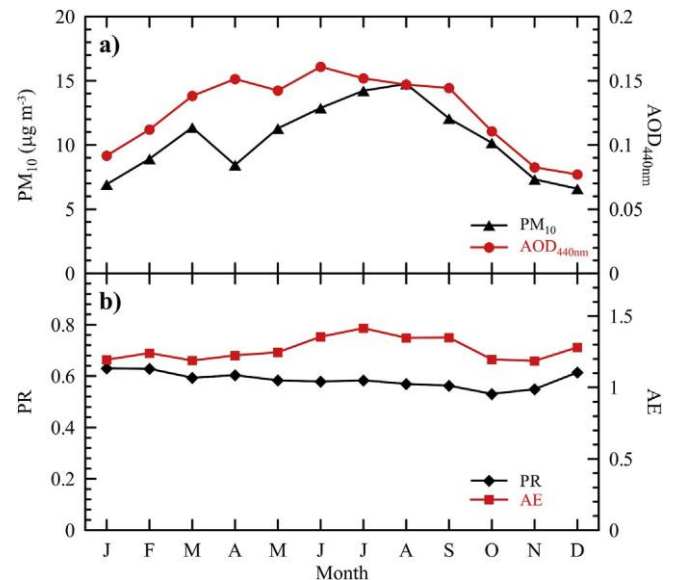


Fig. 2. Monthly mean annual cycle based on daily data of a) AOD (440 nm) and PM₁₀, b) Ångström exponent and PM ratio for the period 2003e2014.

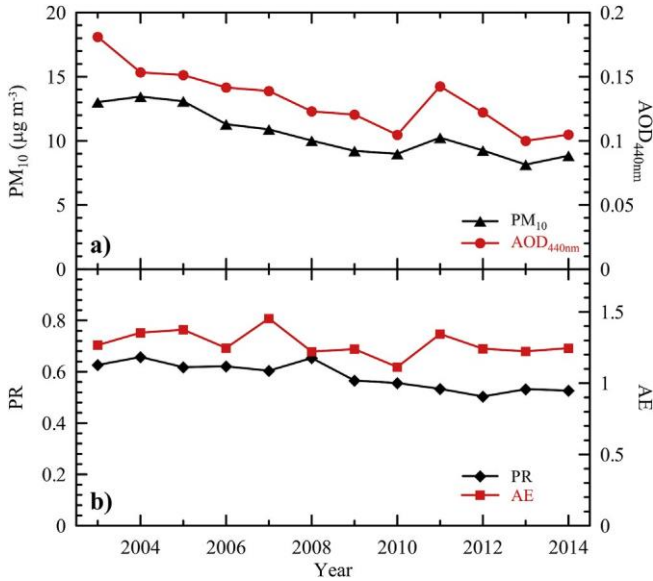


Fig. 3. Evolution of yearly mean data for a) AOD (440 nm) and PM₁₀, b) Angstrom exponent and PM ratio for the period 2003e2014.

summer (~0.15) with increasing (decreasing) values in spring (fall) resulting in a nearly bell shaped annual cycle. However, no relevant minimum in spring appears for the AOD, although a slight minimum can be observed in May. Therefore, the most obvious difference between the mean annual cycles of AOD and PM₁₀ is the presence of these two clear seasonal maxima for PM₁₀.

Although it is not shown here, the climatological curve of PM_{2.5} presents the same variations and shape as that of PM₁₀. The PM₁₀ and PM_{2.5} data are strongly correlated with a Pearson coefficient of R \approx 0.89 and a slope of 0.58, which corresponds to the mean value of PR. Thus the annual cycle of PR (Fig. 2b) shows very little variation in the monthly means with slightly higher values in winter, being nearly constant around the average value of 0.58 ± 0.15 (Table 3). The Ångström exponent is also rather constant throughout the year, with an average value of 1.28 ± 0.37 , but with lower values in winter-spring than during summer-early fall. Therefore, there is a discrepancy between PR and AE annual cycles during summer months. For both PR and AE parameters, day-to-day variations within a month are generally large for all months as indicated by the great variability associated to the means (Tables 2 and 3 and Fig. 2), but they present monthly means around their total average and hence these two parameters correlate poorly, as discussed later. From the analysed variations it seems

Table 2

Monthly statistics of the AOD (440 nm) and AE parameters for the period 2003e2014 based on daily values, with the number of days (with percentage in parentheses), mean, median, percentiles (P25, P75, P5, P95), minimum (Min) and maximum (Max) values.

| Month | N. days (%) | Mean \pm STD | Median | P25 | P75 | P5 | P95 | Min | Max |
|-----------------------------------|---------------|-----------------|--------|------|------|-------|------|-------|------|
| Aerosol Optical Depth, AOD | | | | | | | | | |
| Jan | 134 (36.02%) | 0.09 ± 0.08 | 0.06 | 0.05 | 0.11 | 0.026 | 0.23 | 0.014 | 0.71 |
| Feb | 215 (63.42%) | 0.11 ± 0.08 | 0.09 | 0.05 | 0.15 | 0.033 | 0.27 | 0.019 | 0.51 |
| Mar | 230 (61.83%) | 0.14 ± 0.09 | 0.11 | 0.07 | 0.17 | 0.046 | 0.29 | 0.028 | 0.80 |
| Apr | 223 (61.94%) | 0.15 ± 0.09 | 0.13 | 0.09 | 0.18 | 0.058 | 0.34 | 0.036 | 0.57 |
| May | 296 (79.57%) | 0.14 ± 0.07 | 0.12 | 0.09 | 0.17 | 0.061 | 0.29 | 0.045 | 0.40 |
| Jun | 258 (71.67%) | 0.16 ± 0.09 | 0.13 | 0.09 | 0.21 | 0.059 | 0.34 | 0.034 | 0.61 |
| Jul | 333 (89.52%) | 0.15 ± 0.11 | 0.12 | 0.08 | 0.19 | 0.050 | 0.37 | 0.024 | 0.87 |
| Aug | 320 (86.02%) | 0.15 ± 0.11 | 0.10 | 0.07 | 0.19 | 0.044 | 0.37 | 0.027 | 0.65 |
| Sep | 312 (86.67%) | 0.14 ± 0.09 | 0.13 | 0.07 | 0.19 | 0.042 | 0.34 | 0.026 | 0.61 |
| Oct | 255 (68.55%) | 0.11 ± 0.08 | 0.08 | 0.06 | 0.14 | 0.038 | 0.26 | 0.016 | 0.61 |
| Nov | 199 (55.28%) | 0.08 ± 0.05 | 0.07 | 0.05 | 0.10 | 0.028 | 0.18 | 0.017 | 0.38 |
| Dec | 172 (46.24%) | 0.08 ± 0.05 | 0.07 | 0.05 | 0.09 | 0.030 | 0.17 | 0.021 | 0.30 |
| Total | 2947 (67.24%) | 0.13 ± 0.09 | 0.11 | 0.07 | 0.16 | 0.039 | 0.31 | 0.014 | 0.87 |
| Ångström Parameter, AE | | | | | | | | | |
| Jan | 134 (36.02%) | 1.19 ± 0.34 | 1.27 | 0.94 | 1.45 | 0.61 | 1.65 | 0.188 | 1.77 |
| Feb | 215 (63.42%) | 1.25 ± 0.38 | 1.32 | 0.95 | 1.56 | 0.53 | 1.72 | 0.145 | 1.89 |
| Mar | 230 (61.83%) | 1.19 ± 0.38 | 1.24 | 0.95 | 1.48 | 0.49 | 1.72 | 0.015 | 1.83 |
| Apr | 223 (61.94%) | 1.23 ± 0.35 | 1.25 | 1.01 | 1.46 | 0.60 | 1.77 | 0.186 | 2.04 |
| May | 296 (79.57%) | 1.25 ± 0.28 | 1.25 | 1.08 | 1.42 | 0.74 | 1.68 | 0.299 | 2.05 |
| Jun | 258 (71.67%) | 1.36 ± 0.35 | 1.40 | 1.16 | 1.59 | 0.78 | 1.85 | 0.153 | 2.07 |
| Jul | 333 (89.52%) | 1.42 ± 0.37 | 1.48 | 1.27 | 1.64 | 0.65 | 1.88 | 0.086 | 2.53 |
| Aug | 320 (86.02%) | 1.35 ± 0.39 | 1.43 | 1.16 | 1.60 | 0.56 | 1.85 | 0.188 | 2.29 |
| Sep | 312 (86.67%) | 1.35 ± 0.33 | 1.38 | 1.15 | 1.58 | 0.75 | 1.81 | 0.233 | 2.25 |
| Oct | 255 (68.55%) | 1.20 ± 0.38 | 1.25 | 0.99 | 1.47 | 0.41 | 1.73 | 0.083 | 2.08 |
| Nov | 199 (55.28%) | 1.19 ± 0.39 | 1.29 | 0.89 | 1.47 | 0.46 | 1.72 | 0.082 | 1.86 |
| Dec | 172 (46.24%) | 1.28 ± 0.34 | 1.33 | 1.11 | 1.53 | 0.66 | 1.72 | 0.262 | 1.87 |
| Total | 2947 (67.24%) | 1.28 ± 0.37 | 1.34 | 1.06 | 1.54 | 0.60 | 1.79 | 0.015 | 2.53 |

aerosol load in the study area representative of a rural regional background.

3.1.1. Climatological annual cycle

The climatological annual cycle of PM₁₀ (see Fig. 2a) is characterized by high values in late-winter/early-spring and summer, and low values in winter and fall, with two maxima, one in March (11.4 mg m^{-3}) and the other in August (14.7 mg m^{-3}), with a pronounced minimum between them. Like for PM₁₀, the lowest values of the AOD are found in winter (~0.09) and the highest values in

that PR is relatively less sensitive to particle size variations as compared to AE. This may be also noted when analysing in detail major desert dust events that lead to an important decrease of the AE parameter while PR values remain little affected in these cases (Cachorro et al., 2013, 2014). These results show that on average aerosol particles of intermediate size are representative of the north central area of the Iberian Peninsula.

As mentioned, the area of "Castilla y León" is characterized by prevalent clean atmospheric conditions with the occurrence of moderate-to-strong desert dust intrusions or long-range

Table 3

Monthly statistics of the PM₁₀ and PM ratio for the period 2003–2014 based on daily values, with the number of days (with percentage in parentheses), mean, median, percentiles (P25, P75, P5, P95), minimum (Min) and maximum (Max) values.

| Month | N. days (%) | Mean ± STD | Median | P25 | P75 | P5 | P95 | Min | Max |
|-------------------------------------------------------|---------------|-------------|--------|------|------|------|------|------|------|
| PM₁₀ | | | | | | | | | |
| Jan | 281 (75.54%) | 6.9 ± 4.9 | 5 | 4 | 8 | 3 | 17 | 2 | 36 |
| Feb | 297 (87.61%) | 8.9 ± 6.8 | 7 | 4 | 12 | 3 | 22 | 1 | 50 |
| Mar | 344 (92.47%) | 11.4 ± 12.5 | 8 | 5 | 13 | 3 | 29 | 2 | 143 |
| Apr | 332 (92.22%) | 8.4 ± 6.1 | 7 | 5 | 10 | 3 | 18 | 2 | 48 |
| May | 352 (94.62%) | 11.3 ± 7.5 | 9 | 7 | 14 | 4 | 25 | 2 | 68 |
| Jun | 336 (93.33%) | 12.9 ± 8.8 | 10 | 8 | 15 | 5 | 27 | 3 | 90 |
| Jul | 356 (95.70%) | 14.2 ± 13.6 | 11 | 9 | 16 | 6 | 29 | 4 | 197 |
| Aug | 354 (95.16%) | 14.7 ± 11.7 | 11 | 8 | 16 | 6 | 35 | 3 | 94 |
| Sep | 331 (91.94%) | 12.1 ± 5.9 | 11 | 7 | 15 | 5 | 23 | 3 | 39 |
| Oct | 342 (91.94%) | 10.2 ± 7.1 | 8 | 5 | 12 | 3 | 24 | 2 | 45 |
| Nov | 321 (89.17%) | 7.3 ± 5.5 | 6 | 4 | 8 | 3 | 15 | 2 | 49 |
| Dec | 303 (81.45%) | 6.6 ± 4.7 | 5 | 4 | 8 | 3 | 14 | 2 | 39 |
| Total | 3949 (90.1%) | 10.6 ± 9.0 | 8 | 5 | 13 | 3 | 25 | 1 | 197 |
| PM ratio PR ¼ PM_{2.5}/PM₁₀ | | | | | | | | | |
| Jan | 254 (68.28%) | 0.63 ± 0.17 | 0.66 | 0.50 | 0.75 | 0.33 | 0.87 | 0.08 | 0.94 |
| Feb | 282 (83.19%) | 0.63 ± 0.18 | 0.67 | 0.50 | 0.78 | 0.33 | 0.87 | 0.18 | 0.97 |
| Mar | 330 (88.71%) | 0.60 ± 0.16 | 0.60 | 0.50 | 0.71 | 0.33 | 0.83 | 0.25 | 0.93 |
| Apr | 305 (84.72%) | 0.60 ± 0.14 | 0.60 | 0.50 | 0.71 | 0.33 | 0.82 | 0.17 | 0.92 |
| May | 338 (90.86%) | 0.58 ± 0.14 | 0.60 | 0.50 | 0.67 | 0.33 | 0.80 | 0.22 | 0.96 |
| Jun | 321 (89.17%) | 0.58 ± 0.13 | 0.58 | 0.50 | 0.67 | 0.37 | 0.80 | 0.12 | 0.92 |
| Jul | 345 (92.74%) | 0.58 ± 0.12 | 0.59 | 0.50 | 0.67 | 0.30 | 0.76 | 0.27 | 0.92 |
| Aug | 346 (93.01%) | 0.57 ± 0.12 | 0.57 | 0.50 | 0.67 | 0.37 | 0.70 | 0.19 | 0.94 |
| Sep | 318 (88.33%) | 0.56 ± 0.12 | 0.56 | 0.50 | 0.64 | 0.37 | 0.76 | 0.17 | 0.90 |
| Oct | 322 (86.56%) | 0.53 ± 0.14 | 0.51 | 0.42 | 0.63 | 0.30 | 0.70 | 0.02 | 0.86 |
| Nov | 304 (84.44%) | 0.55 ± 0.15 | 0.50 | 0.44 | 0.67 | 0.30 | 0.80 | 0.04 | 0.88 |
| Dec | 277 (74.46%) | 0.61 ± 0.16 | 0.63 | 0.50 | 0.75 | 0.33 | 0.83 | 0.19 | 0.93 |
| Total | 3742 (85.38%) | 0.58 ± 0.15 | 0.60 | 0.50 | 0.68 | 0.33 | 0.82 | 0.04 | 0.97 |

Table 4

Yearly statistics of the AOD (440 nm) and AE parameters for the period 2003–2014 based on daily values, with the number of days (with percentage in parentheses), mean, median, percentiles (P25, P75, P5, P95), minimum (Min) and maximum (Max) values.

| Year | N. days (%) | Mean ± STD | Median | P25 | P75 | P5 | P95 | Min | Max |
|-----------------------------------|---------------|-------------|--------|------|------|-------|------|-------|------|
| Aerosol Optical Depth, AOD | | | | | | | | | |
| 2003 | 156 (42.74%) | 0.18 ± 0.11 | 0.15 | 0.10 | 0.24 | 0.055 | 0.38 | 0.029 | 0.59 |
| 2004 | 265 (72.40%) | 0.15 ± 0.12 | 0.12 | 0.07 | 0.19 | 0.041 | 0.38 | 0.026 | 0.87 |
| 2005 | 295 (80.82%) | 0.15 ± 0.09 | 0.13 | 0.09 | 0.19 | 0.056 | 0.31 | 0.033 | 0.80 |
| 2006 | 190 (52.05%) | 0.14 ± 0.09 | 0.13 | 0.07 | 0.19 | 0.038 | 0.30 | 0.016 | 0.42 |
| 2007 | 271 (74.25%) | 0.14 ± 0.10 | 0.11 | 0.07 | 0.18 | 0.038 | 0.33 | 0.026 | 0.71 |
| 2008 | 280 (76.50%) | 0.12 ± 0.08 | 0.11 | 0.07 | 0.15 | 0.044 | 0.27 | 0.030 | 0.61 |
| 2009 | 256 (70.14%) | 0.12 ± 0.06 | 0.11 | 0.07 | 0.15 | 0.045 | 0.26 | 0.032 | 0.35 |
| 2010 | 244 (66.85%) | 0.11 ± 0.08 | 0.08 | 0.05 | 0.13 | 0.031 | 0.26 | 0.022 | 0.53 |
| 2011 | 269 (73.70%) | 0.14 ± 0.09 | 0.12 | 0.08 | 0.19 | 0.053 | 0.32 | 0.032 | 0.57 |
| 2012 | 252 (68.85%) | 0.12 ± 0.09 | 0.09 | 0.07 | 0.14 | 0.044 | 0.33 | 0.031 | 0.47 |
| 2013 | 220 (60.27%) | 0.10 ± 0.09 | 0.08 | 0.05 | 0.11 | 0.027 | 0.30 | 0.017 | 0.61 |
| 2014 | 249 (68.22%) | 0.11 ± 0.07 | 0.08 | 0.06 | 0.13 | 0.034 | 0.23 | 0.014 | 0.37 |
| Total | 2947 (67.24%) | 0.13 ± 0.09 | 0.11 | 0.07 | 0.16 | 0.04 | 0.31 | 0.014 | 0.87 |
| Ångström Parameter, AE | | | | | | | | | |
| 2003 | 156 (42.74%) | 1.27 ± 0.30 | 1.33 | 1.06 | 1.51 | 0.76 | 1.64 | 0.291 | 1.81 |
| 2004 | 265 (72.40%) | 1.35 ± 0.40 | 1.41 | 1.10 | 1.66 | 0.61 | 1.87 | 0.086 | 2.07 |
| 2005 | 295 (80.82%) | 1.38 ± 0.34 | 1.44 | 1.23 | 1.63 | 0.63 | 1.76 | 0.225 | 1.91 |
| 2006 | 190 (52.05%) | 1.25 ± 0.40 | 1.32 | 1.04 | 1.52 | 0.50 | 1.74 | 0.082 | 1.97 |
| 2007 | 270 (73.97%) | 1.46 ± 0.43 | 1.51 | 1.21 | 1.79 | 0.69 | 2.08 | 0.145 | 2.53 |
| 2008 | 280 (76.50%) | 1.22 ± 0.34 | 1.29 | 0.99 | 1.49 | 0.61 | 1.65 | 0.015 | 1.89 |
| 2009 | 256 (70.14%) | 1.24 ± 0.27 | 1.26 | 1.07 | 1.44 | 0.73 | 1.61 | 0.370 | 1.87 |
| 2010 | 244 (66.85%) | 1.11 ± 0.33 | 1.18 | 0.89 | 1.36 | 0.53 | 1.56 | 0.183 | 1.83 |
| 2011 | 269 (73.70%) | 1.35 ± 0.34 | 1.42 | 1.18 | 1.60 | 0.66 | 1.77 | 0.186 | 1.85 |
| 2012 | 252 (68.85%) | 1.24 ± 0.34 | 1.34 | 1.08 | 1.47 | 0.59 | 1.69 | 0.153 | 1.82 |
| 2013 | 220 (60.27%) | 1.22 ± 0.34 | 1.30 | 1.01 | 1.48 | 0.60 | 1.72 | 0.222 | 1.83 |
| 2014 | 249 (68.22%) | 1.25 ± 0.38 | 1.30 | 1.01 | 1.54 | 0.45 | 1.79 | 0.176 | 1.88 |
| Total | 2947 (67.24%) | 1.28 ± 0.37 | 1.34 | 1.06 | 1.54 | 0.60 | 1.79 | 0.015 | 2.53 |

transported pollutants of anthropogenic origin (see P95 percentiles in Tables 2 and 3). We must bear in mind that in this area only desert dust (DD) outbreaks contribute substantially to the values of PM_x, whereas fine particles which characterize anthropogenic pollution aerosols events, have relatively less influence over mass concentration. On the contrary, AOD is impacted in a similar way by

both types of events. This fact partly explains the differences between both annual cycles, one of the most important causes being the vertical distribution of aerosols and the complex deposition processes introducing different time delay between surface and columnar detections. Another reason is the intrinsic differences in measurement techniques of both quantities, as already mentioned.

Table 5

Yearly statistics of the PM₁₀ and PM ratio for the period 2003e2014 based on daily values, with the number of days (with percentage in parentheses), mean, median, percentiles (P25, P75, P5, P95), minimum (Min) and maximum (Max) values.

| Year | N. days (%) | Mean ± STD | Median | P25 | P75 | P5 | P95 | Min | Max |
|-------------------------------------------------------|---------------|---------------|--------|------|------|------|------|------|------|
| PM₁₀ | | | | | | | | | |
| 2003 | 330 (90.41%) | 13.02 ± 10.0 | 10 | 6 | 17 | 3 | 32 | 2 | 62 |
| 2004 | 338 (92.35%) | 13.45 ± 14.70 | 10 | 7 | 15 | 4 | 30 | 3 | 197 |
| 2005 | 330 (90.41%) | 13.09 ± 12.97 | 10 | 6 | 16 | 4 | 29 | 2 | 143 |
| 2006 | 339 (92.88%) | 11.30 ± 7.44 | 10 | 6 | 15 | 3 | 27 | 2 | 49 |
| 2007 | 336 (92.05%) | 10.89 ± 7.72 | 9 | 6 | 13 | 4 | 23 | 1 | 68 |
| 2008 | 317 (86.61%) | 10.02 ± 6.88 | 9 | 5 | 13 | 3 | 24 | 2 | 45 |
| 2009 | 329 (90.14%) | 9.22 ± 5.26 | 8 | 5 | 12 | 3 | 19 | 2 | 34 |
| 2010 | 331 (90.68%) | 8.99 ± 8.35 | 8 | 5 | 11 | 3 | 18 | 2 | 94 |
| 2011 | 340 (93.15%) | 10.25 ± 6.99 | 9 | 5 | 12 | 3 | 23 | 2 | 48 |
| 2012 | 315 (86.07%) | 9.26 ± 8.43 | 7 | 5 | 11 | 3 | 20 | 2 | 90 |
| 2013 | 328 (89.86%) | 8.15 ± 5.57 | 7 | 4 | 10 | 3 | 19 | 2 | 43 |
| 2014 | 316 (86.58%) | 8.84 ± 6.27 | 7 | 5 | 11 | 3 | 20 | 2 | 45 |
| Total | 3949 (90.1%) | 10.56 ± 9.01 | 8 | 5 | 13 | 3 | 25 | 1 | 197 |
| PM ratio PR % PM_{2.5}/PM₁₀ | | | | | | | | | |
| 2003 | 308 (84.38%) | 0.63 ± 0.13 | 0.65 | 0.56 | 0.71 | 0.39 | 0.82 | 0.25 | 0.94 |
| 2004 | 323 (88.25%) | 0.66 ± 0.13 | 0.67 | 0.57 | 0.75 | 0.43 | 0.86 | 0.25 | 0.96 |
| 2005 | 326 (89.32%) | 0.63 ± 0.14 | 0.62 | 0.50 | 0.71 | 0.36 | 0.83 | 0.14 | 0.93 |
| 2006 | 318 (87.12%) | 0.62 ± 0.15 | 0.63 | 0.50 | 0.75 | 0.36 | 0.60 | 0.17 | 0.93 |
| 2007 | 317 (86.85%) | 0.60 ± 0.14 | 0.60 | 0.50 | 0.70 | 0.38 | 0.82 | 0.20 | 0.93 |
| 2008 | 299 (81.69%) | 0.65 ± 0.14 | 0.67 | 0.57 | 0.75 | 0.40 | 0.86 | 0.17 | 0.94 |
| 2009 | 315 (86.30%) | 0.57 ± 0.13 | 0.56 | 0.50 | 0.67 | 0.37 | 0.77 | 0.24 | 0.90 |
| 2010 | 319 (87.40%) | 0.56 ± 0.13 | 0.55 | 0.50 | 0.67 | 0.33 | 0.77 | 0.20 | 0.88 |
| 2011 | 326 (89.32%) | 0.53 ± 0.14 | 0.50 | 0.42 | 0.63 | 0.33 | 0.80 | 0.20 | 0.92 |
| 2012 | 299 (81.69%) | 0.50 ± 0.15 | 0.50 | 0.39 | 0.62 | 0.29 | 0.75 | 0.19 | 0.97 |
| 2013 | 305 (83.56%) | 0.53 ± 0.13 | 0.55 | 0.44 | 0.63 | 0.33 | 0.73 | 0.08 | 0.86 |
| 2014 | 287 (78.63%) | 0.53 ± 0.14 | 0.50 | 0.42 | 0.63 | 0.30 | 0.79 | 0.04 | 0.92 |
| Total | 3742 (85.38%) | 0.58 ± 0.15 | 0.60 | 0.50 | 0.68 | 0.33 | 0.82 | 0.04 | 0.97 |

3.1.2. Interannual variability and trends

A moderate year-to-year variability of both PM₁₀ and AOD data is observed in Fig. 3a with a similar decreasing trend during the period 2003e2014. Using the Mann-Kendall Trend Test with the Sen's Slope method (e.g., Mateos et al., 2015), PM₁₀ gives a trend of -0.42 mg m⁻³ per year with a 95% confidence interval of [-0.55, -0.3], thus resulting in a reduction of 40% during the period 2003e2014. The AOD trend is -0.005 (-38%) with a confidence interval of [-0.007, -0.004]. Hence, both parameters show similar reduction, which suggests that the evolution of one of these parameters can be inferred from the other. These decreasing trends and possible causes have been analysed recently by various authors for PMx data (Barmpadimos et al., 2012; Cusack et al., 2012; Querol et al., 2014; Mateos et al., 2015) and for AOD (Mateos et al., 2014, 2015) over the Iberian Peninsula. Although not relevant, the differences between the results of these authors can be attributed to the use of different mean values (yearly or monthly), periods and methods.

Fig. 3b presents the inter-annual variability for the PM ratio and AE parameters, where AE appears to be more variable than PR (also at monthly level, not shown here). Though weak as compared to that of AOD/PM₁₀, there is also a decreasing trend which is more pronounced in PR and less obvious in AE. For each year PM ratio remains relatively constant throughout the seasons with some slight differences between one year and the other during summer (not shown). On the contrary, for AE the shape of the seasonal pattern appears to be different from one year to the next, thus on a monthly level AE parameter is more variable than PR. In order to properly interpret these results, we must bear in mind that AE can vary from 0 to 2.5 while PR range is between 0 and 1. The PR exhibits a reduction trend over the 12 analysed years of 22% (due to the fact that PM_{2.5} presents a reduction of ~60%) whereas AE only shows 8% reduction (value within the range of annual variability), which highlights the fact that each quantity is related to particle size in a different way: PR linked with the strong reduction of

particle concentration and AE more linked with the AOD spectral dependence (remember that the effectivity of particle-radiation interaction is related to the size of particles and the range of wavelength).

It is important to note here that the observed differences between these surface and columnar properties cannot be attributed to different samplings (i.e. total number daily data around 70% for AOD against 90% for "in-situ" data), since the climatological analysis using only PM₁₀-AOD coincident pairs yields to similar results. Bear in mind that PMx measurements are made under all weather conditions including overcast and/or partially cloudy conditions where there are no or few available data for the AOD. Cloud screening in AOD measurements under highly variable turbidity episodes (such as relatively strong desert dust intrusions) affected by clouds is extremely difficult. Therefore, specific cases such as a desert dust episodes clearly detected by PMx data, may not be visible in AOD, leading to discrepancies in monthly means which in turn affect yearly means. In the present data set yearly means are not affected by these sampling issues and correlate strongly as shown later on (section 3.2.2). However, if a high discrepancy in PMx-AOD yearly mean is observed, it is reasonable to suspect possible problems in the database.

3.2. Relationships between AOD-AE, PM₁₀ -PR

In order to better understand the relationship between columnar-surface quantities it is relevant to know previously the distinct behaviour of each pair: AE-AOD on one hand and PR-PM₁₀ on the other.

3.2.1. AE-AOD columnar relationship

Fig. 4 is a plot of the AE parameter versus AOD for daily (Fig. 4aeb) and instantaneous databases (Fig. 4ced) with values of PM₁₀ (a, c) and PR (b, d) represented by a colour scale. For sake of clarity, Figures S1 and S2 (supplementary material) separately

show each category of PM₁₀ or PR and a 3D plot of the AE vs. AOD. These AE-AOD scatterplots of intensive-extensive quantities are part of the general site aerosol characterization and hence frequently used in columnar aerosol studies. Indeed they link particle size with the amount of aerosols allowing to classify or discriminate aerosol types according to defined aerosol climatological models, such as continental, maritime, desert dust, biomass burning, etc. (Hess et al., 1998; Eck et al., 1999; Kim et al., 2004; Vergaz et al., 2005; Toledano et al., 2007a; Kaskaoutis et al., 2009; Kumar et al., 2014). and to quantify their respective contribution. The PM₁₀ and PR range values in the graphs of Fig. 4 allow a comprehensive analysis of these four quantities, and together with Fig. 5 are necessary for a deeper interpretation of the relationship between them.

As it can be seen in Fig. 4a, most AOD-AE daily averages (about 80%) are in the range of 0.0e0.2 and 1.0e2.0 respectively, which are typical of a clean continental area (e.g., Toledano et al., 2009; Bennouna et al., 2013). PM₁₀ values from 0 to 10 mg m⁻³ (50% of total) extend over the whole range of AOD with 47% corresponding to AOD :: 0.10 (inset in Fig. 4a). For these data sets AE parameter also cover all range of sizes from 0 to 2. These values of PM₁₀ below 10 mg m⁻³ together with those between 10 and 20 mg m⁻³ (38% of data) are the most frequent and extend over all the ranges of the plot (dark and light blue points), considerably surpassing the AOD value of 0.2 and even reaching the highest AOD values. Bearing in mind that the average of AOD is 0.13 ± 0.9, mean value plus the

standard deviation is 0.22, therefore values higher than this threshold may be considered events of high turbidity in this area, being considered as high-to-moderate between 0.2 and 0.3 and higher than 0.3 as strong-extreme cases. These cases of high turbidity represent 18% of the total AOD database. On the other hand, PM₁₀ values larger than 20 mg m⁻³ only represent 12% of total data which are represented by green points in Fig. 4a (PM₁₀ between 20 and 40 mg m⁻³ with AOD from 0.1 to 0.6) and red-brown points (PM₁₀ greater than 40 mg m⁻³ are only 2.6% of the total values, thus few days correspond to strong-extreme events of high turbidity) in Fig. 4a.

The same can be observed in Fig. 4c corresponding to instantaneous values, which illustrates a more detailed information and provides a better view of the results. For example, the particularly strong extreme events in AOD correspond to intense desert dust intrusions of very low AE values (bottom branches of brown colour with PM₁₀ values higher than 50 mg m⁻³) or to anthropogenic pollution events coming from far off areas of our region with high values of AE (top branches of green colour). Furthermore, mixed aerosol type (blue light colour) with values of AE in 1e1.5 but moderate PM₁₀ values (10e20 mg m⁻³ interval) are clearly visible in the center of Fig. 4c. Although these two Fig. 4(a, c) allow a good characterization of aerosols, we must note that in general there is a great mixing between the different range of values of both PM₁₀ and AOD data. This behaviour means a weak connection between AOD and PM₁₀ under certain conditions when taking daily data, as

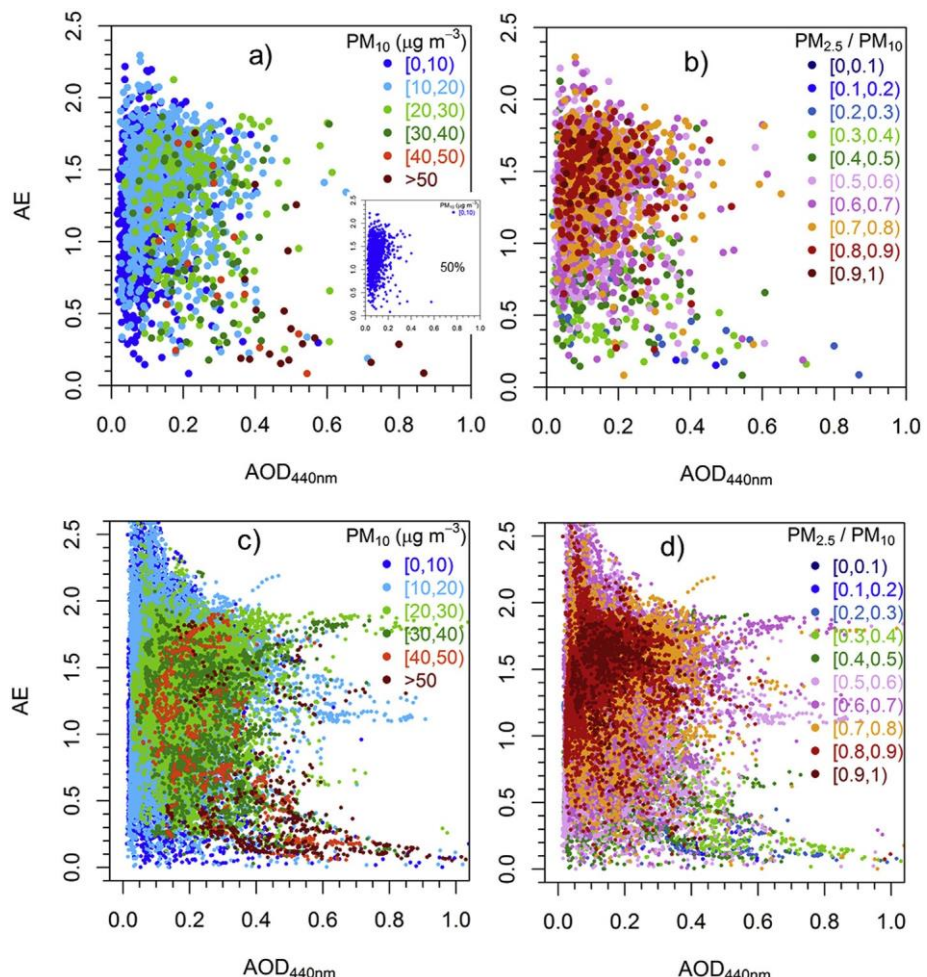


Fig. 4. Scatterplots of AE vs. AOD for (a, b) daily and (c, d) instantaneous data with the corresponding colour scale range of (a, c) PM₁₀ and (b, d) PM ratio, for the period 2003e2014.

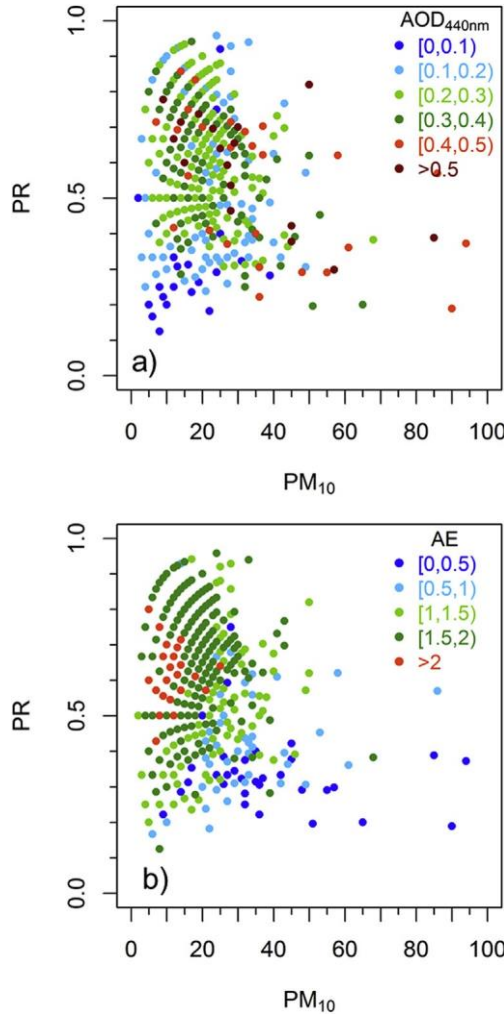


Fig. 5. Scatterplots of PM ratio vs. PM₁₀ daily data with the colour scale range for (a) AOD and (b) AE, for the period 2003e2014.

discussed later on.

With respect to particle size Fig. 4b,d illustrate the behaviour of daily and instantaneous AE-AOD values but now with the colour scale representing PR values. Values of PR below 0.3 are not frequent (blue points: 2% of total) and also correspond to the lowest AE values. These values represent very pure desert dust aerosols (or weakly mixed with other aerosol types during transport) with values of AOD beyond 0.2. The PR values between 0.3 and 0.5 (green points, 19%) are largely missing from the figure but they span the whole range of AE (between low values up to ~2) and AOD. The majority of PR daily data (purple points, 50%) range from 0.5 to 0.7 and cover all the ranges on the AE-AOD plot with the exception of extreme desert dust (bottom-right area). These PR values represent medium particle size, also corroborated by AE values (observe the branches at AE ~1.3 and that at 1.8), and include pollution episodes with the highest AOD (right-top branches) which is not the case for PM₁₀. The PR values larger than 0.7 (orange, red and brown colours points, ~23%) point out particles of medium-to-fine size and hence have values of AE greater than 1 and with AOD values up to 0.4. The region around AE ~1.2e1.5 and AOD ~0.1 corresponds to the highest density of data points.

3.2.2. Surface PR-PM₁₀ relationship

Fig. 5a**e**b presents the scatterplots of daily data of PR versus

PM₁₀ (equivalent to Fig. 4a**e**b for AE-AOD) with values of AOD and AE represented by a colour scale. For shake of clarity, Figures S3 and S4 (supplementary material) separately show each category of AOD or AE and a 3D plot of the PR vs. PM₁₀. These scatterplots are not usually analysed in air quality studies based on PMx data. As only daily values are available for these quantities, there is a certain limitation in the information compared to the combination of AOD-AE data (Fig. 4 c**d**e), especially when events must be analysed in detail. The most curious is the shape the data points take in the figure, curves resembling those of "the wings of a butterfly", which are due to the low values of PMx where the points are discretized (integer values for PM₁₀ and PM_{2.5}) and superimposed. As it can be seen, only for very low PR values (less than 0.4) or larger PM₁₀ values (about 20 mg m⁻³) the points appear as scattered points in the figure. This discretized behaviour makes that important information is missing in the figure. Blue points are masked in Fig. 5a (this information can be seen in supplementary material), and they correspond to AOD from 0 to 0.2 and account for the majority of all points.

In Fig. 5b (with AE in the colour scale) only the range of light-green points for AE between 1 and 1.5 are masked by superimposed dark-green points of AE values between 1.5 and 2. Both ranges, representing medium and fine particles, are the most abundant. Obviously, most of the behaviour shown by Fig. 5 is

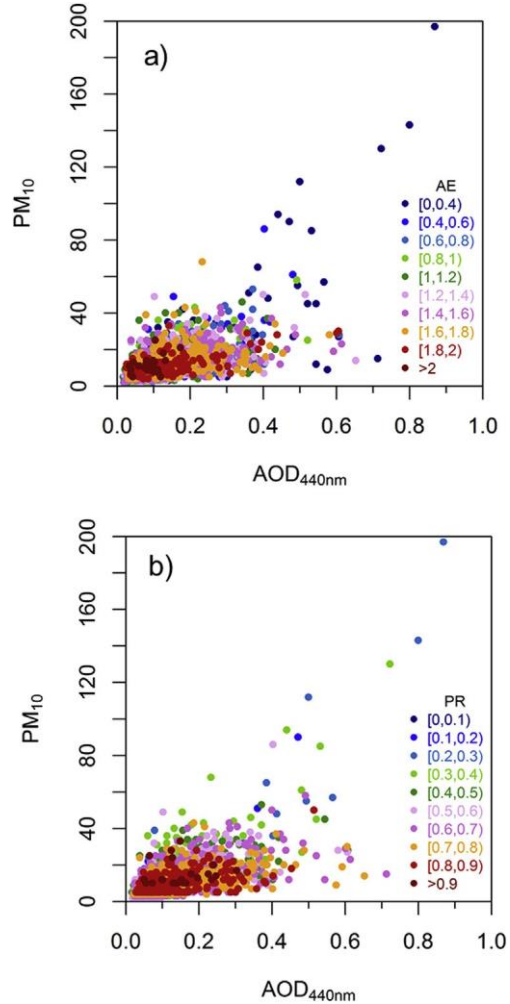


Fig. 6. Scatterplots of PM₁₀ vs. AOD daily data with the colour scale range for (a) AE and (b) PM ratio, for the period 2003e2014.

already described in Fig. 4. However, it is relevant to conclude that AOD-AE scatterplot for daily data contain more useful information than that of PM₁₀-PR. The reason behind this behaviour is that AE has more valuable information about particle size than PR, as mentioned before. Actually, PR is a simple ratio of concentrations but AE contains the spectral AOD dependence, which according to the Mie Theory carries useful information about particle size because of the complex interaction of particle and radiation.

3.3. Relationships between columnar and surface load of aerosols, PM₁₀-AOD

The useful information given by the above plots will help us to better interpret the PM₁₀-AOD relationship. Fig. 6a**b** shows this

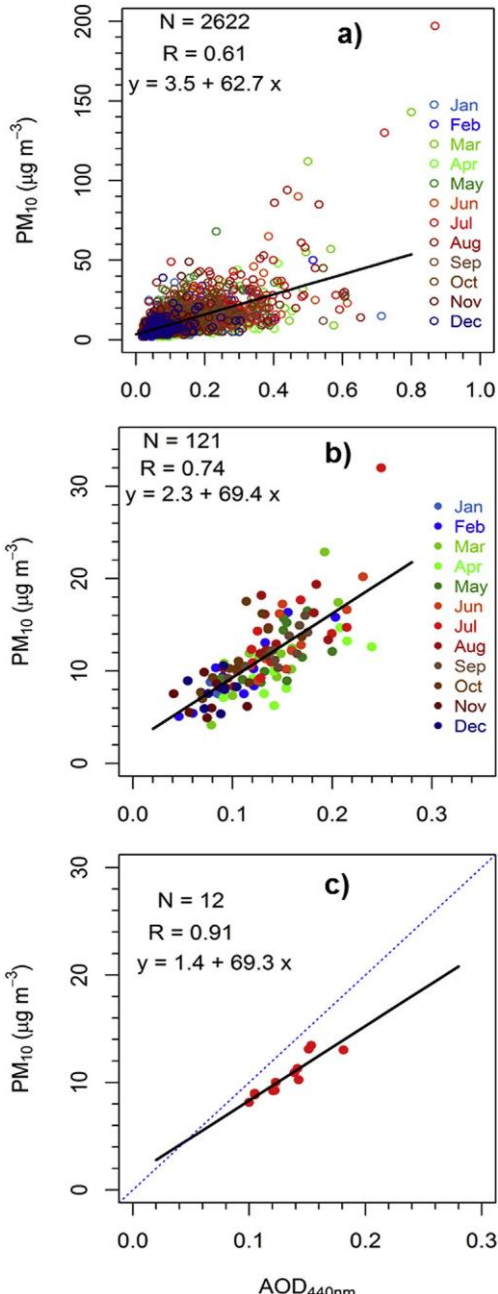


Fig. 7. Scatterplots of PM₁₀ vs. AOD taking (a) daily, (b) monthly and (c) yearly values with associated linear fits.

relationship using the 2622 coincident days where AE and PR values are represented by a colour scale, respectively. The moderated-to-low correlation of PM₁₀-AOD is due to the bulk of points covering the different ranges of values as analysed before. For instance, values of PM₁₀ below 20 $\mu\text{g m}^{-3}$ contain most of the AOD values up to 0.3. There are very few points beyond AOD \approx 0.4 and PM₁₀ \approx 40 $\mu\text{g m}^{-3}$ which are well observed in the graph, most of them corresponding to desert dust intrusions (e.g., Cachorro et al., 2008, 2013; 2014) as it is indicated by the blue colour of AE and PR. Days of anthropogenic pollution are also detected with moderated-to-high values of AE and PR (purple and orange colours). As expected, in general PM₁₀ values increase with AOD but with a wide range of variation. For episodes of high-to-extreme intensity, both AOD and PM₁₀ present high values and their correlation is very dependent on the type of episode (anthropogenic pollution or desert dust) and on atmospheric conditions. For example, in the case of desert dust episodes there are important day-delays between the detection by PM₁₀ and by AOD, which cannot be explained easily due to the complex deposition processes.

The correlation established in Fig. 7a for daily data presents a slope of 62.7 and an intercept of 3.5 (a slope of 80.0 is obtained when the line is constrained to pass through the origin). As expected, and considering other works (e.g., Kacenelenbogen et al.,

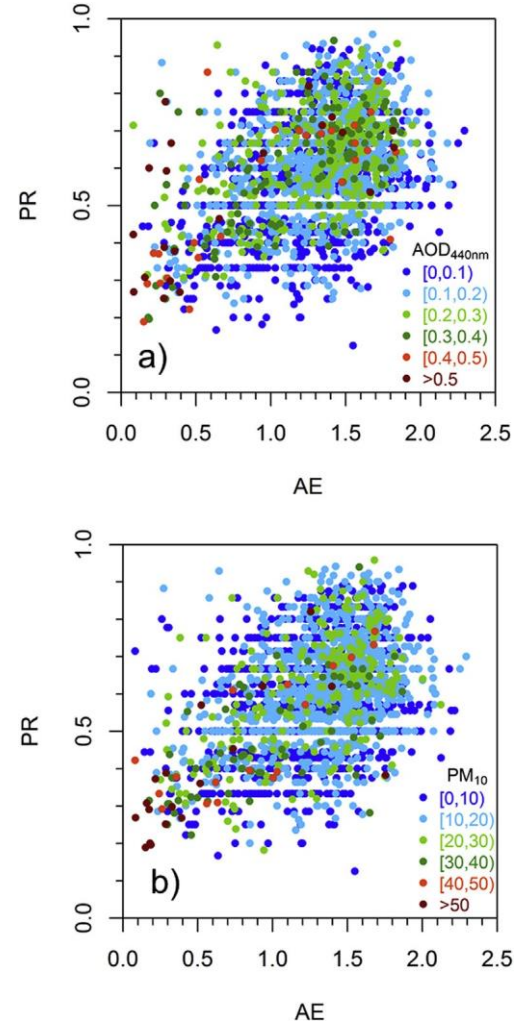


Fig. 8. Scatterplots of PM ratio vs. AE daily data with the colour scale range for (a) AOD and (b) PM₁₀, for the period 2003e2014.

2006; Estelles et al., 2012), these two parameters are moderately correlated with a correlation coefficient of 0.61 (p-value less than 0.001), lying between the 95% confidence interval (0.54e1). The PM₁₀-AOD correlation is improved when considering monthly means (Fig. 7b) increasing the correlation coefficient to 0.74 (p-value less than 0.001), with a slope of 69.4 and an intercept of 2.3. Finally the correlation for yearly data (Fig. 7c) has a similar slope to monthly data and an intercept of 1.4, with a very high correlation coefficient R ≈ 0.9. Indeed, a likely primary reason for this overall moderate correlation is the high variability of aerosols in a short range of AOD and PM₁₀ due to the clean conditions of the area where the prevailing particles (about 85%) are medium-to-fine size with AE between 0.8 and 1.7 and PR between 0.5 and 0.8. These aerosol particles have a large influence on AOD but contribute much less to mass of PM₁₀ in comparison to larger particles.

3.4. Relationships between columnar and surface particle size parameters: PR-AE

Finally, Fig. 8 plots PR versus AE with values of AOD and PM₁₀ represented by a colour scale. For shake of clarity, Figures S5 and S6 (supplementary material) separately show each category of AOD or PM₁₀ and a 3D plot of the PR vs. AE. As can be seen, a very low correlation exists between daily values of both parameters because dark and light blue colours extend everywhere covering all the AE-PR ranges. Green points that represent high turbidity events of moderate-to-high intensity, i.e. AOD in the range (0.2, 0.4) and PM₁₀ in (20, 40 mg m⁻³), are mainly positioned over the range of fine particles (towards the right-top about PR ≈ 0.7 and AE ≈ 1.5) but also extend everywhere. Finally red-brown points of very high and extreme turbidity episodes appear defined by two clusters (although with some sparse points) for AOD (Fig. 8a) but not for PM₁₀ (Fig. 8b). One cluster given by desert dust type (bottom-left) appears in both Fig. 8a,b but the cluster representing anthropogenic aerosols (industrial, urban, or biomass burning, right-top) is

not well defined for PM₁₀ values in Fig. 8b. One possible reason may be that mineral dust particles have a larger density as compared to anthropogenic aerosols for the same AOD value because the former have a larger impact on the mass concentration over the PMx filters.

These established correlations are highly site-dependent and this limits its possible application to other areas but they may be useful when there is a lack of PM₁₀ or AOD data over long time periods. Furthermore, we have observed that the non-correspondence between both quantities for yearly data (for example AOD increase with a PM₁₀ decrease) allows the detection of possible problems in the data series.

3.5. PM₁₀-AOD and PR-AE relationship using binned data

Finally, because of the low correlation in the day-by-day data between the four quantities as described above, in Fig. 9 we have examined using binned data fundamental PM₁₀-AOD and PR-AE relationships but also the complementary relationships PM₁₀-AE and PR-AOD. In Fig. 9a, PM₁₀ is represented as a function of the binned AOD, in the interval 0e1 by steps of 0.05. Each point of the curve corresponds to PM₁₀ average for a given bin of AOD, and the associated standard deviation is represented by vertical bars. As shown, PM₁₀ increases slowly and regularly as the AOD reaches about 0.25, but beyond this value the increasing slope is more irregular until PM₁₀ reaches a maximum of about 47 mg m⁻³ (at AOD ≈ 0.55). For AOD > 0.55 there are only few data (see histogram) with irregular increasing or decreasing behaviour of PM₁₀ values, which correspond to exceptionally strong events of high atmospheric turbidity. These highest AOD with the highest PM₁₀ values (i.e., appearing as scattered points in Figs. 4 and 6) belong in general to desert dust intrusions (as the study case of July 2004 described in Cachorro et al., 2008), while other are due to episodes of anthropogenic pollution or biomass burning.

In these cases both types of data, PM₁₀ and/or AOD data detect

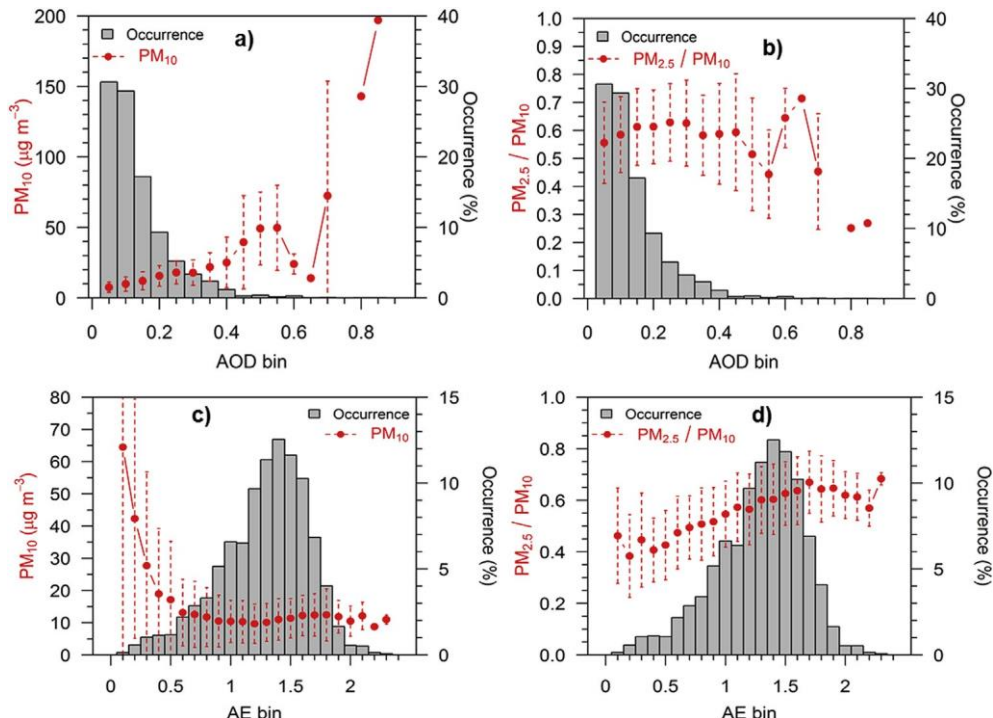


Fig. 9. PM₁₀ as a function of (a) binned AOD data and (c) binned AE data. Idem for PM ratio respectively (b, d). The bars represent the standard deviation for EMEP data within each bin. The data counts for each bin (relative occurrence) are also shown on the superimposed histogram.

the existence of a strong event but do not always correspond in time. In the case of desert dust outbreaks for example, the maximum of AOD is not always coincident with the maximum of PM₁₀ on a daily basis. This is because of the sedimentation process, as it is the case for the episode of low AOD and high PM₁₀ observed in Fig. 7a (dark green point corresponding to the month of May). In the case of strong anthropogenic pollution episodes the high AOD is generally accompanied by lower PM₁₀ values as compared with desert dust intrusions.

These results are corroborated by Fig. 9b, which is analogous to Fig. 9a but this time with PR instead of PM₁₀. The slight increase in PM₁₀-AOD observed in the previous graph for low AOD is reflected here in the nearly constant behaviour of PR around 0.6, being practically independent of the AOD. For the last points with AOD higher than 0.5 (a very irregular zone), PR presents minima in the same AOD bins where the maxima are observed for the PM₁₀ and vice versa, indicating a high correlation between bin-averaged data of PR-PM₁₀. This explains the fact that high episodes are well detected by the two data series of PM₁₀ and AOD, but not necessarily with a systematic day-to-day correlation.

Fig. 9c,d presents analogous plots where the same data are binned according to AE values. As expected and observed in Fig. 9c, PM₁₀ bin-averaged and associated standard deviation are the highest for the lowest AE values, which correspond to the occurrence of desert dust intrusions. The highest PM₁₀ values decrease sharply until AE \approx 0.6, followed by a nearly stable behaviour for AE values above 0.7. This result for PM₁₀-AE highlights the well-known inverse correlation AOD-AE for desert dust episodes. In Fig. 9d, PM ratio increases monotonically and smoothly with the increase of AE in all AE ranges, just breaking at both extremes where irregularities occur under desert dust (left) or high-pollution (right) episodes. This figure emphasizes the existence of a low correlation between these two parameters as illustrated also by Fig. 8. It is only under very high or extreme episodes with very low or very high AE or PR values, when both quantities present a clear correspondence.

4. Conclusions

In this study long-term data (2003e2014) of two nearby background sites in the North-central Iberian Peninsula were used to analyse the relationship between surface and columnar aerosol loads considering PM₁₀, AOD, AE and PR data, where PM₁₀ and AOD indicate the aerosol load, and AE and PR are related with particle size. The different relationships between these four quantities are investigated from a climatological point of view which also provides a general characterization of these key aerosol properties in a regional background environment.

This perspective is different of that presented in previous studies, mainly focused on establishing empirical relations between PM_x ($x \leq 10 \text{ mm}$ or 2.5 mm) and AOD in order to estimate or predict PM_x as a parameter that addresses air quality over big cities or large polluted areas. In most of these cases the AOD is provided by satellite sensors, which indeed presents the great advantage of large spatial coverage, but also carries much larger uncertainty as compared to ground-based measurements. Here, the study is carried out over a clean environment where the synergies between surface and columnar aerosol properties are long-term established.

The different relationships between these surface-columnar quantities are analysed by means of scatterplots because of their ability to show nonlinear relationships between the different parameters. In this study, not only the correlation between the aerosol load represented by PM₁₀ and AOD is thoroughly analysed, but also their relations with AE and PR. Although there is, to a greater or lesser extent, a physical-theoretical basis to support the existent relationships between them, the complex physical processes and

the dependences on other involved factors give rise to consideration of these relations from an empirical point of view. As a consequence, the mathematical expressions sometimes established (e.g., simple linear equation), are not always recommended.

Although the encountered correlations are generally low for daily data, they improve considerably for monthly or yearly means, and give very consistent relationships for binned data. As already mentioned these relationships depend on the aerosol characteristics of the site, and because of the clean and background conditions of our study area, they present a short range of AOD and PM₁₀ values compared to other more polluted areas.

Despite the limitations mentioned throughout the paper, it is shown that for long-term series the synergy between surface and columnar remotely sensed data can still be quantitatively explored to provide useful information for aerosol characterization and general trends from a climatological point of view.

Acknowledgements

The authors are grateful to EMEP and MAGRAMA ("Ministerio de Agricultura, Alimentación y Medio Ambiente" of Spain) for providing PM_x observations. Special thanks also go to NASA/GSFC, PHOTONS/LOA and RIMA/GOA people for their longstanding collaboration and for operating and maintaining the AERONET network. Thanks to Spanish Government (by means of the Ministerio de Economía y Competitividad, MINECO) for the financial support of the: a) FPI grant BES-2012-051868; b) "Juan de la Cierva - Incorporación" grant IJCI-2014-19477; and c) project CMT2015-66742-R. We also thank to the Environmental Council of the CyL Regional Government ("Consejería de Medio Ambiente, Junta de Castilla y León") for supporting this research about atmospheric aerosols as well as Consejería de Educación for supporting the project VA100U14. Furthermore, the research leading to these results has received funding from the European Union Seventh Framework Programme (FP7/2007e2013) under grant agreement Nr. 654109 [ACTRIS 2].

Appendix A. Supplementary data

Supplementary data related to this article can be found at <http://dx.doi.org/10.1016/j.atmosenv.2016.05.061>.

References

- Barmpadimos, I., Keller, J., Oderbolz, D., Hueglin, C., Prévôt, A.S.H., 2012. One decade of parallel fine (PM_{2.5}) and coarse (PM₁₀ePM_{2.5}) particulate matter measurements in Europe: trends and variability. *Atmos. Chem. Phys.* 12, 3189e3203. <http://dx.doi.org/10.5194/acp-12-3189-2012>.
- Bennouna, Y., Cachorro, V.E., Toledano, C., Berjón, A., Prats, N., Fuertes, D., González, R., Rodrigo, R., Torres, B., de Frutos, A., 2011. Comparison of atmospheric aerosol climatologies over southwestern Spain derived from AERONET and MODIS. *Remote Sens. Environ.* 115, 1272e1284. <http://dx.doi.org/10.1016/j.rse.2011.01.011>.
- Bennouna, Y., Cachorro, V.E., Torres, B., Toledano, C., Berjón, A., de Frutos, A., Alonso Fernández-Coppel, I., 2013. Atmospheric turbidity and the annual cycle of aerosol optical depth over north-central Spain with ground (AERONET) and satellite (MODIS) remotely sensed data. *Atmos. Environ.* 67, 352e364.
- Boucher, O., Randall, D., Artaxo, P., Bretherton, C., Feingold, G., Forster, P., Kermanen, V.M., Kondo, Y., Liao, H., Lohmann, U., Rasch, P., Satheesh, S.K., Sherwood, S., Stevens, B., Zhang, X.Y., 2013. Clouds and aerosols. In: Stocker, T.F., Qin, D., Plattner, G.K., Tignor, M., Allen, S.K., Boschung, J., Nauels, A., Xia, Y., Bex, V., Midgley, P.M. (Eds.), *Climate Change 2013: The Physical Science Basis. Contribution of Working Group I to the Fifth Assessment Report of the Intergovernmental Panel on Climate Change* 2013. Cambridge University Press Cambridge, United Kingdom and New York, NY, USA.
- Brown, J.S., Gordon, T., Price, O., Asgharian, B., 2013. Thoracic and respirable particle definitions for human health risk assessment. Part. Fibre Toxicol. 10, 10e12. <http://dx.doi.org/10.1186/1743-8977-10-12>.
- Cachorro, V.E., Tanré, D., 1997. The correlation between particle mass loading and extinction: application to desert dust aerosol content estimation. *Remote Sens. Environ.* 60, 187e194.

- Cachorro, V.E., Duran, P., De Frutos, A.M., Vergaz, R., 2000. Measurements of the atmospheric turbidity of the north-center continental area in Spain: spectral aerosol optical thickness and Angstrom turbidity parameters. *J. Aerosol. Sci.* 31, 687e702.
- Cachorro, V.E., Toledano, C., Prats, N., Sorribas, M., Mogo, S., Berjón, A., Torres, B., Rodrigo, R., de la Rosa, J., De Frutos, A.M., 2008. The strongest desert dust intrusion mixed with smoke over the Iberian Peninsula registered with Sun photometry. *J. Geophys. Res.* 113, D14S04. <http://dx.doi.org/10.1029/2007JD009582>.
- Cachorro, V.E., Burgos, M.A., Bennouna, Y., Toledano, C., Herguedas, A., González Orcajo, J., de Frutos, A.M., 2013. Inventario del Aerosol Desértico en la Región de Castilla y León (2003e2012). In: Costa, María Joao, Silva, Ana Maria, Guerrero Rascado, Juan Luis, Pereira, Sérgio, Bortoli, Daniele, Salgado, Rui (Eds.), Proceedings Book of the 1st Iberian Meeting Aerosol Science and Technology RICTA 2013, Evora, Portugal, ISBN 978-989-20-3962-6. Available at: <http://www.ricta2013.cge.uevora.pt/wp-content/uploads/2013/10/E-ProcBook-RICTA2013.pdf>.
- Cachorro, V.E., Burgos, M.A., Bennouna, Y., Toledano, C., Torres, B., Mateos, D., Marcos, A., de Frutos, A.M., 2014. Characterization of PMx data belonging to the desert-dust inventory based on AOD-alpha RIMA-AERONET data at Palencia-Autilla stations. In: Rosell-Llompart, Joan, Grifoll, Jordi (Eds.), Proceedings Book of the 2nd Iberian Meeting Aerosol Science and Technology RICTA 2014, Tarragona, Spain. Available at: <http://digital.publicacionsurv.cat/index.php/purw/catalog/book/65>.
- Cusack, M., Alastuey, A., Pérez, N., Pey, J., Querol, X., 2012. Trends of particulate matter (PM2.5) and chemical composition at a regional background site in the Western Mediterranean over the last nine years (2002e2010). *Atmos. Chem. Phys.* 12, 8341e8357. <http://dx.doi.org/10.5194/acp-12-8341-2012>.
- Delucchi, M.A., Murphy, J.J., McCubbin, D.R., 2002. The health and visibility cost of air pollution: a comparison of estimation methods. *J. Environ. Manage.* 64, 139e152. <http://dx.doi.org/10.1006/jema.2001.0515>.
- Dubovik, O., Holben, B., Eck, T.F., Smirnov, A., Kaufman, Y.J., King, M.D., Tanré, D., Slutsker, I., 2002. Variability of absorption and optical properties of key aerosol types observed in worldwide locations. *J. Atmos. Sci.* 59, 590e608.
- EC, 1999. Directive 1999/30/EC of the European Parliament and of the Council (22 April 1999) relating to limit values for sulphur dioxide and oxides of nitrogen, PM and lead in ambient air. Official J. Eur. Communities L 163, 41e60.
- EC, 2008. Directive 2008/50/EC of the European parliament and of the Council (21 may 2008) on ambient air quality and cleaner air for Europe. Official J. Eur. Communities L 151, 1e44.
- Eck, T., Holben, B., Reid, J., Dubovik, O., Smirnov, A., O'Neill, N., Slutsker, I., Kinne, S., 1999. Wavelength dependence of the optical depth of biomass burning, urban, and desert dust aerosols. *J. Geophys. Res.* 104, 31333e31349.
- EMEP, 1996. EMEP/CCC-Report 1/95, EMEP Manual for Sampling and Chemical Analysis, Rev 2002. Norwegian Institute for Air Research available at: <http://www.nilu.no/projects/ccc/manual/index.html> (last access: 10 March 2014).
- EMEP, 2011. EMEP/CCC-Report 4/11, EMEP Transboundary Particulate Matter in Europe Status Report 2011. Norwegian Institute for Air Research available at: <http://www.nilu.no/projects/ccc/reports/emep4-2011.pdf> (last access: 10 March 2014).
- EMEP, 2014. EMEP/CCC-Report 3/2014, Data Report 2012 Acidifying and Eutrophying Compounds and Particulate Matter. Norwegian Institute for Air Research available at: <http://www.nilu.no/projects/ccc/reports/CCR3-2014.pdf> (last access: 1 October 2015).
- Escudero, M., Castillo, S., Querol, X., Avila, A., Alarcón, M., Viana, M., Alastuey, A., Cuevas, E., Rodríguez, S., 2005. Wet and dry African dust episodes over eastern Spain. *J. Geophys. Res.* 110, D18208. <http://dx.doi.org/10.1029/2004JD004731>.
- Escudero, M., Querol, X., Avila, A., Cuevas, E., 2007. Origin of the exceedances of the European daily PM limit value in regional background areas of Spain. *Atmos. Environ.* 41, 730e744.
- Estelles, V., Martínez-Lozano, J.A., Pey, J., Sicard, M., Querol, X., Esteve, A.R., Utrillas, M.P., Sorribas, M., Gangoiti, G., Alastuey, A., Rocadenbosch, F., 2012. Study of the correlation between columnar aerosol burden, suspended matter at ground and chemical components in a background European environment. *J. Geophys. Res.* 117, D04201. <http://dx.doi.org/10.1029/2011JD016356>.
- Füssel, H.M., Jol, A., 2012. Climate Change, Impacts and Vulnerability in Europe 2012 an Indicator-based Report. Publications Office of the European Union 2012, Luxembourg.
- Goloub, P., Cachorro, V.E., Cuevas, E., Blarel, L., Berjón, A., Toledano, C., Podvin, T., Lapionak, A., Guirado, C., Ramos, R., González, R., Fuertes, D., 2e7 September, 2012. The AERONET-Europe calibration facility: access within the ACTRIS Project. In: European Aerosol Conference, EAC2012, Granada, Spain.
- Hess, M., Koepke, P., Schult, I., 1998. Optical properties of aerosols and clouds: the software package OPAC. *B. Am. Meteorol. Soc.* 79, 831e844.
- Holben, B.N., Eck, T.F., Slutsker, I., Tanré, D., Buis, J.P., Setzer, A., Vermote, E., Reagan, J.A., Kaufman, Y.J., Nakajima, T., Lavenu, F., Jankowiak, I., Smirnov, A., 1998. AERONET e a federated instrument network and data archive for aerosol characterization. *Remote Sens. Environ.* 66, 1e16.
- Holben, B., Tanré, D., Smirnov, A., Eck, T., Slutsker, I., Abuhaman, N., Newcomb, W., Schafer, J., Chatenet, B., Lavenu, F., Kaufman, Y.J., Vande Castle, J., Setzer, A., Markham, B., Clark, D., Frouin, R., Halthore, R., Karneli, A., O'Neill, N.T., Pietras, C., Pinker, R.T., Voss, K., Zibordi, G., 2001. An emerging ground-based aerosol climatology: aerosol optical depth from AERONET. *J. Geophys. Res.* 106, 12067e12097.
- Kacenelenbogen, M., Léon, J.F., Chiapello, I., Tanré, D., 2006. Characterization of aerosol pollution events in France using ground-based and POLDER-2 satellite data. *Atmos. Chem. Phys.* 6, 4843e4849.
- Kaskaoutis, D.G., Badarinath, K.V.S., Kharol, S.K., Sharma, A.R., Kambezidis, H.D., 2009. Variations in the Aerosol optical properties and Types over the tropical urban site of Hyderabad, India. *J. Geophys. Res.* 114, D22204. <http://dx.doi.org/10.1029/2009JD012423>.
- Kim, D.H., Sohn, B.J., Nakajima, T., Takamura, T., Choi, B.C., Yoon, S.C., 2004. Aerosol optical properties over east Asia determined from ground-based sky radiation measurements. *J. Geophys. Res.* 109, D02209. <http://dx.doi.org/10.1029/2003JD003387>.
- Kokhanovsky, A.A., Prikhach, A.S., Katsev, I.L., Zege, E.P.n., 2009. Determination of particulate matter vertical columns using satellite observations. *Atmos. Meas. Tech.* 2, 327e335. <http://dx.doi.org/10.5194/amt-2-327-2009>.
- Kumar, K.R., Sivakumar, V., Reddy, R.R., Gopal, K.R., Adesina, A.J., 2014. Identification and classification of different aerosol types over a subtropical rural site in Mpumalanga, South Africa: seasonal variations retrieved from the AERONET sunphotometer. *Aerosol Air Qual. Res.* 14, 108e123.
- Mateos, D., Sanchez-Lorenzo, A., Antón, M., Cachorro, V.E., Calbó, J., Costa, M.J., Torres, B., Wild, M., 2014. Quantifying the respective roles of aerosols and clouds in the strong brightening since the early 2000s over the Iberian Peninsula. *J. Geophys. Res. Atmos.* 119, 10382e10393. <http://dx.doi.org/10.1002/2014JD022076>.
- Mateos, D., Cachorro, V.E., Toledano, C., Burgos, M.A., Bennouna, Y., Torres, B., Fuertes, D., González, R., Guirado, C., Calle, A., de Frutos, A.M., 2015. Columnar and surface aerosol load over the Iberian Peninsula establishing annual cycles, trends, and relationships in five geographical sectors. *Sci. Total Environ.* 518e519, 378e392. <http://dx.doi.org/10.1016/j.scitotenv.2015.03.002>.
- Pey, J., Querol, X., Alastuey, A., Forastiere, F., Stafoggia, M., 2013. African dust outbreaks over the Mediterranean Basin during 2001e2011: PM10 concentrations, phenomenology and trends, and its relation with synoptic and mesoscale meteorology. *Atmos. Chem. Phys.* 13, 1395e1410. <http://dx.doi.org/10.5194/acp-13-1395-2013>.
- Pope III, C.A., 2000. Review: epidemiological basis for particulate air pollution health standards. *Aerosol Sci. Tech.* 32, 4e14.
- Pope III, C.A., Dockery, D.W., 2006. Health effects of fine particulate air pollution: lines that connect. *J. Air & Waste Manage. Assoc.* 56, 709e742.
- Pelletier, B., Santer, R., Vidot, J., 2007. Retrieving of particulate matter from optical measurements: a semiparametric approach. *J. Geophys. Res.* 112, D06208. <http://dx.doi.org/10.1029/2005JD006737>.
- Querol, X., Pey, J., Pandolfi, M., Alastuey, A., Cusack, M., Perez, N., Moreno, T., Viana, M., Mihalopoulos, N., Kallos, G., Kleanthous, S., 2009. African dust contributions to mean ambient PM10 mass-levels across the Mediterranean Basin. *Atmos. Environ.* 43, 4266e4277.
- Querol, X., et al., 2014. 2001-2012 trends on air quality in Spain. *Sci. Tot Env.* 490, 957e969.
- Rodríguez, S., Querol, X., Alastuey, A., Kallos, G., Kakaliagou, O., 2001. Saharan dust contributions to PM10 and TSP levels in southern and eastern Spain. *Atmos. Environ.* 35, 2433e2447.
- Rohen, G.J., von Hoynigen-Huene, W., Kokhanovsky, A., Dinter, T., Vountas, M., Burrows, J.P., 2011. Retrieval of aerosol mass load (PM10) from MERIS/Envirsat top of atmosphere spectral reflectance measurements over Germany. *Atmos. Meas. Tech.* 4, 523e534.
- Smirnov, A., Holben, B.N., Eck, T.F., Dubovik, O., Slutsker, I., 2000. Cloud-screening and quality control algorithms for the AERONET database. *Remote Sens. Environ.* 73, 337e349.
- Toledano, C., Cachorro, V.E., Berjón, A., De Frutos, A., Sorribas, M., De la Morena, B., Goloub, P., 2007a. Aerosol optical depth and Ångström exponent climatology at El Arenoso AERONET site (Huelva, Spain). *Q. J. Roy. Meteorol. Soc.* 133, 795e807.
- Toledano, C., Cachorro, V.E., De Frutos, A., Sorribas, M., Prats, N., De la Morena, B., 2007b. Inventory of African desert dust events over the southwestern Iberian Peninsula in 2000e2005 with an AERONET Cimel sun photometer. *J. Geophys. Res.* 112, D21201. <http://dx.doi.org/10.1029/2006JD008307>.
- Toledano, C., Cachorro, V.E., de Frutos, A.M., Torres, B., Berjón, A., Sorribas, M., Stone, R.S., 2009. Airmass classification and analysis of aerosol types at El Arenoso (Spain). *J. Appl. Meteorol. Clim.* 48, 962e981. <http://dx.doi.org/10.1175/2008JAMC2006.1>.
- Toledano, C., Bennouna, Y., Cachorro, V., Ortiz de Galisteo, P., Stohl, A., Stebel, K., Kristiansen, N.I., Olmo, F.J., Lyamani, H., Obregón, M.A., Estelles, V., Wagner, F., Baldasano, J.M., González-Castañedo, Y., Clarisse, L., de Frutos, A., 2012. Aerosol properties of the Eyjafjallajökull ash derived from Sun photometer and satellite observations over the Iberian Peninsula. *Atmos. Environ.* 48, 22e32.
- Tørseth, K., Aas, W., Breivik, K., Fjærås, A.M., Fiebig, M., Hjellbrekke, A.G., Lund Myhre, C., Solberg, S., Yttri, K.E., 2012. Introduction to the European monitoring and evaluation Programme (EMEP) and observed atmospheric composition change during 1972e2009. *Atmos. Chem. Phys.* 12, 5447e5481. <http://dx.doi.org/10.5194/acp-12-5447-2012>.
- Vergaz, R., Cachorro, V.E., De Frutos, A.M., Vilaplana, J.M., De La Morena, B.A., 2005. Columnar characteristics of aerosols by spectroradiometer measurements in the maritime area of the Cadiz Gulf (Spain). *Int. J. Climatol.* 25, 1781e1804.
- WHO, 2006. Air Quality Guidelines: Global Update 2005: Particulate Matter, Ozone, Nitrogen Dioxide and Sulphur Dioxide. World Health Organization, ISBN 9289021926. WHO Regional Office for Europe.

3.2. *Inventario de intrusiones desérticas en el centro-norte de la Península Ibérica durante el periodo 2003-2014*

3.2.1. Resumen gráfico

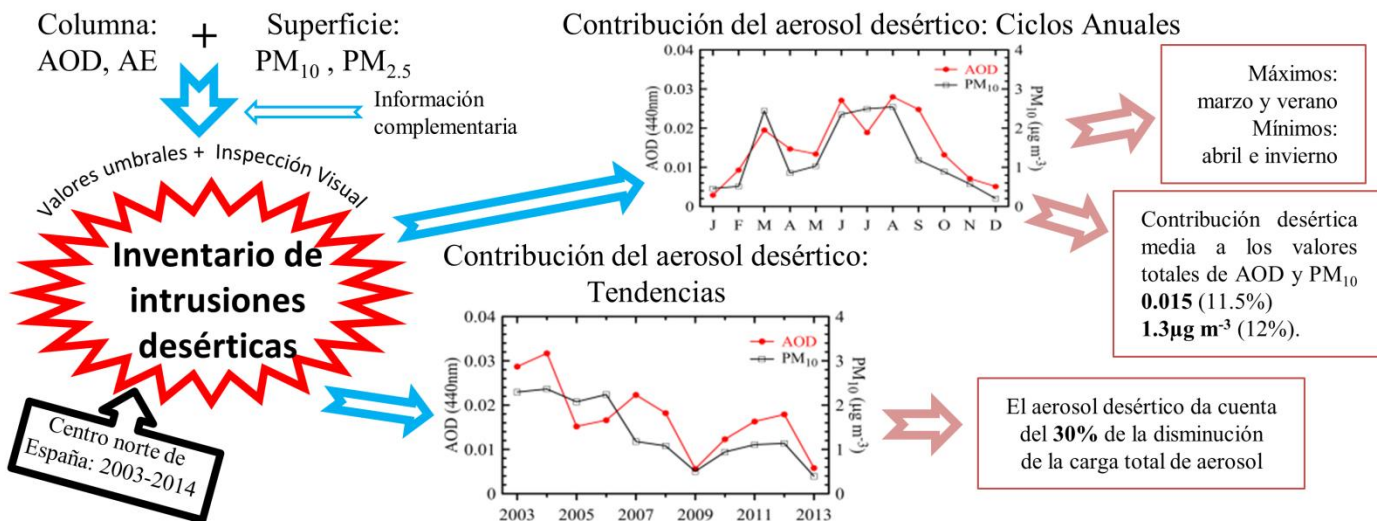


Figura 9: Resumen gráfico del A2.

3.2.2. Resumen

El inventario de intrusiones desérticas obtenido con la metodología explicada en la Sección 2.3 durante el periodo 2003-2014 en nuestra zona de estudio, que puede considerarse representativa de la región de Castilla y León, cuenta con la ventaja de haber sido creado a partir de dos bases de datos complementarias, lo que permite una detección más precisa de los días que presentan intrusión desértica tanto a nivel de superficie como en las capas altas de la atmósfera. Consta de 152 episodios desérticos compuestos por 418 días, alrededor de 13 episodios y 35 días (9.5%) por año. De estos episodios solamente 19 han sido registrados en superficie como excedencias según los valores de PM₁₀ (superando los 50 $\mu\text{g m}^{-3}$ establecidos por las normativas europeas) durante los 12 años de estudio, lo que muestra los bajos niveles de contaminación de la atmósfera en nuestra zona de estudio. Un resultado a destacar es que tener una base de datos con menos días con medida de AOD en comparación a las de PM₁₀,

no supone un hándicap a la hora de detectar intrusiones desérticas utilizando los valores de AOD.

El ciclo anual de la ocurrencia de las intrusiones desérticas presenta dos máximos, en marzo y junio, con un mínimo en abril y la menor ocurrencia registrada durante los meses de invierno. Este comportamiento ha sido corroborado por otros estudios (Pey et al., 2013; Salvador et al., 2014), en esta zona y en otras zonas de la PI usando datos PM_x. La ocurrencia de días con intrusión desértica presenta una gran variabilidad interanual. Así, nos encontramos con años como 2006 en que se registran 67 días de intrusión y otros como 2013 en los que apenas se han registrado 15. Además, no hay relación entre los años con más (o menos) número de días con intrusión desértica y los eventos más (o menos) intensos registrados, como se observa al estudiar las medias de los valores de AOD y PM₁₀. Aunque con una gran variabilidad, se obtiene una tendencia interanual estadísticamente significativa de ~3 días menos por año con presencia de aerosol desértico.

El ciclo anual de las intrusiones desérticas guarda gran relación con los escenarios sinópticos que favorecen la entrada de masas de aire africanas a la Península. En particular, se observa que la baja térmica en el norte de África durante los meses de verano es la responsable del mayor número de intrusiones en la PI (~53%).

El punto más importante de éste estudio se centra en el cálculo cuantitativo, tanto climatológico como interanual, de la contribución de las intrusiones desérticas sobre los valores totales de AOD, PM₁₀, PM_{2.5} y PM_{2.5-10} (ver Sección 2.2). En general, los promedios de contribución desértica a los valores de AOD, PM₁₀, PM_{2.5} y PM_{2.5-10} son de 0.015 (11.5%), 1.3 µg m⁻³ (12%), 0.6 µg m⁻³ (9%) y 0.8 µg m⁻³ (16%), respectivamente. Los ciclos anuales del impacto de las intrusiones desérticas sobre AOD y PM₁₀ presentan dos máximos: en marzo (13.4% y 20.1%, respectivamente) y en verano (~17% y ~16.8%, respectivamente). Además, dichos ciclos muestran una evolución bastante similar durante todo el año salvo para los meses de julio y septiembre, con los resultados actuales. Un hecho diferencial es que el ciclo anual de la contribución desértica a los valores de AOD no sigue la misma evolución que el ciclo anual de los valores totales de AOD (comportamiento cercano a una campana de Gauss) mientras que para el PM₁₀, ambos ciclos (contribución desértica a los valores de PM₁₀ y valores totales de PM₁₀) muestran una forma similar.

El cálculo interanual de la contribución de las intrusiones desérticas sobre los niveles de AOD y PM₁₀ muestra un decrecimiento progresivo. Esta reducción en los niveles de aerosol

desértico puede explicar el 30% de la reducción de la carga total de aerosoles observada en la zona de estudio durante el periodo 2003-2014 indicada en la Sección 3.1.2.

Como último punto en relación a la contribución de las intrusiones desérticas, se han calculado las relaciones entre la contribución a nivel de superficie y de columna, obteniéndose coeficientes de correlación de 0.81 para los promedios anuales.

Los errores asociados al cálculo de la contribución de aerosol desértico a la carga total de aerosol dependerán fuertemente del procedimiento de detección de eventos utilizado. Por este motivo, se ha estimado una incertidumbre asociada a la detección de eventos (es decir el error asociado al número de días al año en que hay intrusión desértica) y se ha estudiado cómo repercute en el cálculo de la contribución, obteniendo valores de ~10% de error para la contribución del ciclo anual del AOD, ~8% para los valores interanuales de AOD y entre 8-14% para el ciclo anual y los valores interanuales de PM₁₀. Debemos mencionar la dificultad en la estimación de los errores asociados a estas evaluaciones.

Es relevante la importancia de este estudio, no solo porque se usan por primera vez medidas de superficie y columna como elementos complementarios sino por el hecho de que es el primer inventario de estas características que nosotros conocemos. Además se realiza por primera vez la evaluación de la contribución de los aerosoles desérticos al AOD total, así como a los niveles de la fracciones de PM_{2.5} y PM_{10-2.5}, tanto en el ciclo anual como en la evaluación interanual. La alta correlación existente entre los valores anuales totales de AOD y PM₁₀ observada durante los 12 años de estudio permite estimar los valores anuales de una u otra variable en el caso de que existan huecos en la base de datos. La correlación existente entre los valores correspondientes a la contribución de los aerosoles desérticos al total en los últimos años también es un resultado a considerar.

3.2.3. Artículo 2



Inventory of African desert dust events in the north-central Iberian Peninsula in 2003–2014 based on sun-photometer–AERONET and particulate-mass–EMEP data

Victoria E. Cachorro¹, María A. Burgos¹, David Mateos¹, Carlos Toledano¹, Yasmine Bennouna¹, Benjamín Torres¹, Ángel M. de Frutos¹, and Álvaro Herguedas²

¹Grupo de Óptica Atmosférica, Facultad de Ciencias, Universidad de Valladolid, Paseo Belén 7, CP 47011, Valladolid, Spain

²Departamento de Control de Calidad y Cambio Climático, Consejería de Fomento y Medio Ambiente de la Junta de Castilla y León, Valladolid, Spain

Correspondence to: Victoria E. Cachorro (chiqui@goa.uva.es)

Received: 15 January 2016 – Published in Atmos. Chem. Phys. Discuss.: 19 February 2016

Revised: 3 June 2016 – Accepted: 6 June 2016 – Published: 8 July 2016

Abstract. A reliable identification of desert dust (DD) episodes over north-central Spain is carried out based on the AErosol RObotic NETwork (AERONET) columnar aerosol sun photometer (aerosol optical depth, AOD, and Ångström exponent, α) and European Monitoring and Evaluation Programme (EMEP) surface particulate-mass concentration (PM_x , $x = 10$, 2.5, and 2.5–10 μm) as the main core data. The impact of DD on background aerosol conditions is detectable by means of aerosol load thresholds and complementary information provided by HYSPLIT (Hybrid Single Particle Lagrangian Integrated Trajectory Model) air mass back trajectories, MODIS (Moderate Resolution Imaging Spectroradiometer) images, forecast aerosol models, and synoptic maps, which have been carefully reviewed by a human observer for each day included in the DD inventory. This identification method allows the detection of low and moderate DD intrusions and also of mixtures of mineral dust with other aerosol types by means of the analysis of α . During the period studied (2003–2014), a total of 152 DD episodes composed of 418 days are identified. Overall, this means ~ 13 episodes and ~ 35 days per year with DD intrusion, representing 9.5 % days year $^{-1}$. During the identified DD intrusions, 19 daily exceedances over 50 $\mu\text{g m}^{-3}$ are reported at the surface. The occurrence of DD event days during the year peaks in March and June, with a marked minimum in April and lowest occurrence in winter. A large interannual variability is observed showing a statistically significant temporal decreasing trend of ~ 3 days year $^{-1}$. The DD impact

on the aerosol climatology is addressed by evaluating the DD contribution in magnitude and percent (in brackets) for AOD, PM_{10} , $PM_{2.5}$, and $PM_{2.5-10}$, obtaining mean values of 0.015 (11.5 %), 1.3 $\mu\text{g m}^{-3}$ (11.8 %), 0.55 $\mu\text{g m}^{-3}$ (8.5 %) and 0.79 $\mu\text{g m}^{-3}$ (16.1 %), respectively. Annual cycles of the DD contribution for AOD and PM_{10} present two maxima – one in summer (0.03 and 2.4 $\mu\text{g m}^{-3}$ for AOD in June and PM_{10} in August) and another in March (0.02 for AOD and 2.2 $\mu\text{g m}^{-3}$ for PM_{10}) – both displaying a similar evolution with exceptions in July and September. The seasonal cycle of the DD contribution to AOD does not follow the pattern of the total AOD (close to a bell shape), whereas both PM_{10} cycles (total and DD contribution) are more similar to each other in shape, with an exception in September. The interannual evolution of the DD contribution to AOD and PM_{10} has evidenced a progressive decrease. This decline in the levels of mineral dust aerosols can explain up to 30 % of the total aerosol load decrease observed in the study area during the period 2003–2014. The relationship between columnar and surface DD contribution shows a correlation coefficient of 0.81 for the interannual averages. Finally, synoptic conditions during DD events are also analysed, observing that the north African thermal low causes most of the events (~ 53 %). The results presented in this study highlight the relevance of the area studied since it can be considered representative of the clean background in the western Mediterranean Basin where DD events have a high impact on aerosol load levels.

1 Introduction

Atmospheric aerosol particles play a key role in the radiation scattering and absorption physical processes that contribute to the Earth's radiative budget (Trenberth et al., 2009; Wild et al., 2013). Their impact on Earth's climate is represented by their direct radiative forcing (Haywood and Boucher, 2000; Boucher et al., 2013), but aerosols also act as cloud condensation nuclei modifying cloud properties and giving rise to a set of feedback processes that constitute the indirect radiative effect (Lohmann and Feichter, 2005; Lohmann et al., 2010; Boucher et al., 2013). All these aerosol climate effects have been enhanced due to anthropogenic aerosol particles (mainly sulfate and carbonaceous substances), which have increased the mean global temperature in the last century and have modified the atmospheric composition substantially (Boucher et al., 2013). Aerosol radiative properties, such as aerosol optical depth (AOD) or single scattering albedo (d'Almeida et al., 1991; Cachorro et al., 2000; Eck et al., 2010) are important issues to consider when studying the impact of atmospheric aerosol on climate.

Beside the climatological aspect of atmospheric aerosols, another element to be considered is their direct effect on air quality (Ganor et al., 2009; Kulmala et al., 2009; Querol et al., 2013). In environmental studies, particulate matter is mostly represented by its level of mass concentration at the surface represented by various size fractions (PM₁₀, PM_{2.5}, PM₁, etc., where the subscript indicates the upper cut-off of the aerodynamic diameter of particles and PM_X is used here as a general term referring to these fractions) and by the chemical speciation of its components: sulfates, nitrates, carbonaceous material, and minerals, among others. Aerosols can have a strong adverse impact on human health (e.g. Pope, 2000; Pérez et al., 2012) and ecosystems (Mahowald et al., 2010).

Desert or mineral dust aerosol is one of the main natural types of atmospheric aerosol particles, with a strong impact on the Earth system due to its worldwide distribution and temporal variability (Goudie and Middleton, 2006; Knippertz and Stuut, 2014; Viana et al., 2014). The injections of desert dust (DD) into the atmosphere, from the main two Sahara dust sources (Bodélé depression and eastern Mauritania) by different resuspension processes, can result in aerosol layers at high altitude being transported long distances to the Atlantic Ocean and Europe (e.g. Prospero, 1999; Prospero et al., 2002; Escudero et al., 2006, 2011; Engelstaedter and Washington, 2007; Knippertz and Todd, 2012; Guirado et al., 2014).

Our interest in this work focuses on atmospheric aerosol studies over the Iberian Peninsula (IP), which constitutes a peculiar area due to the large spatio-temporal variability in aerosol properties, types, and mixing processes as a result of the contrasting influences of the Atlantic Ocean, Mediterranean Sea, European continent, and the Saharan area. Based on sun-photometer data studies, different sectors of the IP,

defined by their topography or geography, can exhibit different aerosol climatologies (Alados-Arboledas et al., 2003; Vergaz et al., 2005; Estellés et al. 2007; Toledano et al., 2007a; Obregón et al., 2012; Bennouna et al., 2013; Mateos et al., 2014a). In particular, the Sahara and Sahel desert areas are the most important natural sources of mineral aerosols for the IP. The closeness of the IP to the African continent intensifies the impact of desert dust events on the aerosol load, measured as the whole atmospheric column (AOD) and at the surface (PM_X). Different synoptic weather conditions and circulation patterns influence the arrival of desert dust intrusions in the IP, resulting in differences in the seasonal behaviour (Escudero et al., 2005, 2006; Toledano et al., 2007b; Basart et al., 2009; Valenzuela et al., 2012a; Pey et al., 2013a; Salvador et al., 2013, 2014). These intrusions are characterized by isolated or episodic events of short duration (around 2–3 days). However, episodes in summer months are longer and more frequent than in other seasons, so that often successive episodes are linked due to the recirculation of air masses producing feedback processes, which give rise to a long residence time of desert dust particles in the atmosphere when there is low precipitation (Rodríguez et al., 2002; Escudero et al., 2005). Therefore, desert dust aerosols are one of the most important types over the IP, having an important influence on the air quality and radiative properties, and hence their detection, quantification, and characterization are important research tasks.

There are different ways to approach the detection or identification of desert dust events depending on the objectives of each study. The detection depends on the different techniques used: surface measurements, remote sensing (satellite or ground-based), back-trajectory evaluation, aerosol models, or a combination of these. Air mass trajectories are one of the first and most used techniques to identify the origin of the transport of mineral dust aerosols to different regions worldwide (e.g. Hogan and Rosmond, 1991; Prospero et al., 2002; Kallos et al., 2003; Pace et al., 2006). Although there is abundant literature about mineral dust over southern Europe or the Mediterranean areas, most of the studies about detection, characterization, and/or the impact of desert dust aerosols are focused on case studies or particularly strong episodes: e.g. in Italy (e.g. Meloni et al., 2007; di Sarra et al., 2011; Bègue et al., 2012), Greece (e.g. Kaskaoutis et al., 2008), or the Iberian Peninsula (e.g. Lyamani et al., 2005; Cachorro et al., 2006, 2008; Pérez et al., 2006; Guerrero-Rascado et al., 2009; Córdoba-Jabonero et al., 2011). Few studies are based on long-term datasets of desert dust using different techniques, such as sun photometers (Toledano et al., 2007b; Valenzuela et al., 2012b), satellite sensors (Kaufman et al., 2005, Kaskaoutis et al., 2012; Gkikas et al., 2013, 2015), lidar measurements (Mona et al., 2006, 2014; Papayannis et al., 2008), or PM_X data (Escudero et al., 2005; Pey et al., 2013a; Salvador et al., 2013, 2014; Rodríguez et al., 2015). As can be seen from this list only recent studies

contain long-term data sets and only in some of them is the net contribution to the aerosol load of DD evaluated.

The PM_X observations provided by different networks have constituted one of the most frequent tools for the establishment of DD inventories (e.g. Escudero et al., 2005; Pey et al., 2013a; Salvador et al., 2013, 2014) in order to evaluate their contribution to PM_X levels required by the EU directives. The EU 2008/50/EC directive (EC, 2008) on air quality establishes threshold values for the concentration of particles with an aerodynamic diameter below 10 (PM_{10}) and 2.5 ($\text{PM}_{2.5}$) μm : an annual mean and 24 h mean of 40 and $50 \mu\text{g m}^{-3}$ for PM_{10} and an annual $\text{PM}_{2.5}$ average of $25 \mu\text{g m}^{-3}$. In this sense it is necessary to know the contribution of natural and anthropogenic components to the total aerosol load. Therefore, the contribution of mineral dust in south Europe is important because of the link between PM_{10} exceedances and DD intrusions or outbreaks.

Once the identification of DD African aerosols is carried out, the next task is to quantify their contribution to the total aerosol load. The evaluation of the contribution of DD episodes to PM_X data is viable by means of a chemical speciation analysis (Rodríguez et al., 2001, 2002, 2015), but this method requires high manpower and has poor temporal sampling. Hence, in order to avoid this expensive technique, other methods have been developed using PM_X (Escudero et al., 2007; Ganor et al., 2009) and AOD data (Toledano et al., 2007b). As reported by Viana et al. (2010) and taking into account more recent publications (e.g. MAGRAMA, 2013, 2015), no more than three methods are currently used with PM_X , including receptor models (Pey et al., 2013b; Belis et al., 2013). However, these techniques would need to be updated to the measuring site for DD contribution estimates. In a similar way columnar aerosol algorithms can facilitate the apportioning of the different aerosol types (Dubovik et al., 2002; O'Neill et al., 2003) to the total aerosol load.

The advantage of remote sensing techniques, such as sun photometry, for DD detection is the spectral information recorded by their AOD measurements and given by the Ångström exponent, α . This is a powerful tool in the identification and classification of the different aerosol types (Eck et al., 1999; Toledano et al., 2007a) but also allows “near-real-time” processing of data by means of reasonably sophisticated algorithms (Dubovik et al., 2002; O'Neill et al., 2003) that retrieve aerosol properties. The evolutions of surface PM_X and columnar AOD differ in the seasonal cycles (see, e.g., Bennouna et al., 2014; Mateos et al., 2015), and hence their DD impact can also present some discrepancies in that cycle. The PM_X sampling used here is based on daily filter records (see Aas et al., 2013), while sun photometers provide instantaneous measurements of the columnar load but their sampling is limited to daytime cloud-free conditions (Toledano et al., 2007a, b).

The usefulness of a DD inventory is that it opens the possibility of the evaluation of the desert dust contribution to the total aerosol load. However, very few studies have ac-

complished this task over a long period and from a multi-year perspective. To our knowledge, only the inventory of Toledano et al. (2007b) addressed the DD contribution to AOD between 2000 and 2005 at a Spanish south-western site (El Arenosillo). For PM_X data we have found various studies, such as the more recent publication by Salvador et al. (2013, 2014) and Pey et al. (2013a). Salvador et al. (2013) reported a DD inventory, and the corresponding contribution of DD is determined over the Madrid area over the period 2001–2011, which is extended to several stations covering the whole IP by Salvador et al. (2014). Pey et al. (2013a), with the same methodology as Salvador et al. (2013), analysed the period 2001–2011 for PM_{10} at different sites over the whole Mediterranean Basin. In these three studies, the method used for the evaluation of the DD contribution to PM_X is different to that for AOD. Therefore, the development of methodologies for the evaluation of DD contribution is an open area of research, for instance, to obtain the near real-time DD contribution value.

Within this framework, the main purpose of this study is to establish an inventory of DD episodes together with the evaluation of their contribution to the total aerosol load, using both AOD and PM_X data. This is the first time, to our knowledge, that DD events are identified by the simultaneous use of both columnar (AOD and α) and surface (PM_X) aerosol observations. The methodology is applied over one of the cleanest atmospheric areas in south-western Europe, the north-central area (Castilla y León region) of the Iberian Peninsula, for a long time period spanning more than 1 decade (2003–2014). Regarding the columnar aerosol data, the reliable measurements performed within the AErosol RObotic NETwork, AERONET (Holben et al., 1998), are used. For the study area, the only available aerosol long-term data set is recorded at the Palencia site (41.9°N , 4.5°W ; 750 m a.s.l.). Regarding surface aerosols, we use the high-quality particulate-matter data recorded by the European Monitoring and Evaluation Programme (EMEP) network in the nearby Peñausende station (41.28°N , 5.87°W ; 985 m a.s.l.), with similar background conditions to Palencia. In this way, the use of these two worldwide extended and high-quality networks will ensure the feasibility of implementing the proposed method in other regions. The long-term inventory described hereafter has been employed to establish the main characteristics of the DD episodes in north-central Spain: their climatology, interannual behaviour, trends for the number of episodes and associated days, and occurrence under different synoptic scenarios. In addition, the evaluation of the DD contribution to the total mean values of AOD and PM_X is also addressed over the period investigated from a climatological and interannual perspective, which emphasizes the correlations between both quantities.

Section 2 describes the region of study and the datasets used. The methodology followed in the DD identification and in the evaluation of its contribution to aerosol load is presented in Sect. 3. In Sects. 4.1–4.3, the seasonal cycles

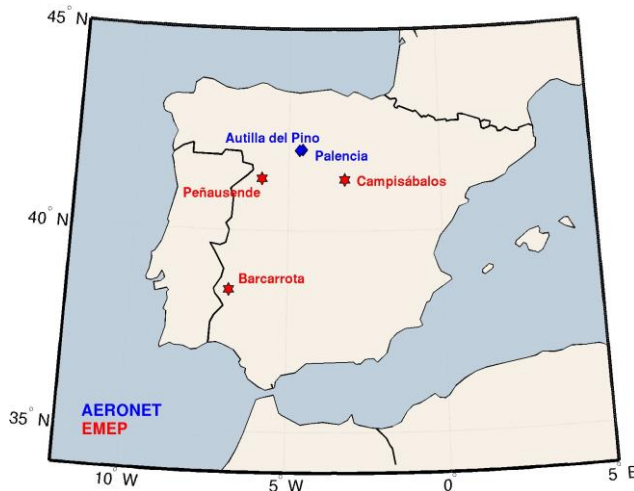


Figure 1. Location of the main sites used in this study belonging to AERONET (blue diamonds) and EMEP (red stars) networks.

and interannual evolution of DD events and dusty days and the DD contribution to AOD and PM_X are investigated. Section 4.4 provides an estimation of the uncertainty in this method and Sect. 4.5 describes the synoptic scenarios associated with the arrival of DD episodes in the north-central Iberian Peninsula. Finally, Sect. 5 summarizes the main findings obtained in this study.

2 Sites of measurements and database

2.1 AERONET network and AOD and Ångström exponent database

The main database for this study includes the instantaneous values of AOD obtained for 440 nm (henceforth AOD for clarity) and the Ångström exponent (α for the 440–870 nm range) measured at the Palencia site of the AERONET-EUROPE network (see Fig. 1 and Table 1). The instrument used to obtain these data is a Cimel CE318 radiometer which measures under clear sky conditions and every 15 minutes. The raw measurements in all-sky conditions (level 1.0 of AERONET criteria), the cloud-screened data (level 1.5), and the high-quality processed data in level 2.0 are used in this study. Lower-quality levels help to reliably determine the duration of each DD episode, in particular, when the event includes cloudiness. Aerosol measurements have been available at the Palencia site since 2003, one of the longest series of aerosol optical measurements in the Iberian Peninsula (Mateos et al., 2014a). The number of available days for every year in this study can be seen in Table 1. The standardization protocols of AERONET require pre- and post-calibration of the instruments after a field measuring period of 12 months, which helps to ensure the quality of the obtained data and associates an uncertainty for $\text{AOD}_{440\text{nm}}$ of

± 0.01 and for the derived α parameter of about ± 0.03 (see, e.g., Toledo et al., 2007a).

The Palencia site is placed in the autonomous region of Castilla y León in the north-central Iberian Peninsula, which is also known as the Castilian plateau, with an average altitude of ~ 800 m. This region is the third-least populated community in Spain due to its large area ($94\,193 \text{ km}^2$) and its low population (2 543 413 inhabitants registered in the census in 2012), with a population density just a bit higher than 27 inhabitants per square kilometre. Palencia is a small city (100 000 inhabitants) located in the north of Castilla y León but the measuring site is located on the outskirts, being surrounded by rural areas, removed from big urban and industrial centres. Hence, this area exhibits an exceptionally clean atmosphere, and aerosol observations are representative of the background conditions for the whole region. Therefore, desert dust intrusions can be observed since they significantly modify the background aerosol properties.

In order to fill the gaps in the Palencia AOD database, the site Autilla (42.00°N , 4.60°W ; 873 m a.s.l.) close to Palencia (7 km apart) has been used (for details see Bennouna et al., 2013). This site is used by GOA (Grupo de Óptica Atmosférica) as the calibration platform for Cimel sun photometers within the AERONET-EUROPE infrastructure and also works as a routine measurement site. Under these considerations, the columnar aerosol data series used in this study is consistent and allows one to perform the inventory of DD events in this region.

2.2 EMEP network and PM database

Daily PM_{10} and $\text{PM}_{2.5}$ measurements provided by the EMEP network constitute the second core database used to carry out this study (see Fig. 1 and Table 1). This network has the objective of regularly providing qualified scientific data to interested organizations in order to analyse and assess the trans-boundary transport and emission of pollutants (e.g. Aas et al., 2013). This is the objective of the LRTAP (Long-Range Transboundary Air Pollution) convention that establishes a framework for cooperative action for reducing the impact of air pollution. Using the PM_{10} and $\text{PM}_{2.5}$ data, the particulate matter associated with coarse particles ($\text{PM}_{2.5-10}$) can be determined by taking the difference of these quantities ($\text{PM}_{10}-\text{PM}_{2.5}$).

PM_{10} and $\text{PM}_{2.5}$ data belonging to the EMEP site of Peñausende have also been used for the detection of dusty days and for the evaluation of the DD contribution to the total PM_X levels. However, in order to better detect the DD episodes that arrive at our study area, two nearby stations (Campisábalos, 41.28°N , 3.14°W , 1360 m a.s.l., and Barcarrota, 38.48°N , 6.92°W , 393 m a.s.l.; see Fig. 1) are taken as complementary sites. All these three sites (Peñausende, Campisábalos, and Barcarrota) are placed in rural areas where background values are measured and the detection of Saharan desert dust intrusions is also possible. Among all

Table 1. Annual sum of days with aerosol data of AERONET and EMEP databases (“all days”) used in this study. Yearly number of dusty days in the DD inventory (“desert dust event days”) identified by criteria of AOD, PM₁₀, AOD, and PM₁₀ and other ancillary information. The relative coverage (percentage) is also given in parenthesis. See Sect. 3 for further details about the criteria used.

| | 2003 | 2004 | 2005 | 2006 | 2007 | 2008 | 2009 | 2010 | 2011 | 2012 | 2013 | 2014 | Total |
|-------------------------------------|---------------|---------------|---------------|---------------|---------------|---------------|---------------|---------------|---------------|---------------|---------------|---------------|----------------|
| All days | | | | | | | | | | | | | |
| Sampling AOD (%) | 156 (42.8) | 265 (72.4) | 295 (80.8) | 190 (52.1) | 271 (74.2) | 280 (76.5) | 256 (70.1) | 244 (66.8) | 269 (73.7) | 252 (68.9) | 220 (63.3) | 249 (68.2) | 2947 (67.2) |
| Sampling PM ₁₀ (%) | 343 (94.0) | 349 (95.4) | 340 (93.2) | 347 (95.1) | 349 (95.6) | 333 (91.0) | 341 (93.4) | 347 (95.1) | 347 (95.1) | 319 (87.2) | 332 (91.0) | 335 (91.8) | 4082 (93.1) |
| Coincident sampling (%) | 149 (40.8) | 256 (69.9) | 279 (76.4) | 183 (50.1) | 259 (71.0) | 255 (69.7) | 243 (66.6) | 238 (65.2) | 256 (70.1) | 219 (59.8) | 200 (57.5) | 234 (64.1) | 2771 (63.2) |
| Desert dust event days | | | | | | | | | | | | | |
| Number of dusty days | 44 | 44 | 41 | 67 | 44 | 31 | 24 | 19 | 32 | 29 | 15 | 28 | 418 |
| Only AOD criterion (%) | 5 (11.4) | 8 (18.2) | 9 (22.0) | 6 (9.0) | 14 (31.8) | 4 (12.9) | 4 (16.7) | 5 (26.3) | 9 (28.1) | 12 (41.4) | 2 (13.3) | 2 (7.1) | 80 (19.1) |
| Only PM ₁₀ criterion (%) | 19 (43.2) | 3 (6.8) | 11 (26.8) | 37 (55.2) | 6 (13.6) | 2 (6.5) | 7 (29.2) | 2 (10.5) | 0 (0) | 1 (3.4) | 8 (53.3) | 18 (64.3) | 114 (27.3) |
| AOD&PM ₁₀ criteria (%) | 20 (45.5) | 33 (75.0) | 21 (51.2) | 23 (34.3) | 22 (50.0) | 25 (80.6) | 11 (45.8) | 9 (47.4) | 23 (71.9) | 15 (51.7) | 4 (26.7) | 8 (28.6) | 214 (51.2) |
| Other criteria (%) | 0 (0) | 0 (0) | 0 (0) | 1 (1.5) | 2 (4.5) | 0 (0) | 2 (8.3) | 3 (15.8) | 0 (0) | 1 (3.4) | 1 (6.7) | 0 (0) | 10 (2.4) |

Spanish EMEP sites, these two complementary sites (Campisábalos and Barcarrota) have not been randomly selected, since their geographical locations help us to have more information about the path followed by the intrusion before arriving in our study area. The direction of arrival can be established by measurements from the west (by the Peñausende site), south-west (by the Barcarrota site), and south-east (by the Campisábalos site).

The available time period for the PM_x data starts in 2001, but the same period (2003–2014) used in the AOD_{440 nm} is considered for the homogenization of the results presented in this study. It is important to emphasize here that in spite of the distance between the Peñausende and Palencia sites (~ 100 km), the absence of any large landforms between them together with their atmospheric and background conditions make possible the joint discrimination and evaluation of these observations of AOD and PM_x for the detection of DD intrusions. Furthermore, an analysis of the air masses at Peñausende and Palencia sites (not shown here) has been carried out, corroborating that the geographical distance between them is negligible for the analysis of regional quantities such as AOD, water vapour, and the ozone column, among others.

The use of AOD_{440 nm}, σ , PM₁₀, and PM_{2.5} observations provides a comprehensive database to carry out an analysis of aerosol load and particle size, both at the surface and in the whole atmospheric column. Table 1 presents a detailed description of the number of days with available data every year for each database. Overall, PM_x presents a larger

amount of days with data than AOD. Particularly, the year 2003 presents the lowest AOD sampling (42 % of 365 days) because of gaps just at the start of the sun photometer measurements.

2.3 Ancillary information

To carry out a more accurate evaluation and discrimination of days that constitute a desert dust intrusion, ancillary information is also considered. Air mass back trajectories arriving at Palencia at 12:00 UTC have been calculated with the HYSPLIT model (Hybrid Single-Particle Lagrangian Integrated Trajectory), version 4 (Draxler et al., 2014; Stein et al., 2015). Due to the fact that desert dust aerosols can be transported to altitude levels higher than the boundary layer, back trajectories have been calculated for three heights (500, 1500, and 3000 m above ground level) and analysed 5 days back in time (120 h), using the model vertical velocity in the calculations. The meteorological database used as input for HYSPLIT is the Global Data Assimilation System (GDAS) GDAS1 dataset (e.g. Su et al., 2015). These three levels are commonly used in these studies to represent the air masses near the surface, in the boundary layer, and in the free troposphere, in order to follow the vertical transport of aerosols.

Information about cloudiness is obtained from MODIS (Moderate Resolution Imaging Radiometer) rapid response imagery products (<https://earthdata.nasa.gov/data/near-real-time-data/rapid-response>). In addition, GIOVANNI (Geospatial Interactive Online Visual-

ization AND aNalysis Infrastructure) MODIS AOD aerosol maps (<http://giovanni.gsfc.nasa.gov/giovanni/>) and those provided by the AERONET website (http://aeronet.gsfc.nasa.gov/cgi-bin/bamgomas_interactive) are used to determine the extension and path followed by the mineral dust air masses for a DD identified event. The NAAPS Global Aerosol model (Navy Aerosol Analysis and Prediction System; available at <http://www.nrlmry.navy.mil/aerosol/>) is also used to test whether model forecasts also detect a given DD episode over the study area.

As shown in previous studies (Escudero et al., 2005; Toledano et al., 2007b) desert dust intrusions over Spain take place under certain synoptic scenarios (see Sect. 4.5 for further details). Through the Earth System Research Laboratory of NOAA (National Oceanic and Atmospheric Administration), the plots of the geopotential height at 700 hPa and mean sea level pressure are obtained in order to evaluate the synoptic scenario associated with a given DD episode among the four possibilities (see Sect. 4.5) proposed by Escudero et al. (2005).

3 Methodology

3.1 Detection of desert dust episodes

This study is based on instantaneous AOD_{440 nm} and α values, as well as daily PM₁₀ and PM_{2.5}/PM₁₀ ratio data. The method for the detection of desert dust (DD) intrusions is a manual inspection of the evolution of these four quantities together with the origin of the air masses at the three levels of altitude at 500, 1500, and 3000 m a.s.l. and the auxiliary material of AOD MODIS maps, aerosol models, and synoptic scenarios. The methodology for detection is similar to that applied in Toledano et al. (2007b) with the added information of PM_x data, and not much different from that used in other studies also based on a set of different observations (Escudero et al., 2005; Pace et al., 2006; Kalivitis et al., 2007; MAGRAMA, 2013). The difference between these methods lies on the weight given to each quantity and the way the information is analysed. For example in our case the AOD–PM_x data are the primary information, but in other studies the primary variable is the origin of the air masses (Pace et al., 2006; Valenzuela et al., 2012a). Meteorological products and forecast aerosol models can also be used for this task (MAGRAMA, 2013). Although automatic methods can be applied in the DD identification, a visual inspection should be performed to corroborate each classification.

This study has been carried out as a year-by-year service to the “Consejería de Medio Ambiente” of the Autonomous Community of Castilla y León by means of two research programmes from 2006 to 2013 entitled “Discrimination, characterization and evaluation of desert dust outbreaks over ‘Castilla y León’ region”. These programmes aim to help im-

plement the “Environmental Quality Improvement Policy” of the EU by the national and regional governments of Spain. The experience gained with this year-by-year identification provides the final DD inventory presented in this study.

Thresholds have been established to identify those conditions which stand above the clean background over the study area. Hence, the choice of these thresholds is based on the aerosol climatology of the site from our investigations (Bennouna et al., 2014; Mateos et al., 2015) and previous results (see, e.g., Querol et al., 2009, 2014). The mean values for the long-term period 2003–2014 are 0.13 ± 0.09 for AOD_{440 nm} and $10 \pm 9 \mu\text{g m}^{-3}$ for PM₁₀. Hence, to detect the DD intrusions a visual inspection of the entire database is performed. When a day shows a group of a number of points of the instantaneous AOD ≥ 0.18 and/or the daily PM₁₀ $\geq 13 \mu\text{g m}^{-3}$, that day is further investigated. The AOD threshold corresponds to the mean value plus half of the standard deviation, approximately; meanwhile that for PM₁₀ is about the mean plus one third of the standard deviation. Hence, these thresholds must be taken as “warning flags” in the sense that these values alone do not define the classification as a dusty day. They also need the ancillary information given by the air mass backwards trajectories, satellite images, weather maps, and model forecasts to determine and corroborate the origin of aerosols and synoptic conditions. Therefore, with all this information, the human observer decides if a day must be included or not in the DD inventory.

In parallel to the above analysis, the evolution of the α quantity is also checked, allowing the identification of two different types of DD intrusions. Those days displaying $\alpha \leq 1.0$ in most of the instantaneous columnar data are identified as the “purer” desert dust intrusions, and they are denoted by a D flag. Those days with α values in the interval $1.0 \leq \alpha \leq 1.5$ (which have been classified as dusty days by their aerosol load and/or the ancillary information) present a mixture with other types (e.g. clean continental aerosols) and they are denoted by an MD (mixed desert) flag. The MD event days may either be a part of an intense event (generally of the D type) or form by themselves a low to moderate intensity event. Previous studies have also shown that DD intrusions into the Mediterranean Basin can present moderate AOD associated with large α values (e.g. Pace et al., 2006; Tafuro et al., 2006; Boselli et al., 2012). The limit of $\alpha \leq 1$ for identifying coarse particles has been established by previous studies in different worldwide areas (e.g. Eck et al., 1999, 2010; Dubovik et al., 2002; Meloni et al., 2007; Boselli et al., 2012), making this threshold suitable for our study area. It is important to emphasize here that the α parameter allows a more accurate identification of desert dust events. In particular, it allows the identification of those of low intensity, which have less of the characteristics identifying a desert origin (overall, the larger the AOD of a desert event, the lower the α) because they are generally mixed with other aerosol types and are not accounted for in many DD studies (e.g. Gkikas et al., 2013). These DD events of low intensity are more difficult to detect

because of the low signal of mineral dust aerosols, and hence it is more difficult to evaluate their contribution or impact on AOD and PM_X daily values. In fact, although the aerosol load threshold used in this study might seem very low, we must note again here that all these quantities are manually supervised by the expert observer who will take the final decision of the inclusion or not of a dusty day, bearing in mind all the available information given by these data and all the complementary material.

Another problem to be considered in the identification of a dusty day is when AOD and PM_{10} measurements show different information. For instance, AOD fingerprints seem to indicate a possible desert dust presence meanwhile PM_{10} does not. It must be taken into account that the PM_{10} quantity does not necessarily follow the same temporal behaviour as the AOD and possible time delays in PM_{10} concentration due to the fact that deposition processes can occur. Desert dust events can reach the IP at high-altitude layers (e.g. above 2000 m; Gkikas et al., 2015), and dry deposition can last various hours day^{-1} . Assuming an average speed of deposition of around 0.6 cm s^{-1} (Zender et al., 2003), DD particles can remain in the troposphere for up to 2 days after an episode ends (Escudero et al., 2007). Hence, these possible time delays between columnar air masses and surface PM_{10} are very variable (e.g. Kalivitis et al., 2007; Pey et al., 2013a). Therefore, AOD and PM_{10} observations must be considered to be complementary information to detect mineral dust aerosols since with the evolution of both quantities it is easier to identify DD fingerprints.

It is worth mentioning that in the general detection of both intensity and duration of a particular event, DD causes an increase in the $\text{AOD}_{440\text{nm}}$ and PM_{10} values, which then surpass or just reach the corresponding threshold, together with a decrease in the σ and $\text{PM}_{2.5}/\text{PM}_{10}$ values, giving rise to an increase in the mean size of the particle distribution. The duration of each intrusion can be established, since the low typical values, characteristic of the regional background, are recovered when the event finishes. The central or most intense days of each event are easy to detect due to the large increment of aerosol load with large particles (σ even close to zero) but low to moderate events are more difficult to detect. Although the events vary in their nature, the first and last days of a DD event show a low or moderate signature of mineral dust particles because of its mixture with other aerosol types (e.g. clean continental aerosol in our study area), with the exception of the strong DD events which generally have a notable impact on the aerosol load levels from the first day of the episode.

In the inspection of the instantaneous columnar dataset, non-reliable records are identified and removed due to their high spread in the data likely attributed to cloudy conditions. In the corroboration of some critical decisions made by the expert observer the ancillary information (see Sect. 2.3) constitutes a key point of the methodology. For instance, the verification of cloudy conditions can be supported by means of a

comparison between AOD instantaneous data from different levels, 1.0 (all-sky conditions) and 1.5 (cloud-screened data), and the visualization of cloud systems in MODIS true-colour and cloud product images. If there are signs of cloud presence, instantaneous AOD data are carefully checked to discern between cloud-contaminated data and a DD intrusion.

Once aerosol load measurements for a given day indicate the likely classification as a dusty day, the air mass back trajectories (calculated as described in Sect. 2.3) are visualized to check if the origin of the path or the path followed crosses the north African region and/or its surroundings. Therefore, the air mass back-trajectory analysis and the geopotential maps (establishing a particular synoptic scenario, see Sects. 2.3 and 4.5) lead to the final decision with respect to a DD event day classification, even for those days showing cloudiness. Finally, to help in the understanding of the general situation regarding the geographical distribution of the aerosol plumes, AOD MODIS maps and NAAPS forecasts are also visualized for ensuring the final choice. The consistency of the information used provides a reliable identification of the DD event.

It is worth mentioning here that the final decision to include a day as D or MD is made by the human observer with all the available information at hand. Perhaps this methodology is not the most adequate to apply for a big area with a high number of sites and long-term databases, but it is necessary for developing methodologies, because it will allow the validation of other more automatic methods (e.g. those only based on threshold criteria), most of them using satellite observations (e.g. Gkikas et al., 2013, 2015).

3.2 Evaluation of desert dust contribution to total AOD and total PM_{10} concentration

Once the DD inventory is established, the evaluation of the DD contribution can be addressed on seasonal and annual scales. Following Toledano et al. (2007b), the contribution of the DD events to AOD can be obtained as the difference of the multi-annual monthly means considering all days and the corresponding value without including the desert dust cases. This procedure was also used for PM_{10} data in a 3-year evaluation of net DD contribution at several sites in the Mediterranean Basin (Querol et al., 2009). In this study, the annual cycle of the DD contribution to AOD/ PM_X is evaluated with this same methodology over the entire period 2003–2014, using the DD event days classified in the inventory. Furthermore, the relative DD contribution to AOD/ PM_X can be obtained by dividing each one with respect to the corresponding total AOD/ PM_X value. Regarding the seasonal evaluations, the classification is as follows: winter (December–January–February), spring (March–April–May), summer (June–July–August), and autumn (September–October–November). Analogously, the yearly AOD/ PM_X means excluding dusty days are subtracted from the yearly AOD/ PM_X means for all days to obtain the DD contribution on an annual timescale.

Table 2. Main results of the DD inventory. Legend: N.E. (number of episodes), N.D. (number of days), P.D. (percentage of days), and M.D. (mean duration). Yearly mean values of AOD, σ , and PM_x data of desert dust events are also reported.

| | 2003 | 2004 | 2005 | 2006 | 2007 | 2008 | 2009 | 2010 | 2011 | 2012 | 2013 | 2014 | Total | Mean |
|----------------------------------------------------|-------------|-------------|-------------|-------------|-------------|-------------|-------------|-------------|-------------|-------------|-------------|-------------|-------|-------------|
| N.E. | 15 | 13 | 16 | 17 | 12 | 14 | 10 | 12 | 15 | 12 | 7 | 9 | 152 | 12.7 |
| N.D. | 44 | 44 | 41 | 67 | 44 | 31 | 24 | 19 | 32 | 29 | 15 | 28 | 418 | 34.8 |
| P.D. (%) | 12.05 | 12.02 | 11.23 | 18.36 | 12.05 | 8.47 | 6.58 | 5.21 | 8.77 | 7.92 | 4.11 | 7.67 | 9.5 | 9.5 |
| M.D. (days) | 2.93 | 3.14 | 2.56 | 4.00 | 3.67 | 2.21 | 2.40 | 1.58 | 2.13 | 2.42 | 2.14 | 3.11 | 2.7 | 2.7 |
| Mean AOD _{440 nm} | 0.32 ± 0.11 | 0.33 ± 0.16 | 0.28 ± 0.13 | 0.24 ± 0.08 | 0.29 ± 0.11 | 0.27 ± 0.10 | 0.20 ± 0.05 | 0.31 ± 0.11 | 0.27 ± 0.09 | 0.27 ± 0.10 | 0.18 ± 0.11 | 0.19 ± 0.09 | — | 0.26 ± 0.05 |
| Mean σ | 0.98 ± 0.33 | 0.92 ± 0.40 | 0.95 ± 0.44 | 0.88 ± 0.32 | 1.17 ± 0.40 | 1.02 ± 0.44 | 0.92 ± 0.27 | 0.91 ± 0.50 | 0.90 ± 0.36 | 0.83 ± 0.48 | 1.22 ± 0.29 | 0.63 ± 0.41 | — | 0.94 ± 0.15 |
| Mean PM ₁₀ ($\mu\text{g m}^{-3}$) | 28.7 ± 13.0 | 30.0 ± 32.7 | 29.8 ± 28.5 | 21.2 ± 8.0 | 19.3 ± 12.0 | 21.5 ± 8.0 | 16.0 ± 6.5 | 25.0 ± 25.8 | 21.8 ± 11.0 | 23.2 ± 20.4 | 16.4 ± 4.8 | 22.3 ± 8.8 | — | 22.9 ± 4.7 |
| Mean PM _{2.5} ($\mu\text{g m}^{-3}$) | 14.9 ± 6.3 | 14.4 ± 8.9 | 14.7 ± 10.0 | 12.0 ± 3.7 | 10.0 ± 4.1 | 13.8 ± 4.4 | 8.5 ± 5.0 | 10.6 ± 9.4 | 8.7 ± 3.1 | 7.9 ± 3.3 | 8.5 ± 3.7 | 8.1 ± 2.6 | — | 11.0 ± 2.8 |
| Mean PM _{2.5–10} ($\mu\text{g m}^{-3}$) | 13.9 ± 9.1 | 15.9 ± 25.1 | 14.7 ± 20.9 | 9.2 ± 6.5 | 9.3 ± 8.4 | 7.6 ± 5.8 | 7.6 ± 3.1 | 14.4 ± 16.5 | 12.5 ± 8.1 | 15.5 ± 17.7 | 7.6 ± 4.7 | 14.6 ± 8.0 | — | 11.9 ± 3.4 |

4 Results and discussion

4.1 Evaluation of the number of episodes and days: annual cycle and year-to-year variability

4.1.1 Evaluation of the number of episodes and dusty days

The inventory of desert dust intrusions includes the following: information on each episode and its associated days; the daily mean AOD, σ , PM₁₀, and PM_{2.5}; and cloudiness, synoptic scenarios, and air mass origin at three altitude levels (500, 1500, and 3000 m a.s.l.). Tables 1 and 2 show the information used to classify DD events and the main statistics for this inventory, respectively.

The PM₁₀ sampling presents the best coverage of the measuring time period with 93.1 % of the days, AOD is available 67.2 % of the time, and the coincident sampling is available 63.2 % of the time. As can be deduced from Table 1, the majority (51.2 %) of the DD event days composing the inventory are noticeable in both AOD and PM₁₀ datasets. However, 46.4 % of the total detected days are over the required

thresholds only in one quantity (AOD or PM_{10}). This is the advantage of the proposed inventory because DD outbreaks are identified with two complementary quantities about the aerosol load. The reasons behind this 46.4 % (19.1 % only with AOD and 27.3 % only with PM_{10}) are due to time delays between columnar and surface levels related to deposition phenomena and also are due to the lack of AOD or PM_{10} measurements. Therefore, if the inventory is addressed by only one quantity, a large number of dusty days can be lost in their identification. Finally, a smaller number of cases (2.4 %) are identified as dusty days using the ancillary information when AOD and PM_{10} data are not available.

The smaller amount of available data in the AOD time series (see Table 1), in comparison with PM_{10} , is not a major handicap in DD detection. There are several years (2004, 2007, 2008, 2010, 2011, and 2012) with more DD days detected only by AOD than only by PM_{10} , in spite of the smaller AOD sampling (between 53 and 103 days less per year). However, years 2003 and 2006, which present less than 200 daily AOD data, require the use of PM_{10} to better identify DD intrusions.

As reported in Table 2, during 2003–2014, a total number of 152 episodes has been identified, composed of 418 days. Among them, 242 days have been classified as days with desert aerosols (D) and 176 days with mixed aerosols (MD). Overall, this means 13 episodes and 35 days per year with desert dust intrusion, representing 9.5 % of the days each year. The duration of DD episodes is very variable, ranging from 1 to 13 days, but a value of 2.7 days is obtained as the mean episode duration. Due to the high variability in the intensity of these intrusions it is difficult to distinguish when an event has ended or its intensity has simply fallen below our threshold. During summer, the recirculation of air masses in the IP is very frequent and the DD episodes are subject to large intensity variations. We have considered separate DD episodes when there is, at least, 1 day that does not meet the DD requirements between two DD episodes.

Our percentage of dusty days of 9.5 % is lower than that reported by Salvador et al. (2013), which is around 18 % (18 episodes and 65 days per year). Salvador et al. (2013) analysed DD intrusions over the central Iberian Peninsula (Madrid area) between 2001 and 2008. This large difference between two nearby areas (separated by ~ 200 km) can be explained by the different time periods considered and the existence between these areas of a high mountain range (Sistema Central), with peaks up to 2400 m a.s.l. For the north-eastern area of the Iberian Peninsula, Escudero et al. (2005) reported 15 % of DD intrusions (16 episodes and 54 days per year) in the period 1996–2002, and Pey et al. (2013a) obtained 17–18 % between 2001 and 2011.

4.1.2 Annual cycle of the number of episodes and days

The annual cycles of the number of episodes and number of days with DD conditions are presented in Fig. 2. In gen-

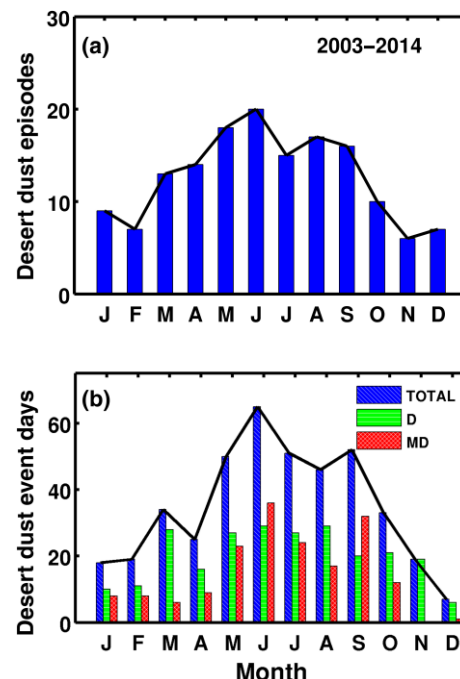


Figure 2. Annual cycle of (a) total number of episodes per month for total DD intrusions; (b) total (blue bars) number of days per month for total DD intrusions and for desert (D, green bars) and mixed desert (MD, red bars) categories in 2003–2014. Mean values per month can be derived by dividing by 12.

eral, the seasonal pattern along the year followed by the number of episodes (Fig. 2a) and dusty days (Fig. 2b) is similar, with a significant increase in the DD occurrence in March (13 events and 34 dusty days), a weak fall of DD event days in April (14 events and 25 dusty days), a notable increment between May and September (around 17 events and 53 dusty days per month), and a progressive decline to the minima in November and December. The number of episodes and event days peaks in June (20 events and 65 dusty days). A noteworthy feature of this figure is the local minimum in the number of DD episodes in July (15 episodes in 2003–2014) which is shifted to August in the number of DD event days (46 dusty days in 2003–2014). Figure 2b is similar in shape to that reported by Salvador et al. (2013) with the exception of September, and it is also similar to that of Escudero et al. (2005) with the exception of October. Concerning the two types of DD conditions distinguished in our inventory, the D type controls the annual cycle in the March maximum and April minimum, while the MD type controls the evolution between August and October.

Some features mentioned above regarding the seasonal behaviour of DD events for the north-central Spanish region are also observed for other areas of the IP. For instance, the March maximum and April minimum are common features in south-western (Toledano et al., 2007b; Obregón et al., 2012), north-eastern (Escudero et al., 2005; Papayannis et al.,

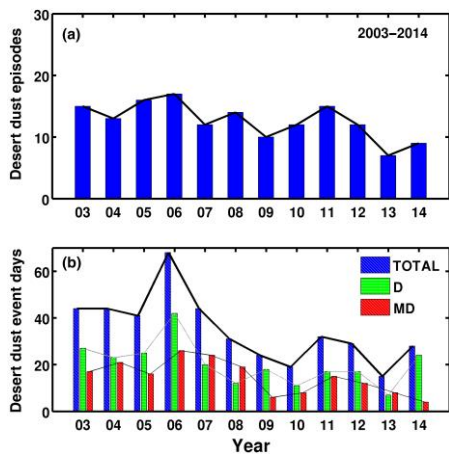


Figure 3. Interannual variability of (a) total number of episodes; (b) total (blue bars) number of days for the desert dust (DD) intrusions and for desert (D, green bars) and mixed desert (MD, red bars) categories.

2008), and central (Salvador et al., 2013) Spain. In spite of the different measuring instruments (sun photometer, lidar, or particulate-mass concentration), time periods, and methodologies employed in the DD event identification, its impact over (almost) all of the Iberian Peninsula follows the same pattern with the two maxima – one in late winter/early spring (March) and the other in summer – and the accentuated minimum of winter. Several minor discrepancies are found for the rest of the year; for example, the maximum number of DD event days during the summer months with a local minimum (in July) between them seems to be a characteristic of the annual cycles of the south-western (Toledano et al., 2007b) and north-central areas. Conversely, the eastern region presents a local maximum in October (Escudero et al., 2005; Pey et al., 2013a) which is not seen in our study region. These results confirm that different areas have different aerosol properties in the IP (Mateos et al., 2015). The larger occurrence of dusty days in summer and in certain spring and fall months is also observed in other Mediterranean areas using lidar networks to identify the occurrence of DD outbreaks (e.g. Mona et al., 2006; Papayannis et al., 2008).

4.1.3 Interannual variability and trends of the number of episodes and days with DD

The year-to-year variability for the number of both the episodes and days is reported in Table 2 and illustrated in Fig. 3. A large interannual variability is observed, which is more accentuated for the number of DD event days (Fig. 3b) with an apparent decreasing trend during the analysed period. A large number of dusty days is reported during the first 5 years (2003–2007), the maximum being in 2006 (67 days).

After 2007 there is a decline in DD event days up to 19 days in 2010, and a small upturn is observed in 2011, 2012, and 2014, with a sharp reduction in 2013. The lowest occurrence of DD events was in 2013 with only seven episodes and 15 dusty days that year (4.11 %). By contrast, the largest number of events took place in 2016 with 17 episodes composed of 67 days of dust intrusion (18.4 %). Nevertheless, the number of episodes and the number of days are not directly linked. For instance, 12 episodes are observed in both 2007 and 2010 but the former registered 44 days of intrusion, whereas the latter registered just 19 days. Furthermore, even though 2006 is the year with the highest occurrence of dusty days, it is not linked with the most intense events. Both $\text{AOD}_{440\text{ nm}}$ and PM_{10} means (for DD days) are lower in 2006 than for previous years, in which a smaller occurrence of DD conditions is observed. The minimum load during DD days is registered in 2013 for the $\text{AOD}_{440\text{ nm}}$ (0.18) and in 2009 for the PM_{10} ($16 \mu\text{g m}^{-3}$), while the maximum occurred in 2004 (0.33 for AOD and $30 \mu\text{g m}^{-3}$ for PM_{10}). Concerning the two classifications of DD event days (D and MD types), the years 2003, 2006, 2009, 2012, and 2014 are governed by the purer D type intrusions.

To quantify the decreasing trends in the number of episodes and associated days, the Theil–Sen estimator and Mann–Kendall test for significance have been used. The trends for the number of DD episodes and days are reported in Table 3 for the yearly values. A statistically significant trend at the 95 % significance level presents a p value below 0.05 (e.g. Sanchez-Lorenzo et al., 2013). The total number of dusty days has decreased by 2.7 days per year (p value of 0.02) between 2003 and 2014. This change, however, does not cause a significant trend in the number of episodes, which presents a decrease of 0.67 episodes per year with a p value around 0.03 (~ 97 % of significance level). These figures corroborate a significant decrease in the DD events seen in the north-central area of the Iberian Peninsula over the past decade. This result is in line with the findings obtained by Gkikas et al. (2013) for the whole Mediterranean Basin using MODIS data between 2000 and 2007 and considering only very intense DD events selected by a high AOD threshold.

4.2 Desert dust contribution to total AOD: seasonal cycle, interannual variability, and trends

4.2.1 Annual seasonal cycle

Figure 4 and Table 4 show the annual cycle of the DD contribution (small red bars in the figure) together with the multi-annual monthly means considering all days and only days without DD aerosols (the difference between these two values gives the DD contribution). Overall, the mean DD contribution to AOD is 0.015 or 11.5 % in 2003–2014.

The total AOD annual cycle representing the climatology follows the well-known pattern previously reported and ex-

Table 3. Temporal trends (Theil–Sen estimator), p value, and confidence interval ([i1, i2]) given by the quantities considered for all days and for the contribution of DD. For the DD inventory the number of episodes and DD event days is also included. Negative trend means a decrease in the quantity analysed.

| | Quantity | Trend | p value | i1 | i2 | Trend units | Trend (% per year) |
|--------------|-----------------------------------------|---------|-----------|--------|--------|-------------------------------|-----------------------|
| All days | AOD | -0.006 | < 0.01 | -0.009 | -0.003 | AOD units per year | -4.6 |
| | PM ₁₀ | -0.46 | < 0.01 | -0.66 | -0.30 | $\mu\text{g m}^{-3}$ per year | -4.5 |
| | PM _{2.5} | -0.38 | < 0.01 | -0.49 | -0.30 | $\mu\text{g m}^{-3}$ per year | -6.3 |
| | PM _{2.5–10} | -0.07 | 0.19 | -0.19 | 0.07 | $\mu\text{g m}^{-3}$ per year | -1.6 |
| DD inventory | Number of episodes | -0.67 | 0.03 | -1.00 | 0.00 | N.E. per year | -5.2 |
| | Number of DD event days | -2.7 | 0.02 | -4.2 | -1.30 | N.D. per year | -8.0 |
| | DD contribution to AOD | -0.0019 | 0.016 | -0.003 | -0.000 | AOD units per year | -11.2 |
| | DD contribution to PM ₁₀ | -0.14 | 0.06 | -0.26 | 0.01 | $\mu\text{g m}^{-3}$ per year | -10.1 |
| | DD contribution to PM _{2.5} | -0.079 | < 0.01 | -0.12 | -0.04 | $\mu\text{g m}^{-3}$ per year | -13.7 |
| | DD contribution to PM _{2.5–10} | -0.085 | 0.06 | -0.16 | 0.00 | $\mu\text{g m}^{-3}$ per year | -10.0 |

Table 4. Monthly mean contribution of DD to total AOD and PM_X, in absolute (“abs.”, AOD units and $\mu\text{g m}^{-3}$) and relative (“rel.”, %) values during the 2003–2013 period.

| | | Jan | Feb | Mar | Apr | May | Jun | Jul | Aug | Sep | Oct | Nov | Dec | Total |
|----------------------|------|-------|-------|-------|-------|-------|-------|-------|-------|-------|-------|-------|-------|-------|
| AOD _{440nm} | abs. | 0.006 | 0.011 | 0.018 | 0.014 | 0.014 | 0.027 | 0.018 | 0.026 | 0.023 | 0.014 | 0.008 | 0.004 | 0.015 |
| | rel. | 6.05 | 9.94 | 13.38 | 9.37 | 9.86 | 17.07 | 12.07 | 17.42 | 15.66 | 12.37 | 9.55 | 5.40 | 11.51 |
| PM ₁₀ | abs. | 0.51 | 0.58 | 2.23 | 0.81 | 0.96 | 2.28 | 2.35 | 2.38 | 1.16 | 1.37 | 0.83 | 0.23 | 1.31 |
| | rel. | 7.70 | 6.73 | 20.13 | 9.78 | 8.54 | 17.69 | 16.51 | 16.13 | 9.61 | 13.57 | 11.57 | 3.64 | 11.80 |
| PM _{2.5} | abs. | 0.36 | 0.43 | 0.66 | 0.28 | 0.33 | 0.88 | 1.12 | 1.12 | 0.58 | 0.50 | 0.28 | 0.08 | 0.55 |
| | rel. | 7.85 | 7.16 | 10.50 | 5.60 | 5.00 | 11.99 | 13.64 | 13.40 | 8.33 | 9.71 | 7.26 | 1.88 | 8.53 |
| PM _{2.5–10} | abs. | 0.20 | 0.17 | 1.67 | 0.47 | 0.69 | 1.40 | 1.25 | 1.33 | 0.58 | 0.93 | 0.56 | 0.17 | 0.79 |
| | rel. | 8.18 | 5.55 | 32.84 | 13.89 | 14.28 | 24.76 | 20.59 | 20.90 | 11.26 | 18.50 | 16.34 | 6.57 | 16.14 |

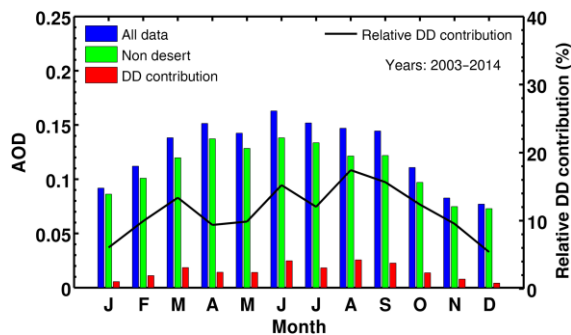


Figure 4. Annual cycle for DD contribution to the total monthly AOD means in absolute (red bar) and relative values (black line) in 2003–2014. Blue bars (also indicated as all data) represent the annual cycle of total AOD and green bars the corresponding values without including the days of desert dust (indicated as non desert).

plained for the Palencia site (see, e.g., Bennouna et al., 2013; Mateos et al., 2014a). To summarize: the increasing values from January to June (just when the maximum is found), with a slight reduction in May and a decreasing trend to the end

of the year, almost provide a well-defined bell shape. As for the climatology with the DD episodes excluded, it preserves the bell pattern found before for the general case, except for some minor discrepancies. For instance, the change between May and June is not noticeable for the curve with the DD excluded, in contrast with the larger increment observed for the general case.

However, the seasonal pattern followed by the DD contribution displays two maxima: the first one in March (late winter/early spring) with 0.018 or 13.4 % and the strongest one occurring in the summer period (June and August) with ~ 0.027 or ~ 17 %. Together with these maxima, there are two local minima: in April–May (around 0.014 or 9.5 %) and in July (0.018 or 12 %). After August, a progressive decline in the DD contribution is observed with the minimum in winter (December and January show similar values about 0.004 or 5.4 %). It is worth mentioning here the different characters of the two local minima occurring in April–May and July. The former generally occurs in the IP (linked to the precipitation cycle), while the latter is more typical of the central and south-western areas of Spain. For instance, the July min-

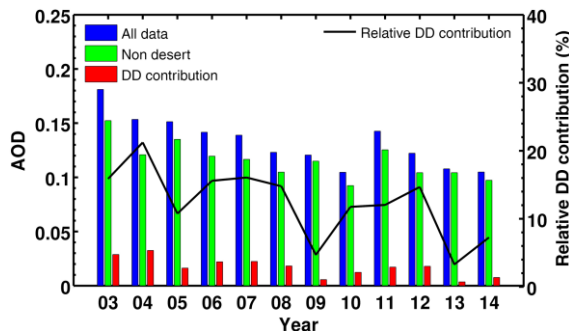


Figure 5. Interannual variability of DD contribution to the total yearly AOD in absolute (red bar) and relative values (black line). Blue bars (also indicated as all data) represent the mean yearly AOD value and green bars the corresponding values without including the days of desert dust (also indicated as non desert).

imum seems to be related to the arrival of drier air masses in the low troposphere as it is observed in the precipitable water vapour cycle (Ortiz de Galisteo et al., 2013).

The annual cycle of the DD contribution to the Palencia site (representing north-central Spain) presents a similar shape to that obtained in the El Arenosillo site (south-western area) by Toledano et al. (2007b) for an inventory of 6 years, from 2000 to 2005. This is an important result in two aspects: one related to the shape of the annual cycle or seasonal behaviour and the other one related to the different contribution of north and south areas of the IP. In relation to the geographical gradient of the African dust contribution, a quantitative difference is observed between these two areas. The total AOD signal is clearly impacted by DD events in the southern Iberian coast (with relative contributions being over 30 %), while in the north-central region the DD influence is weaker; thus, a south–north-decreasing gradient over the IP is observed regarding the DD contribution to AOD values. This behaviour is well known in the IP from earlier aerosol studies based on PM_X data (Querol et al., 2009; Pey et al., 2013a; Salvador et al., 2013, 2014), but this is the first time this is confirmed by an inventory of AOD data.

4.2.2 Interannual variability and trends

With respect to the interannual change in the DD contribution to AOD, Fig. 5 and Table 5 show its annual values between 2003 and 2014 (using the methodology explained in Sect. 3.2). In a quick-look analysis, both total AOD and DD contributions have a significant year-to-year variability with a decreasing trend during the period studied. The maximum DD contribution with a value of 0.033 or 21.2 % took place in 2004 and also showed a maximum in the total AOD around 0.15 (the mean value of 2003 is clearly affected by the low sampling: 42.7 %, compared to the 72.4 % in 2004). The year 2013 presents the absolute minimum of the DD contribution to AOD with 0.004 or ~ 4 %, with a low contribution in 2009

too (0.006 or ~ 5 %). There is a weak evolution of the DD contribution until 2008, although 2005 presents a marked local minimum (DD contribution to AOD around 0.016 or 11 %). There are years with simultaneous decreases (2008, 2009, 2013) or increases (2011, 2014) in both total AOD and its DD contribution, but in other years they present the opposite behaviour (2005 and 2006). The solid line in Fig. 5 illustrating the evolution of the relative DD contribution to AOD highlights the minima of 2013, 2009, and 2005 and the maxima of 2004 and 2012. The high interannual variability can be explained by the typical variability of the different African source areas and associated emission processes together with the atmospheric conditions and transport patterns of DD aerosols that can reach the Iberian Peninsula (Prospero et al. 2002; Kaufman et al., 2005; Escudero et al., 2006; Knippertz and Todd, 2012; Salvador et al., 2014).

The temporal trends in total AOD and in the DD contribution to AOD are also evaluated and shown in Table 3. The decrease in the total AOD in the Palencia site in 2003–2014 is 0.006 AOD units per year (with a P value < 0.01) or 4.6 % per year, which is in line with previous findings for the same site by Bennouna et al. (2014) and Mateos et al. (2014b) for shorter (4 and 3 years, respectively) periods. With respect to the DD contribution to AOD, a decrease of 0.0019 AOD units per year (P value = 0.02) or 11.2 % per year is calculated. Therefore, this rate represents 30 % of the total AOD decreasing trend. Hence, the natural decrease in DD aerosols has notably affected AOD levels over the north-central Iberian Peninsula during the study period.

4.3 Desert dust contribution to PM_x levels: annual cycle, interannual variability, and trends

4.3.1 Annual seasonal cycle

In the same way as for AOD, the contribution of desert dust events to mean values of PM_{10} , $\text{PM}_{2.5}$, and $\text{PM}_{2.5-10}$ have also been calculated. The annual cycle and the interannual evolution of these three quantities and the corresponding DD contributions are reported in Tables 4 and 5 and also illustrated by Figs. 6 and 7, respectively.

The DD contribution to the total PM_{10} , $\text{PM}_{2.5}$, and $\text{PM}_{2.5-10}$ is not usually evaluated at the same time. To our knowledge, this is the first time that fine- and coarse-mode contributions are evaluated in a long-term desert dust inventory of this type. Furthermore, the temporal trends for the interannual DD contributions are also discussed. It is worth mentioning here that as PM_{10} and $\text{PM}_{2.5}$ are obtained from independent filters (see Sect. 2.2) while $\text{PM}_{2.5-10}$ is only available with simultaneous PM_X data, the amount of data used in the evaluation of DD contribution for each quantity differs slightly.

According to Table 4, the mean DD contributions to PM_X during the study period are $1.3 \mu\text{g m}^{-3}$ (12 %) for PM_{10} , $0.6 \mu\text{g m}^{-3}$ (9 %) for $\text{PM}_{2.5}$, and $0.8 \mu\text{g m}^{-3}$ (16 %)

Table 5. Mean annual contribution of DD to total AOD and PM_X in absolute (“abs.”, AOD units, and $\mu\text{g m}^{-3}$, respectively) and relative (“rel.”, %) values during the 2003–2013 period.

| | | 2003 | 2004 | 2005 | 2006 | 2007 | 2008 | 2009 | 2010 | 2011 | 2012 | 2013 | 2014 |
|----------------------|------|-------|-------|-------|-------|-------|-------|-------|-------|-------|-------|-------|-------|
| AOD _{440nm} | abs. | 0.029 | 0.033 | 0.016 | 0.022 | 0.022 | 0.018 | 0.006 | 0.012 | 0.017 | 0.018 | 0.004 | 0.008 |
| | rel. | 15.87 | 21.22 | 10.76 | 15.59 | 16.06 | 14.78 | 4.68 | 11.75 | 12.03 | 14.67 | 3.76 | 7.25 |
| PM ₁₀ | abs. | 2.29 | 2.35 | 2.07 | 2.39 | 1.18 | 1.08 | 0.50 | 0.94 | 1.11 | 1.14 | 0.39 | 1.25 |
| | rel. | 18.12 | 17.80 | 16.10 | 21.49 | 11.02 | 11.04 | 5.59 | 10.81 | 10.92 | 12.36 | 4.87 | 14.54 |
| PM _{2.5} | abs. | 1.04 | 0.87 | 0.92 | 1.23 | 0.52 | 0.68 | 0.25 | 0.34 | 0.31 | 0.31 | 0.16 | 0.30 |
| | rel. | 13.07 | 10.27 | 11.95 | 17.79 | 8.10 | 10.36 | 4.76 | 6.92 | 5.99 | 6.88 | 3.52 | 6.55 |
| PM _{2.5–10} | abs. | 1.38 | 1.61 | 1.21 | 1.21 | 0.73 | 0.42 | 0.27 | 0.65 | 0.71 | 0.91 | 0.18 | 1.01 |
| | rel. | 27.00 | 30.99 | 22.91 | 26.97 | 15.85 | 12.52 | 6.72 | 15.34 | 14.42 | 18.31 | 4.88 | 22.57 |

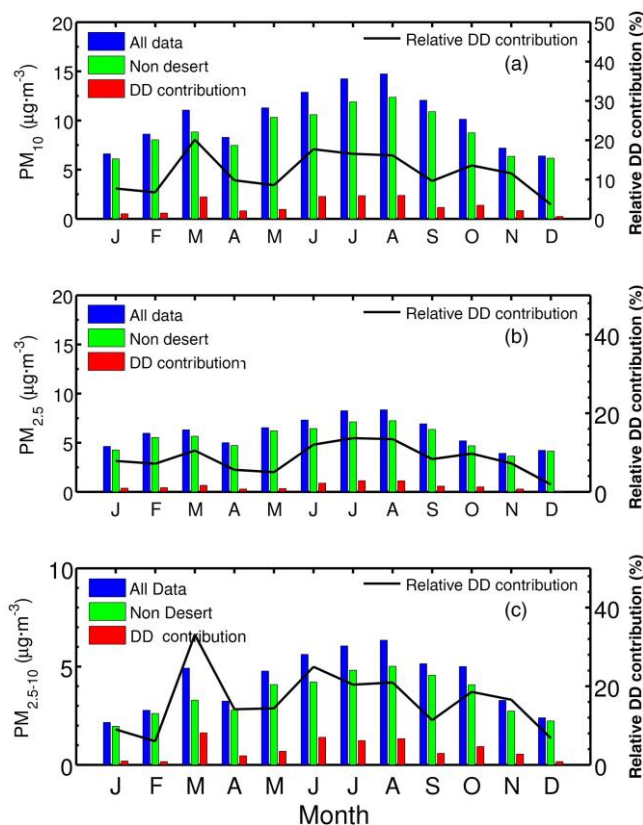


Figure 6. Annual cycle for DD contribution to the total monthly PM₁₀ (a), PM_{2.5} (b), and PM_{2.5–10} (c) means in absolute (red bar) and relative values (black line) in 2003–2014. Blue bars represent the annual cycle of total PM₁₀ (a), PM_{2.5} (b), and PM_{2.5–10} (c) and green bars the corresponding values without including the days of desert dust.

for PM_{2.5–10}. Our findings during 2003–2014 are in line with those given by Querol et al. (2009): 2 $\mu\text{g m}^{-3}$ for a 3 year period (2004–2006) of PM₁₀ data at the Peñausende site. A decreasing south to north gradient of African dust contribution to PM₁₀ (e.g. Querol et al., 2009; Pey et al., 2013a) is found

for the north-central area of the IP. In particular, PM₁₀ is similar to the averages in the north-eastern area ($< 2 \mu\text{g m}^{-3}$) and smaller than the values obtained at southern sites (up to 5–6 $\mu\text{g m}^{-3}$). Our relative contribution is in line with the lowest values of the ranges reported by Salvador et al. (2013) using a chemical speciation analysis at three different sites near Madrid.

The total PM₁₀ annual cycle (see Fig. 6) is well known in the north-central area of the Iberian Peninsula (see, e.g., Bennouna et al., 2014; Mateos et al., 2015); There are two maxima: a major one in summer and a secondary one in early spring (considering our seasonal classification with March as part of the spring). There is also a winter minimum and another minimum in April. This general behaviour for the entire dataset is also followed if the DD events are excluded. The evolution of these two latter curves is also followed by the DD contribution to PM₁₀. The largest DD contribution is observed in March (2.2 $\mu\text{g m}^{-3}$ or 20 %) and in the summer months of June to August ($\sim 2.3 \mu\text{g m}^{-3}$ or $\sim 17\%$). The months of April and May ($\sim 0.9 \mu\text{g m}^{-3}$ or $\sim 9\%$) display a notable decrease with respect to March. After summer, there is a sharp fall in September (1.2 $\mu\text{g m}^{-3}$ or 10 %) producing a local minimum and beyond October a progressive decline leading to the weakest effect ($< 8\%$) of the African intrusions during winter months (DJF). The maximum relative DD contribution to PM₁₀ can reach 20 %, which is within the range (10–50 %) observed by Pey et al. (2013a) for the eastern Spanish coast. Comparing the seasonal cycles of DD contribution to PM₁₀ in the latter area with respect to north-central Iberian Peninsula, some common features appear (March maximum, April–May decrease, summer increase, and September drop) but the maximum in October seen on the Mediterranean coast does not happen in the north-central area.

Even though both AOD and PM₁₀ express the aerosol load, these quantities present noticeable differences. To facilitate the comparison of the results shown above, Fig. S1 (Supplement) shows the annual cycles of AOD and PM₁₀ total means and their DD contributions together. The annual cycle of the

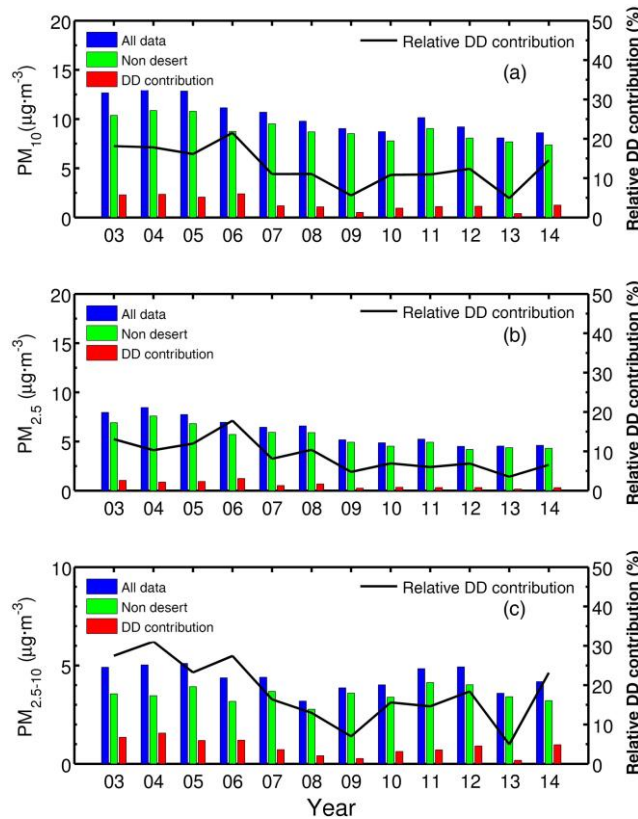


Figure 7. Interannual variability of DD contribution to the total yearly PM₁₀ (a), PM_{2.5} (b), and PM_{2.5–10} (c) in absolute (red bar) and relative values (black line). Blue bars represent the mean year PM₁₀ (a), PM_{2.5} (b), and PM_{2.5–10} (c) value and green bars the corresponding values without including the days of desert dust.

two quantities, total AOD and PM₁₀, for the complete dataset follows a similar behaviour between August and March, with differences in April (local PM minimum) and May (local AOD minimum), and a slightly different evolution in June–July. These discrepancies between these quantities lead to a moderately high correlation coefficient of 0.82 between AOD and PM₁₀, but their physical meaning is uncertain, taking into account the discrepancies in the two annual cycles. The seasonal cycles of DD contribution (both absolute and relative), to AOD and PM₁₀ differ in July (with a local minimum of AOD) and September (sharp fall of PM₁₀). Furthermore, it is worth mentioning that the maximum of March is more intense for the DD contribution to PM₁₀ than the DD contribution to AOD. Hence, the correlation factors between the DD contribution to PM₁₀ and to AOD are moderately high: 0.84 and 0.74 for the absolute and relative values, respectively.

The fine mode, represented by the PM_{2.5} data, follows the same pattern as PM₁₀ in the total and DD contribution curves (Table 4 and Fig. 6b). The DD contribution to PM_{2.5} is below 10 % for most of the year, with a mean value of ~9 %.

The total coarse-mode (PM_{2.5–10}) curve is also similar to that obtained for the total PM₁₀, although the mean contribution of the DD events is 16 % of the total PM_{2.5–10}, in contrast to the 12 % of the PM₁₀ (see Table 4). The DD contribution to PM_{2.5–10} (Table 4 and Fig. 6c) exhibits a strong maximum in March (1.7 $\mu\text{g m}^{-3}$ or 33 %), a reduction in April and May (around 14 %), large values in June (1.4 $\mu\text{g m}^{-3}$ or 25 %) followed by a weak decrease in July and August (1.3 $\mu\text{g m}^{-3}$ or 21 %), and low values in autumn and winter.

4.3.2 Interannual variability and trends

The interannual variations of total PM₁₀, PM_{2.5}, and PM_{2.5–10} and the corresponding DD contributions to these PM_x concentrations are plotted in Fig. 7 and reported in Table 5. In the shape of the DD contribution we can distinguish two periods associated with the strong minimum of 2009. The first period has a decreasing trend from 2003 to 2009 where the first 4 years have similar DD contributions among them. The second period starts with a strong rise of the DD contribution from 2009 to 2012, followed by a significant fall in 2013 and a final rise in 2014. The absolute maximum DD contribution occurs in 2006 (2.4 $\mu\text{g m}^{-3}$ or 21 %) and the absolute minimum is observed in 2013 with 0.4 $\mu\text{g m}^{-3}$ or 5 %, although it is very similar to the value in 2009. The solid line in Fig. 7 illustrating the evolution of the relative contribution highlights the minima of 2005, 2009 and 2013 and the maxima of 2004, 2006, 2012, and 2014.

The interannual evolutions of the total PM₁₀ and AOD are very similar (see Fig. S2, Supplement) with a correlation coefficient of around 0.9 in 2003–2014. With respect to the yearly values of DD contributions to AOD and PM₁₀, they show a correlation coefficient of 0.81. The agreement is also quite good for the relative DD contributions to AOD and PM₁₀ (correlation coefficient around 0.7). This high agreement, extremely good during 2009–2013, is not seen for some years. For instance, the reason behind the low DD contribution to AOD in 2006 can be explained by the poor sampling during that year (see Table 1). So far, no reasonable explanation has been found for the strong fall between 2004 and 2005 in the DD contribution to AOD despite the fact that total AOD and PM₁₀ display the same behaviour. The DD contribution to PM₁₀ is notably larger than that obtained for AOD in 2014. The high interannual variability of these quantities highlights the necessity of longer time periods to assess this kind of relationships, bearing in mind that the net contribution of DD aerosols is represented by very low values with a high uncertainty; hence this variability falls within the expected range of change. These results are of interest for long-term studies of columnar and surface aerosol loads in relation to their evolution and trends for climate studies be-

cause tropospheric aerosols have a strong regional signature and the area studied presents exceptional background conditions representative of the western Mediterranean Basin.

The weak impact of the DD events on the PM_{2.5} levels (fine mode, see Fig. 7b and Table 5) is reflected in the low relative contribution with only 3 years (2003, 2005, and 2006) presenting values higher than 12 %. The last years of the period analysed (2009–2014) present a notable low DD contribution to PM_{2.5} below 7 %. By contrast, PM_{2.5–10} (Fig. 7c and Table 5) still follows the PM₁₀ pattern. The initial years are the ones with the largest contributions (around 27 % until 2006), while 2013 shows the minimum values (around 5 %) together with 2009 (~ 7 %).

There is a decreasing trend of all the quantities shown in Fig. 7. The general decrease in PM_X levels has been previously reported for the Peñausende site and for shorter periods (e.g. Barmpadimos et al., 2012; Bennouna et al., 2014; Mateos et al., 2014b; Querol et al., 2014), and it has been corroborated by the temporal trends obtained in this study (see Table 3). Cusack et al. (2012) pointed out a percentage reduction ranging between 7 to 41 % in the yearly PM_{2.5} from 2002 and 2010 at 11 Spanish sites. To quantify the observed decrease in the DD impact, Table 3 also presents the temporal trends of the DD contribution of PM₁₀, PM_{2.5}, and PM_{2.5–10}. The general decrease in PM₁₀ (0.46 µg m⁻³ per year, with a *p* value < 0.01) at the Peñausende site for the period 2003–2014 is in line with previous studies (e.g. Querol et al., 2014; Mateos et al., 2015). Regarding the DD contribution, the fall in the three quantities is quantified as around –10 % per year. In particular, the DD contribution to PM₁₀ has decreased by an absolute amount of 0.14 µg m⁻³ per year (*p* value of 0.06) and 0.08 µg m⁻³ per year (*p* value < 0.01) for PM_{2.5}. The reduction observed in the DD event days (see Sect. 4.1.3) has also led to a significant fall in total particulate matter. Comparing the temporal trends of the PM₁₀ DD contribution and the rate for the total quantity, the DD impact has caused 30 % of the total PM₁₀ decrease in north-central Spain. This percentage is smaller (about 21 %) for the PM_{2.5} case. In the north-eastern region, Querol et al. (2014) showed that crustal matter accounted for 14 % of the total PM_{2.5} decrease between 2001 and 2012.

4.4 Estimation of associated uncertainty of the methodology

No quantification has been done for the associated uncertainties in the number of events and associated days in most of the literature. The same happens for the uncertainty linked to the DD contribution, which can be evaluated as a consequence of the earlier error of DD detection. One way to estimate a possible range of the real uncertainty is the comparison of results obtained from different methodologies. This task was addressed by the above-mentioned study of Viana et al. (2010) showing relative differences in the number of dusty days of about 12 and 28–50 % for the DD absolute con-

tribution. A big step took place when the proposed methodology by Escudero et al. (2007) was taken as the official standard method. However, the 30 days moving percentile used to establish the regional background has been changed from 30 % (reported by Escudero et al., 2007) to 40 % (Pey et al., 2013a; Salvador et al., 2013, 2014). There is evidence that this percentile may be site dependent, thus demonstrating the difficulty of this evaluation. Otherwise, it must be borne in mind that a big difference exists between the Escudero et al. (2007) methodology and that applied by us. This subsection describes a first attempt to estimate the uncertainty associated with the method used in our study.

Fingerprints of each DD event day are visible on at least one of the quantities related to aerosol load (columnar or surface) analysed in the inventory evaluation (see Sect. 3), plus the additional information on air mass back trajectories, satellite images, and synoptic scenarios. Usually, several of these variables simultaneously corroborate the DD presence, especially due to the low background values that characterize the north-central Spanish region. Therefore, the thorough inspection of all the information provided by different sources at the same time causes the error in the DD identification to be minimal. From our experience during these 12 years of data, we consider that possible error sources can be, mainly, the following: gaps in the data series, classification or not of a day when the aerosol load is close to the threshold values, and uncertainty of the instrumental techniques and the ancillary tools. Therefore, we can estimate that about 3–5 days per year could be missed in the annual sum of dusty days. This assumption is based on our long-term expertise in this evaluation when the DD inventory has been re-evaluated to ensure its accuracy. So the associated relative uncertainty, considering the average of 35 DD event days per year, is ~ 9–15 %, which is in line with the results reported by Viana et al. (2010) as mentioned above. This estimation gives a realistic range for the error associated with this methodology of visual inspection. The 5 days per year uncertainty (or 15 %) can overestimate the real error, but even this percentage can be considered acceptable as the maximum average error. Regarding the sum of dusty days in the seasonal cycle, the same range of error can be assumed in every monthly interannual value.

The possibility of missing these few days with DD fingerprints (~ 3–5 per year and per interannual month) leads to an uncertainty in the evaluation of the DD contribution to AOD values. Hence, to quantify the uncertainty in the seasonal cycle of the DD contribution to AOD each interannual monthly database is extended adding 9 % of DD event days (considering that 3 days are missed). For these “extra” days the AOD is assumed as the mean value during the DD events in that month. For instance, 4 days are added in June with a mean AOD of 0.27 and 1 day is added in January with AOD_{440 nm} = 0.18. The DD contribution is calculated for the new data series, evaluating the differences with those values shown in Sect. 4.2 (from the original database). The results

show a small change in the DD contribution to AOD, always below 0.002. For instance, for June the relative uncertainty caused by the added days is 6.7 % (the absolute DD contribution for the original evaluation is 0.027). However, those months with less absolute DD contribution to AOD cause a relative difference between 15 and 20 % (such as January and December). Overall, the mean uncertainty is 0.0013 or 9.7 % when the uncertainties of the 12 multi-annual monthly values are averaged. This relative uncertainty is in line with the 10 % calculated by receptor modelling studies (Viana et al., 2010). The same procedure is applied for the interannual DD contribution to AOD. On average, the inclusion of 9 % DD extra days causes an uncertainty of 0.0014 or 8.3 %. If the assumption of a missing 3 days per year is even increased to 5 days per year, the uncertainties caused regarding the DD contribution to AOD values only increase up to 14 %. Hence, the reliability of the method followed here is demonstrated because of the low changes in the results when the DD inventory is augmented with possible dusty days missed.

In the same way, the study of the uncertainties of the DD contribution to PM_{10} is also addressed with the same method (adding 9–15 % extra DD event days). The results for PM_{10} indicate a mean uncertainty of 0.1–0.13 $\mu\text{g m}^{-3}$ or 8–14 % in the evaluation of both annual cycle and interannual evolution. Hence, this relative uncertainty can be also extrapolated to the $\text{PM}_{2.5}$ and $\text{PM}_{2.5-10}$ DD contributions showing the feasibility of this method.

4.5 Analysis of the synoptic scenarios during desert dust episodes

Using the ancillary information used in the final choice of the DD identification, the synoptic scenarios that favour the arrival of air masses originating in the north of Africa are also studied. These scenarios are those defined and described by Escudero et al. (2005): via the Atlantic Arch (North Africa High located at surface level, NAH-S), directly from northern Africa by deep low pressure (Atlantic Depression, AD) or by a convective system (North African High located at upper levels, NAH-A), and from the Mediterranean area (North African Depression, NAD). Overall, the geographical positions and heights of the high- and low-pressure systems produce the mineral aerosols that reach the IP. Figure 8 presents the annual cycle and interannual variability of the number of episodes associated with each synoptic scenario. The synoptic scenario of each episode has been established considering all the daily meteorological maps during the episode.

The synoptic scenario analysis of the DD events (see Fig. 8a) has shown a predominance of the NAH-A (81 out of 152 episodes), in particular, during the warm season (from May to October). This scenario is produced by an intense solar heating of the Saharan desert. These air masses present large DD loads which can arrive at high altitudes (up to 5 km a.s.l.). In our study region, the NAH-S scenario governs (38 out of 152 episodes) the DD intrusions between Decem-

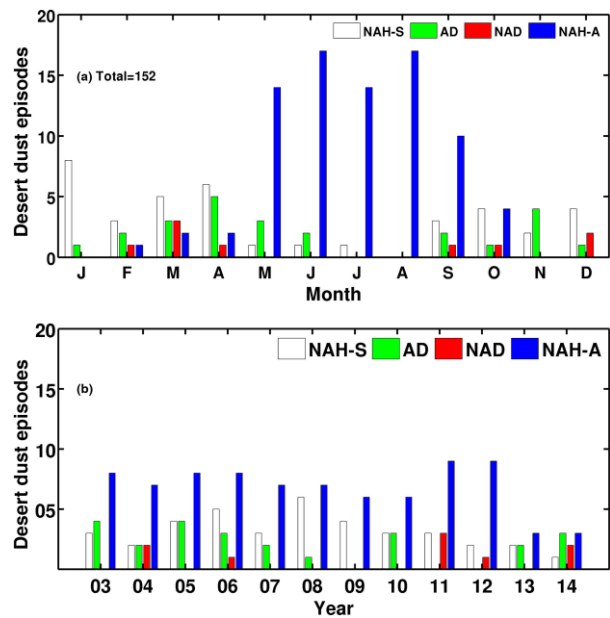


Figure 8. Annual cycle (a) and interannual (b) variability of DD episodes classified in terms of their synoptic scenarios: NAH-S (white bars), AD (green bars), NAD (red bars), and NAH-A (blue bars). The four synoptic scenarios are described in the text (see Sect. 4.5).

ber and April (being also significant in October) and generates transport at the lower atmospheric levels (generally below 1 km a.s.l.). The AD scenario plays a minor role (24 out of 152 episodes) but with an influence confined to between February and May, September, and November. The NAD scenario only presents an important contribution in March and December (9 out of 152 episodes).

The fingerprints of the evolution of these synoptic scenarios are reflected in the climatology of the DD episodes shown in Fig. 2. The rapid increase in DD events in March (see Fig. 2) is caused by a larger influence of NAH-S (3 to 5 DD events with respect to February), the marked appearance of NAD (3 events), and a slight increase in AD (2 to 3 DD events with respect to February). The synoptic situation in April changes and the NAD scenario almost disappears while NAH-S and AD increase their influence. The local summer minimum in July is caused by the lower occurrence of the NAH-A conditions. Previous studies have found this minimum for other columnar quantities, such as the vertical precipitable water vapour (Ortiz de Galisteo et al., 2013). The absolute DD event minimum of November is caused by the total disappearance of the NAH-A scenario.

Comparing these results with previous inventories performed in other geographical areas of the IP, the synoptic scenario climatology presents some discrepancies. Toledano et al. (2007b) have also found a predominance of the NAH-A conditions during summer for the El Arenosillo site (south-western IP) in the period 2000–2005. However, the role

played by the NAH-S seems to be minor during winter compared to the north-central area. The DD inventory in the northern Mediterranean Spanish coast has been analysed by Escudero et al. (2005) between 1996 and 2002. They also obtained the major predominance of the NAH-A during summer, although the NAD scenario shows a notable impact on the DD events in May and November. These outbreaks arriving from the Mediterranean area are also reported in the months of February, March, and November in the El Arenosillo inventory.

The interannual distribution of DD events and the four synoptic scenarios (see Fig. 8b) corroborate the predominance of the synoptic scenario NAH-A every year. Overall, there is a mean of seven episodes per year due to this scenario in the north-central area of the IP, the maximum influence being in 2012 where 9 out 12 events occurred in this situation. A special feature is the simultaneous appearance of the four scenarios only in the years 2004, 2006, and 2014. The last 2 years of the analysed period (2013–2014) have shown a decrease in the number of episodes that can be attributed to the absence of synoptic conditions favouring mineral dust transport during summer (NAH-A scenario). The occurrence of the NAH-S and AD scenarios presents high interannual variability but the number of DD episodes they caused is always smaller than those caused by NAH-A. Finally, NAD conditions in the north-central IP are only relevant in 2004, 2011, and 2014 with 2, 3, and 2 events, respectively. However, this scenario plays a key role in the north-eastern area of the IP (e.g. Escudero et al., 2005), which shows that DD intrusions arriving through the Mediterranean area rarely reach the north-central region of Spain.

5 Conclusions

In this study, a methodology to obtain a reliable identification of desert dust (DD) intrusions is proposed and applied to the north-central area of the Iberian Peninsula. Long-term datasets of AOD and PM_X for the background sites of Palencia and Peñausende (representative of the study area) have been used as core information for the detection of desert dust intrusions in this area during an 12-year period (from January 2003 to December 2014). The analysis of ancillary information, such as air mass back trajectories at three altitude levels (500, 1500, and 3000 m a.s.l.), MODIS-AOD and true-colour images, and meteorological maps, has been used to establish the duration of each desert dust episode, creating a reliable inventory of desert dust episodes. The main conclusions can be summarized as follows:

1. The simultaneous consideration of surface and columnar aerosols has been shown to be a reliable tool in DD identification. More than half of the inventory has been detected by $\text{AOD}_{440\text{nm}}$ and PM_{10} data at the same time. However, each quantity can provide DD detection by itself in a large number of cases (114 and 80 out of 418 days detected by only PM_{10} and AOD data, respectively). The smaller coverage of AOD sampling is not a major handicap in this process.
2. A total of 152 episodes composed of 418 days presented desert dust aerosols during the entire period. The annual cycles of the number of DD episodes and days follow a similar pattern: an increase in March, a weak fall of event days in April, a notable increment between May and September, and a progressive decline to the absolute minimum in winter, with the absolute maximum in June and local minimum in July or August. Interannual variability of the number of DD episodes and dusty days is high, ranging between 7 episodes (15 dusty days) in 2013 and 17 episodes (67 dusty days) in 2006. A temporal trend of -2.7 dusty days per year (95 % significance level) highlights the decrease between 2003 and 2014. Therefore, a reduction in the DD outbreaks in the north-central area of the Iberian Peninsula is found during the period studied.
3. Overall, the mean DD contribution to $\text{AOD}_{440\text{nm}}$ is 0.015 or 11.5 %, while for the surface concentration PM_{10} , $\text{PM}_{2.5}$, and $\text{PM}_{2.5-10}$ this is $1.3 \mu\text{g m}^{-3}$ (11.8 %), $0.55 \mu\text{g m}^{-3}$ (8.5), and $0.79 \mu\text{g m}^{-3}$ (16.1 %), respectively.
4. The annual cycle of the DD contribution to the aerosol load peaks in March, decreases in April–May, notably increases during summer months (the AOD curve has a local minimum in July), and experiences a progressive decline after summer (with a significant fall in September for the PM_{10} curve) towards minimum values in winter. The maximum DD contribution to AOD occurs in June and August close to 0.03, while the PM_{10} maximum DD contribution reaches $\sim 2.4 \mu\text{g m}^{-3}$ in August.
5. The interannual variability of the DD contribution to the aerosol load is at a maximum in 2004 for AOD with 0.03 and 2006 for PM_{10} with $2.4 \mu\text{g m}^{-3}$ and at a minimum in 2013 (0.004 for $\text{AOD}_{440\text{nm}}$ and $0.4 \mu\text{g m}^{-3}$ for PM_{10}). The correlation coefficient between the DD contribution to $\text{AOD}_{440\text{nm}}$ and PM_{10} yearly means is 0.81.
6. The temporal trends of the DD contribution to AOD, PM_{10} , and $\text{PM}_{2.5}$ have values of -0.0019 (p value of 0.02), $-0.14 \mu\text{g m}^{-3}$ (p value of 0.06) per year, and $-0.08 \mu\text{g m}^{-3}$ (p value < 0.01) per year in the analysed period, respectively. All these negative rates indicate a decrease in the levels of natural mineral dust aerosols, which represents around 30 % of the total aerosol load decrease shown by AOD (columnar) and PM_{10} (surface) in 2003–2014. This decrease is around 20 % for the $\text{PM}_{2.5}$ case.
7. DD outbreaks have mainly reached the north-central Iberian Peninsula directly from northern Africa by a

convective system (NAH-A synoptic scenario), with clear predominance in the summer months. The NAH-S (via the Atlantic Arch) and AD (directly from northern Africa by a deep low pressure) scenarios present a variable influence thorough the year, while the NAD (from the Mediterranean area) conditions are only important in March and December.

The proposed inventory is the first one based on long-term AOD-PM data series. The use of worldwide networks (EMEP and AERONET) ensures that this method can be implemented in other regions with background aerosol observations, as long as nearby PM_x and AOD measurement sites in clear remote (background) locations are analysed.

With careful inspection of all the information, the inventory can be a useful tool to develop and validate automated methodologies which use other instruments such as Raman lidars and ceilometers or which use model forecasts. The comparison between different methodologies allows a more reliable estimation of uncertainties in DD detection and its contribution to total aerosol load. Future studies based on this inventory will be focused on a global characterization of microphysical and radiative properties of desert dust including the evaluation of its radiative forcing over the study region. Therefore, these results are useful for assessing regional climate change studies linked to atmospheric aerosols because of the excellent clean background conditions of the area, which may be considered one of the few sites or areas in south-western Europe with these conditions.

6 Data availability

Data used in this study are freely available from AERONET and EMEP networks. The specific inventory dataset is the intellectual property of the research group that carried out this work.

The Supplement related to this article is available online at doi:10.5194/acp-16-8227-2016-supplement.

Acknowledgements. The authors are grateful to Spanish MINECO for the financial support of the FPI grant BES-2012-051868 and project CGL2012-33576. Thanks are due to EMEP (especially to MAGRAMA and AEMET) and AERONET-PHOTONS-RIMA staff for providing observations and for the maintenance of the networks. The research leading to these results has received funding from the European Union Seventh Framework Programme (FP7/2007-2013) under grant agreement Nr. 262254 [ACTRIS 2]. We also thank “Consejería de Fomento y Medio Ambiente” for their support to desert dust studies in the Castilla y León region, as well as “Consejería de Educación de Junta de Castilla y León” for financing the project (VA100U14).

Edited by: W. Lahoz

References

- Aas, W., Espen Yttri, K., Stohl, A., Lund Myhre, C., Karl, M., Tyro, S., Marecková, K., Wankmüller, R., Klimont, Z., Heyes, C., Alastuey, A., Querol, X., Pérez, N., Moreno, T., Lucarelli, F., Areskoug, H., Balan, V., Cavalli, F., Putaud, J. P., Cape, J. N., Catrambone, M., Ceburnis, D., Conil, S., Gevorgyan, L., Jaffrezo, J. L., Hueglin, C., Mihalopoulos, N., Mitosinkova, M., Riffault, V., Sellegri, K., Spindler, G., Schuck, T., Pfeffer, U., Breuer, L., Adolfs, D., Chuntonova, L., Arabidze, M., and Abdulazizov, E.: Transboundary particulate matter in Europe Status report 2013, EMEP Report, 4/2013 (Ref. O-7726), 2013.
- Alados-Arboledas, L., Lyamani, H., and Olmo, F. J.: Aerosol size properties at Armilla, Granada (Spain), Q. J. Roy. Meteor. Soc., 129, 1395–1413, doi:10.1256/qj.01.207, 2003.
- Barmpadimos, I., Keller, J., Oderbolz, D., Hueglin, C., and Prévôt, A. S. H.: One decade of parallel fine (PM_{2.5}) and coarse (PM₁₀–PM_{2.5}) particulate matter measurements in Europe: trends and variability, Atmos. Chem. Phys., 12, 3189–3203, doi:10.5194/acp-12-3189-2012, 2012.
- Basart, S., Pérez, C., Cuevas, E., Baldasano, J. M., and Gobbi, G. P.: Aerosol characterization in Northern Africa, Northeastern Atlantic, Mediterranean Basin and Middle East from direct-sun AERONET observations, Atmos. Chem. Phys., 9, 8265–8282, doi:10.5194/acp-9-8265-2009, 2009.
- Bègue, N., Tulet, P., Chaboureau, J. P., Roberts, G., Gomes, L., and Mallet, M.: Long-range transport of Saharan dust over north-western Europe during EUCAARI 2008 campaign: Evolution of dust optical properties by scavenging, J. Geophys. Res., 117, D17201, doi:10.1029/2012JD017611, 2012.
- Belis, C. A., Karagulian, F., Larsen, B. R., and Hopke, P. K.: Critical review and met-analysis of ambient particulate matter source apportionment using receptor models in Europe, Atmos. Environ., 69, 94–108, doi:10.1016/j.atmosenv.2012.11.009, 2013.
- Bennouna, Y. S., Cachorro, V. E., Torres, B., Toledano, C., Berjón, A., de Frutos, A. M., and Alonso Fernández Coppel, I.: Atmospheric turbidity determined by the annual cycle of the aerosol optical depth over north-center Spain from ground (AERONET) and satellite (MODIS), Atmos. Environ., 67, 352–364, doi:10.1016/j.atmosenv.2012.10.065, 2013.
- Bennouna, Y. S., Cachorro, V., Burgos, M. A., Toledano, C., Torres, B., and de Frutos, A.: Relationships between columnar aerosol optical properties and surface particulate matter observations in north-central Spain from long-term records (2003–2011), Atmos. Meas. Tech. Discuss., 7, 5829–5882, doi:10.5194/amtd-7-5829-2014, 2014.
- Boselli, A., Caggiano, R., Cornacchia, C., Madonna, F., Mona, L., Macchiato, M., Pappalardo, G., and Trippetta, S.: Multi year sun-photometer measurements for aerosol characterization in a Central Mediterranean site, Atmos. Res., 104–105, 98–110, doi:10.1016/j.atmosres.2011.08.002, 2012.
- Boucher, O., Randall, D., Artaxo, P., Bretherton, C., Feingold, G., Forster, P., Kermanen, V. M., Kondo, Y., Liao, H., Lohmann, U., Rasch, P., Satheesh, S. K., Sherwood, S., Stevens, B., and Zhang, X. Y.: Clouds and aerosols, in: Climate Change 2013: The Phys-

- ical Science Basis, Contribution of Working Group I to the Fifth Assessment Report of the Intergovernmental Panel on Climate Change, edited by: Stocker, T. F., Qin, D., Plattner, G.-K., Tignor, M., Allen, S. K., Boschung, J., Nauels, A., Xia, Y., Bex, V., and Midgley, P. M., 571–657, Cambridge University Press, Cambridge, United Kingdom and New York, NY, USA, 2013.
- Cachorro, V. E., Durán, P., Vergaz, R., and de Frutos, A. M.: Columnar physical and radiative properties of atmospheric aerosols in north central Spain, *J. Geophys. Res.*, 105, 7161–7175, doi:10.1029/1999JD901165, 2000.
- Cachorro, V. E., Vergaz, R., de Frutos, A. M., Vilaplana, J. M., Henriques, D., Laulainen, N., and Toledano, C.: Study of desert dust events over the southwestern Iberian Peninsula in year 2000: two case studies, *Ann. Geophys.*, 24, 1493–1510, doi:10.5194/angeo-24-1493-2006, 2006.
- Cachorro, V. E., Toledano, C., Prats, N., Sorribas, M., Mogo, S., Berjón, A., Torres, B., Rodrigo, R., de la Rosa, J., and De Frutos, A. M.: The strongest desert dust intrusion mixed with smoke over the Iberian Peninsula registered with Sun photometry, *J. Geophys. Res.*, 113, D14S04, doi:10.1029/2007JD009582, 2008.
- Córdoba-Jabonero, C., Sorribas, M., Guerrero-Rascado, J. L., Adame, J. A., Hernández, Y., Lyamani, H., Cachorro, V., Gil, M., Alados-Arboledas, L., Cuevas, E., and de la Morena, B.: Synergetic monitoring of Saharan dust plumes and potential impact on surface: a case study of dust transport from Canary Islands to Iberian Peninsula, *Atmos. Chem. Phys.*, 11, 3067–3091, doi:10.5194/acp-11-3067-2011, 2011.
- Cusack, M., Alastuey, A., Pérez, N., Pey, J., and Querol, X.: Trends of particulate matter ($\text{PM}_{2.5}$) and chemical composition at a regional background site in the Western Mediterranean over the last nine years (2002–2010), *Atmos. Chem. Phys.*, 12, 8341–8357, doi:10.5194/acp-12-8341-2012, 2012.
- d'Almeida, G., Koepke, P., and Shettle, E.: Atmospheric Aerosols: Global Climatology and Radiative Characteristics, Studies in Geophysical Optics and Remote Sensing, A. Deepak Pub., Hampton, Va, 561 pp., 1991.
- di Sarra, A., Di Biagio, C., Meloni, D., Monteleone, F., Pace, G., Pugnaghi, S., and Sferlazzo, D.: Shortwave and longwave radiative effects of the intense Saharan dust event of 25–26 March 2010 at Lampedusa (Mediterranean Sea), *J. Geophys. Res.*, 116, D23209, doi:10.1029/2011JD016238, 2011.
- Draxler, R. A., Stunder, B., Rolph, G., Stein, A., and Taylor, A.: HYSPLIT4 User's Guide, Air Resources Laboratory, National Oceanic and Atmospheric Administration (NOAA), Silver Spring, MD, 2014.
- Dubovik, O., Holben, B. N., Eck, T. F., Smirnov, A., Kaufman, Y. J., King, M. D., Tanré, D., and Slutsker, I.: Variability of absorption and optical properties of key aerosol types observed in worldwide locations, *J. Atmos. Sci.*, 59, 590–608, 2002.
- EC: Directive 2008/50/EC of the European Parliament and of the Council (21 May 2008) on Ambient Air Quality and Cleaner Air for Europe, Official Journal of the European Communities, L 151, 1–44, available at: <http://eur-lex.europa.eu/legal-content/EN/TXT/?uri=CELEX:32008L0050> (last access: 7 December 2015), 2008.
- Eck, T. F., Holben, B. N., Reid, J. S., Dubovik, O., Smirnov, A., O'Neill, N. T., Slutsker, I., and Kinne, S.: The wavelength dependence of the optical depth of biomass burning, urban and desert dust aerosols, *J. Geophys. Res.*, 104, 31333–31350, 1999.
- Eck, T. F., Holben, B. N., Sinyuk, A., Pinker, R. T., Goloub, P., Chen, H., Chatenet, B., Li, Z., Singh, R. P., Tripathi, S. N., Reid, J. S., Giles, D. M., Dubovik, O., O'Neill, N. T., Smirnov, A., Wang, P., and Xia, X.: Climatological aspects of the optical properties of fine/coarse mode aerosol mixtures, *J. Geophys. Res.*, 115, D19205, doi:10.1029/2010JD014002, 2010.
- Engelstaedter, S. and Washington, R.: Atmospheric controls on the annual cycle of North African dust, *J. Geophys. Res.*, 112, D03103, doi:10.1029/2006JD007195, 2007.
- Escudero, M., Castillo, S., Querol, X., Avila, A., Alarcón, M., Viana, M. M., Alastuey, A., Cuevas, E., and Rodríguez, S.: Wet and dry African dust episodes over eastern Spain, *J. Geophys. Res.*, 110, D18S08, doi:10.1029/2004JD004731, 2005.
- Escudero, M., Stein, A., Draxler, R. R., Querol, X., Alastuey, A., Castillo, S., and Avila, A.: Determination of the contribution of northern Africa dust source areas to PM_{10} concentrations over the central Iberian Peninsula using the hybrid single-particle lagrangian integrated trajectory model (HYSPPLIT) model, *J. Geophys. Res.*, 111, D06210, doi:10.1029/2005JD006395, 2006.
- Escudero, M., Querol, X., Pey, J., Alastuey, A., Pérez, N., Ferreira, F., Alonso, S., and Cuevas, E.: A methodology for the quantification of the net African dust load in air quality monitoring networks, *Atmos. Environ.*, 41, 5516–5524, doi:10.1016/j.atmosenv.2007.04.047, 2007.
- Escudero, M., Stein, A. F., Draxler, R. R., Querol, X., Alastuey, A., Castillo, S., and Avila, A.: Source apportionment for African dust outbreaks over the western Mediterranean using the HYSPPLIT model, *Atmos. Res.*, 99, 518–527, doi:10.1016/j.atmosres.2010.12.002, 2011.
- Estellés, V., Martínez-Lozano, J. A., Utrillas, M. P., and Campanelli, M.: Columnar aerosol properties in Valencia (Spain) by ground-based Sun photometry, *J. Geophys. Res.*, 112, D11201, doi:10.1029/2006JD008167, 2007.
- Ganor, E., Stupp, A., and Alpert, P.: A method to determine the effect of mineral dust aerosol on air quality. *Atmos. Environ.*, 43, 5463–5468, doi:10.1016/j.atmosenv.2009.07.028, 2009.
- Gkikas, A., Hatzianastassiou, N., Mihalopoulos, N., Katsoulis, V., Kazadzis, S., Pey, J., Querol, X., and Torres, O.: The regime of intense desert dust episodes in the Mediterranean based on contemporary satellite observations and ground measurements, *Atmos. Chem. Phys.*, 13, 12135–12154, doi:10.5194/acp-13-12135-2013, 2013.
- Gkikas, A., Basart, S., Hatzianastassiou, N., Marinou, E., Amiridis, V., Kazadzis, S., Pey, J., Querol, X., Jorba, O., Gassó, S., and Baldasano, J. M.: Mediterranean desert dust outbreaks and their vertical structure based on remote sensing data, *Atmos. Chem. Phys. Discuss.*, 15, 27675–27748, doi:10.5194/acpd-15-27675-2015, 2015.
- Goudie, A. S. and Middleton, N. J.: Desert Dust in the Global System, Springer-Verlag Berlin Heidelberg, Berlin, Germany, 288 pp., 2006.
- Guerrero-Rascado, J. L., Olmo, F. J., Avilés-Rodríguez, I., Navas-Guzmán, F., Pérez-Raírez, D., Lyamani, H., and Alados Arboledas, L.: Extreme Saharan dust event over the southern Iberian Peninsula in September 2007: active and passive remote sensing from surface and satellite, *Atmos. Chem. Phys.*, 9, 8453–8469, doi:10.5194/acp-9-8453-2009, 2009.
- Guirado, C., Cuevas, E., Cachorro, V. E., Toledano, C., Alonso-Pérez, S., Bustos, J. J., Basart, S., Romero, P. M., Camino,

- C., Mimouni, M., Zeudmi, L., Goloub, P., Baldasano, J. M., and de Frutos, A. M.: Aerosol characterization at the Saharan AERONET site Tamanrasset, *Atmos. Chem. Phys.*, 14, 11753–11773, doi:10.5194/acp-14-11753-2014, 2014.
- Haywood, J. M. and Boucher, O.: Estimates of the direct and indirect radiative forcing due to tropospheric aerosols: A review, *Rev. Geophys.*, 38, 513–543, doi:10.1029/1999RG000078, 2000.
- Hogan, T. and Rosmond, T.: The description of the Navy Operational Global Atmospheric Predictions System's spectral forecast model, *Mon. Weather Rev.*, 119, 1786–1815, doi:10.1175/1520-0493(1991)119<1786:TDOTNO>2.0.CO;2, 1991.
- Holben, B. N., Eck, T. F., Slutsker, I., Tanré, D., Buis, J. P., Setzer, A., Vermote, E., and Smirnov, A.: AERONET – A federated instrument network and data archive for aerosol characterization, *Remote Sens. Environ.*, 66, 1–16, doi:10.1016/S0034-4257(98)00031-5, 1998.
- Kalivitis, N., Gerasopoulos, E., Vrekousis, M., Kouvarakis, G., Kubilay, N., Hatzianastassiou, N., Vardavas, I., and Mihalopoulos, N.: Dust transport over the Eastern Mediterranean from TOMS, AERONET and surface measurements, *J. Geophys. Res.*, 112, D03202, doi:10.1029/2006JD007510, 2007.
- Kallos, G., Papadopoulos, A., and Katsafados, P.: Model-derived seasonal amounts of dust deposited on Mediterranean Sea and Europe. In Building the European Capacity in Operational Oceanography. Proceedings of the Third International Conference on EuroGOOS, Athens, Greece 3–6 December 2002, edited by: Dahlin, H., Flemming, N. C., Nittis, K., and Petersson, S. E., Elsevier Oceanography Series, 69, 57–63, 2003.
- Kaskaoutis, D., Kambezidis, H., Nastos, P., and Kosmopoulos, P.: Study on an intense dust storm over Greece, *Atmos. Environ.*, 42, 6884–6896, 2008.
- Kaskaoutis, D. G., Kosmopoulos, P. G., Nastos, P. T., Kambezidis, H. D., Sharma, M., and Mehdi, W.: Transport pathways of Sahara dust over Athens, Greece as detected by MODIS and TOMS, *Geomat. Nat. Hazards Risk*, 3, 35–54, 2012.
- Kaufman, Y. J., Koren, I., Remer, L. A., Tanré, D., Ginoux, P., and Fan, S.: Dust transport and deposition observed from the terra-moderate resolution imaging spectroradiometer (MODIS) space-craft over the Atlantic ocean, *J. Geophys. Res.*, 110, D10S12, doi:10.1029/2003JD004436, 2005.
- Knippertz, P. and Stuut, J.-B. W.: Mineral Dust: A Key Player in the Earth System, Springer Netherlands, Dordrecht, Netherlands, 509 pp., 2014.
- Knippertz, P. and Todd, M.C.: Mineral dust aerosols over the Sahara: Meteorological controls on emission and transport and implications for modeling, *Rev. Geophys.*, 50, RG1007, doi:10.1029/2011RG000362, 2012.
- Kulmala, M., Asmi, A., Lappalainen, H. K., Carslaw, K. S., Pöschl, U., Baltensperger, U., Hov, Ø., Brenquier, J.-L., Pandis, S. N., Facchini, M. C., Hansson, H.-C., Wiedensohler, A., and O'Dowd, C. D.: Introduction: European Integrated Project on Aerosol Cloud Climate and Air Quality interactions (EUCAARI) – integrating aerosol research from nano to global scales, *Atmos. Chem. Phys.*, 9, 2825–2841, doi:10.5194/acp-9-2825-2009, 2009.
- Lohmann, U. and Feichter, J.: Global indirect aerosol effects: a review, *Atmos. Chem. Phys.*, 5, 715–737, doi:10.5194/acp-5-715-2005, 2005.
- Lohmann, U., Rotstayn, L., Storelvmo, T., Jones, A., Menon, S., Quaas, J., Ekman, A. M. L., Koch, D., and Ruedy, R.: Total aerosol effect: radiative forcing or radiative flux perturbation?, *Atmos. Chem. Phys.*, 10, 3235–3246, doi:10.5194/acp-10-3235-2010, 2010.
- Lyamani, H., Olmo, F. J., and Alados-Arboledas, L.: Saharan dust outbreak over southeastern Spain as detected by sun photometer, *Atmos. Environ.*, 39, 7276–7284, doi:10.1016/j.atmosenv.2005.09.011, 2005.
- MAGRAMA: Ministerio de Agricultura, Alimentación y Medio Ambiente. “Procedimiento para la identificación de episodios naturales de PM₁₀ y PM_{2.5}, y la demostración de causa en lo referente a las superaciones del valor límite diario de PM₁₀”, Madrid, Spain, Abril 2013, available at: http://www.magrama.gob.es/es/calidad-y-evaluacion-ambiental/temas/atmosfera-y-calidad-del-aire/Metodolog%C3%ADA_para_episodios_naturales_2012_tcm7-281402.pdf (last access: 7 December 2015), 2013.
- MAGRAMA: Ministerio de Agricultura, Alimentación y Medio Ambiente, “Episodios naturales de partículas 2014”, Madrid, Spain, Abril 2015, available at: http://www.magrama.gob.es/es/calidad-y-evaluacion-ambiental/temas/atmosfera-y-calidad-del-aire/episodiosnaturales2014_tcm7-379247.pdf (last access: 7 December 2015), 2015.
- Mahowald, N. M., Kloster, S., Engelstaedter, S., Moore, J. K., Mukhopadhyay, S., McConnell, J. R., Albani, S., Doney, S. C., Bhattacharya, A., Curran, M. A. J., Flanner, M. G., Hoffman, F. M., Lawrence, D. M., Lindsay, K., Mayewski, P. A., Neff, J., Rothenberg, D., Thomas, E., Thornton, P. E., and Zender, C. S.: Observed 20th century desert dust variability: impact on climate and biogeochemistry, *Atmos. Chem. Phys.*, 10, 10875–10893, doi:10.5194/acp-10-10875-2010, 2010.
- Mateos, D., Antón, M., Toledano, C., Cachorro, V. E., Alados-Arboledas, L., Sorribas, M., Costa, M. J., and Baldasano, J. M.: Aerosol radiative effects in the ultraviolet, visible, and near-infrared spectral ranges using long-term aerosol data series over the Iberian Peninsula, *Atmos. Chem. Phys.*, 14, 13497–13514, doi:10.5194/acp-14-13497-2014, 2014a.
- Mateos, D., Sanchez-Lorenzo, A., Antón, M., Cachorro, V. E., Calbo, J., Costa, M. J., Torres, B., and Wild, M.: Quantifying the respective roles of aerosols and clouds in the strong brightening since the early 2000s over the Iberian Peninsula, *J. Geophys. Res. Atmos.*, 119, 10382–10393, doi:10.1002/2014JD022076, 2014b.
- Mateos, D., Cachorro, V. E., Toledano, C., Burgos, M. A., Bennouna, Y., Torres, B., Fuertes, D., González, R., Guirado, C., Calle, A., and de Frutos, A. M.: Columnar and surface aerosol load over the Iberian Peninsula establishing annual cycles, trends, and relationships in five geographical sectors, *Sci. Total Environ.*, 518–519, 378–392, doi:10.1016/j.scitotenv.2015.03.002, 2015.
- Meloni, D., di Sarra, A., Biavati, G., De Luisi, J. J., Monteleone, F., Pace, G., Piacentino, S., and Sferlazzo, D. M.: Seasonal behavior of Saharan dust events at the Mediterranean island of Lampedusa in the period 1999–2005, *Atmos. Env.*, 41, 3041–3056, doi:10.1016/j.atmosenv.2006.12.001, 2007.
- Mona, L., Amodeo, A., Pandolfi, M., and Pappalardo, G.: Saharan dust intrusions in the mediterranean area: Three years of raman lidar measurements, *J. Geophys. Res.*, 111, D16203, doi:10.1029/2005JD006569, 2006.

- Mona, L., Papagiannopoulos, N., Basart, S., Baldasano, J., Bini-
etoglou, I., Cornacchia, C., and Pappalardo, G.: EARLINET
dust observations vs. BSC-DREAM8b modeled profiles: 12-
year-long systematic comparison at Potenza, Italy, *Atmos. Chem.
Phys.*, 14, 8781–8793, doi:10.5194/acp-14-8781-2014, 2014.
- Obregón, M. A., Pereira, S., Wagner, F., Serrano, A., Cancillo, M.
L., and Silva, A. M.: Regional differences of column aerosol pa-
rameters in western Iberian Peninsula, *Atmos. Environ.*, 62, 208–
219, doi:10.1016/j.atmosenv.2012.08.016, 2012.
- O'Neill, N. T., Eck, T. F., Smirnov, A., Holben, B. N., and Thulasir-
aman, S.: Spectral discrimination of coarse and fine mode optical
depth, *J. Geophys. Res.*, 108, 4559, doi:10.1029/2002JD002975,
2003.
- Ortiz de Galisteo, J. P., Bennouna, Y., Toledano, C., Cachorro, V.,
Romero, P., Andrés, M. I., and Torres, B.: Analysis of the annual
cycle of the precipitable water vapour over Spain from 10-year
homogenized series of GPS data, *Q. J. Roy. Meteor. Soc.*, 140,
397–406, doi:10.1002/qj.2146, 2013.
- Pace, G., di Sarra, A., Meloni, D., Piacentino, S., and Chamard,
P.: Aerosol optical properties at Lampedusa (Central Medi-
terranean). 1. Influence of transport and identification of dif-
ferent aerosol types, *Atmos. Chem. Phys.*, 6, 697–713,
doi:10.5194/acp-6-697-2006, 2006.
- Papayannis, A., Amiridis, V., Mona, L., Tsaknakis, G., Balis, D.,
Bosenberg, J., Chaikovski, A., De Tomasi, F., Grigorov, I., Mat-
tis, I., Mitev, V., Muller, D., Nickovic, S., Perez, C., Pietruczuk,
A., Pisani, G., Ravetta, F., Rizi, V., Sicard, M., Trickl, T., Wie-
igner, M., Gerdung, M., Mamouri, R. E., D'Amico, G., and Pappa-
lardo, G.: Systematic lidar observations of Saharan dust over
Europe in the frame of EARLINET (2000–2002), *J. Geophys.
Res.*, 113, D10204, doi:10.1029/2007jd009028, 2008.
- Pérez, C., Nickovic, S., Baldasano, J. M., Sicard, M., Rocaden-
bosch, F., and Cachorro, V. E.: A long Saharan dust event over
the western mediterranean: Lidar, sun photometer observations,
and regional dust modeling, *J. Geophys. Res.*, 111, D15214,
doi:10.1029/2005JD006579, 2006.
- Pérez, L., Tobías, A., Querol, X., Pey, J., Alastuey, A., Díaz, J., and
Sunyer, J.: Saharan dust, particulate matter and cause-specific
mortality: A case-crossover study in Barcelona (Spain), *Environ.
Int.*, 48, 150–155, doi:10.1016/j.envint.2012.07.001, 2012.
- Pey, J., Querol, X., Alastuey, A., Forastiere, F., and Stafoggia,
M.: African dust outbreaks over the Mediterranean Basin during
2001–2011: PM₁₀ concentrations, phenomenology and trends,
and its relation with synoptic and mesoscale meteorology, *At-
mos. Chem. Phys.*, 13, 1395–1410, doi:10.5194/acp-13-1395-
2013, 2013a.
- Pey, J., Alastuey, A., and Querol, X.: PM₁₀ and PM_{2.5} source at the
insular location in the western Mediterranean by using source ap-
portionment techniques, *Sci. Total Environ.*, 456–457, 267–277,
doi:10.1016/j.scitotenv.2013.03.084, 2013b.
- Pope, C. A.: Review: Epidemiological basis for particulate air
pollution health standards, *Aerosol Sci. Tech.*, 31, 4–14,
doi:10.1080/027868200303885, 2000.
- Prospero, J. M.: Long-term measurements of the transport of
African mineral dust to the Southeastern United States: Impli-
cations for regional air quality, *J. Geophys. Res.*, 104, 15.917–
15.927, doi:10.1029/1999JD900072, 1999.
- Prospero, J. M., Ginoux, P., Torres, O., Nicholson, S. E., and Gill,
T. E.: Environmental characterization of global sources of atmo-
- spheric soil dust identified with the nimbus 7 total ozone map-
ping spectrometer (TOMS) absorbing aerosol product, *Rev. Geo-
phys.*, 40, 2-1-2-31, doi:10.1029/2000RG000095, 2002.
- Querol, X., Pey, J., Pandolfi, M., Alastuey, A., Cusack, M.,
Pérez, N., Moreno, T., and Kleanthous, S.: African dust
contributions to mean ambient PM₁₀ mass-levels across
the Mediterranean Basin, *Atmos. Environ.*, 43, 4266–4277,
doi:10.1016/j.atmosenv.2009.06.013, 2009.
- Querol, X., Alastuey, A., Viana, M., Moreno, T., Reche, C., Min-
guillón, M. C., Ripoll, A., Pandolfi, M., Amato, F., Karanasiou,
A., Pérez, N., Pey, J., Cusack, M., Vázquez, R., Plana,
F., Dall’Osto, M., de la Rosa, J., Sánchez de la Campa,
A., Fernández-Camacho, R., Rodríguez, S., Pio, C., Alados-
Arboledas, L., Titos, G., Artiñano, B., Salvador, P., García Dos
Santos, S., and Fernández Patier, R.: Variability of carbonaceous
aerosols in remote, rural, urban and industrial environments in
Spain: implications for air quality policy, *Atmos. Chem. Phys.*,
13, 6185–6206, doi:10.5194/acp-13-6185-2013, 2013.
- Querol, X., Alastuey, A., Pandolfi, M., Reche, C., Pérez, N.,
Minguillón, M. C., Moreno, T., Viana, M., Escudero, M.,
Orio, A., Pallarés, M., and Reina, F.: 2001–2012 trends
on air quality in Spain, *Sci. Total Environ.*, 490, 957–969,
doi:10.1016/j.scitotenv.2014.05.074, 2014.
- Rodríguez, S., Querol, X., Alastuey, A., Kallos, G., and Kakaliagou,
O.: Saharan dust contributions to PM₁₀ and TSP levels in
Southern and Eastern Spain, *Atmos. Environ.*, 35, 2433–2447,
doi:10.1016/S1352-2310(00)00496-9, 2001.
- Rodríguez, S., Querol, X., Alastuey, A., and Plana, F.: Sources
and processes affecting levels and composition of atmospheric
aerosol in the western Mediterranean, *J. Geophys. Res.*, 107,
4777, doi:10.1029/2001JD001488, 2002.
- Rodríguez, S., Cuevas, E., Prospero, J. M., Alastuey, A., Querol,
X., López-Solano, J., García, M. I., and Alonso-Pérez, S.: Mod-
ulation of Saharan dust export by the North African dipole, *At-
mos. Chem. Phys.*, 15, 7471–7486, doi:10.5194/acp-15-7471-
2015, 2015.
- Salvador, P., Artiñano, B., Molero, F., Viana, M., Pey, J., Alastuey,
A., and Querol, X.: African Dust Contribution to Ambient
Aerosol Levels Across Central Spain: Characterization of Long-
Range Transport Episodes of Desert Dust, *Atmos. Res.*, 127,
117–129, doi:10.1016/j.atmosres.2011.12.011, 2013.
- Salvador, P., Alonso-Pérez, S., Pey, J., Artiñano, B., de Bustos, J.
J., Alastuey, A., and Querol, X.: African dust outbreaks over the
western Mediterranean Basin: 11-year characterization of atmo-
spheric circulation patterns and dust source areas, *Atmos. Chem.
Phys.*, 14, 6759–6775, doi:10.5194/acp-14-6759-2014, 2014.
- Sanchez-Lorenzo, A., Calbó, J., and Wild, M.: Global and dif-
fuse solar radiation in Spain: Building a homogeneous dataset
and assessing trends, *Global Planet. Change*, 100, 343–352,
doi:10.1016/j.gloplacha.2012.11.010, 2013.
- Stein, A., Draxler, R., Rolph, G., Stunder, B., Cohen, M., and
Ngan, F.: NOAA’s HYSPLIT atmospheric transport and disper-
sion modeling system, *Bull. Am. Meteorol. Soc.*, 96, 2059–2077,
doi:10.1175/BAMS-D-14-00110.1, 2015.
- Su, L., Yuan, Z., Fung, J. C. H., and Lau, A. K. H.: A comparison
of HYSPLIT backward trajectories generated from two GDAS
datasets, *Sci. Total Environ.*, 506–507, 527–537, 2015.

- Tafuro, A. M., Barnaba, F., De Tomasi, F., Perrone, M. R., and Gobbi, G. P.: Saharan dust particle properties over the central Mediterranean, *Atmos. Res.*, 81, 67–93, 2006.
- Toledano, C., Cachorro, V. E., Berjon, A., de Frutos, A. M., Sorribas, M., de la Morena, B., and Goloub, P.: Aerosol optical depth and Ångström exponent climatology at El Arenosillo AERONET site (Huelva, Spain), *Q. J. Roy. Meteor. Soc.*, 133, 795–807, doi:10.1002/qj.54, 2007a.
- Toledano, C., Cachorro, V. E., de Frutos, A. M., Sorribas, M., and Prats, N.: Inventory of African Desert Dust Events Over the Southwestern Iberian Peninsula in 2000–2005 with an AERONET Cimel Sun Photometer, *J. Geophys. Res.*, 112, D21201, doi:10.1029/2006JD008307, 2007b.
- Trenberth, K. E., Fasullo, J. T., and Kiehl, J.: Earth's Global Energy Budget, *B. Am. Meteorol. Soc.*, 90, 311–323, doi:10.1175/2008BAMS2634.1, 2009.
- Valenzuela, A., Olmo, F. J., Lyamani, H., Antón, M., Quirantes, A., and Alados-Arboledas, L.: Classification of aerosol radiative properties during African desert dust intrusions over southeastern Spain by sector origins and cluster analysis, *J. Geophys. Res.*, 117, D06214, doi:10.1029/2011JD016885, 2012a.
- Valenzuela, A., Olmo, F. J., Lyamani, H., Antón, M., Quirantes, A., and Alados-Arboledas, L.: Aerosol radiative forcing during African desert dust events (2005–2010) over Southeastern Spain, *Atmos. Chem. Phys.*, 12, 10331–10351, doi:10.5194/acp-12-10331-2012, 2012b.
- Vergaz, R., Cachorro, V. E., de Frutos, A. M., Vilaplana, J. M., and de la Morena, B. A.: Columnar characteristics of aerosols by spectroradiometer measurements in the maritime area of the Cadiz gulf (Spain), *Int. J. Climatol.*, 25, 1781–1804, doi:10.1002/joc.1208, 2005.
- Viana, M., Salvador, P., Artiñano, B., Querol, X., Alastuey, A., Pey, J., Latz, A. J., Cabañas, M., Moreno, T., García, S., Herce, M., Diez, P., Romero, D., and Fernández, R.: Assessing the performance of methods to detect and quantify African dust in airborne particulates, *Environ. Sci. Technol.*, 44, 8814–8820, doi:10.1021/es1022625, 2010.
- Viana, M., Pey, J., Querol, X., Alastuey, A., de Leeuw, F., and Lükewille, A.: Natural Sources of Atmospheric Aerosols Influencing Air Quality Across Europe, *Sci. Total Environ.*, 472, 825–833, doi:10.1016/j.scitotenv.2013.11.140, 2014.
- Wild, M., Folini, D., Schar, C., Loeb, N., Dutton, E. G., and König-Langlo, G.: The global energy balance from a surface perspective, *Clim. Dynam.*, 40, 3107–3134, doi:10.1007/S00382-012-1569-8, 2013.
- Zender, C. S., Bian, H., and Newman, D.: Mineral Dust Entrainment and Deposition (DEAD) model: Description and 1990s dust climatology, *J. Geophys. Res.*, 108, 4416, doi:10.1029/2002JD002775, 2003.

3.3. Propiedades microfísicas y ópticas del aerosol desértico y sus mezclas en estaciones de fondo regional del centro-norte de la Península Ibérica

3.3.1. Resumen gráfico

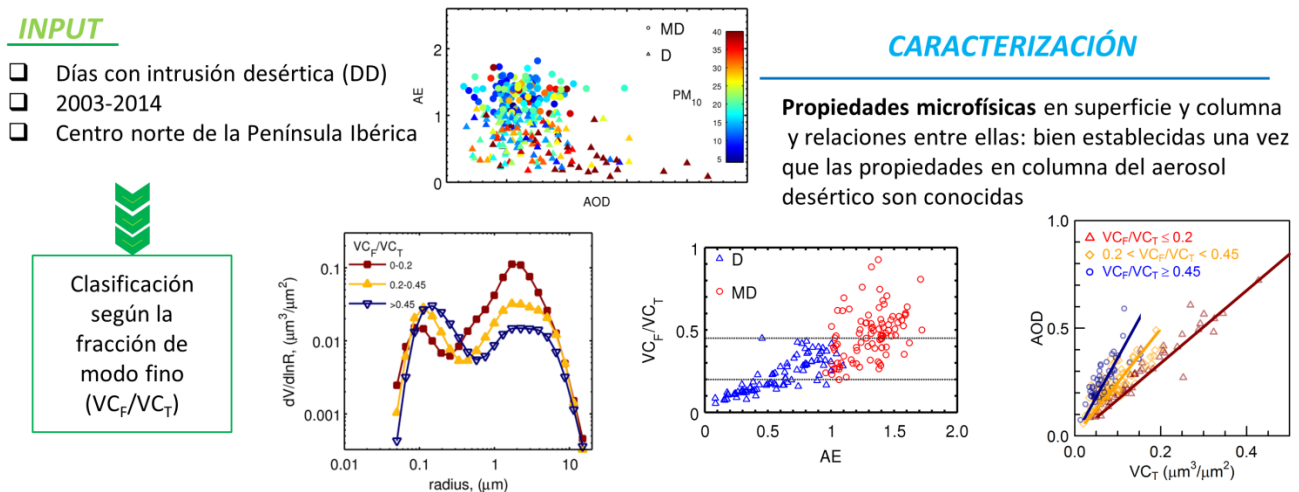


Figura 10: Resumen gráfico del A3.

3.3.2. Resumen

Este tercer trabajo se ha centrado en analizar las propiedades ópticas y microfísicas, y las relaciones entre éstas, del aerosol desértico que conforma el inventario creado en el trabajo o artículo anterior. En esta sección es relevante destacar que además de trabajar con AOD-AE haremos uso de otras magnitudes obtenidas al aplicar un algoritmo de inversión cuando se cumplen ciertas condiciones, lo que produce una notable disminución en el número de datos finales. Las propiedades en columna obtenidas de la red de AERONET que se analizarán serán, además del AOD y el AE, la distribución de tamaños, el volumen de concentración (VC), la esfericidad, el radio efectivo, el albedo de dispersión simple y el factor de asimetría. Se sigue trabajando con los datos de PM_x a fin de completar sus relaciones con estos nuevos parámetros que definen las propiedades en columna de los aerosoles atmosféricos.

Bajo la hipótesis de que los aerosoles son aproximadamente partículas esféricas (hipótesis fundamentada en que en promedio una gran cantidad de partículas de forma irregular se comportan como si fueran esféricas), introduciremos la función de distribución de tamaños (FDTA) que muestra la variación de la concentración de éstos en función de su tamaño, bien diámetro o radio. Su importancia radica en que es la base para derivar propiedades microfísicas de los aerosoles y en ella se pueden diferenciar varios modos característicos: las partículas ultrafinas son aquellas que pertenecen al modo de nucleación (diámetro entre 0.001 y 0.01 μm) y al modo Aitken (diámetro entre 0.01 y 0.1 μm). El modo de acumulación está compuesto por partículas cuyo diámetro varía entre 0.1 y 1 μm y el modo grueso por aquellas con diámetro superior a 1 μm . Esta clasificación de los modos de la FDTA es la que se considera en las medidas de tipo “*in situ*” pero para el estudio de la FTDA en los aerosoles en columna solo se diferencian el modo fino (que contiene a los otros 3 ya enumerados) y el modo grueso. De ella se derivan las siguientes magnitudes representativas de la microfísica de las partículas: la concentración volúmica y radio efectivo para las partículas finas, gruesas y el total (VC_F , VC_C , VC_T , ER_F , ER_C , y ER_T respectivamente). La fracción de esfericidad es un parámetro que caracteriza la forma predominante de las partículas, tomando valores que varían entre 0 (partículas no esféricas) y 1 (partículas esféricas). Por tanto, todas estas magnitudes junto con el AE se utilizan para obtener información sobre el tamaño y forma de los aerosoles analizados.

Entre las magnitudes representativas de las propiedades ópticas o radiativas de los aerosoles tenemos el albedo de dispersión simple (SSA), que se define como la fracción de radiación dispersada con respecto al total de radiación extinguida cuando hablamos de interacción entre la radiación incidente en la atmósfera y las partículas constituyentes de ésta. Sus valores varían entre 0 (absorción total) y 1 (no hay absorción), siendo su valor más habitual por encima de 0.9. El factor de asimetría, se utiliza para describir la direccionalidad de la radiación dispersada, situándose sus valores entre 0.6-0.8 para la mayoría de los tipos de aerosoles. Las relaciones entre las propiedades microfísicas en columna y las magnitudes representativas de la concentración másica, PM_{10} , $PM_{2.5}$ y el PM ratio a nivel de superficie, han sido también analizadas para completar el estudio de las relaciones entre las propiedades de columna y superficie para los aerosoles desérticos.

En primer lugar hemos de realizar la caracterización de los aerosoles desérticos evaluando el ciclo anual e interanual y las estadísticas correspondientes a los días de los episodios desérticos para los parámetros AOD, PM_{10} , AE y PM ratio. El valor medio obtenido para el

AOD es de 0.27 ± 0.12 y de $24 \pm 18 \mu\text{gm}^{-3}$ para el PM₁₀, así como AE= 0.94 ± 0.40 y PM_{2.5}/PM₁₀= 0.54 ± 0.16 . Los ciclos anuales de AOD y PM₁₀ de los aerosoles desérticos muestran que los máximos de intensidad aparecen en marzo y verano y valores mínimos en invierno como cabía esperar. A continuación se realizó la caracterización de la FDTM.

Un punto principal de este estudio ha sido la diferenciación entre las intrusiones de aerosol desértico y aquellas que presentan mezcla con otros aerosoles. Se han encontrado 3 tipos de episodios desérticos en función de sus propiedades:

- a) Casos típicos de aerosol ‘puramente’ desértico: con una nula relevancia del modo fino ($\text{VC}_F/\text{VC}_T \leq 0.2$), valores del AE por debajo de 0.6 y máximos de concentración en partículas en torno a los $2 \mu\text{m}$, radio total efectivo mayor a $0.5 \mu\text{m}$, no esfericidad, mayor poder de absorción para longitudes de onda pequeña y menor dependencia espectral del factor de asimetría.
- b) Casos de mezcla dominados por el aerosol desértico: caracterizados por valores de $\text{VC}_F/\text{VC}_T \in [0.2, 0.45]$ y del AE $\in [1.0, 1.5]$, radio total efectivo entre 0.2 y $0.5 \mu\text{m}$, partículas más esféricas, valores más pequeños de SSA indicando mayor poder absorbente en todas las longitudes de onda y mayor dependencia espectral del factor de asimetría.
- c) Casos de mezcla en los que la presencia de aerosol desértico no es dominante sino que hay una prevalencia de partículas finas y vienen caracterizados por valores de $\text{VC}_F/\text{VC}_T \geq 0.45$ y de $\text{AE} > 1.5$. Las demás magnitudes muestran características comunes con las partículas mezcla del caso anterior, b).

Si estamos estudiando las partículas cuyas características definen el aerosol mineral o desértico es difícil entender esta última mezcla que aparece en nuestro inventario, dominada por partículas finas. Sin embargo, como se ha visto al explicar la metodología de detección de estos eventos, y el hecho de que la pieza base es incluir o no un día completo cuya señal bien en AOD o PM₁₀ supere los niveles umbrales (no necesariamente coincidentes), hace que puedan aparecer este tipo de datos o casos. Debemos de tener en cuenta el hecho de que junto a las partículas gruesas también viajan partículas finas, como se observa en el aumento de la concentración del modo fino en la FDTA. En general todos estos parámetros que representan a estas propiedades microfísicas y ópticas presentan una amplia variabilidad para los casos con predominancia de la fracción fina.

Se han analizado varias relaciones entre estos parámetros o variables, como por ejemplo VC_F/VC_T frente al AE, PM ratio o esfericidad, AE frente a esfericidad, así como éstas con el radio efectivo... En concreto, de la relación entre el AOD y la concentración volúmica, VC, se puede definir el factor de eficiencia de extinción, que toma valores entre 1.7 y $3.7 \mu\text{m}^2/\mu\text{m}^3$ dependiendo de la fracción VC_F/VC_T considerada. En promedio se ha obtenido un valor de $2.1 \pm 0.06 \mu\text{m}^2/\mu\text{m}^3$.

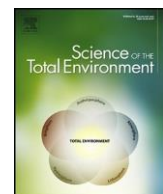
A partir de la relación entre el PM_{10} y la concentración volúmica se puede obtener el factor de escala, que da cuenta de la altura hasta la que una capa homogénea de aerosol con un coeficiente de extinción dado se tendría que extender para tener un valor de AOD determinado. En nuestro estudio se ha obtenido un valor medio de ~ 9 km, llegando para algunas categorías a los 10 km. Hemos pues de resaltar la obtención de estos resultados ya que no son determinados frecuentemente en los estudios de aerosoles, como los relativos al factor de eficiencia y a la altura de escala, por cuanto entraña trabajar con datos de superficie y columna, pertenecientes a campos de trabajo bastante diferentes en el amplio mundo de estudio de los aerosoles atmosféricos.

3.3.3. Artículo 3



Contents lists available at ScienceDirect

Science of the Total Environment

journal homepage: www.elsevier.com/locate/scitotenv

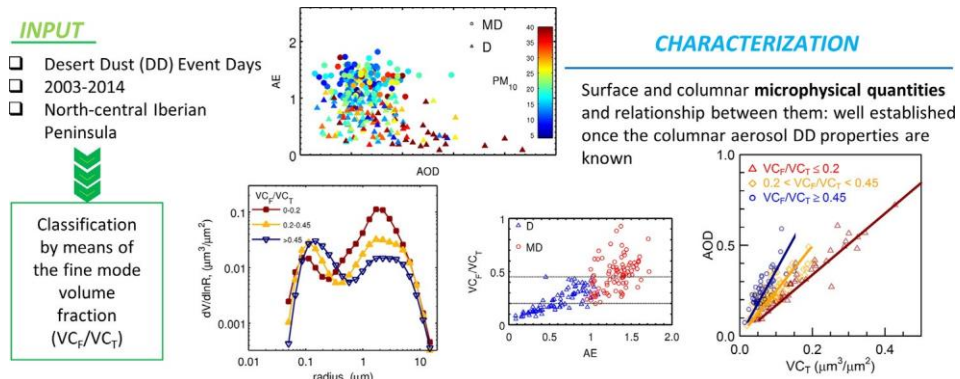
Aerosol properties of mineral dust and its mixtures in a regional background of north-central Iberian Peninsula

M.A. Burgos, D. Mateos, V.E. Cachorro*, C. Toledoano, A.M. de Frutos

Grupo de Óptica Atmosférica, Universidad de Valladolid, Paseo Belén 7, CP 47011 Valladolid, Spain

HIGHLIGHTS

- Long-term characterization of mineral dust aerosols and its role in mixtures
- Volume extinction efficiency for mineral dust ranges between 1.7 and 3.7 $\mu\text{m}^2/\mu\text{m}^3$.
- Aerosol scale height factor is about 9 km in the columnar-surface analysis.

GRAPHICAL ABSTRACT**article info****Article history:**

Received 31 May 2016

Received in revised form 13 July 2016

Accepted 1 August 2016

Available online xxxx

Editor: D. Barcelo

Keywords:

African desert dust and mixtures

AOD and PM10

Aerosol scale height factor

Columnar volume extinction efficiency

Surface and columnar aerosol data

abstract

To broaden the knowledge about desert dust (DD) aerosols in western Mediterranean Basin, their fingerprints on optical and microphysical properties are analyzed during DD episodes in the north-central plateau of the Iberian Peninsula between 2003 and 2014. Aerosol columnar properties obtained from the AErosol RObotic NETwork (AERONET), such as aerosol optical depth (AOD), Ångström exponent (AE), volume particle size distribution, volume concentration (VC), sphericity, single scattering albedo, among others, are analyzed in order to provide a general characterization, being some of them compared to particle mass surface concentrations PM₁₀, PM_{2.5}, and their ratio, data obtained from EMEP network. The mean intensity of DD episodes exhibits: AOD_{440nm} = 0.27 ± 0.12, PM₁₀ = 24 ± 18 $\mu\text{g}/\text{m}^3$, AE = 0.94 ± 0.40 and PM_{2.5}/PM₁₀ = 0.54 ± 0.16. The AOD and PM₁₀ annual cycles show maximum intensity in March and summer and minima in winter. A customized threshold of AE = 1 distinguishes two types of dusty days, those with a prevailing desert character and those of mixed type, which is corroborated by sphericity values. Three well established intervals are obtained with the fine mode volume fraction (VC_F/VC_T). Coarse-mode-dominated cases (VC_F/VC_T ≤ 0.2) present a mineral dust character: e.g., particle maximum concentration about 2 μm , non-sphericity, stronger absorption power at shorter wavelengths, among others. The relevance of the fine mode is noticeable in mixtures with a predominance of particles about 0.2–0.3 μm radii. Conditions characterized by 0.2 < VC_F/VC_T < 0.45 and VC_F/VC_T ≥ 0.45 present a larger variability in all investigated aerosol properties. Relationships between AOD and columnar particle volume concentration give volume extinction efficiencies between 1.7 and 3.7 $\mu\text{m}^2/\mu\text{m}^3$ depending on VC_F/VC_T. Aerosol scale height is obtained from relationships between surface and columnar concentrations displaying very large values up to

* Corresponding author.

E-mail address: chiqui@goa.uva.es (V.E. Cachorro).

10 km. The uncertainty associated with the transformation between AOD and PM₁₀ can be partially reduced when the aerosol microphysical properties are known.

© 2016 Elsevier B.V. All rights reserved.

1. Introduction

Airborne dust is a key player in the atmospheric science studies since it is considered to impact climate, air quality and human health by causing respiratory diseases and infections or even certain epidemics; Earth's radiative budget by scattering/absorbing solar radiation; life cloud cycle acting as cloud condensation nuclei or ice nuclei; air visibility that can affect traffic or military operations; different continental and maritime ecosystems by changing the provided nutrients; and the soil erosion in agriculture (e.g., Horvath, 1998; Dubovik et al., 2002; Eck et al., 2010; Yannopoulos et al., 2015; Gkikas et al., 2013; Knippertz and Stuut, 2014). Mineral dust accounts for 13% of the total natural emissions in the Earth's system (e.g., Viana et al., 2014), being the Sahara and Sahel deserts the most relevant natural sources of crustal aerosols in the Northern Hemisphere (Prospero et al., 2002) with N200 Tg per year emitted to the atmosphere and transported over the Atlantic Ocean (Kaufman et al., 2005). The injection of desert dust (DD) into the atmosphere from the Sahara's two major dust sources (Bodélé depression and eastern Mauritania) by different re-suspension processes can achieve high atmospheric layers, being responsible for high aerosol loads that are transported very large distances, to the northern Atlantic Ocean, Caribbean Sea, Amazon Basin, Mediterranean Basin, and European continent (e.g., Goudie and Middleton, 2001).

Focusing on the studies devoted to the analysis of DD over the Iberian Peninsula (IP), it has been observed that different areas exhibit different behavior and annual cycle of DD events because of the orography and the uneven synoptic conditions along the IP (Silva et al., 2002; Estellés et al., 2007; Toledano et al., 2007; Obregón et al., 2015; Mateos et al., 2014). The closeness of the IP to the African continent enhances the impact of these high turbidity events on different aspects. For example, DD outbreaks impact on air quality by increasing aerosol load, being the main responsible of the daily exceedances over 50 µg m⁻³ (limit established by the 2008/50/EC European Directive) in the particulate matter with aerodynamic diameter less than 10 micrometers (PM₁₀) levels (e.g., Escudero et al., 2007; Querol et al., 2014; Salvador et al., 2013, 2014). This is reinforced by long residence times of dust particles in the atmosphere favored by the low precipitation levels (e.g., Escudero et al., 2005; Cabello et al., 2012). Moreover, aerosol seasonal patterns are modulated by mineral dust producing two maxima along the year of PM or aerosol optical depth (AOD) in certain areas of the IP (e.g., Mateos et al., 2015). The DD aerosols also present influence on the radiative budget with an aerosol forcing efficiency about -70 Wm⁻² at the surface in south-eastern IP (Valenzuela et al., 2014). Acute effects on human health also occur during DD events in Spain, accelerating cardiovascular and respiratory mortality (Pérez et al., 2012; Reyes et al., 2014).

Different methodologies have been recently developed in order to detect and identify DD intrusions by means of PM_x (x refers here to the upper particle cut-off) or AOD data. Likewise, other tools are used to identify DD outbreaks, such as aerosol model forecasts, air mass back trajectories, satellite images, among others (e.g., Pace et al., 2006; Tafuro et al., 2006; Escudero et al., 2007; Toledano et al., 2007; Querol et al., 2009; Cabello et al., 2012; Pey et al., 2013; Salvador et al., 2014; and Cachorro et al., 2016). All these tools can be used in very different and combined ways in order to carry out the DD detection and the evaluation of its occurrence, intensity and impact, as for example over the entire Mediterranean Basin.

An extensive work about desert dust studies has been carried out during the last years in the Mediterranean area. Pace et al. (2006) and

Meloni et al. (2007) obtained occurrence maxima in May and July in the Lampedusa island (Central Mediterranean) using MFRSR measurements and air mass backward trajectories in the DD detection. A summer maximum (June and August) is reported by Toledano et al. (2007) in south-western Spain by a combination of Sun photometer data and back-trajectory analysis of air mass origin. Valenzuela et al. (2012) reported the maximum of annual occurrence in July over south-eastern Spain by analyzing air mass back trajectories. Pey et al. (2013) obtained a shifted annual maximum from April to July between eastern and western Mediterranean Basin in the 2000s using PM_x surface data and a combination of meteorological products, aerosol maps, satellite images and air mass back-trajectories. Cachorro et al. (2016) obtained an annual cycle of dusty day occurrence over north-central IP of similar characteristics to that reported by Salvador et al. (2013) for Madrid area, but with lower occurrence.

The application of the mentioned methodologies for DD detection allows further characterization studies, which are related to the evaluation of the different properties that define DD aerosols. However, only some of these properties are used in the methodology of DD identification. In our case, columnar AOD and Ångström exponent (AE), and surface PM₁₀ concentration are used for detection. These quantities will be characterized in the present study, together with other properties, such as volume particle size distribution (VPSD), asymmetry parameter (g) or single scattering albedo (SSA).

Previous studies in the African surroundings have shown that mineral dust aerosols are dominated by large particles beyond 0.6 µm, and they exhibit non-sphericity and a pronounced absorption in the blue spectral range, among others (e.g., Dubovik et al., 2002; Eck et al., 2010; Giles et al., 2012). These are however the expected properties for pure dust near the sources. The dust over our study region has experienced long-range transport, with possible apportioning of other aerosol particles as well as mixture with local aerosol. So it is to expect that some variability and differences with respect to pure dust properties are found in the intensive properties.

The aerosol characterization developed in this article is based on a DD inventory previously reported by Cachorro et al. (2016). This inventory is composed by DD event days occurring in the north-central area of the Iberian Peninsula between January 2003 and December 2014. The methodology behind the inventory simultaneously uses columnar and surface aerosol data to identify DD events. Once the DD fingerprint is recognized in one or both of these core variables, a thorough manual inspection of the data is carried out together with the analysis of air mass backward trajectories, meteorological maps, satellite images, and model forecasts, in order to corroborate the right classification of each DD outbreak.

As a natural continuation of the inventory analysis, the aim of this study is to carry out the characterization of the main optical and microphysical properties during mineral dust events, for a better understanding of mineral aerosol over the IP. One of the most interesting results reported by Cachorro et al. (2016) is the analysis of the two sub-groups of DD aerosols, one labeled as desert (D) and the other one labeled as mixed-desert (MD). These groups were discriminated by means of the Ångström exponent. Such kind of study is required in those areas where aerosol mixtures play a non-negligible role caused by different reasons (large distance to the sources, orography, presence of big industrial cities or other aerosol types, among others) and where the DD identification is complicated since the boundaries among well-known (pure) aerosol types are ambiguous.

A detailed analysis of the aerosol surface concentration and columnar optical and microphysical properties is carried out here using

EMEP (European Monitoring and Evaluation Programme) and AERONET (AErosol RObotic NETwork, Holben et al., 1998) observations. These data allow the study about how columnar and surface quantities are related. Relationship between different size parameters are studied, like AE, effective radius (ER), the fraction of the fine mode volume concentration (VC_F/VC_T) and surface $PM_{2.5}/PM_{10}$ ratio. Relationships between columnar volume concentrations and aerosol loads by columnar AOD and surface PM_x are also reported to better define their validity during high turbidity dust events as one of the most relevant results. To the best of our knowledge, some of these relationships are established for the first time. Finally, radiative quantities are also investigated to provide a general insight about absorbing and scattering properties: sphericity fraction, single scattering albedo and asymmetry factor during DD events. Hence, this is the first DD aerosol characterization based on a long-term inventory with emphasis on the relationship between columnar and surface properties.

2. Desert dust inventory: sites, databases and method

2.1. Sites and databases

The monitoring sites for the columnar and surface properties are placed in "Castilla y León" region, covering the north-central part of the Iberian Peninsula in an elevated plateau (~800 m a.s.l., called "Meseta Central"), surrounded by three mountain systems in the north, south and east. These large landforms (up to 2500 m a.s.l.) make it difficult the arrival of air masses from southern areas. The study area exhibits a clean continental aerosol background, isolated from any large urban or industrial centres, which implies that aerosol observations are representative of the whole region. The detection of moderate or even minor DD aerosol intrusions is possible since they notably modify the background properties.

Columnar aerosol data measured by CIMEL CE-318 (Holben et al., 1998) Sun photometers from AERONET contains instantaneous values of spectral AOD (at 7 different wavelengths) and its associated Ångström exponent (AE) at Palencia site (41.9° N, 4.5° W, and 750 m a.s.l.), which are completed with the nearby Autilla site (41.9° N, 4.6° W, and 870 m a.s.l., 7 km away) when gaps appear in the database. The Sun photometer performs direct sun measurements every 15 min during daytime. The AOD at 440 nm wavelength is selected in this study to perform the DD characterization. Furthermore, the CIMEL instrument hourly measures sky radiances, both in almucantar and principal plane geometries, at 440, 670, 870, and 1020 nm wavelengths. Table 1 summarizes the aerosol properties used in this study. Further details about the inversion algorithm were deeply described by, e.g., Dubovik and King (2000); Dubovik et al. (2006); Holben et al. (2006), and Eck et al. (2008). All the instantaneous columnar aerosol data are daily averaged in the characterization presented in this study. As can be seen in Table 1, a notable reduction in the number of inversion products compared to AOD is due to the fewer radiance measurement

sampling and the quality constraints imposed by AERONET inversion algorithm.

The closest site to Palencia with measurements of aerosol surface concentrations (PM_{10} and $PM_{2.5}$) belonging to EMEP network is located in Peñausende (41.28°N, 5.87°W, and 985 m a.s.l.). These PM_{10} and $PM_{2.5}$ concentrations are obtained daily by gravimetric determinations. These are the official data reported to the European Commission and their high quality is guaranteed (e.g., Pey et al., 2013). The PM ratio ($PM_{2.5}/PM_{10}$) gives also an idea of the predominance of fine (large ratio) or coarse (low ratio) particle modes.

Apart from the conceptual differences between columnar and surface aerosol load represented by AOD and PM_x , there exist some significant differences in relation with the sampling of both aerosol concentration measurements. The CIMEL Sun photometer measures nearly instantaneous data under clear-sky conditions during daytime, whereas PM_x data give surface information integrated over 24 h under all sky conditions. Details and discussion about the AOD-AE and PM_x measurements and their sampling can be seen in Bennouna et al. (2016).

2.2. Methodology

The employed methodology for desert outbreak identification based on columnar and surface aerosol data (AOD/AE/ PM_{10}) is explained in detail by Cachorro et al. (2016) and therefore only a short description is provided here. A set of thresholds for AOD (440 nm) and PM_{10} (0.18 and 13 $\mu g m^{-3}$, respectively) are selected taking into account a long-term statistical analysis. Moreover, other important ancillary information is also taken into account together with aerosol information: air mass backward trajectories, satellite images, meteorological maps and aerosol model forecasting, which are manually analyzed. Therefore this methodology does not restrict DD events identification to those days with aerosol data. It is worth mentioning here that the DD inventory of dusty days is elaborated with instantaneous AOD data when available while the foregoing characterization is performed on a daily basis. The use of the instantaneous data allowed us to detect the sharp time when the intrusion arrives, although DD conditions are attributed to that day regardless the arrival time. Therefore, for those days showing the arrival of dust after midday, daily means can present slightly modified values with respect to the "expected" DD aerosol properties. These "non-typical" values have been thoroughly investigated in order to accurately accomplish the DD characterization.

The AE threshold to separate DD event days into two sub-groups is set to 1.0, since it corresponds to a typical value assigned to separate fine and coarse mode predominant aerosols (e.g., Toledano et al., 2007; Di Biagio et al., 2010; Guirado et al., 2014). Those days with mean AE values below 1.0 are noted as "D type". However, during Saharan dust intrusions, mixing with other aerosol types can occur, being DD aerosols a fraction of that mixture (with a wide range of concentrations), therefore the values of the aerosol properties may not be the

Table 1

Information on the columnar and surface quantities used in this study. ND is the number of days with available data into the DD dataset (a total of 418 days in 2003–2014).

| Network | Site | Quantities | Time resolution used for daily means | ND | +Info |
|---------|--------------------|-------------------------------------|--------------------------------------|-----|------------------------------------------------------------------------|
| AERONET | Palencia + Autilla | AOD, AE | 15-min | 324 | Level 2.0 |
| | | VPSD | 1 h | 182 | Level 1.5 + other criteria ^a |
| | | ER _{T/F/C} | | | |
| | | VC _{T/F/C} | | | |
| | | Sphericity | 1 h | 122 | Level 1.5 + other criteria ^b |
| | | SSA, g | 1 h | 163 | Level 1.5 + other criteria ^c |
| EMEP | Peñausende | PM ₁₀ | 24 h | 399 | PM ₁₀ and PM _{2.5} obtained from different filters |
| | | PM _{2.5} | | 403 | |
| | | PM _{2.5} /PM ₁₀ | | 387 | |
| | | | | | |

^a Same AERONET level 2.0 criteria (solar zenith angle N50°, number of symmetrical angles, and sky error between 5% and 8% depending on AOD), but there is no filter with respect to AOD.

^b Same AERONET level 2.0 criteria but with AOD ≥ 0.2 (see Dubovik et al., 2006).

^c Same AERONET level 2.0 criteria but with AOD ≥ 0.15 (see Mallet et al., 2013; Mateos et al., 2014).

ones expected for pure mineral dust (e.g., Pace et al., 2006; Tafuro et al., 2006; Basart et al., 2009; Eck et al., 2010). In our inventory, this category can be represented by 1 b AE b 1.5 and is indicated by MD type. It must be highlighted that "mixture" conditions mean the possible superposition of different aerosol layers located at different heights and loaded with different aerosol types. The measurements of the aerosol optical properties of the entire column take into account all such layers and, therefore, their values are not attributed to one specific aerosol type. Generally, a desert dust episode is composed of D and MD event days, because the majority of the detected DD episodes are of moderate intensity. The selection of criteria to differentiate between fine and coarse particle predominance is not an easy task due to the strong site dependency (local aerosol) and the variable characteristics of the DD events (origin and formation, the followed path, among others). Therefore, many different thresholds used by different authors worldwide can be found in the literature (e.g., Gkikas et al., 2016).

Overall, the number of DD event days is 418 for the 12-year period (2003–2014) according to the inventory described by Cachorro et al. (2016), but only 304 coincident days are available for AOD and PM₁₀. Hence, the available DD database is reduced by almost 30% in the aerosol characterization study. The DD database contains 162 days of D type and 142 of MD type. Fig. 1 shows daily aerosol loads for the two types together with the non-DD event days (a total of 2466) that comprise the whole database for both AOD (Fig. 1a) and PM₁₀ (Fig. 1b) during the analyzed period. As it can be seen, dusty days represent ~11% of the total. DD outbreaks are responsible for 45% of the moderate and high-turbidity days showing AOD N 0.2. This percentage increases up to 52% for those days with PM₁₀ N 20 µg m⁻³. The remaining percentage can be attributed to other high-turbidity episodes such as biomass burning or industrial aerosol.

3. Results and discussion

3.1. Characteristics of AOD, PM₁₀, AE, and PM_{2.5}/PM₁₀ during DD events

3.1.1. Frequency histograms

The frequency histograms of the daily values of AOD, PM₁₀, AE, and PM_{2.5}/PM₁₀ for D and MD event days are shown in Fig. 2. Aerosol load during the DD events presents most AOD daily values in the range 0.15–0.35 (~72%) and between 15 and 35 µg m⁻³ for PM₁₀ (~60%). The occurrence frequency for AOD peaks in 0.2 for both subgroups and decreases forwards. A similar behavior is observed for PM₁₀ quantity with the maximum about 15–20 µg m⁻³ depending on the category

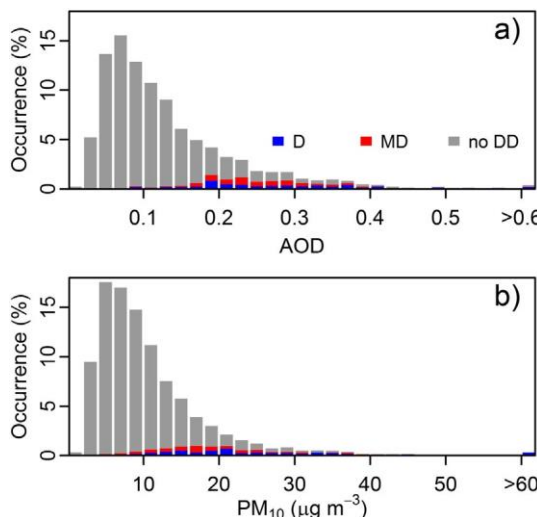


Fig. 1. Frequency histograms of AOD (a), PM₁₀ (b) during no DD (gray), D (blue), and MD (red) event days in the period 2003–2014. (For interpretation of the references to color in this figure legend, the reader is referred to the web version of this article.)

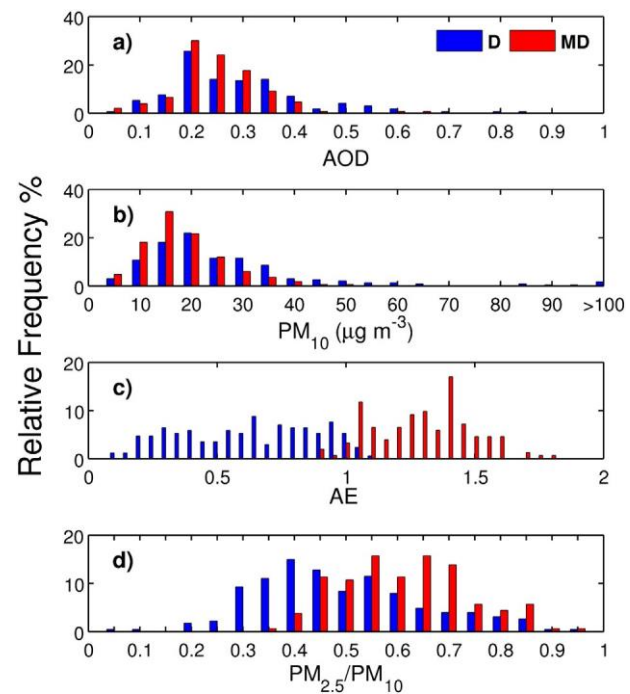


Fig. 2. Frequency histograms of AOD (a), PM₁₀ (b, in µg m⁻³), AE (c), and PM_{2.5}/PM₁₀ (d) during D and MD event days in the period 2003–2014.

or subgroup. The most intense events present AOD and PM₁₀ mean values over 0.40 and 40 µg m⁻³, respectively representing about 10% of the total dusty days. In particular, exceedances beyond 50 µg m⁻³, threshold established by the 2008/50/EC European Directive, are achieved in 19 cases or the ~5% of the total dusty days in the period 2003–2014.

With respect to the aerosol size predominance, represented by the AE, Fig. 2c illustrates the threshold values used for the discrimination between D and MD categories. Around 76% of AE values fall between 0.5 and 1.5, displaying an even distribution. The lowest AE values (b0.5), that indicates strong coarse mode predominance, represent about 18% of the DD event days.

The PM_{2.5}/PM₁₀ is useful to complete the analysis since this is the only variable not (directly) used in the DD identification. The PM ratio values span from 0.1 to 0.95, with most of the data concentrated in the range 0.4–0.7 (~62%). The extreme categories 0–0.4 and 0.7–1.0 present similar weight (~19%). The PM ratio frequencies considerably mix up D and MD categories, with a wider interval for D type.

Daily mean values out of the established thresholds (see Section 2) are registered due to two possible situations. On one hand, daily averages are considered in the characterization meanwhile the thresholds to detect a DD event day are established for the instantaneous AOD values within a day (as mentioned above). Thus, if an outbreak occurs after midday, it is possible to detect it thanks to the instantaneous values in spite of the fact that the daily mean does not overcome the corresponding threshold. On the other hand, the followed methodology allows identifying an outbreak when its impact is only visible at high layers or only at surface level, in which case only the AOD or PM₁₀ quantity overcomes its established threshold. These cases highlight the advantage of this methodology. Overall the daily mean values out of the thresholds represent the ~15% (~18%) of the total event days for AOD (PM₁₀).

Table 2 briefly summarizes the statistics of AOD, PM₁₀, AE, and PM_{2.5}/PM₁₀ quantities for desert dust intrusion days. Overall, DD outbreaks showing large aerosol loads rule the mean value since this statistical parameter stays above the median. However, this effect is weaker in the MD subset. The differences between mean and median values are generally larger for PM₁₀ quantity than for AOD. This fact can be

Table 2

Mean and standard deviation (SD), median and quartile deviation (QD), percentiles 5 (P5) and 95 (P95), maximum, skewness (s) and kurtosis (k) for AOD, PM_{10} (in $\mu\text{g m}^{-3}$), AE, and $\text{PM}_{2.5}/\text{PM}_{10}$ for each D, MD, and D + MD event days.

| Event days | Quantity | Mean \pm SD | Median \pm QD | P5 | P95 | Max. | s | k |
|------------|----------------------------------|-----------------|-----------------|------|-------|------|-------|-------|
| D + MD | AOD | 0.27 \pm 0.12 | 0.25 \pm 0.07 | 0.12 | 0.50 | 0.87 | 1.49 | 7.05 |
| | AE | 0.94 \pm 0.41 | 0.98 \pm 0.33 | 0.25 | 1.54 | 1.82 | -0.19 | 2.02 |
| | PM_{10} | 24 \pm 18 | 20 \pm 7 | 8 | 49 | 197 | 4.44 | 33.75 |
| | $\text{PM}_{2.5}/\text{PM}_{10}$ | 0.54 \pm 0.16 | 0.54 \pm 0.12 | 0.31 | 0.82 | 0.94 | 0.07 | 2.62 |
| D | AOD | 0.29 \pm 0.13 | 0.26 \pm 0.08 | 0.11 | 0.54 | 0.87 | 1.31 | 5.61 |
| | AE | 0.62 \pm 0.26 | 0.63 \pm 0.23 | 0.19 | 1.00 | 1.10 | -0.14 | 1.87 |
| | PM_{10} | 27 \pm 22 | 21 \pm 9 | 8.15 | 60.55 | 197 | 3.80 | 24.16 |
| | $\text{PM}_{2.5}/\text{PM}_{10}$ | 0.49 \pm 0.16 | 0.46 \pm 0.11 | 0.28 | 0.8 | 0.93 | 0.41 | 2.89 |
| MD | AOD | 0.25 \pm 0.09 | 0.24 \pm 0.05 | 0.12 | 0.38 | 0.65 | 1.07 | 6.89 |
| | AE | 1.30 \pm 0.19 | 1.32 \pm 0.14 | 1.01 | 1.59 | 1.82 | 0.07 | 2.48 |
| | PM_{10} | 18 \pm 8 | 17 \pm 5 | 7.8 | 36 | 50 | 1.04 | 4.51 |
| | $\text{PM}_{2.5}/\text{PM}_{10}$ | 0.61 \pm 0.12 | 0.63 \pm 0.14 | 0.43 | 0.83 | 0.94 | 0.20 | 2.39 |

understood from the histograms shown in Fig. 2, where surface aerosols present a wider interval, achieving concentrations above $100 \mu\text{g m}^{-3}$. However, AE and $\text{PM}_{2.5}/\text{PM}_{10}$ present very similar values of the mean and median, indicating a more even distribution of their data. The AOD, PM_{10} , AE, and $\text{PM}_{2.5}/\text{PM}_{10}$ data sets do not follow a normal distribution. The AOD and PM_{10} exhibit a log-normal shape (O'Neill et al., 2000), whereas AE and $\text{PM}_{2.5}/\text{PM}_{10}$ frequency distributions present platykurtic shapes. These behaviors are linked with the frequency histograms shown in Fig. 2. The stronger loads and larger particles associated to D type are corroborated by the percentile values (larger P95 of AOD and PM_{10} , and lower P5 of AE and $\text{PM}_{2.5}/\text{PM}_{10}$).

3.1.2. Scatter plots

Fig. 3 shows the AE-AOD scatterplot for all daily means and dusty days including information about the corresponding PM_{10} or $\text{PM}_{2.5}/\text{PM}_{10}$ values. In order to obtain a better visualization in Fig. 3b, an upper threshold of $40 \mu\text{g m}^{-3}$ has been established for PM_{10} values. The right identification of DD events with the employed method is corroborated in Fig. 3a, in which dusty days stand out among the entire dataset. The shape of this diagram for D type is similar to that reported by the analysis of DD aerosols performed in previous studies about nearby areas (e.g., Toledano et al., 2007; Di Biagio et al., 2010; Valenzuela et al., 2012; Obregón et al., 2015). The mixing of dust with other aerosol types associated to MD type put the DD intrusions of this sub-group in the unexpected area (AE $>$ 1) of this kind of diagram.

Previous studies have also stated that DD intrusions in the Mediterranean Basin can present moderate AOD values associated with large AE values (e.g., Pace et al., 2006; Tafuro et al., 2006). The same has been shown by Pey et al. (2013) when analyzing the intensity of DD outbreaks by PM_x values for the whole Mediterranean basin. In order to analyze the intensity of the DD outbreaks and following the AOD criterion used by Gkikas et al. (2016), the mean plus four times standard deviation, our extreme DD events are those with an AOD larger than 0.5. This extreme subset represents 16 dusty days (about 5% of the total DD event days). Strong episodes, determined with the AOD interval between mean plus two and four times the standard deviation, range between 0.3 and 0.5. There are 85 cases (26% of days). Finally, 223 days (69%) are low-moderate DD outbreaks and exhibit an AOD below 0.3.

The relationships among AOD, AE and surface concentrations under DD intrusions display different behaviors (see Fig. 3b and c). For the D subset, the four most intense columnar events (AOD $>$ 0.7) are linked with large surface concentrations too ($\text{PM}_{10} > 40 \mu\text{g m}^{-3}$), with a predominance of the coarse mode ($\text{PM}_{2.5}/\text{PM}_{10} > 0.5$ and AE > 0.6). For instance, Fig. 4b shows the time series of all the quantities during a strong event in October 2008: AOD values about 0.6 and a maximum PM_{10} larger than $40 \mu\text{g m}^{-3}$. It is worth mentioning that during this episode, there was high temporal agreement between columnar and surface aerosol load, although the PM ratio only reached values close to 0.4 meanwhile AE was close to zero.

Overall, most of the strong and extreme DD intrusions of AOD (N0.3) also present PM_{10} values $> 25 \mu\text{g m}^{-3}$. However, the discrepancy between surface and columnar impact of DD aerosols frequently occurs due to delays in the deposition phenomena. There are PM_{10} values below $15 \mu\text{g m}^{-3}$ and $\text{PM}_{2.5}/\text{PM}_{10} > 0.5$ with a high AOD. For instance, on September 5th, 2004 ($\text{PM}_{10} = 12 \mu\text{g m}^{-3}$, AOD = 0.54, AE = 0.33, and $\text{PM}_{2.5}/\text{PM}_{10} = 0.67$, see Fig. 4a) is enclosed in a 10-day event (1st-10th September 2004) which represents a DD outbreak with more impact on high atmospheric levels than at the surface. This DD event is also reported in south-western Spain by Prats et al. (2008) in

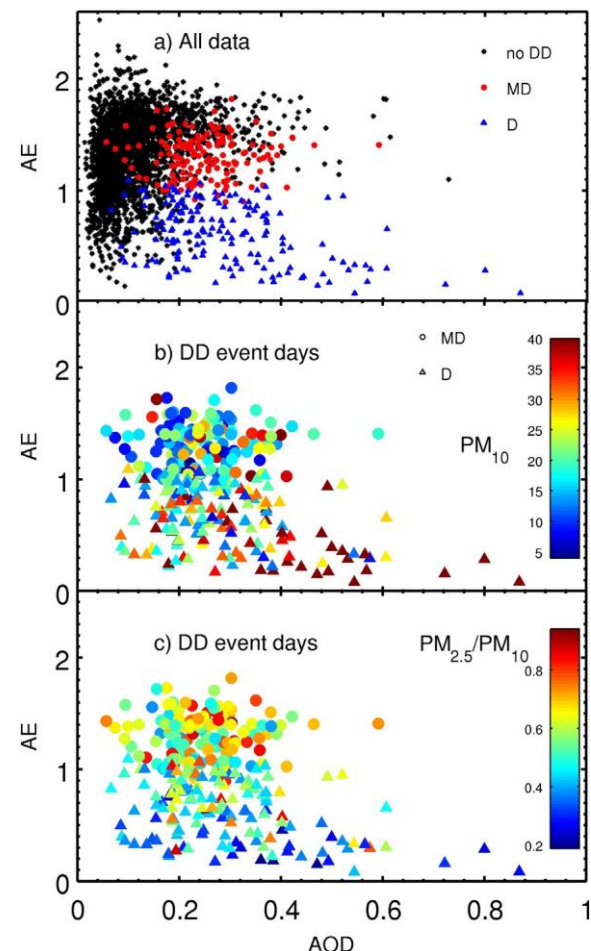


Fig. 3. AE-AOD scatterplot for all data (a) and for DD intrusions (b, c), with the corresponding daily value of PM_{10} (b) and $\text{PM}_{2.5}/\text{PM}_{10}$ (c) in colour scale. The two types of DD intrusions are represented by triangles (D type) and circles (MD type). (For interpretation of the references to color in this figure legend, the reader is referred to the web version of this article.)

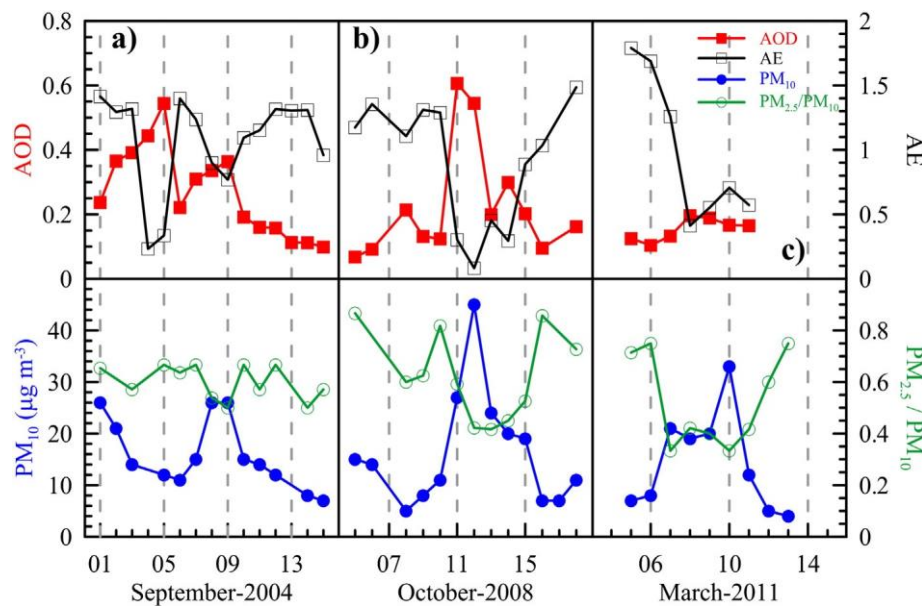


Fig. 4. Time series of AOD (solid squares), AE (open squares), PM₁₀ (solid circles), and PM_{2.5}/PM₁₀ (open circles) during three particular DD events quoted in the text.

the first fortnight of September-2004. The possible delay in deposition to the ground, considering the 24 h filter sampling in the surface concentration, could also produce large PM₁₀ and low PM_{2.5}/PM₁₀ values with simultaneous weak columnar loads (AOD \approx 0.3) when the event is starting/finishing.

For the MD subset, the intensity of columnar events is in general low to moderate, with AOD values \leq 0.4, the majority of surface concentrations under 25 $\mu\text{g m}^{-3}$ and PM_{2.5}/PM₁₀ ranging from 0.5 to 0.7. Overall, MD event days show lower PM₁₀ and higher PM_{2.5}/PM₁₀ values than D type due to the presence of aerosol mixtures. In particular, there is larger frequency of biomass burning or anthropogenic aerosol events during summer (e.g., Mateos et al., 2015). Large variability of the PM₁₀ occurs for the MD type and AOD ranges between 0.2 and 0.4. Overall, low AOD (\leq 0.2) implies PM₁₀ \leq 20 $\mu\text{g m}^{-3}$ with intermediate values of the PM_{2.5}/PM₁₀ ratio. However, large PM₁₀ and low PM_{2.5}/PM₁₀ values can also occur for this AOD range. For instance, a 3-day event from 8th to 10th March 2011 (see Fig. 4c) represents a case with more impact at low atmospheric layers than in the column (e.g., PM₁₀ = 33 $\mu\text{g m}^{-3}$, AOD = 0.16, AE = 0.7, and PM_{2.5}/PM₁₀ = 0.33 on March 3rd, 2011). The 4-day event shows low AE values and AOD about 0.2 with surface concentrations ranging between 20 and 30 $\mu\text{g m}^{-3}$ and PM_{2.5}/PM₁₀ about 0.4.

3.1.3. Relationships of columnar and surface quantities: PM₁₀-AOD and PM ratio-AE

One important task carried out in aerosol studies in the last years has been the development of a method for monitoring surface aerosol levels (generally accomplished by air quality networks) by means of remote sensing data, such as the AOD data provided by satellite sensors (e.g., Liu et al., 2004; Kacenelenbogen et al., 2006; Rohen et al., 2011). A theoretical background supports this analysis between AOD and PM₁₀ quantities (for further details see Bennouna et al., 2016). In the present study, the AOD-PM₁₀ and AE-PM_{2.5}/PM₁₀ relationships are reported in Fig. S1 only for mineral dust aerosols (the general comparison for the entire long-term database was presented by Bennouna et al., 2016). Overall the correlation or Pearson's coefficient (R) is around 0.6 for PM₁₀ vs AOD relationship, being lower (R \sim 0.5) for PM_{2.5}/PM₁₀ vs AE. During DD intrusions the change of PM₁₀ is larger than that shown by AOD (see linear fits in Fig. S1). This fact can also be proved with the range of surface concentration values achieving a maximum of \sim 200 $\mu\text{g m}^{-3}$, meanwhile AOD does not reach 1.0. If the total mean values in the 2003-2014 period are used as reference (PM₁₀ =

10.3 $\mu\text{g m}^{-3}$ and AOD = 0.13), the mentioned maxima correspond to changes around 20 and 8 times the mean values of PM₁₀ and AOD, respectively. Therefore, although the surface-columnar relationship presents limitations, there are still similarities that point out the usefulness of the joint interpretation of these two quantities during high turbidity events such as DD outbreaks.

3.2. Annual cycle of AOD, PM₁₀, AE, and PM_{2.5}/PM₁₀ during DD events

The annual cycles for DD event days obtained for AOD, PM₁₀, AE, and PM_{2.5}/PM₁₀ are shown in Fig. 5. Regarding AOD, Fig. 5a illustrates the intensity of the dusty days (D + MD curve). Maximum values about 0.32 appear in March and the summer months of July and August, local minimum in May and absolute minimum during the winter months (0.15 in January). The three annual cycles (D, MD, and D + MD) exhibit very similar AOD values in February, April, June and August. Overall, DD intensity is governed by D type but certain differences are noticeable. The maximum in March is governed by D type (reaching values up to 0.36) because MD event days have stable AOD from February to April. The decrease on the DD outbreak intensity in May is observed in both subsets, being more intense for the MD type. The slight AOD decrease in June in the D curve is counteracted by the large increase in the MD type. In July, the D type presents a more marked maximum with a notable fall in August, again, counteracted by the load increase during MD events. The behavior in September and October is ruled by MD type while D is the only event type encountered in November and December. To our knowledge, this study presents the first evaluation of the DD intensity monthly cycle for AOD in the western Mediterranean area. The seasonal means of AOD intensity during DD outbreaks over 4-year period (2003-2006) in Palencia site are studied by Basart et al. (2009) obtaining values in the interval 0.23-0.33 (taking the wavelength of 670 nm). This range is proven here to be still acceptable for a longer period (2003-2014) with values (at 440 nm): 0.22 (DJF), 0.28 (MAM), 0.30 (JJA), and 0.24 (SON). With respect to the AE, the variation of seasonal means in this study is almost negligible between 0.91 (MAM) and 0.96 (DJF and JJA) with the D type exhibiting seasonal values around 0.61. These figures are higher than those reported by Basart et al. (2009) around 0.45. This discrepancy can be attributed to the different AE criteria used to identify dusty days, established in 0.7 (Basart et al., 2009) or 1.0 (Cachorro et al., 2016).

Some of the main characteristics shown for AOD are similar in the PM₁₀ annual cycle for D + MD curve (see Fig. 5b): maximum in

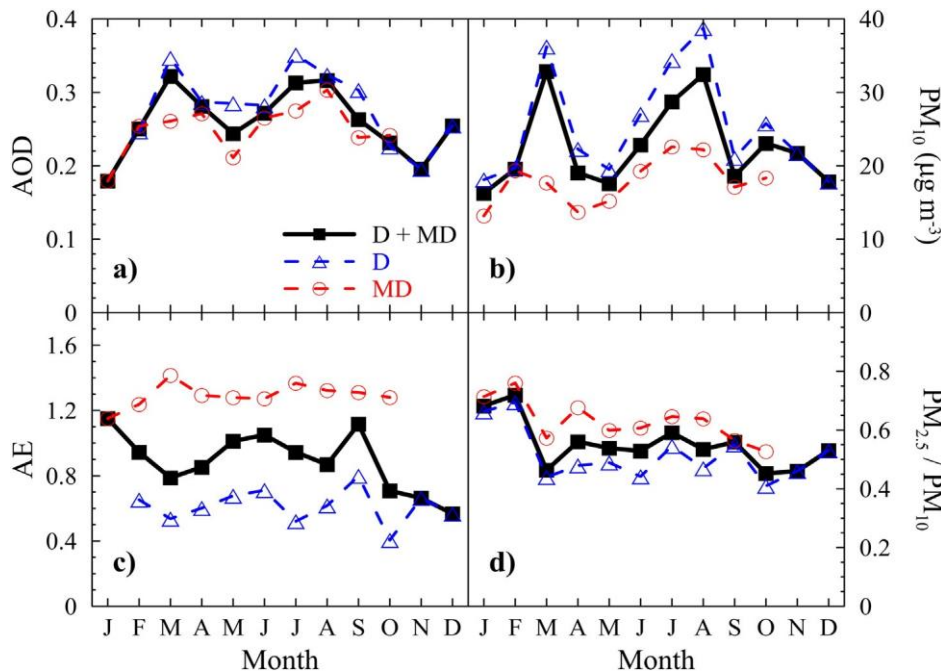


Fig. 5. Annual cycles of AOD (a), PM_{10} (b, in $\mu\text{g m}^{-3}$), AE (c) and $\text{PM}_{2.5}/\text{PM}_{10}$ ratio (d) for the DD inventory (squares) and the two subsets or categories of desert dust aerosols, D (triangles) and MD (circles).

March ($34 \mu\text{g m}^{-3}$) and summer months (being in this case more prominent the month of August), local minima in April and May and absolute minimum during winter ($16\text{--}18 \mu\text{g m}^{-3}$). The D + MD seasonality is only governed by the D type, reaching its absolute maximum in August with almost $40 \mu\text{g m}^{-3}$. The MD type shows a more stable pattern throughout the year, without marked changes. We have compared the magnitude of the PM_{10} seasonal cycle with that obtained in other regions of the Iberian Peninsula by Pey et al. (2013). These authors have reported the seasonal cycle intensity for the NE and SE sectors, which is quantitatively larger than our results for the north-central area.

The value of AE parameter, linked to particle size predominance (see Fig. 5c), corroborates the well-known behavior mentioned above for DD intrusions by decreasing and increasing in an opposite way than AOD. Thus, the AOD maximum of March becomes a minimum of AE (about 0.8) and the same occurs during summer months. For D subset, the largest coarse particle predominance observed in October (annual minimum of AE, ~ 0.45) is not linked to the most intense loads. However, the low AE observed in March and July, occur with the strongest events. The MD type follows an even distribution throughout the year.

Finally, the $\text{PM}_{2.5}/\text{PM}_{10}$ ratio (see Fig. 5d) presents a strong minimum (larger concentration of coarse mode) in March of ~ 0.5 and a weak variability in the rest of the year. A particular difference with respect to AE is observed in July: the ratio values increase from June and AE decreases indicating a different weight of fine/coarse particles at the surface and the entire column. The minimum of D type in the AE in October is also observed in the $\text{PM}_{2.5}/\text{PM}_{10}$ ratio but this is not as pronounced as in the AE (local minimum compared to September and November). There is a small difference between $\text{PM}_{2.5}/\text{PM}_{10}$ values for the D and MD types. In addition, for most of the year their behavior is similar, being only remarkable the difference in August and September.

3.3. Characterization of columnar microphysical properties during DD events

3.3.1. Columnar volume particle size distribution

AE and PM ratio are simple derived parameters used to represent the particle size predominance. The columnar microphysical properties

obtained by inversion methods (Dubovik and King, 2000; Dubovik et al., 2006; Torres et al., 2014) are more explicit quantities, such as the columnar volume particle size distribution and its derived parameters: volume concentration, effective radius for total, fine and coarse modes, fine mode volume fraction, etc. Therefore, these columnar microphysical properties have been investigated during DD events in the study area. As a first step, VPSD during these outbreaks is compared to the overall mean of available AERONET inversion data, in Fig. 6a. The VPSD for all data exhibits a clear bimodality, the fine mode peaks at $0.15 \mu\text{m}$ and the coarse mode at $2.24 \mu\text{m}$ (but with a large flat shape between 1 and $3.5 \mu\text{m}$), being the concentrations about $0.011 \mu\text{m}^3/\mu\text{m}^2$. This feature is already reported by, e.g., Prats et al. (2011) in southern Spain but only during the cold season (November through February), since in the summer months the southern area has a clear coarse particle predominance. This fact highlights the difference between northern and southern areas of the Iberian Peninsula with respect to the aerosol properties and seasonality.

However, these characteristics are strongly modified during DD events. For the total number of DD event days (D + MD curve), the increase of the coarse mode concentration is evident and presents a slimmer shape compared to the former. Besides, a more prominent maximum appears about $2 \mu\text{m}$ radius, which is in the size range ($1\text{--}3.5 \mu\text{m}$) reported by Ryder et al. (2013) in the Central Sahara and is similar to the values reported at other sites affected by African desert dust (e.g., Cuesta et al., 2008; Guirado et al., 2014). The fine mode concentration does not suffer any reduction during these events, as it was also reported by previous studies in other Mediterranean sites (e.g. Gkikas et al., 2013). In this mode, the center of the peak is also shifted to smaller radii ($0.11 \mu\text{m}$).

Concerning the D type, the mean VPSD peaks at $1.7 \mu\text{m}$ ($0.08 \mu\text{m}^3/\mu\text{m}^2$). It is noticeable that for both fine and coarse mode, the maxima are shifted to smaller radii with respect to the overall mean (black line in Fig. 6a). In presence of mixtures with dust (MD curve) the fine mode concentration is on average higher than the coarse mode. The fine mode peaks at $0.15 \mu\text{m}$, slightly shifted to larger radii when compared to the D curve but with a similar concentration. The features presented here about VPSD for DD are in line with previous studies in the

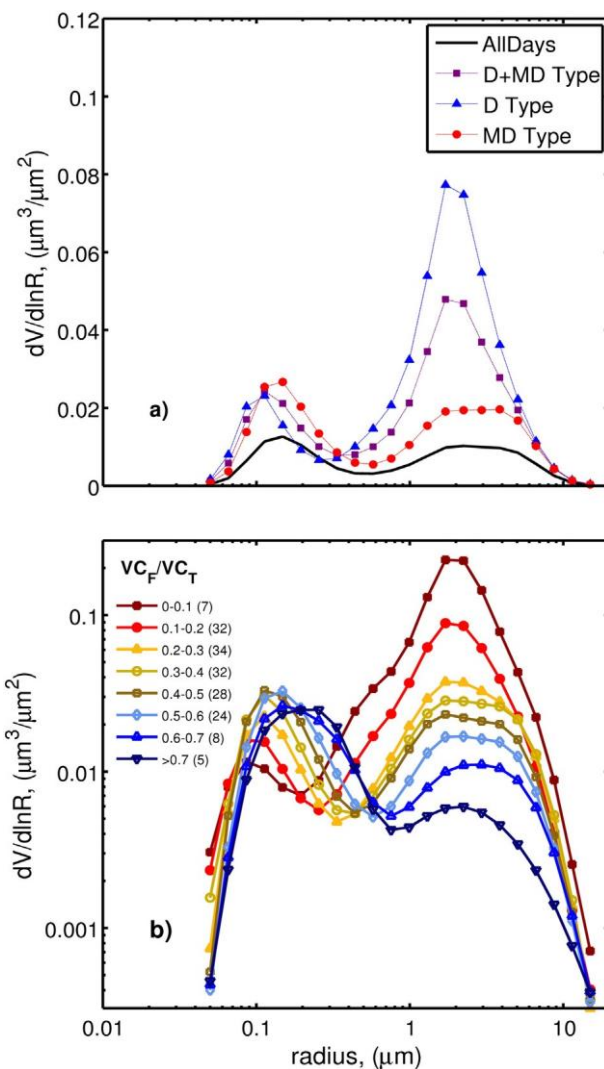


Fig. 6. Aerosol volume size distribution at Palencia AERONET site in 2003–2014: a) for All days (solid black line), all dusty days (D + MD, lilac squares), and D (blue triangles) and MD (red circles) event days; b) for the entire $V_C/F/V_C/T$ range. (For interpretation of the references to color in this figure legend, the reader is referred to the web version of this article.)

Mediterranean Basin for particular or strong DD episodes (e.g., Tafuro et al., 2006; Cachorro et al., 2008; Prats et al., 2008; Valenzuela et al., 2012; among others).

Eck et al. (2010) obtained a notable dependence of VPSD curves on the fine mode volume fraction, presenting large fine mode concentrations under certain mixture conditions of desert dust with biomass burning at Ilorin site in Nigeria. Similar results were reported by Toledano et al. (2011) for Cape Verde islands, when DD episodes occurring at different heights and mixed with biomass burning aerosols were analyzed. Fig. 6b shows the VPSD dependence on $V_C/F/V_C/T$ (the ratio of volume concentration for the fine mode, V_C/F , to the total one, V_C/T). The VPSD curves for the strongest coarse concentrations (corresponding to $V_C/F/V_C/T \leq 0.2$) present the maximum concentration at about 2 μm radii and the fine mode is almost negligible. Furthermore, a small concentration increase about 0.6 μm is found, which could be analogous to the third mode reported by Eck et al. (2010) and Toledano et al. (2011) for dust observed nearby the Sahara desert. This third mode is an unusual characteristic in most worldwide aerosol sites. Hence, DD intrusions observed in our study area with $V_C/F/V_C/T \leq 0.2$ show the expected characteristics for Saharan mineral dust aerosols. The feature at 0.6 μm disappears in Fig. 6b for larger fine mode fractions; in contrast to the previous studies nearby Sahara, which present this extra-mode

until intermediate fine mode fractions. In the 0.2 b $V_C/F/V_C/T$ b 0.5 range, bimodality is evident with similar concentration in the fine and coarse modes. With respect to the coarse mode, the maximum concentration is shifted to larger radii between 2 and 4 μm for increasing fine mode fraction, while the fine mode peaks around 0.1 μm. When the fine mode predominates ($V_C/F/V_C/T \geq 0.5$), its radius for the maximum concentration is shifted to larger values, between 0.15 and 0.30 μm.

To understand the role played by mixtures during African dust episodes in central Iberian Peninsula, Salvador et al. (2013) reported the mean source contributions to PM_{10} values in the Madrid region for short field campaigns. Their results highlight that mineral contribution can achieve the 66% of the total bulk of PM_{10} during dusty days for a rural environment, while the remaining 'non-negligible' percentage is attributed to road traffic, secondary inorganic aerosol, sea salt, among others. Furthermore, no b 25% of other sources are even present when the daily limit value of $PM_{10} = 50 \mu g m^{-3}$ is overcome during intense DD intrusions.

3.3.2. Relationships between the size and shape parameters: AE, fine mode volume fraction, sphericity, and $PM_{2.5}/PM_{10}$

Different parameters representing the aerosol size are directly derived from the VPSD, such as the effective radius or the fine mode volume fraction ($V_C/F/V_C/T$). This latter quantity may be considered analogous to the surface PM ratio ($PM_{2.5}/PM_{10}$). Besides, the AE obtained from the AOD spectral dependence is also related to the prevailing aerosol size (Eck et al., 2008). A relevant quantity provided by the AERONET inversion algorithm (Dubovik et al., 2006) is the sphericity (portion of spherical particles), ranging from 0 to 1 and thus indicating the spherical (values near 1) or non-spherical (values near 0) shape of the aerosol particles. The relationships between these four quantities related to the aerosol size and shape in different ways are studied in this subsection, with focus on their general features as part of the aerosol characterization of mineral dust and its mixtures over our study area.

Fig. 7a shows how the $V_C/F/V_C/T$ ratio is related to the Ångström exponent, which is a more simple parameter to obtain. Overall, the correlation between $V_C/F/V_C/T$ and AE is in general poor, as obtained by previous studies such as Prats et al. (2011) for "El Arenoso" site in the south-western Iberian Peninsula; Rodríguez et al. (2012) and Toledano et al. (2012) in Sub-Arctic areas. However, the correlation is higher when only D-type intrusions are analyzed, with a correlation coefficient ~ 0.8 showing an almost linear dependence for AE values up to 1.0. The correlation is much lower for the MD type ($R \sim 0.4$) without any marked dependence. In order to extend the columnar analysis to the surface, the $V_C/F/V_C/T$ vs $PM_{2.5}/PM_{10}$ scatterplot is shown in Fig. 7b. High dispersion leading to a weak correlation is observed. The highest correlation is obtained for D event days with $R \sim 0.6$ (~ 0.3 for MD type). Overall, an increasing trend of $PM_{2.5}/PM_{10}$ from 0.2 to 0.9 is observed in the entire range of $V_C/F/V_C/T$. This novel result must be highlighted because of the different techniques used to derive PM ratio values and columnar inversion products. The lower sampling frequency of Sun photometer inversion products (V_C/T , V_C/F and Sphericity, see Table 1) have also caused a notable reduction in the number of available data, 182 in Fig. 7a and 165 in Fig. 7b, from the total of 304 with simultaneous AOD and PM_{10} data. Hence, this fact difficults the usage of these quantities in the DD detection process.

A general feature can be drawn from Fig. 7a–b: three zones have been identified considering the type of DD intrusions falling in each one. First at all, those intrusions with a predominant coarse mode ($V_C/F/V_C/T \leq 0.2$) are only of D type, with AE below 0.7 and $PM_{2.5}/PM_{10}$ between 0.2 and 0.6. This behavior is an indicator of strong coarse particle predominance in the atmospheric column meanwhile weak mixture conditions can occur at the surface. About a quarter of all the available points fall in this interval of $V_C/F/V_C/T$. In contrast, there is a zone where the fine mode predominates even in the presence of dust ($V_C/F/V_C/T \geq 0.45$, AE N 1.2 and 0.5 b $PM_{2.5}/PM_{10}$ b 1.0) being all classified as MD type. The presence of mineral dust is always ensured by the

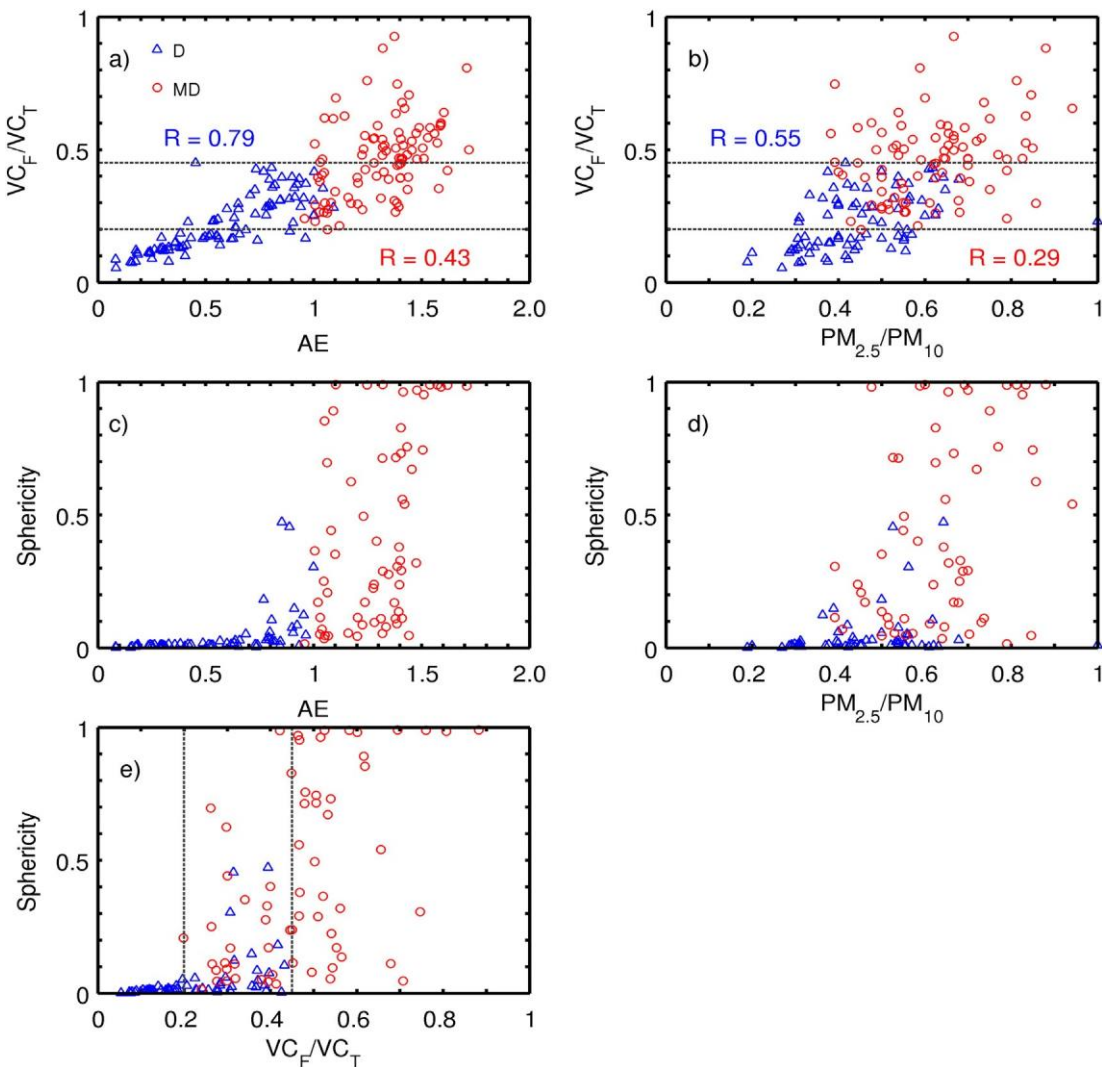


Fig. 7. Scatterplots of: a) VC_F/VC_T vs AE, b) VC_F/VC_T vs $PM_{2.5}/PM_{10}$, c) Sphericity vs AE, d) Sphericity vs $PM_{2.5}/PM_{10}$, and e) Sphericity vs VC_F/VC_T for the D (blue triangles) and MD (red circles) event days. (For interpretation of the references to color in this figure legend, the reader is referred to the web version of this article.)

analysis of the ancillary information described in Section 2.2. Furthermore, the intermediate zone ($0.2 \leq VC_F/VC_T \leq 0.45$) presents both D and MD types with a wide range of AE (0.6–1.8) and PM ratio (0.3–0.8) values, which corroborates the relevance of analyzing aerosol mixtures including mineral dust over our site. About 75% of the total DD event days with columnar inversion products present mixtures in greater or lesser extent. These three established zones of VC_F/VC_T can be considered a main feature in the study of other aerosol properties during DD outbreaks.

The non-spherical shape of mineral dust aerosols has been extensively demonstrated (e.g., Dubovik et al., 2006; Eck et al., 2005; Prats et al., 2008; Bedareva et al., 2014; Taylor et al., 2015), hence this is a key parameter in the aerosol characterization studies. The AERONET retrievals of sphericity fraction (e.g., Dubovik et al., 2006) are used in this section. Fig. 7c–e show the sphericity vs AE, $PM_{2.5}/PM_{10}$, and VC_F/VC_T scatterplots, respectively. Overall, the mean sphericity fraction during DD episodes is 0.25, being as low as 0.05 for D type and about 0.4 for MD type. As expected, most of aerosols present non-spherical shapes (sphericity fraction values below 0.20 in the 64% of the cases), but a non-negligible part (16%) nearly displays a predominant spherical shape (sphericity fraction beyond 0.70). For the D type, most of the sphericity fractions are below 0.20 pointing out the predominance of non-spherical particles, whereas sphericity in the MD type spans in

the entire 0–1 interval indicating mixtures of spherical and non-spherical particles in different proportions.

Fig. 7c clearly shows two well defined areas below and above $AE = 1$, demonstrating that aerosols with AE values below 1 are very predominantly DD aerosol because of the very low sphericity fraction, whereas above $AE = 1$ we can find a mixture of particle shapes with a high variability in the sphericity fractions. On the other hand, as can be seen in Fig. 7d, PM ratio and sphericity do not follow any correspondence, thus demonstrating the less ability of PM ratio for DD detection.

In terms of the VC_F/VC_T ranges established above, the mean sphericity fraction is about 0.01 for $VC_F/VC_T \leq 0.2$. Hence, those cases showing AE values below 0.7 and $PM_{2.5}/PM_{10}$ between 0.2 and 0.6 present non-sphericity, as it is typical in Saharan surroundings (e.g., Dubovik et al., 2006). For the interval $0.2 \leq VC_F/VC_T \leq 0.45$, the mean portion of spherical particles increases up to 0.17. These two fractions are in line with previous studies analyzing areas with notable weight of dust particles (e.g., Taylor et al., 2015). The mean sphericity values in these two first intervals of VC_F/VC_T (where coarse mode predominates) highlight that the choice of the selected threshold of $AE = 1$ in order to distinguish between D and MD dusty days in our study area is reliable and correct, since this quantity hardly reaches values of 0.17. Finally, those cases with $VC_F/VC_T \geq 0.45$ show a mean sphericity fraction of 0.56, thus indicating a minor role of mineral dust particles.

All the results presented in this subsection, with a wide range of AE, VC_F/VC_T , PM ratio, and sphericity fraction, point out a mixture of aerosols, but the purer DD intrusions are reliably detected too. The large number of mixture cases is due to the low-moderate DD events registered. Besides, these results again highlight that the detection of strong DD events could be affordable using AE, VC_F/VC_T or sphericity, but bearing in mind that the amount of available columnar inversion data is much less than AOD and AE observations. Hence, the most suitable quantity to carry out this task is the Ångström exponent, which can present DD fingerprints even in low and moderate episodes.

3.3.3. Effective radius and its relation with other particle size parameters

Effective radius is the most important parameter representing the size of the VPSD, thus its relation with the other quantities related to the particle size is of general interest for atmospheric aerosol community. Fig. 8 displays the Effective Radius (ER) for the total (ER_T), fine (ER_F), and coarse (ER_C) modes vs AE, VC_F/VC_T , and $PM_{2.5}/PM_{10}$ size parameters. Fig. 8c is the first attempt, to our knowledge, of establishing a relationship between columnar microphysical and surface aerosol size properties. Both ER_F and ER_C span in the following tight intervals: (0.1, 0.22 μm) and (1.3, 3 μm), respectively. Therefore, as it can be seen in Fig. 8a they are practically independent of AE, VC_F/VC_T or $PM_{2.5}/PM_{10}$. On the contrary, ER_T shows a wider range between 0.15 and 1.2 μm , and certain correlation with AE, VC_F/VC_T or $PM_{2.5}/PM_{10}$ is to be expected in spite of the different size information contained in each quantity. The correlation coefficients for our DD database are -0.8 for ER_T vs AE, -0.9 for ER_T vs VC_F/VC_T , and -0.6 for ER_T vs $PM_{2.5}/PM_{10}$. I.e., the larger the AE or VC_F/VC_T or $PM_{2.5}/PM_{10}$, the smaller the total effective radius.

The largest particles during DD outbreaks are placed in the ER_T range of 0.5–1.2 μm and they correspond to AE values below 0.5, $VC_F/VC_T \leq 0.2$, and PM ratio up to ~ 0.5 , being only D type intrusions. However, there are similar $PM_{2.5}/PM_{10}$ values occurring for smaller particles (ER_T of 0.2–0.5 μm for D and MD types), which does not happen in the AE and VC_F/VC_T intervals. Overall, the mean ER_T during all events is 0.40 μm , which increases up to 0.50 μm for D type cases and decreases until 0.31 μm for MD type cases.

The highest correlation between AE and ER_T is found for the D type with a correlation coefficient of -0.78 , which is also noticeable ($R = -0.88$) in the ER_T vs VC_F/VC_T scatterplot and slightly lower in the ER_T vs $PM_{2.5}/PM_{10}$ scatterplot ($R = -0.6$). The scatterplots present different behaviors: ER_T vs AE and $PM_{2.5}/PM_{10}$ exhibit linear relationship (Fig. 8a and c) while power functions are used to fit ER_T vs VC_F/VC_T (Fig. 8b). Note that logarithmic scale is used for the y axis. With respect to MD event days, high correlation ($R \sim 0.8$) is observed in Fig. 8b in the VC_F/VC_T analysis, whilst AE and $PM_{2.5}/PM_{10}$ are almost independent on ER_T (with slope of linear fits close to 0 and R below 0.5).

The analysis of dusty days allows establishing a consistent relationship between the total effective radius and AE (Prats et al., 2008). The higher correlation for the ER_T vs VC_F/VC_T study is related to the fact that the both variables are retrieved in the same inversion process (e.g., Gonzi et al., 2002; Prats et al., 2011; Rodríguez et al., 2012). Finally, Fig. 8c shows certain correlation ($R = -0.58$) between the total effective radius and PM ratio recorded at surface for the D type aerosol. All these features are in line with previous results discussed in Figs. 6 and 7.

3.3.4. Columnar volume particle concentration and its relationship with AOD and surface mass concentration

Columnar aerosol load can also be expressed by means of the columnar volume (or mass) particle concentration derived from the VPSD, where we can separate the concentration of the fine and the coarse modes. Aerosol optical depth can be expressed as a function of the columnar volume (or mass) particle concentration (e.g., Fraser et al., 1984; Kokhanovsky et al., 2009), defining the columnar volume efficiency factor E_V . Empirical relationships between AOD and total volume particle concentration (VC_T) were analyzed in previous studies (Prats et al., 2011; Toledano et al., 2012). These studies highlight that the

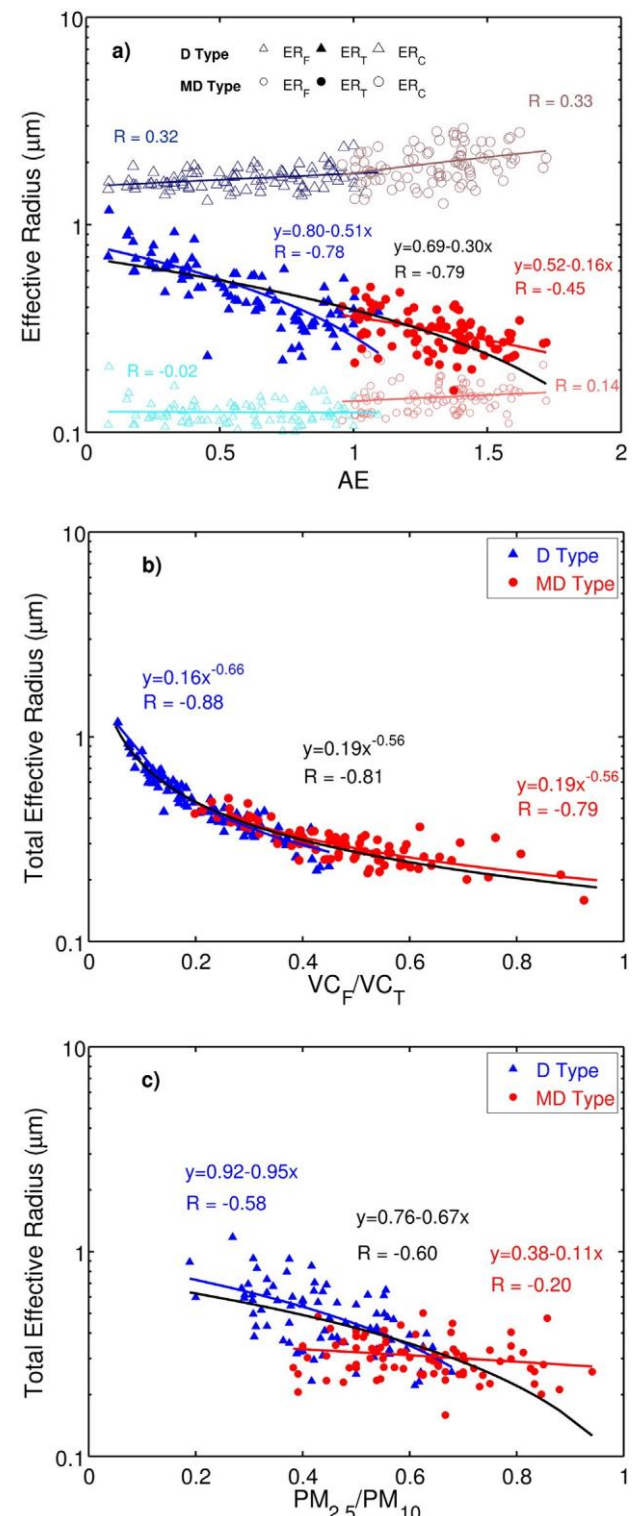


Fig. 8. Scatterplots of: a) effective radius for total, coarse, and fine modes vs Ångström exponent for D (blue triangles) and MD (red circles) event days; b) idem for VC_F/VC_T ; and c) idem for $PM_{2.5}/PM_{10}$. Solid lines are the fits of each analysis, being the black one the fit for the total DD database. (For interpretation of the references to color in this figure legend, the reader is referred to the web version of this article.)

relationship between these two columnar quantities represented by E_V is ruled by the VC_F/VC_T ratio. In order to empirically prove this kind of relationship for dusty days in north-central Iberian Peninsula, Table 3 and Fig. 9 illustrate the linear relationship between different columnar and surface quantities during DD events using the three intervals

established in Fig. 7. Fig. 9 is depicted as an example of visualization of this kind of scatterplots for the AOD vs VC_T , PM_{10} vs VC_T , and AOD vs $PM_{2.5}$ cases. Linear fits without intercept have been assumed in order to avoid the lack of physical meaning for no aerosol conditions.

For the coarse-mode-dominated cases ($VC_F/VC_T \leq 0.2$), there is an excellent agreement between VC_T and AOD (Fig. 9a), with R values about 0.98. The slopes of these fits are the columnar volume extinction efficiencies (e.g., Toledano et al., 2012) which present units of $\mu\text{m}^2/\mu\text{m}^3$. Hence, for a given AOD, the larger the slope the smaller the VC_T . For strong DD outbreaks observed in south-western Spain in summer 2004, Prats et al. (2011) reported a mean efficiency value of $1.8 \mu\text{m}^2/\mu\text{m}^3$, with an extreme threshold of $1.4 \mu\text{m}^2/\mu\text{m}^3$ for coarse particles. Our columnar volume extinction efficiency for this category ($1.7 \mu\text{m}^2/\mu\text{m}^3$) falls between these two values. As the fine mode gains weight, the slope becomes larger, up to a value of $3.7 \mu\text{m}^2/\mu\text{m}^3$ for $VC_F/VC_T \geq 0.45$. This figure is in line with previous results for fine particles in southern Spain (Prats et al., 2011) and Sub-Arctic areas (Toledano et al., 2012). The VC_F/VC_T governs the columnar volume extinction efficiency, related to different aerosol types. Overall, the mean columnar volume extinction efficiency obtained during all dusty days is about $2.1 \pm 0.06 \mu\text{m}^2/\mu\text{m}^3$.

To correctly interpret the slope of PM_{10} vs VC_T fit (Fig. 9b and Table 3), it must be born in mind that the ratio between the columnar aerosol optical depth and the horizontal extinction coefficient defines the scale height H (e.g., Horvath et al., 2002), which can be understood as the height a homogenous aerosol layer with given extinction coefficient would extend in order to have the given optical depth. The scale height factor makes the transformation from surface to columnar quantities. Besides, the slope of the fit between PM_{10} and VC_T gives the ratio between two particle concentrations, one expressed by mass and the other one by volume, thus this slope is the ratio between aerosol particle density ρ (in g cm^{-3} , in this case of desert dust particles) and the scale height H. In this sense, the slope between the surface and columnar concentration can provide an estimate of the scale height or the particle density, depending on the known quantities.

Table 3 presents the linear fits between PM_{10} and VC_T , $PM_{2.5}$ and VC_F , and $PM_{2.5-10}$ and VC_C . These three linear fits exhibit correlations coefficients about 0.9 with the expected exceptions of the fine mode fit in the $VC_F/VC_T \leq 0.2$ category and the coarse mode fit in the $VC_F/VC_T \geq 0.45$ one. The PM_{10} vs VC_T exhibits increasing slopes as the fine mode fraction gains weight. The opposite is observed in the $PM_{2.5}$ vs VC_F fit. The slopes of these fits in Table 3 are in g m^{-4} (or $\mu\text{g cm}^{-4}$).

Table 3

Linear fits ($y = b x$) for three different categories of VC_F/VC_T ratio: c1) $VC_F/VC_T \leq 0.2$, c2) $0.2 < VC_F/VC_T \leq 0.45$, and c3) $VC_F/VC_T \geq 0.45$. The 'StE', 'R', and 'N' are the standard error, correlation coefficient and number of data, respectively. The 'H' column in the PM_x vs VC_x fits is the corresponding scale height, assuming a particle density for crustal material of 2.2 g cm^{-3} (e.g., Sorribas et al., 2015). See text for units.

| Fit | VC_F/VC_T category | b | StE | R | N | H (m) |
|-------------------------|----------------------|--------|--------|------|----|--------|
| AOD vs VC_T | c1 | 1.68 | 0.05 | 0.98 | 41 | - |
| | c2 | 2.49 | 0.07 | 0.97 | 76 | - |
| | c3 | 3.74 | 0.14 | 0.97 | 48 | - |
| PM_{10} vs VC_T | c1 | 226 | 16 | 0.91 | 41 | 9725 |
| | c2 | 236 | 12 | 0.92 | 76 | 9329 |
| | c3 | 272 | 19 | 0.90 | 48 | 8080 |
| $PM_{2.5}$ vs VC_F | c1 | 620 | 64 | 0.84 | 41 | 3546 |
| | c2 | 377 | 19 | 0.92 | 76 | 5843 |
| | c3 | 309 | 21 | 0.91 | 48 | 7117 |
| $PM_{2.5-10}$ vs VC_C | c1 | 172 | 13 | 0.91 | 41 | 12,781 |
| | c2 | 163 | 10 | 0.88 | 76 | 13,517 |
| | c3 | 217 | 25 | 0.79 | 48 | 10,157 |
| AOD vs PM_{10} | c1 | 0.0062 | 0.0005 | 0.89 | 41 | - |
| | c2 | 0.0091 | 0.0005 | 0.92 | 76 | - |
| | c3 | 0.0114 | 0.0008 | 0.90 | 48 | - |
| AOD vs $PM_{2.5}$ | c1 | 0.0184 | 0.0015 | 0.89 | 41 | - |
| | c2 | 0.0169 | 0.0009 | 0.92 | 76 | - |
| | c3 | 0.0186 | 0.0012 | 0.91 | 48 | - |

If the assumption of crustal material having a density of 2.2 g cm^{-3} is considered (Wagner et al., 2009; Sorribas et al., 2015), the scale factors H obtained with the PM_{10} vs VC_T slope (shown in Table 3) range between ~ 8000 and $\sim 10,000$ m depending on the VC_F/VC_T interval. When fine particles are analyzed ($PM_{2.5}$ vs VC_F and $VC_F/VC_T \geq 0.45$ category) the scale factor is ~ 7000 m, assuming the same density (Sorribas et al., 2015). Finally, for the coarse particles a larger scale height H around 13,000 m is obtained for the categories $VC_F/VC_T \leq 0.2$ and $0.2 < VC_F/VC_T \leq 0.45$. All these large scale factors indicate that a relevant portion of dust is contained in high layers with limited impact on the extinction at the ground. When there is no impact of neither desert dust nor other high turbidity events, the scale height H takes a mean value about 2700 m, which is in line with the results reported by Horvath et al. (2002) in two sites in Spain and Austria during short campaigns, who obtained values ranging from 3000 to 5000 m.

With this information, the ratio between AOD and PM_{10} or $PM_{2.5}$ can be understood as an efficiency factor, with units of m^3/g . Hence, analogously to the efficiency introduced at the surface by Waggoner et al. (1981), the AOD/ PM_{10} and AOD/ $PM_{2.5}$ ratios represent the mass extinction efficiency for the whole atmospheric column. The slopes for AOD vs PM_{10} fits are strongly dependent on the VC_F/VC_T category, meanwhile AOD vs $PM_{2.5}$ presents similar slopes for the three intervals. If the AOD quantity is estimated from the surface PM_{10} concentrations, a high dispersion is expected during DD outbreaks although the right identification of the aerosol microphysical properties can help to reduce the uncertainty.

3.4. Aerosol radiative properties during DD events

One of the most relevant aerosol parameter related to the aerosol absorption is the single scattering albedo (SSA). In order to characterize this quantity during DD events, its spectral dependence is shown in Fig. 10a. The SSA values indicate a less absorbing power when mineral dust aerosols are identified, since they increase compared to non-dusty days for all wavelengths. For instance, the SSA values for D type increases with respect to the non-dusty conditions: from 0.89 to 0.94 at 675 nm and from 0.85 to 0.94 at 1020 nm. The curve for the all the DD episodes (D + MD curve, with a mean SSA about 0.92) is almost wavelength independent but still contains the fingerprint of the increasing values from the UV to near-infrared (NIR) range that characterizes the mineral dust aerosol (see the D type curve). The marked increase between 440 and 670 nm is found for Saharan dust (Dubovik et al., 2002; Kim et al., 2011; García et al., 2008; Eck et al., 2010; Toledano et al., 2011; Giles et al., 2012, among others) but also at various Spanish and Mediterranean sites during desert dust events (e.g., Meloni et al., 2006; Cachorro et al., 2008, 2010; Valenzuela et al., 2012). The less absorbing character of DD aerosol still remains when analyzing the MD type but SSA decreases with wavelength, similarly to the non-dusty days. In this case, the fine mode becomes more relevant and the difference between SSA for MD and non-DD event days is weaker (e.g., from 0.89 to 0.91 at 675 nm and from 0.85 to 0.89 at 1020 nm).

As it was shown by Eck et al. (2010) at Ilorin site, the SSA displays a strong dependence on the fine mode volume fraction VC_F/VC_T , including its spectral behavior. Actually, the larger the fine mode volume fraction, the smaller the differences among the spectral SSA values; i.e., there is a notable SSA increase with wavelength for VC_F/VC_T up to about 0.5, while beyond this threshold there is no spectral change. In order to corroborate this behavior in our study area, Fig. 10b shows the SSA spectral dependence in the three categories of VC_F/VC_T for the D + MD cases. Our results for $VC_F/VC_T \leq 0.2$ change from SSA = 0.91 at 440 nm to SSA = 0.96 at 1020 nm, thus indicating the typical less absorbing power at longer wavelengths. The SSA curve for the intermediate range ($0.2 < VC_F/VC_T \leq 0.45$) remains even, about 0.91, meanwhile those conditions ruled by the fine mode ($VC_F/VC_T \geq 0.45$) present a SSA decrease from 0.93 at 440 nm to 0.89 at 1020 nm, pointing out most absorbing aerosols at longer wavelengths. Focusing on SSA at 440 nm, very similar values

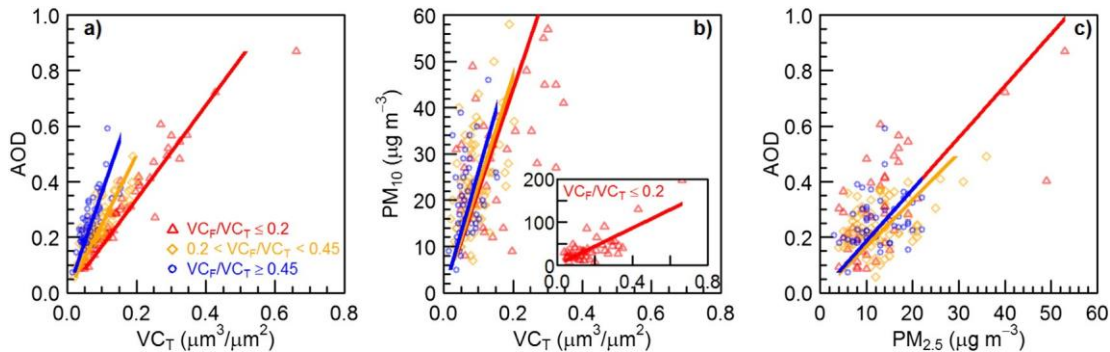


Fig. 9. AOD vs VC_T (a), PM_{10} vs VC_T (b), and AOD vs $PM_{2.5}$ (c) for three different intervals of VC_F/VC_T during DD episodes. Linear fits are reported in Table 3.

are obtained for our three VC_F/VC_T categories, which is in line with previous findings by Eck et al. (2010) for Kampur and XiangHe sites. This effect suggests that there is not any change on absorption power at 440 nm among all the DD episodes in the inventory regardless the fine mode volume fraction. Another important intensive aerosol quantity related to the scattering processes is the asymmetry factor (g) which gives information about the angular distribution of the light scattered by particles and spans from 0.6 to 0.8 for most of the aerosol types. Similarly to the SSA analysis, Fig. 11 shows the g spectral dependence for different DD intrusion types and VC_F/VC_T fractions. The non-dusty days are described by strong decreasing wavelength dependence from 0.71 at 440 nm to 0.6 at 1020 nm. This decrease is softened for DD outbreaks (with larger values for the D event days, about 0.70–0.72), because g increases with the particle size (Horvath, 1998; Cachorro et al., 2000). This feature is also noticeable when studying g dependence on VC_F/VC_T for the D + MD cases. The categories of $VC_F/VC_T \leq 0.2$ and $0.2 < VC_F/VC_T \leq 0.45$ present similar values being g about 0.74–0.70 at 440 nm and 0.72–0.67 at 1020 nm, respectively. Finally, for the fine-mode-dominated cases ($VC_F/VC_T \geq 0.45$), g strongly decreases with wavelength (0.72–0.62). Dubovik et al. (2002) reported ranges of 0.69–0.65 and 0.73–0.71 at Solar Village and Cape Verde sites between 440 and 1020 nm for a desert dust and oceanic environment. In a DD characterization study in Granada (southern Iberian Peninsula) by Valenzuela et al. (2012), these authors obtained similar values for g spectral dependence, i.e. from 0.7 to 0.66 in the 440–1020 nm interval.

4. Conclusions

The main statistics and characterization of aerosol size and load involving both surface and columnar properties of dusty days over north-central IP for a long-term period (2003–2014) is presented here. This study is based on a reliable inventory of DD intrusions

obtained by the simultaneous usage of surface and columnar data (Cachorro et al., 2016). As a relevant result, the study reveals that most of the DD outbreaks contain desert dust aerosols mixed with other aerosol types, mainly anthropogenic pollution, biomass burning, or marine aerosols. Some of the aerosol properties studied are directly derived from measurements, like surface PM_{10} and $PM_{2.5}$ and its ratio, or columnar data like AOD or AE, and others are retrieved from a more complex inversion algorithm which requires sky radiance measurements, like the columnar particle size distribution and its derived parameters: effective radius, volume particle concentration, etc. Besides, optical parameters like the asymmetry factor and single scattering albedo are also considered.

This study highlights the relevance of the joint interpretation of surface and columnar aerosol data which includes certain relationships for DD episodes. Examples of these relationships are the total effective radius versus AE, the fine mode volume fraction or the PM ratio, and the VC_T vs AOD or PM_{10} , allowing the determination of the volume extinction factor or the scale height factor. For the first time, PM_x measurements are linked to columnar inversion products during DD events for long term data, which is one of the novelties of the present study. The surface-columnar relationships are well established once the columnar aerosol DD properties are known. For instance, the slopes of the fits for each interval of VC_F/VC_T range are obtained with high correlation coefficients.

Characterization aerosol studies are site-dependent due to the specific local conditions occurring over each site, but they are required to better understand how aerosol properties change over certain areas, particularly those relatively far away from the sources which receive frequent desert dust intrusions likely mixed, in greater or lesser extent, with other aerosol types. Our results are mostly in line with previous DD characterization studies carried out in the Mediterranean Basin and northern African surroundings. For the purest mineral dust events, all

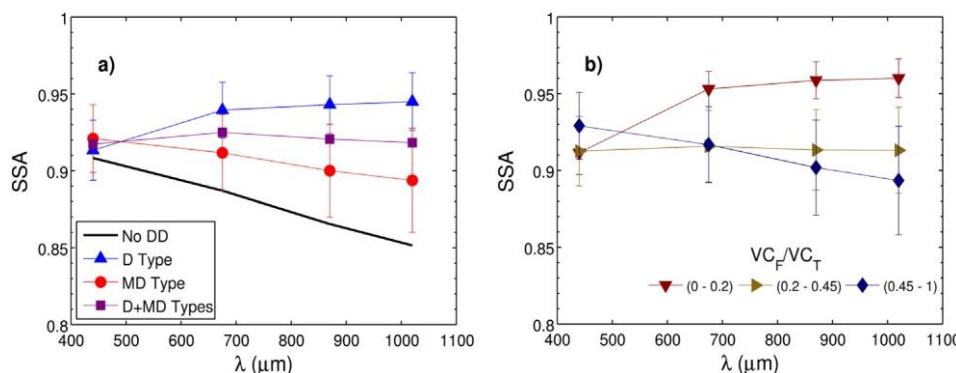


Fig. 10. Spectral single scattering albedo: a) during DD and no DD episodes; b) for three different intervals of VC_F/VC_T .

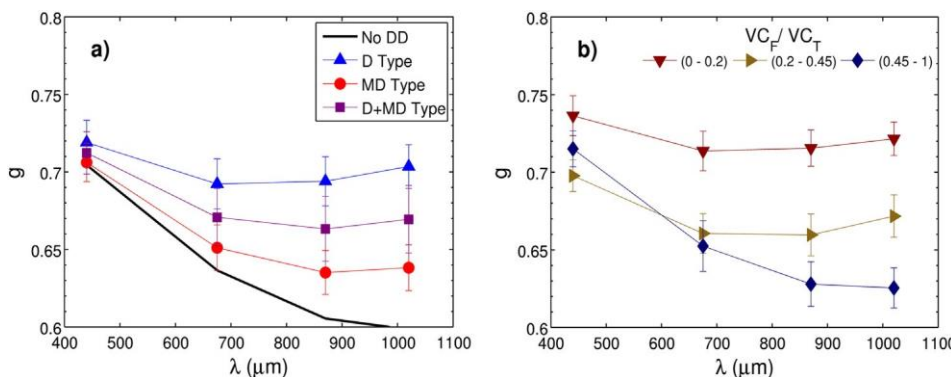


Fig. 11. Asymmetry factor: a) during DD and no DD episodes; b) for the three different intervals of VC_F/VC_T .

the aerosol properties present their typical values. The size (AE, PM ratio and total effective radius) and concentration (AOD, PM_x , and volume particle concentration) quantities exhibit significant correlation (in a greater or lesser extent). Furthermore, other microphysical and radiative properties such as non-sphericity and single scattering albedo are also congruent with previous results. Those cases showing fine mode volumen fraction below 0.2 represent 25% of the DD database with columnar inversion data. The remaining part (~75%) highlights the large relevance of mixtures with mineral dust, which produce a wide range of aerosol properties. For instance, VC_F/VC_T can be above 0.45, sphericity fraction can overcome 0.7, effective radii can reach 0.3 μm , and fair correlations ($R > 0.6$) between $\text{PM}_{10}/\text{PM}_{2.5}$ and columnar volume concentrations can be found.

Analyzing the results of this study, some parameters seem to be more suitable than others to detect and classify desert dust aerosols, like AE and sphericity fraction. Defined ranges of these parameters allow the classification in different aerosol categories, as those given by AE or VC_F/VC_T . A threshold of $AE=1$ is suitable for our area to distinguish between intrusions composed of aerosols with a strong prevailing DD character and those presenting a mixture of aerosols. This classification is corroborated by the non-sphericity and low values of VC_F/VC_T . The advantage of using AE quantity relies on its larger sampling compared to the other inversion products.

Overall, the rapport between surface and columnar aerosol properties during DD intrusions here reported is relevant due to the different measurement techniques that are involved. The 12-years inventory is an extraordinary tool to investigate how DD fingerprints on aerosol properties change at both levels during different types of DD episodes. In particular, the columnar and surface retrievals about aerosol speciation during this kind of events can be a very interesting topic for further studies. Hence, this study is required to better understand their behavior along the whole Mediterranean Basin and can be used to validate DD forecast models or satellite DD products.

Supplementary data to this article can be found online at <http://dx.doi.org/10.1016/j.scitotenv.2016.08.001>.

Acknowledgements

The authors are grateful to Spanish MINECO for the financial support of the FPI grant BES-2012-051868, project CGL2012-33576, and "Juan de la Cierva – Incorporación" grant IJCI-2014-19477. The research leading to these results has received funding from the European Union under grant agreement Nr. 654109 [ACTRIS 2]. Thanks are due to EMEP (especially to MAGRAMA and AEMET) and AERONET-PHOTONS-RIMA staff for providing observations and for the maintenance of the networks. We also thank "Consejería de Fomento y Medio Ambiente" for their support to desert dust studies in Castilla y León region, as well as Consejería de Educación of Junta de Castilla y León for supporting the project (VA100U14).

References

- Basart, S., Pérez, C., Cuevas, E., Baldasano, J.M., Gobbi, G.P., 2009. Aerosol characterization in Northern Africa, Northeastern Atlantic, mediterranean basin and middle east from direct-sun AERONET observations. *Atmos. Chem. Phys.* 9 (21), 8265–8282.
- Bedareva, T.V., Sviridenkov, M.A., Zhuravleva, T.B., 2014. Retrieval of dust aerosol optical and microphysical properties from ground-based Sun-sky radiometer measurements in approximation of randomly oriented spheroids. *J. Quant. Spectrosc. Radiat.* 146, 140–157. <http://dx.doi.org/10.1016/j.jqsrt.2014.05.006>.
- Bennouna, Y., Cachorro, V.E., Mateos, D., Burgos, M.A., Toledano, C., Torres, B., de Frutos, A.M., 2016. Long-term comparative study of columnar and surface mass concentration aerosol properties in a background environment. *Atmos. Environ.* 140, 261–272.
- Cabello, M., Orza, J.A.G., Barrero, M.A., Gordo, E., Berasaluce, A., Cantón, L., Dueñas, C., Fernández, M.C., Pérez, M., 2012. Spatial and temporal variation of the impact of an extreme Saharan dust event. *J. Geophys. Res.* 117, D11204. <http://dx.doi.org/10.1029/2012JD017513>.
- Cachorro, V.E., Burgos, M.A., Mateos, D., Toledano, C., Bennouna, Y., Torres, B., de Frutos, A.M., Herguedas, A., 2016. Inventory of African desert dust events in the North-central Iberian Peninsula in 2003–2014 based on sun photometer and PM_x data. *Atmos. Chem. Phys.* 16, 8227–8248. <http://dx.doi.org/10.5194/acp-16-8227-2016>.
- Cachorro, V.E., Duran, P., Vergaz, R., de Frutos, A.M., 2000. Columnar physical and radiative properties of atmospheric aerosols in north central Spain. *J. Geophys. Res.-Atmos.* 105 (D6), 7161–7175.
- Cachorro, V.E., Toledano, C., Antón, M., Berjón, A., de Frutos, A.M., Vilaplana, J.M., Arola, A., Krotkov, N.A., 2010. Comparison of UV irradiances from Aura/Ozone monitoring instrument (OMI) with brewer measurements at el Arenosillo (Spain) – part 2: analysis of site aerosol influence. *Atmos. Chem. Phys.* 10, 11867–11880. <http://dx.doi.org/10.5194/acp-10-11867-2010>.
- Cachorro, V.E., Toledano, C., Prats, N., Sorribas, M., Mogo, S., Berjón, A., Torres, B., Rodrigo, R., de la Rosa, J., de Frutos, A.M., 2008. The strongest desert dust intrusion mixed with smoke over the Iberian Peninsula registered with Sun photometry. *J. Geophys. Res.* 113, D14S04. <http://dx.doi.org/10.1029/2007JD009582>.
- Cuesta, J., Edouart, D., Mimouni, M., Flamant, P.H., Loth, C., Gibert, F., Marnas, F., Bouklila, A., Kharef, M., Ouchene, B., Kadi, M., Flamant, C., 2008. Multiplatform observations of the seasonal evolution of the Saharan atmospheric boundary layer in Tamanrasset, Algeria, in the framework of the African Monsoon Multidisciplinary Analysis field campaign conducted in 2006. *J. Geophys. Res.-Atmos.* 113, D00C07. <http://dx.doi.org/10.1029/2007jd009417>.
- Di Biagio, C., di Sarra, A., Meloni, D., 2010. Large atmospheric shortwave radiative forcing by Mediterranean aerosols derived from simultaneous ground-based and spaceborne observations and dependence on the aerosol type and single scattering albedo. *J. Geophys. Res.* 115, D10209. <http://dx.doi.org/10.1029/2009JD012697>.
- Dubovik, O., King, M.D., 2000. A flexible inversion algorithm for retrieval of aerosol optical properties from sun and sky radiance measurements. *J. Geophys. Res.* 105 (D16), 20673–20696.
- Dubovik, O., Holben, B., Eck, T.F., Smirnov, A., Kaufman, Y.J., King, M.D., Tanre, D., Slutsker, I., 2002. Variability of absorption and optical properties of key aerosol types observed in worldwide locations. *J. Atmos. Sci.* 59, 590–608.
- Dubovik, O., Sinyuk, A., Lapyonok, T., Holben, B.N., Mishchenko, M., Yang, P., Eck, T.F., Volten, H., Munoz, O., Veihelmann, B., van der Zande, W.J., Leon, J.F., Sorokin, M., Slutsker, I., 2006. Application of spheroid models to account for aerosol particle nonsphericity in remote sensing of desert dust. *J. Geophys. Res.-Atmos.* 111 (D11), 2156–2202. <http://dx.doi.org/10.1029/2005JD006619>.
- Eck, T.F., Holben, B.N., Dubovik, O., Smirnov, A., Goloub, P., Chen, H.B., Chatenet, B., Gomes, L., Zhang, X.Y., Tsay, S.C., Ji, Q., Giles, D., Slutsker, I., 2005. Columnar aerosol optical properties at AERONET sites in central eastern Asia and aerosol transport to the tropical mid-Pacific. *J. Geophys. Res.* 110, D06202.
- Eck, T.F., Holben, B.N., Reid, J.S., Sinyuk, A., Dubovik, O., Smirnov, A., Giles, D., O'Neill, N.T., Tsay, S.C., Ji, Q., Al Mandoos, A., Ramzan Khan, M., Reid, E.A., Schafer, J.S., Sorokin, M., Newcomb, W., Slutsker, I., 2008. Spatial and temporal variability of column-integrated aerosol optical properties in the southern Arabian Gulf and United Arab Emirates in summer. *J. Geophys. Res.* 113 (D01204).
- Eck, T.F., Holben, B.N., Sinyuk, A., Pinker, R.T., Goloub, P., Chen, H., Chatenet, B., Li, Z., Singh, R.P., Tripathi, S.N., Reid, J.S., Giles, D.M., Dubovik, O., O'Neill, N.T., Smirnov, A., Wang, P., Xia, X., 2010. Climatological aspects of the optical properties of fine/coarse mode

- aerosols mixtures. *J. Geophys. Res.* 115, D19205. <http://dx.doi.org/10.1029/2010JD014002>.
- Escudero, M., Castillo, S., Querol, X., Avila, A., Alarcón, M., Viana, M.M., Alastuey, A., Cuevas, E., Rodríguez, S., 2005. Wet and dry African dust episodes over eastern Spain. *J. Geophys. Res.* 110, D18S08. <http://dx.doi.org/10.1029/2004JD004731>.
- Escudero, M., Querol, X., Pey, J., Alastuey, A., Pérez, N., Ferreira, F., Alonso, S., Cuevas, E., 2007. A methodology for the quantification of the net African dust load in air quality monitoring networks. *Atmos. Environ.* 41 (26), 5516–5524. <http://dx.doi.org/10.1016/j.atmosenv.2007.04.047>.
- Estellés, V., Martínez-Lozano, J.A., Utrillas, M.P., 2007. Influence of air mass history on the columnar aerosol properties at Valencia, Spain. *J. Geophys. Res.* 112, D15211. <http://dx.doi.org/10.1029/2007JD008593>.
- Fraser, R.S., Kaufman, Y.J., Mahoney, R.L., 1984. Satellite measurements of aerosol mass and transport. *Atmos. Environ.* 18, 2577–2584.
- García, O.E., Diaz, A.M., Exposito, F.J., Diaz, J.P., Dubovik, O., Dubuisson, P., Roger, J.-C., Eck, T.F., Sinyuk, A., Derimian, Y., Dutton, E.G., Schafer, J.S., Holben, B.N., García, C.A., 2008. Validation of AERONET estimates of atmospheric solar surface fluxes and aerosol radiative forcing by ground-based broadband measurements. *J. Geophys. Res.* 113, D21207. <http://dx.doi.org/10.1029/2008JD010211>.
- Giles, D.M., Holben, B.N., Eck, T.F., Sinyuk, A., Smirnov, A., Slutsker, I., Dickerson, R.R., Thompson, A.M., Schafer, J.S., 2012. An analysis of AERONET aerosol absorption properties and classifications representative of aerosol source regions. *J. Geophys. Res.* 117, D17203. <http://dx.doi.org/10.1029/2012JD018127>.
- Gkikas, A., Hatzianastassiou, N., Mihalopoulos, N., Katsoulis, V., Kazadzis, S., Pey, J., Querol, X., Torres, O., 2013. The regime of intense desert dust episodes in the Mediterranean based on contemporary satellite observations and ground measurements. *Atmos. Chem. Phys.* 13 (23), 12135–12154. <http://dx.doi.org/10.5194/acp-13-12135-2013>.
- Gkikas, A., Hatzianastassiou, N., Mihalopoulos, N., Torres, O., 2016. Characterization of aerosol episodes in the greater Mediterranean Sea area from satellite observations (2000–2007). *Atmos. Environ.* 118, 286–304. <http://dx.doi.org/10.1016/j.atmosenv.2015.11.056>.
- Gonzi, S., Baumgartner, D., Putz, E., 2002. Aerosol Climatology and Optical Properties of Key Aerosol Types Observed in Europe, IGAM/UG Technical Report for EU No. 1/2002 EDUCUE. <http://www.uni-graz.at/en/igam1/wwwgonzi/educe.b.pdf>.
- Goudie, A.S., Middleton, N.J., 2001. Saharan dust storms: nature and consequences. *Earth-Sci. Rev.* 56, 179–204. [http://dx.doi.org/10.1016/S0012-8252\(01\)00067-8](http://dx.doi.org/10.1016/S0012-8252(01)00067-8).
- Guirado, C., Cuevas, E., Cachorro, V.E., Toledano, C., Alonso-Pérez, S., Bustos, J.J., Basart, S., Romero, P.M., Camino, C., Mimouni, M., Zeudmi, L., Goloub, P., Baldasano, J.M., de Frutos, A.M., 2014. Aerosol characterization at the Saharan AERONET site Tamanras-set. *Atmos. Chem. Phys.* 14 (21), 11753–11773. <http://dx.doi.org/10.5194/acp-14-11753-2014>.
- Holben, B., Eck, T., Slutsker, I., Smirnov, A., Sinyuk, A., Schafer, J., Giles, D., Dubovik, O., 2006. AERONET's Version 2.0 Quality Assurance Criteria, Remote Sensing of the Atmosphere and Clouds, Proc. SPIE 6408, 64080Q. <http://dx.doi.org/10.1117/12.706524>.
- Holben, B.N., Eck, T.F., Slutsker, I., Tanré, D., Buis, J.P., Setzer, A., Vermote, E., Smirnov, A., 1998. AERONET – a federated instrument network and data archive for aerosol characterization. *Remote Sens. Environ.* 66 (1), 1–16. [http://dx.doi.org/10.1016/S0034-4257\(98\)00031-5](http://dx.doi.org/10.1016/S0034-4257(98)00031-5).
- Horvath, H., 1998. Influence of Atmospheric Aerosols upon the Global Radiation Balance. Atmospheric Particles. John Wiley & Sons Ltd.
- Horvath, H., Alados Arboledas, L., Olmo, F.J., Jovanovic, O., Gangl, M., Kaller, W., Sánchez, C., Sauerzopf, H., Seidl, S., 2002. Optical characteristics of the aerosol in Spain and Austria and its effect on radiative forcing. *J. Geophys. Res.* 107 (D19), 4386. <http://dx.doi.org/10.1029/2001JD001472>.
- Kacenelenbogen, M., Léon, J.F., Chiapello, I., Tanré, D., 2006. Characterization of aerosol pollution events in France using ground-based and POLDER-2 satellite data. *Atmos. Chem. Phys.* 6, 4843–4849.
- Kaufman, Y.J., Koren, I., Remer, L.A., Tanré, D., Ginoux, P., Fan, S., 2005. Dust transport and deposition observed from the Terra-Moderate Resolution Imaging Spectroradiometer (MODIS) spacecraft over the Atlantic Ocean. *J. Geophys. Res.* 110, D10S12. <http://dx.doi.org/10.1029/2003JD004436>.
- Kim, D., Chin, M., Yu, H., Eck, T.F., Sinyuk, A., Smirnov, A., Holben, B.N., 2011. Dust optical properties over North Africa and Arabian Peninsula derived from the AERONET dataset. *Atmos. Chem. Phys.* 11, 10733–10741. <http://dx.doi.org/10.5194/acp-11-10733-2011>.
- Knippertz, P., Stuut, J.-B.W., 2014. Chapter 1 Introduction. In: Knippertz, P., Stuut, J.-B.W. (Eds.), Mineral Dust: A Key Player in the Earth System. Springer, New York, pp. 1–14. <http://dx.doi.org/10.1007/978-94-017-8978-3>.
- Kokhanovsky, A.A., Prikhach, A.S., Katsev, I.L., Zege, E.P., 2009. Determination of particulate matter vertical columns using satellite observations. *Atmos. Meas. Tech.* 2, 327–335. <http://dx.doi.org/10.5194/amt-2-327-2009>.
- Liu, Y., Park, R.J., Jacob, D.J., Li, Q., Kilaru, V., Sarnat, J.A., 2004. Mapping annual mean ground-level PM_{2.5} concentrations using multiangle imaging spectroradiometer aerosol optical thickness over the contiguous United States. *J. Geophys. Res. D: Atmos.* 109 (22), 1–10.
- Mallet, M., Dubovik, O., Nabat, P., Dulac, F., Kahn, R., Sciare, J., Paronis, D., Léon, J.F., 2013. Absorption properties of Mediterranean aerosols obtained from multi-year ground-based remote sensing observations. *Atmos. Chem. Phys.* 13 (18), 9195–9210.
- Mateos, D., Antón, M., Toledano, C., Cachorro, V.E., Alados-Arboledas, L., Sorribas, M., Baldasano, J.M., 2014. Aerosol radiative effects in the ultraviolet, visible, and near-infrared spectral ranges using long-term aerosol data series over the Iberian Peninsula. *Atmos. Chem. Phys.* 14 (24), 13497–13514. <http://dx.doi.org/10.5194/acp-14-13497-2014>.
- Mateos, D., Cachorro, V.E., Toledano, C., Burgos, M.A., Bennouna, Y., Torres, B., Fuertes, D., González, R., Guirado, C., Calle, A., de Frutos, A.M., 2015. Columnar and surface aerosol load over the Iberian Peninsula establishing annual cycles, trends, and relationships in five geographical sectors. *Sci. Total Environ.* 518–519, 378–392. <http://dx.doi.org/10.1016/j.scitotenv.2015.03.002>.
- Meloni, D., di Sarra, A., Biavati, G., DeLisi, J.J., Monteleone, F., Pace, G., Piacentino, S., Sferlazzo, D.M., 2007. Seasonal behavior of Saharan dust events at the Mediterranean island of Lampedusa in the period 1999–2005. *Atmos. Environ.* 41 (14), 3041–3056. <http://dx.doi.org/10.1016/j.atmosenv.2006.12.001>.
- Meloni, D., di Sarra, A., Pace, G., Monteleone, F., 2006. Optical properties of aerosols over the central Mediterranean. 2. Determination of single scattering albedo at two wavelengths for different aerosol types. *Atmos. Chem. Phys.* 6, 715e727.
- Obregón, M.A., Serrano, A., Cancillo, M.L., Cachorro, V.E., Toledano, C., 2015. Aerosol radiometric properties at Western Spain (Cáceres station). *Int. J. Climatol.* 35 (6), 981–990. <http://dx.doi.org/10.1002/joc.4031>.
- O'Neill, N.T., Ignatov, A., Holben, B.N., Eck, T.F., 2000. The lognormal distribution as a reference for reporting aerosol optical depth statistics: Empirical tests using multi-year, multi-site AERONET Sunphotometer data. *Geophys. Res. Lett.* 27, 3333–3336. <http://dx.doi.org/10.1029/2000GL011581>.
- Pace, G., di Sarra, A., Meloni, D., Piacentino, S., Chamard, P., 2006. Aerosol optical properties at Lampedusa (Central Mediterranean). 1. Influence of transport and identification of different aerosol types. *Atmos. Chem. Phys.* 6, 697–713. <http://dx.doi.org/10.5194/acp-6-697-2006>.
- Pérez, L., Tobías, A., Querol, X., Pey, J., Alastuey, A., Díaz, J., Sunyer, J., 2012. Saharan dust, particulate matter and cause-specific mortality: a case/crossover study in Barcelona (Spain). *Environ. Int.* 48, 150–155. <http://dx.doi.org/10.1016/j.envint.2012.07.001>.
- Pey, J., Querol, X., Alastuey, A., Forastiere, F., Stafoggia, M., 2013. African dust outbreaks over the Mediterranean Basin during 2001–2011: PM₁₀ concentrations, phenomenology and trends, and its relation with synoptic and mesoscale meteorology. *Atmos. Chem. Phys.* 13 (3), 1395–1410. <http://dx.doi.org/10.5194/acp-13-1395-2013>.
- Prats, N., Cachorro, V.E., Berjón, A., Toledano, C., de Frutos, A.M., 2011. Column-integrated aerosol microphysical properties from an AERONET sun photometer over southwestern Spain. *Atmos. Chem. Phys.* 11, 12535–12547. <http://dx.doi.org/10.5194/acp-11-12535-2011>.
- Prats, N., Cachorro, V.E., Sorribas, M., Mogo, S., Berjón, A., Toledano, C., de Frutos, A.M., de la Rosa, J., Lauilainen, N., de la Morena, B.A., 2008. Columnar aerosol properties during "El Arenoso 2004 summer campaign". *Atmos. Environ.* 42, 2643–2653. <http://dx.doi.org/10.1016/j.atmosenv.2007.07.041>.
- Prospero, J.M., Ginoux, P., Torres, O., Nicholson, S.E., Gill, T.E., 2002. Environmental characterization of global sources of atmospheric soil dust identified with the Nimbus 7 total ozone mapping spectrometer (TOMS) absorbing aerosol product. *Rev. Geophys.* 40 (1), 2–1–2–31. <http://dx.doi.org/10.1029/2000RG000095>.
- Querol, X., Alastuey, A., Pandolfi, M., Reche, C., Pérez, N., Minguillón, M.C., Moreno, T., Viana, M., Escudero, M., Orio, A., Pallarés, M., Reina, F., 2014. 2001–2012 trends on air quality in Spain. *Sci. Total Environ.* 490, 957–969. <http://dx.doi.org/10.1016/j.scitotenv.2014.05.074>.
- Querol, X., Pey, J., Pandolfi, M., Alastuey, A., Cusack, M., Pérez, N., Moreno, T., Kleanthous, S., 2009. African dust contributions to mean ambient PM₁₀ mass levels across the Mediterranean Basin. *Atmos. Environ.* 43 (28), 4266–4277. <http://dx.doi.org/10.1016/j.atmosenv.2009.06.013>.
- Reyes, M., Díaz, J., Tobías, A., Montero, J.C., Linares, C., 2014. Impact of Saharan dust particles on hospital admissions in Madrid (Spain). *Int. J. Environ. Health Res.* 24 (1), 63–72. <http://dx.doi.org/10.1080/09603123.2013.782604>.
- Rodríguez, E., Toledano, C., Cachorro, V.E., Ortiz, P., Stebel, K., Berjón, A., Blindheim, S., Gausa, M., de Frutos, A.M., 2012. Aerosol characterization at the sub-Arctic site Andenes (69°N, 16°E), by the analysis of columnar optical properties. *Q.J.R. Meteorol. Soc.* 138, 471–482. <http://dx.doi.org/10.1002/qj.921>.
- Rohen, G.J., von Hoyningen-Huene, W., Kokhanovsky, A., Dinter, T., Vountas, M., Burrows, J.P., 2011. Retrieval of aerosol mass load (PM₁₀) from MERIS/Envisat top of atmosphere spectral reflectance measurements over Germany. *Atmos. Meas. Tech.* 4, 523–534. <http://dx.doi.org/10.5194/amt-4-523-2011>.
- Ryder, C.L., Highwood, E.J., Lai, T.M., Sodemann, H., Marsham, J.H., 2013. Impact of atmospheric transport on the evolution of microphysical and optical properties of Saharan dust. *Geophys. Res. Lett.* 40, 2433–2438. <http://dx.doi.org/10.1002/grl.50482>.
- Salvador, P., Alonso-Pérez, S., Pey, J., Artíñano, B., de Bustos, J.J., Alastuey, A., Querol, X., 2014. African dust outbreaks over the western Mediterranean Basin: 11-year characterization of atmospheric circulation patterns and dust source areas. *Atmos. Chem. Phys.* 14, 6759–6775. <http://dx.doi.org/10.5194/acp-14-6759-2014>.
- Salvador, P., Artíñano, B., Molero, F., Viana, M., Pey, J., Alastuey, A., Querol, X., 2013. African dust contribution to ambient aerosol levels across Central Spain: characterization of long-range transport episodes of desert dust. *Atmos. Res.* 127, 117–129. <http://dx.doi.org/10.1016/j.atmosres.2011.12.011>.
- Silva, A., Bugalho, M., Costa, M.J., von Hoyningen-Huene, V., Shmidt, T., Heintzenberg, J., Henning, S., 2002. Aerosol optical properties from columnar data during the second aerosol characterization experiment on the south coast of Portugal. *J. Geophys. Res.* 107 (D22), 4642. <http://dx.doi.org/10.1029/2002JD000219>.
- Sorribas, M., Ogren, J.A., Olmo, F.J., Quirantes, A., Fraile, R., Gil-Ojeda, M., Alados-Arboledas, L., 2015. Assessment of African desert dust episodes over the southwest Spain at sea level using in situ aerosol optical and microphysical properties. *Tellus B* 67, 27482.
- Tafuro, A.M., Barnaba, F., de Tomasi, F., Perrone, M.R., Gobbi, G.P., 2006. Saharan dust particle properties over the central Mediterranean. *Atmos. Res.* 81–1, 67–93.
- Taylor, M., Kazadzis, S., Amiridis, V., Kahn, R.A., 2015. Global aerosol mixtures and their multiyear and seasonal characteristics. *Atmos. Environ.* 116, 112–129.
- Toledano, C., Cachorro, V.E., de Frutos, A.M., Sorribas, M., Prats, N., 2007. Inventory of African Desert dust events over the Southwestern Iberian Peninsula in 2000–2005 with an AERONET Cimel sun photometer. *J. Geophys. Res.* 112 (D21201). <http://dx.doi.org/10.1029/2006JD008307>.

- Toledano, C., Cachorro, V.E., Gausa, M., Stebel, K., Altonen, V., Berjón, A., Ortiz de Galisteo, J.P., de Frutos, A.M., Bennouna, Y., Blindheim, S., Myhra, C.L., Zibordi, G., Wehrli, C., Kratzer, S., Hakansson, B., Carlund, T., de Leeuw, G., Herber, A., Torres, B., 2012. Overview of sun photometer measurements of aerosol properties in Scandinavia and Svalbard. *Atmos. Environ.* 52, 18–28. <http://dx.doi.org/10.1016/j.atmosenv.2011.10.022>.
- Toledano, C., Wiegner, M., Groß, S., Freudenthaler, V., Gasteiger, J., Müller, D., Müller, T., Schladitz, A., Weinzierl, B., Torres, B., O'Neill, N.T., 2011. Optical properties of aerosol mixtures derived from sun-sky radiometry during SAMUM-2. *Tellus B* 63, 635–648.
- Torres, B., Dubovik, O., Toledano, C., Berjón, A., Cachorro, V.E., Lapyonok, T., Litvinov, P., Goloub, P., 2014. Sensitivity of aerosol retrieval to geometrical configuration of ground-based sun/sky radiometer observations. *Atmos. Chem. Phys.* 14, 847–875. <http://dx.doi.org/10.5194/acp-14-847-2014>.
- Valenzuela, A., Olmo, F.J., Lyamani, H., Antón, M., Quirantes, A., Alados-Arboledas, L., 2012. Aerosol radiative forcing during African desert dust events (2005–2010) over South-eastern Spain. *Atmos. Chem. Phys.* 12 (21), 10331–10351. <http://dx.doi.org/10.5194/acp-12-10331-2012>.
- Valenzuela, A., Olmo, F.J., Lyamani, H., Granados-Muñoz, M.J., Antón, M., Guerrero-Rascado, J.L., Quirantes, A., Toledano, C., Pérez-Ramírez, D., Alados-Arboledas, L., 2014. Aerosol transport over the western Mediterranean basin: evidence of the contribution of fine particles to desert dust plumes over Alborán Island. *J. Geophys. Res.-Atmos.* 119 (24), 14028–14044. <http://dx.doi.org/10.1002/2014JD022044>.
- Viana, M., Pey, J., Querol, X., Alastuey, A., de Leeuw, F., Lükeville, A., 2014. Natural sources of atmospheric aerosols influencing air quality across Europe. *Sci. Total Environ.* 472, 825–833. <http://dx.doi.org/10.1016/j.scitotenv.2013.11.140>.
- Waggoner, A.P., Weiss, R., Ahlquist, N., Covert, D., Will, S., Charlson, R., 1981. Optical characteristics of atmospheric aerosols. *Atmos. Environ.* 15, 1891–1909.
- Wagner, F., Bortoli, D., Pereira, S., Costa, M.J., Silva, A.M., Weinzierl, B., Esselborn, M., Petzold, A., Rasp, K., Heinold, B., Tegen, I., 2009. Properties of dust aerosol particles transported to Portugal from the Sahara desert. *Tellus B* 61B, 297–306.
- Yannopoulos, S.I., Lyberatos, G., Theodosiou, N., Li, W., Valipour, M., Tamburino, A., Angelakis, A.N., 2015. Evolution of water lifting devices (pumps) over the centuries worldwide. *Water* 7, 5031–5060. <http://dx.doi.org/10.3390/w7095031>.

CONCLUSIONES

El trabajo presentado en esta tesis doctoral consta de un estudio detallado de las propiedades de los aerosoles en el centro norte de la Península Ibérica en el periodo 2003-2014, haciendo especial hincapié en las intrusiones de origen desértico. La característica principal subyacente a los tres artículos que componen la tesis es el análisis simultáneo y las relaciones entre las bases de datos de superficie (estación: Peñausende, red: EMEP) y columna (estación: Palencia, red: AERONET). Las magnitudes principales analizadas han sido: AOD y PM₁₀ en relación a la carga total del aerosol y AE y PM ratio (PM_{2.5}/PM₁₀), derivadas de las anteriores, en cuanto al tamaño de los aerosoles. Trabajar con series de datos de larga duración ha permitido realizar todos los análisis desde un punto de vista climatológico, estableciendo por primera vez determinadas relaciones entre propiedades de superficie y columna.

Los principales resultados y conclusiones que se han obtenido son:

1. Los ciclos anuales de AOD y PM₁₀ presentan una clara diferencia, pues si bien ambos muestran el máximo en verano, el ciclo de PM₁₀ exhibe otro máximo secundario bien definido en Marzo. Esta diferencia es debida al mayor peso de las intrusiones desérticas sobre el PM₁₀ que sobre el AOD, más influenciado por los eventos dominados por las partículas finas. La variabilidad interanual, entre 2003-2014, muestra una tendencia decreciente similar para el AOD y el PM₁₀, cuantificada en torno al 40%, y con una correlación del 0.9.
2. Las correlaciones AOD-PM₁₀ son generalmente pobres al analizar datos diarios (coeficientes de correlación R, menores a 0.6) y mejoran considerablemente si se trabaja con medias mensuales o anuales. No se ha podido determinar ningún tipo de relación entre las variables AE y PM ratio, que representan el tamaño medio predominante del aerosol en columna o en superficie. Los resultados muestran que las relaciones entre esas variables deben establecerse por intervalos de valores (bines) y bajo una perspectiva climatológica. No se han mejorado las correlaciones de este tipo de relaciones cuando se analizan los valores exclusivamente durante los eventos desérticos.

3. Se ha propuesto y aplicado una metodología para la detección de eventos desérticos a partir del análisis conjunto de magnitudes en superficie y columna. El uso del AE permite además diferenciar intrusiones con un marcado carácter desértico y condiciones de mezcla. El análisis de información complementaria, como retrotrayectorias de las masas de aire e imágenes satelitales, ha sido clave para la identificación de determinados eventos dudosos (alta nubosidad, etc...) o que carecen de datos experimentales y que forman parte del inventario de las intrusiones desérticas. La mitad de los eventos han sido registrados simultáneamente a partir de los datos de AOD y PM₁₀. Un punto fuerte de la metodología es que permite, además, detectar aquellos eventos que sólo han dejado huella en una de las bases de datos, AOD o PM₁₀. El menor muestreo en la base de datos de AOD no implica un hándicap a la hora de detectar las intrusiones de aerosol desértico.
4. El inventario de intrusiones desérticas cuenta con 152 episodios entre 2003-2014 compuestos por 418 días, con una media de 35 días por año (9,6% de días al año). De esos 418 días, 243 son de tipo aerosol desértico puro (D) y 175 de mezcla con predominio de aerosol desértico o tipo MD. El año con mayor número de intrusiones ha sido 2006 con 67 días y 17 episodios, mientras que en 2013 se ha registrado el mínimo con 15 días que componen 7 episodios. Se ha determinado una reducción en el número de intrusiones de aerosol desértico en el área de estudio con una tendencia decreciente de 2.7 días por año entre 2003 y 2014 estadísticamente significativa.
5. El ciclo anual del número de días y episodios desérticos se comporta aproximadamente de forma similar con máximos en marzo y de mayo a septiembre (máximo absoluto en junio con 65 días) y mínimos en abril e invierno (no superando las 20 días de intrusión en el caso de los meses de invierno). De los 4 tipos de escenarios sinópticos que dan lugar a la llegada de intrusiones desérticas a la Península Ibérica desde el continente africano, ha sido el escenario denominado NAH-A (North African High Located at Upper Levels, que se produce por un fuerte calentamiento del Sahara), el responsable de propiciar la llegada de 81 episodios al área de estudio, cobrando mayor importancia durante los meses de verano.
6. La contribución desértica media es de 0.015 para el AOD y de 1.3 $\mu\text{g m}^{-3}$ para el PM₁₀, representando el ~12% del valor total de ambas magnitudes. El ciclo anual presenta máximos de contribución en los meses de Marzo y de verano. La evolución

interanual muestra que el año de mayor contribución desértica al AOD fue 2004 y 2006 para el PM₁₀, mientras que el año con menor contribución es 2013 en ambas bases de datos. La evolución temporal de la contribución anual de aerosoles desérticos ha disminuido un ~10% por año en el periodo 2003-2014 (respecto a su valor medio), tanto en AOD como en PM₁₀. Esta disminución supone un 30% de la reducción de la carga total de aerosol observada en el área de estudio.

7. La caracterización del ciclo anual de los aerosoles desérticos presenta, tanto para el AOD como para el PM₁₀, la clara bimodalidad ya mostrada por del ciclo anual del PM₁₀ total, con un máximo en marzo y el otro máximo en los meses de verano. El establecimiento de las relaciones entre las propiedades microfísicas entre sí (concentración volúmica, radio efectivo, esfericidad, fracción del modo fino) y con las variables AOD-AE y las variables de superficie PM₁₀ y PM ratio definen las características de los aerosoles desérticos en la región de CyL, determinando los valores del factor de extinción y el factor altura de escala.
8. Las intrusiones con un fuerte carácter desértico están caracterizadas por partículas gruesas y casi nulo peso del modo fino (AE<0.6 y VC_F/VC_T < 0.2), pérdida de poder absorbente con el aumento la longitud de onda como muestra el SSA, no esfericidad, un radio total efectivo entre 0.5-1.2 μm, un alto factor de escala que llega hasta 10 km y un eficiencia de extinción en columna de 1.78 μm⁻²/μm⁻³.
9. Los episodios de mezcla con presencia asegurada de aerosol desértico vienen caracterizados por: aumento de influencia del modo fino (AE > 0.6 y VC_F/VC_T > 0.2), cambio en la dependenciapectral del SSA, aumento de la fracción de esfericidad (0.17-1, barren prácticamente todo el rango de valores), radio total efectivo entre 0.2 y 0.5 μm, factor de escala bajando hasta unos 8 km, y una eficiencia de extinción en columna de hasta 3.74 μm⁻²/μm⁻³.

La consideración simultánea de propiedades en superficie-columna de los aerosoles (incluyendo un análisis detallado de cierta información complementaria) se ha probado como una herramienta útil y eficaz en la detección de eventos desérticos. Este estudio es necesario para ampliar el conocimiento sobre el comportamiento de los aerosoles desérticos en el área Mediterránea, donde presentan una gran influencia, así como para validar los modelos de predicción de aerosoles desérticos o los productos de satélites relativos a estos.

Tareas futuras

El trabajo desarrollado durante esta tesis doctoral puede continuar mediante las vías de investigación que se detallan a continuación:

1. Identificación y caracterización de eventos de alta turbiedad atmosférica de origen antropogénico y sus mezclas.
2. Aplicación de la metodología propuesta a cualquier otra zona que cuente con estaciones de fondo regional que proporcionen valores de PM₁₀ y AOD.
3. Comparativa de la metodología propuesta con otras metodologías existentes, como la que conforma la base de datos CALIMA o la propuesta mediante el algoritmo de O'Neill, aplicada en las estaciones de AERONET.
4. Desarrollo de métodos automáticos de detección de los aerosoles desérticos que puedan ser aplicados en grandes áreas y validación de dichos métodos usando el inventario creado en esta tesis.
5. Validación de productos de satélites (AOD-MODIS) y modelos de predicción de aerosoles desérticos (BSC-Dream, NAAPS...).

REFERENCIAS

- Alados-Arboledas, L., Lyamani, H., Olmo, F.J., 2003. Aerosol size properties at Armilla, Granada (Spain). *Quart. J. Roy. Meteor. Soc.*, 129(590), 1395–1413, doi: 10.1256/qj.01.207.
- Barmpadimos, I., Keller, J., Oderbolz, D., Hueglin, C., Prévôt, A.S.H., 2012. One decade of parallel fine ($PM_{2.5}$) and coarse ($PM_{10}-PM_{2.5}$) particulate matter measurements in Europe: trends and variability. *Atmos. Chem. Phys.*, 12, 3189–3203, doi: 10.5194/acp-12-3189-2012.
- Basart, S., Pérez, C., Cuevas, E., Baldasano, J.M., Gobbi, G.P., 2009. Aerosol characterization in Northern Africa, Northeastern Atlantic, Mediterranean Basin and Middle East from direct-sun AERONET observations. *Atmos. Chem. Phys.*, 9, 8265–8282, doi: 10.5194/acp-9-8265-2009.
- Bennouna, Y.S., Cachorro, V.E., Torres, B., Toledano, C., Berjón, A., de Frutos, A.M., Alonso Fernández Coppel, I., 2013. Atmospheric turbidity determined by the annual cycle of the aerosol optical depth over north-center Spain from ground (AERONET) and satellite (MODIS). *Atmos. Environ.*, 67, 352–364, doi: 10.1016/j.atmosenv.2012.10.065.
- Bennouna, Y.S., Cachorro, V.E., Burgos, M.A., Toledano, C., Torres, B., de Frutos, A.M., 2014. Relationships between columnar aerosol optical properties and surface particulate matter observations in north-central Spain from long-term records (2003–2011). *Atmos. Meas. Tech. Discuss.*, 7, 5829–5882, doi: 10.5194/amtd-7-5829-2014.
- Boucher, O., Randall, D., Artaxo, P., Bretherton, C., Feingold, G., Forster, P., Kerminen, V.M., Kondo, Y., Liao, H., Lohmann, U., Rasch, P., Satheesh, S.K., Sherwood, S., Stevens, B., Zhang, X.Y., 2013. Clouds and Aerosols, In: Climate Change 2013: The Physical Science Basis. Contribution of Working Group I to the Fifth Assessment Report of the Intergovernmental Panel on Climate Change 2013 [Stocker, T.F., Qin, D., Plattner, G.K., Tignor, M., Allen, S.K., Boschung, J., Nauels, A., Xia, Y., Bex, V., Midgley, P.M.]. Cambridge University Press, Cambridge, United Kingdom and New York NY, USA.
- Cachorro, V.E., and Tanré, D., 1997. The correlation between particle mass loading and extinction: application to desert dust aerosol content estimation. *Remote Sens. Environ.*, 60, 187–194.
- Cachorro, V.E., Durán, P., de Frutos, A.M., Vergaz, R., 2000a. Measurements of the atmospheric turbidity of the north-center continental área in Spain: spectral aerosol optical thickness and Ångstrom turbidity parameters. *J. Aerosol Sci.*, 31, 687–702.
- Cachorro, V.E., Durán, P., Vergaz, R., de Frutos, A.M., 2000b. Columnar physical and radiative properties of atmospheric aerosols in north central Spain. *J. Geophys. Res.*, 105(D6), 7161–7175, doi:10.1029/1999JD901165.
- Cachorro, V.E., Burgos, M.A., Mateos, D., Toledano, C., Bennouna, Y., Torres, B., de Frutos, A.M., Herguedas, A., 2016. Inventory of African desert dust events in the North-central Iberian Peninsula in 2003–2014 based on Sun photometer and PMx data. *Atmos. Chem. Phys.*, 16, 8227–8248, doi: 10.5194/acp-16-8227-2016.
- Cusack, M., Alastuey, A., Pérez, N., Pey, J., Querol, X., 2012. Trends of particulate matter ($PM_{2.5}$) and chemical composition at a regional background site in the Western Mediterranean over the last nine years (2002–2010). *Atmos. Chem. Phys.*, 12, 8341–8357, doi: 10.5194/acp-12-8341-2012.
- D’Almeida, G.A., Koepke, P., Shettle, E.P., 1991. Atmospheric Aerosol: Global Climatology and Radiative Characteristics. A. Deepak, Hampton, Va.
- de Deckker, P., Abed, R.M.M., de Beer, D., Hinrichs, K., O’Loingsigh, T., Schefuß, E., Stuut, J.-B., Tapper, N.J., van der Kaars, S., 2008. Geochemical and microbiological fingerprinting of airborne dust that fell in

Canberra, Australia, in October 2002. *Geochem. Geophys. Geosyst.*, 9, Q12Q10, <http://dx.doi.org/10.1029/2008GC002091>.

Dockery, D.W., 2001. Epidemiologic evidence of cardiovascular effects of particulate air pollution. *Environ. Health Perspect.*, 109 (4), 483–486.

Draxler, R.A., Stunder, B., Rolph, G., Stein, A., Taylor, A., 2014. HYSPLIT4 User's Guide, Air Resources Laboratory, National Oceanic and Atmospheric Administration (NOAA). Silver Spring, MD.

EC. Directive 2008/50/EC of the European Parliament and of the Council (21 May 2008) on Ambient Air Quality and Cleaner Air for Europe. Official Journal of the European Communities, 2008. L 151: 1–44.

Eck, T., Holben, B., Reid, J., Dubovik, O., Smirnov, A., O'Neill, N., Slutsker, I., Kinne, S., 1999. Wavelength dependence of the optical depth of biomass burning, urban, and desert dust aerosols. *J. Geophys. Res.*, 104, 31333–31349.

EMEP/CCC-Report 1/95. EMEP Manual for Sampling and Chemical Analysis, rev 2002. Norwegian Institute for Air Research, 1996. Available at: <http://www.nilu.no/projects/ccc/manual/index.html>.

EMEP/CCC-Report 4/11. EMEP Transboundary Particulate Matter in Europe Status report 2011. Norwegian Institute for Air Research, 2011. Available at: <http://www.nilu.no/projects/ccc/reports/emep4-2011.pdf>.

EMEP/CCC-Report 3/2014. Data Report 2012 Acidifying and eutrophying compounds and particulate matter. Norwegian Institute for Air Research, 2014. Available at: <http://www.nilu.no/projects/ccc/reports/ccc3-2014.pdf>.

Escudero, M., Castillo, S., Querol, X., Avila, A., Alarcón, M., Viana, M.M., Alastuey, A., Cuevas, E., Rodríguez, S., 2005. Wet and dry African dust episodes over eastern Spain. *J. Geophys. Res.*, 110, D18S08, doi:10.1029/2004JD004731.

Estellés, V., Martínez-Lozano, J.A., Utrillas, M.P., Campanelli, M., 2007. Columnar aerosol properties in Valencia (Spain) by ground-based Sun photometry. *J. Geophys. Res.*, 112, D11201, doi:10.1029/2006JD008167.

Formenti, P., Schütz, L., Balkanski, Y., Desboeufs, K., Ebert, M., Kandler, K., 2011. Recent Progress in understanding physical and chemical properties of mineral dust. *Atmos. Chem. Phys.*, 11, 8231–8256.

Fraser, R.S., Kaufman, Y.J., Mahoney, R.L., 1984. Satellite measurements of aerosol mass and transport. *Atmos. Environ.*, 18, 2577–2584.

Goudie, A.S., and Middleton, N. J., 2006. Desert Dust in the Global System. Springer-Verlag Berlin Heidelberg, Berlin, Germany, 288 pp., 2006.

Guirado, C., Cuevas, E., Cachorro, V.E., Toledano, C., AlonsoPérez, S., Bustos, J.J., Basart, S., Romero, P.M., Camino, C., Mimouni, M., Zeudmi, L., Goloub, P., Baldasano, J.M., de Frutos, A.M., 2014. Aerosol characterization at the Saharan AERONET site Tamanrasset. *Atmos. Chem. Phys.*, 14, 11753–11773, doi: 10.5194/acp-14-11753-2014.

Haywood, J.M., and Boucher, O., 2000. Estimates of the direct and indirect radiative forcing due to tropospheric aerosols: A review. *Rev. Geophys.*, 38, 513–543, doi: 10.1029/1999RG000078.

Hess, M., Koepke, P., Schult, I., 1998. Optical properties of aerosols and clouds: the software package OPAC. *B. Am. Meteorol. Soc.*, 79, 831–844.

Holben, B.N., Eck, T.F., Slutsker, I., Tanré, D., Buis, J.P., Setzer, A., Vermote, E., Reagan, J.A., Kaufman, Y.J., Nakajima, T., Lavenu, F., Jankowiak, I., Smirnov, A., 1998. AERONET – a federated instrument network and data archive for aerosol characterization. *Remote Sens. Environ.*, 66, 1–16.

- Kaufman, Y.J., Koren, I., Remer, L.A., Tanré, D., Ginoux, P., Fan, S., 2005. Dust transport and deposition observed from the terramoderate resolution imaging spectroradiometer (MODIS) spacecraft over the Atlantic ocean. *J. Geophys. Res.*, 110, D10S12, doi: 10.1029/2003JD004436.
- Knippertz, P., and Stuut, J-B.W., 2014. Mineral Dust: A Key Player in the Earth System, 509 pp. Springer Netherlands. Dordrecht, Netherlands.
- Kokhanovsky, A.A., Prikhach, A.S., Katsev, I.L., Zege, E.P., 2009. Determination of particulate matter vertical columns using satellite observations. *Atmos. Meas. Tech.*, 2, 327–335, doi: 10.5194/amt-2-327-2009.
- Künzli, N., Kaier, R., Medina, S., Studnicka, M., Chanel, O., Filliger, P., Herry, M., Jr F.H., Puybonniewx-Texier, V., Quénel, P., Schneider, J., Seethaler, R., Vergnaud, J.C., Sommer H., 2000. Public health impact of outdoor and traffic related air pollution: a European assessment. *The Lancet*, 356, 795-801.
- Lohmann, U., Rotstayn, L., Storelvmo, T., Jones, A., Menon, S., Quaas, J., Ekman, A.M.L., Koch, D., Ruedy, R., 2010. Total aerosol effect: radiative forcing or radiative flux perturbation? *Atmos. Chem. Phys.*, 10, 3235–3246, doi: 10.5194/acp-10-3235-2010.
- Martinez-Garcia, A., Rosell-Melé, A., Jaccard, S.L., Geibert, W., Sigman, D.M., Haug, G.H., 2011. Southern Ocean dust–climate coupling over the past four million years. *Nature*, 476, 312–315.
- Mateos, D., Antón, M., Toledano, C., Cachorro, V.E., Alados-Arboledas, L., Sorribas, M., and Baldasano, J.M., 2014a. Aerosol radiative effects in the ultraviolet, visible, and near-infrared spectral ranges using long-term aerosol data series over the Iberian Peninsula. *Atmos. Chem. Phys.*, 14(24), 13497-13514, doi: 10.5194/acp-14-13497-2014.
- Mateos, D., Sanchez-Lorenzo, A., Antón, M., Cachorro, V.E., Calbó, J., Costa, M.J., Torres, B., Wild, M., 2014b. Quantifying the respective roles of aerosols and clouds in the strong brightening since the early 2000s over the Iberian Peninsula. *J. Geophys. Res. Atmos.*, 119, 10, 382–10, 393. doi:10.1002/2014JD022076.
- Mateos, D., Cachorro, V.E., Toledano, C., Burgos, M.A., Bennouna, Y., Torres, B., Fuertes, D., González, R., Guirado, C., Calle, A., de Frutos, A.M., 2015. Columnar and surface aerosol load over the Iberian Peninsula establishing annual cycles, trends, and relationships in five geographical sectors. *Sci. Total Environ.*, 518-519, 378-392, doi: 10.1016/j.scitotenv.2015.03.002.
- McTanish, G.H., Lynch, A.W., Burgess, R.C., 1990. Wind erosion in eastern Australia. *Aust. J. Soil. Res.*, 28, 323-339.
- Pelletier, B., Santer, R., Vidot, J., 2007. Retrieving of particulate matter from optical measurements: A semiparametric approach. *J. Geophys. Res.*, 112, D06208, doi: 10.1029/2005JD006737.
- Pérez, L., Tobías, A., Querol, X., Pey, J., Alastuey, A., Díaz, J., Sunyer, J., 2012. Saharan dust, particulate matter and cause-specific mortality: A case-crossover study in Barcelona (Spain). *Environ. Int.*, 48, 150-155, doi: 10.1016/j.envint.2012.07.001.
- Pey, J., Querol, X., Alastuey, A., Forastiere, F., Stafiggia, M., 2013. African dust outbreaks over the Mediterranean Basin during 2001-2011: PM₁₀ concentrations, phenomenology and trends, and its relation with synoptic and mesoscale meteorology. *Atmos. Chem. Phys.* 13(3), 1395-1410, doi:10.5194/acp-13-1395-2013.
- Pope III, C.A., 2000. Review: epidemiological basis for particulate air pollution health standards. *Aerosol Sci. Tech.*, 32, 4–14.
- Prats, N., Cachorro, V.E., Berjón, A., Toledano, C., de Frutos, A.M., 2011. Column-integrated aerosol microphysical properties from an AERONET Sun photometer over southwestern Spain. *Atmos. Chem. Phys.*, 11, 12535–12547, doi: 10.5194/acp-11-12535-2011.

Prospero, J.M., 1999. Long-term measurements of the transport of African mineral dust to the Southeastern United States: Implications for regional air quality. *J. Geophys. Res.*, 104, 15.917–15.927, doi: 10.1029/1999JD900072.

Prospero, J.M., Ginoux, P., Torres, O., Nicholson, S.E., Gill, T.E., 2002. Environmental characterization of global sources of atmospheric soil dust identified with the nimbus 7 total ozone mapping spectrometer (TOMS) absorbing aerosol product. *Rev. Geophys.*, 40, 2-1–2-31, doi: 10.1029/2000RG000095.

Querol, X., Alastuey, A., Pandolfi, M., Reche, C., Pérez, N., Minguillón, M.C., Moreno, T., Viana, M., Escudero, M., Orio, A., Pallarés, M., Reina, F., 2014. 2001–2012 trends on air quality in Spain. *Sci. Tot. Env.*, 490, 957–969.

Reyes, M., Díaz, J., Tobias, A., Montero, J.C., Linares, C., 2014. Impact of Saharan dust particles on hospital admissions in Madrid (Spain). *Int. J. Environ. Health Res.*, 24(1), 63–72, doi: 10.1080/09603123.2013.782604.

Rodrigo Fernández, R., 2012. Caracterización de aerosoles atmosféricos en la Comunidad de Castilla y León. Tesis Doctoral. Dpto de Física Teórica, Atómica y Optica. Universidad de Valladolid.

Rodríguez, S., Querol, X., Alastuey, A., Plana, F., 2002. Sources and processes affecting levels and composition of atmospheric aerosol in the western Mediterranean. *J. Geophys. Res.*, 107(D24), 4777, doi: 10.1029/2001JD001488.

Salvador, P., Alonso-Pérez, S., Pey, J., Artíñano, B., de Bustos, J.J., Alastuey, A., Querol, X., 2014. African dust outbreaks over the western Mediterranean Basin: 11-year characterization of atmospheric circulation patterns and dust source areas. *Atmos. Chem. Phys.*, 14, 6759–6775, doi: 10.5194/acp-14-6759-2014.

Sanchez-Romero, A., Sanchez-Lorenzo, A., González, J.A., Calbó, J., 2016. Reconstruction of long-term aerosol optical depth series with sunshine duration records. *Geophys. Res. Lett.*, 43, 1296–1305, doi:10.1002/2015GL067543.

Schwartz, J., Dockery, D.W., Neas, L.M., 1996. Is daily mortality associated specifically with fine particles? *J. Air Waste Manage. Assoc.*, 46, 927–939.

Schaap, M., Apituley, A., Timmermans, R.M.A., Koelemeijer, R.B.A., de Leeuw, G., 2009. Exploring the relation between aerosol optical depth and PM_{2.5} at Cabauw, the Netherlands. *Atmos. Chem. Phys.*, 9, 909–925.

Smirnov, A., Holben, B.N., Eck, T.F., Dubovik, O., Slutsker, I., 2000. Cloud-screening and quality control algorithms for the AERONET database. *Remote Sens. Environ.*, 73, 337–349.

Stein, A.F., Draxler, R.R., Rolph, G.D., Stunder, B.J.B., Cohen, M.D., and Ngan, F., 2015. NOAA's HYSPLIT atmospheric transport and dispersion modeling system. *Bull. Amer. Meteor. Soc.*, 96, 2059–2077.

Toledano, C., Cachorro, V.E., Berjón, A., de Frutos, A.M., Sorribas, M., de la Morena, B., Goloub, P., 2007a. Aerosol optical depth and Ångström exponent climatology at El Arenosillo AERONET site (Huelva, Spain). *Q. J. Roy. Meteor. Soc.*, 133, 795–807.

Toledano, C., Cachorro, V.E., de Frutos, A.M., Sorribas, M., Prats, N., de la Morena, B.A., 2007b. Inventory of African desert dust events over the southwestern Iberian Peninsula in 2000–2005 with an AERONET Cimel Sun photometer. *J. Geophys. Res. [Atmos.]*, 112, D21201, doi:10.1029/2006JD008307.

Toledano, C., Cachorro, V.E., Gausa, M., Stebel, K., Aaltonen, V., Berjón, A., Ortiz de Galisteo, J.P., de Frutos, A.M., Bennouna, Y., Blindheim, S., Myhre, C.L., Zibordi, G., Wehrli, C., Kratzer, S., Hakansson, B., Carlund, T., de Leeuw, G., Herber, A., Torres, B., 2012. Overview of sun photometer measurements of aerosol properties in Scandinavia and Svalbard. *Atmos. Env.*, 52, 18–28, doi:10.1016/j.atmosenv.2011.10.022.

Tørseth, K., Aas, W., Breivik, K., Fjæraa, A.M., Fiebig, M., Hjellbrekke, A.G., Lund Myhre, C., Solberg, S., Yttri, K.E., 2012. Introduction to the European Monitoring and Evaluation Programme (EMEP) and observed atmospheric composition change during 1972–2009. *Atmos. Chem. Phys.*, 12, 5447–5481, doi: 10.5194/acp-12-5447-2012.

Valenzuela, A., Olmo, F.J., Lyamani, H., Antón, M., Quirantes, A., Alados-Arboledas, L., 2012. Aerosol radiative forcing during African desert dust events (2005–2010) over Southeastern Spain. *Atmos. Chem. Phys.*, 12(21), 10331–10351, doi: 10.5194/acp-12-10331-2012.

Valenzuela, A., Olmo, F.J., Lyamani, H., Granados-Muñoz, M.J., Antón, M., Guerrero-Rascado, J.L., Quirantes, A., Toledano, C., Perez-Ramírez, D., Alados-Arboledas, L., 2014. Aerosol transport over the western Mediterranean basin: Evidence of the contribution of fine particles to desert dust plumes over Alborán Island. *J. Geophys. Res.-Atmos.*, 119 (24), 14028–14044, doi: 10.1002/2014JD022044.

Vergaz, R., Cachorro, V.E., de Frutos, A.M., Vilaplana, J.M., de la Morena, B.A., 2005. Columnar characteristics of aerosols by spectroradiometer measurements in the maritime area of the Cadiz gulf (Spain). *Int. J. Climatol.*, 25(13), 1781–1804, doi: 10.1002/joc.1208.

Viana, M., Pey, J., Querol, X., Alastuey, A., de Leeuw, F., Lükewille, A., 2014. Natural Sources of Atmospheric Aerosols Influencing Air Quality Across Europe. *Sci. Total Environ.*, 472, 825–833, doi: 10.1016/j.scitotenv.2013.11.140.

WHO, 2006. Air Quality Guidelines: Global Update 2005: Particulate Matter, Ozone, Nitrogen Dioxide and Sulphur Dioxide. World Health Organization. WHO Regional Office for Europe. ISBN 9289021926.

Willeke, K., and Baron, P.A., Editors. *Aerosol Measurement. Principles. Techniques and Applications*. John Wiley & Sons, 1993.



Grupo de Óptica Atmosférica

Departamento de Física Teórica, Atómica y Óptica

Universidad de Valladolid